OAK RIDGE NATIONAL LABORATORY LIBRARY
3 4456 0044453 4

NUREG/CR-4249
(ORNL-6163)

ornl

OAK RIDGE NATIONAL LABORATORY

MARTIN MARIETTA

Pressure Vessel Fracture Studies Pertaining to the PWR Thermal-Shock Issue: Experiments TSE-5, TSE-5A, and TSE-6

R. D. Cheverton
D. G. Ball
S. E. Bolt
S. K. Iskander
R. K. Nanstad

OAK RIDGE NATIONAL LABORATORY
CENTRAL RESEARCH LIBRARY
CIRCULATION SECTION
4500N ROOM 175
LIBRARY LOAN COPY
DO NOT TRANSFER TO ANOTHER PERSON
If you wish someone else to see this report, send in name with report and the library will arrange a loan.

Prepared for the U.S. Nuclear Regulatory Commission
Office of Nuclear Regulatory Research
Under Interagency Agreements DOE 40-551-75 and 40-552-75

OPERATED BY
MARTIN MARIETTA ENERGY SYSTEMS, INC.
FOR THE UNITED STATES
DEPARTMENT OF ENERGY

NOTICE

This report was prepared as an account of work sponsored by an agency of the United States Government. Neither the United States Government nor any agency thereof, or any of their employees, makes any warranty, expressed or implied, or assumes any legal liability or responsibility for any third party's use, or the results of such use, of any information, apparatus product or process disclosed in this report, or represents that its use by such third party would not infringe privately owned rights.

Available from

Superintendent of Documents
U.S. Government Printing Office
Post Office Box 37082
Washington, D.C. 20013-7982

and

National Technical Information Service
Springfield, VA 22161

NUREG/CR-4249
ORNL-6163
Dist. Category RF

Engineering Technology Division

PRESSURE VESSEL FRACTURE STUDIES PERTAINING TO THE PWR THERMAL-SHOCK ISSUE: EXPERIMENTS TSE-5, TSE-5A, AND TSE-6

R. D. Cheverton S. E. Bolt
D. G. Ball S. K. Iskander
R. K. Nanstad

Manuscript Completed — May 13, 1985
Date Published — June 1985

Prepared for the
U.S. Nuclear Regulatory Commission
Office of Nuclear Regulatory Research
under Interagency Agreements DOE 40-551-75 and 40-552-75

NRC FIN No. B0119

Prepared by the
OAK RIDGE NATIONAL LABORATORY
Oak Ridge, Tennessee 37831
operated by
MARTIN MARIETTA ENERGY SYSTEMS, INC.
for the
U.S. DEPARTMENT OF ENERGY
under Contract No. DE-AC05-84OR21400

OAK RIDGE NATIONAL LABORATORY LIBRARY
3 4456 0044453 4

CONTENTS

	Page
LIST OF FIGURES	vii
LIST OF TABLES	xv
NOMENCLATURE AND ACRONYMS	xvii
FOREWORD	xix
ACKNOWLEDGMENTS	xxvii
ABSTRACT	1
1. INTRODUCTION AND SUMMARY	1
References	18
2. PURPOSE AND SCOPE OF TSE-5, TSE-5A, AND TSE-6	21
3. METHODS OF ANALYSIS FOR CALCULATING K_I FOR TWO- AND THREE-DIMENSIONAL INNER-SURFACE FLAWS	22
References	24
4. PRETEST ANALYSIS AND SPECIFICATION OF TEST CONDITIONS	25
4.1 Preliminary Selection of Test Conditions	25
4.1.1 Test-cylinder dimensions	25
4.1.2 Test-cylinder material	28
4.1.3 Influence of existing forgings on specification of test-cylinder characteristics	31
4.1.4 Severity of thermal shock	31
4.2 Final Pretest Analysis	31
4.2.1 TSE-5	31
4.2.2 TSE-5A	34
4.2.3 TSE-6	35
References	40
5. TEST-CYLINDER FABRICATION DETAILS AND ASSEMBLY	42
5.1 Test-Cylinder Configuration and Dimensions	42
5.2 Test-Cylinder Fabrication and Heat Treatment	42
5.3 Test-Cylinder Material	42
5.4 Generation of Initial Flaw	46
References	48
6. EXPERIMENTAL TECHNIQUE, EQUIPMENT, AND INSTRUMENTATION	49
6.1 Technique for Achieving Thermal Shock	49
6.2 Heating of Test Cylinder Prior to Thermal Shock	53
6.3 Data Acquisition	53
References	59

Page

7. CHARACTERIZATION OF TEST-CYLINDER MATERIAL 61
7.1 TSE-5 and TSE-6 61
7.2 TSE-5A 71
References 75
8. TSE-5 RESULTS 77
8.1 Heat Transfer 77
8.2 Events During TSE-5 81
8.3 Crack Depths 82
8.4 Fracture-Mechanics Analysis of Primary Flaw 86
8.4.1 Posttest analysis based on design toughness curves 86
8.4.2 K_{Ic} and K_{Ia} values deduced from TSE-5 87
8.4.3 Posttest analysis based on K_{Ic} and K_{Ia} curves deduced from TSE-5 89
8.4.4 Evidence of large scatter in lab K_J data 91
8.4.5 Implications of two-dimensional analysis of flaw 94
8.4.6 Dynamic effects at arrest 95
8.4.7 Warm prestressing 96
8.4.8 Arrest in rising K_I field 96
8.5 Estimate of Crack Depth from COD Data 96
8.6 Crack-Velocity Measurements 98
8.7 Secondary Cracking 99
References 104
9. TSE-5A RESULTS 105
9.1 Heat Transfer 105
9.2 Events During TSE-5A 109
9.3 Crack Depths 111
9.4 Fracture-Mechanics Analysis 114
9.4.1 Posttest analysis based on design toughness curves 114
9.4.2 K_{Ic} and K_{Ia} values deduced from TSE-5A 116
9.4.3 Posttest analysis based on K_{Ic} and K_{Ia} curves deduced from TSE-5A 118
9.4.4 Warm prestressing 118
9.4.5 Arrest in a rising K_I field 119
References 122

Page

10. TSE-6 RESULTS 123

10.1 Heat Transfer 123

10.2 Events During TSE-6 124

10.3 Crack Depths 126

10.4 Fracture-Mechanics Analysis 129

10.4.1 Posttest analysis based on design toughness curves 129

10.4.2 K_{Ic} and K_{Ia} values deduced from TSE-6 129

10.4.3 Posttest analysis based on final set of lab small-specimen K_J and K_{Ia} data 129

10.4.4 Arrest in a rising K_I field 136

Reference 138

11. DISCUSSION OF RESULTS 139

11.1 Comparison of K_{Ic} and K_{Ia} Values Deduced from TSE-4, TSE-5, TSE-5A, and TSE-6, a French Thermal-Shock Experiment and Obtained from "Standard" Lab Specimens ... 139

11.2 Arrest in a Rising K_I Field 143

11.3 Dynamic Effects at Arrest 144

11.4 Comparison of EB-Weld Flaws and Arrested Flaws 144

11.5 Warm Prestressing 144

References 145

APPENDIX A. INFORMATION PERTAINING TO THERMOCOUPLE THIMBLES 147

APPENDIX B. CALIBRATION OF COD GAGES 153

APPENDIX C. MATERIAL PROPERTY DATA 157

APPENDIX D. DIGITAL OUTPUT FROM POSTTEST FRACTURE-MECHANICS ANALYSIS OF TSE-5 173

APPENDIX E. DIGITAL OUTPUT FROM POSTTEST FRACTURE-MECHANICS ANALYSIS OF TSE-5A 187

APPENDIX F. DIGITAL OUTPUT FROM POSTTEST FRACTURE-MECHANICS ANALYSIS OF TSE-6 207

LIST OF FIGURES

Figure		Page
1.1	Schematic cross section of PWR vessel showing path of coolant	3
1.2	Typical instantaneous temperature, stress, fluence, stress-intensity factor, and fracture-toughness distributions through wall of PWR vessel during LBLOCA (long axial flaw; "high" copper, nickel, and fluence; t = 4 min)	4
1.3	Critical-crack-depth curves for LBLOCA (conditions same as for Fig. 1.2)	5
1.4	Stress-intensity factor vs time for LBLOCA (conditions same as for Fig. 1.2)	6
1.5	K_I vs a/w for LBLOCA (conditions same as for Fig. 1.2)	10
1.6	Thermal-shock-induced bending of the wall of a cylinder containing a long axial flaw	11
1.7	Thermal-shock-induced bending of the wall of a cylinder containing a continuous circumferential flaw	12
1.8	K_I vs a/w for long axial and continuous circumferential flaws with and without the bending effect included (conditions same as for Fig. 1.2)	13
1.9	Liquid-nitrogen thermal-shock test facility	15
3.1	A typical finite-element mesh used for calculating K_I via the energy-release-rate method	23
4.1	K_I vs a/w for long axial flaw with and without wall bending included in analysis (typical TSE-5 conditions with t = 3.5 min)	26
4.2	K_I (normalized) for long axial flaw in finite-length cylinder (990-mm OD by 152-mm wall) vs axial distance from midlength of cylinder for $\ell/2$ = 343, 457, 610, and ∞ (TSE-5 loading, a/w = 0.5)	27
4.3	K_{Ic} and K_{Ia} curves used in pretest analysis of TSE-5 (ASME Sect. XI curves with RTNDT = −34°C)	29
4.4	Lower-bound K_J and mean K_{Ia} curves derived from small-specimen data and used in TSE-5A pretest analysis	30

Figure		Page
4.5	K_{Ic} and K_{Ia} curves deduced from TSE-5 and used in TSE-6 pretest analysis	30
4.6	Critical-crack-depth curves for pretest analysis of TSE-5	32
4.7	K_I vs a/w for TSE-5 design conditions	33
4.8	Pretest critical-crack-depth curves for TSE-5A assuming TSE-5 thermal transient and TSE-5A lower-bound K_{IJ} and mean K_{Ia} curves	36
4.9	Pretest critical-crack-depth curves for TSE-6	37
4.10	K_I and K_{Ia} vs a/w for TSE-6 at t = 1.5 min (pretest analysis)	39
4.11	Compressive force and bending moment applied to ligament beyond tip of deep inner-surface long axial flaw during thermal shock to inner surface	40
5.1	Dimensional details for TSE-5, TSE-5A, and TSE-6 test cylinders	43
5.2	Steps in fabrication of TSE-5, TSE-5A, and TSE-6 test cylinders and prolongations	44
5.3	Approximate residual stresses in test-cylinder wall as a result of quench-only heat treatment	45
5.4	Variation with depth in plate of representative mechanical properties for central region of a 3.05-m × 6.10-m × 305-mm plate of ASTM A 533 grade B class 1 steel	46
5.5	Typical setup of test cylinder in EB-weld vacuum box in preparation for generation of axial flaw	47
6.1	Heat transfer coefficients deduced from thermal-shock experiments conducted as a part of surface-coating development effort	50
6.2	Test-cylinder assembly for TSE-5	51
6.3	HSST thermal-shock test facility, showing test-cylinder assembly just prior to its submergence in liquid nitrogen	52
6.4	Test-cylinder assembly positioned on heater	54

Figure		Page
6.5	Developed views of TSE-5 test cylinder showing locations of instrumentation	55
6.6	Developed view of inner surface of TSE-5A test cylinder showing locations of instrumentation	55
6.7	Developed views of TSE-6 test cylinder showing locations of instrumentation	56
6.8	Typical COD gage installation for TSE-5, TSE-5A, and TSE-6	57
6.9	Exterior surface of TSE-6 test cylinder showing locations of UT and acoustic-emission instrumentation	58
7.1	Effect of tempering temperature on the room-temperature tensile properties of TSP-1 after tempering for 4 h and cooling in air	62
7.2	Specimen orientation notation for tensile, CVN, and drop-weight specimens	63
7.3	Tensile properties at the quarter-thickness depth in the 152-mm-thick wall of TSC-1 and TSP-1 after tempering at 613°C	64
7.4	CVN energy and lateral expansion for TSP-1 after tempering for 4 h and cooling in air	65
7.5	K_J data from 1T compact specimens of TSP-1 after tempering at 595, 600, and 650°C	65
7.6	Orientation of compact specimens	66
7.7	K_J and K_{Ia} data for TSP-1, TSP-3, and TSC-3, each tempered at 613°C	67
7.8	K_J data from 0.394T compact specimens of TSP-1 after tempering at 613°C	68
7.9	CVN data for TSC-3 (tempered at 613°C) at a depth location (d/w) = 0.08	69
7.10	CVN data for TSC-3 (tempered at 613°C) at a depth location (d/w) = 0.42	70
7.11	J_J and K_{Ia} data for TSP-2 tempered at 677°C and TSC-2 (tempered at 679°C)	72

Figure		Page
7.12	K_J data from 1T compact specimens of TSP-2 tempered at 707°C	73
7.13	CVN properties for TSP-2 after tempering at 677°C	74
7.14	CVN data for TSP-2 (tempered at 677°C) and for TSC-2 (tempered at 679°C)	75
8.1	Radial temperature distribution at t = 106 s during TSE-5	77
8.2	Radial temperature distribution at t = 178 s during TSE-5	78
8.3	Radial temperature distribution at t = 206 s during TSE-5	78
8.4	Temperature vs a/w for several times in the TSE-5 transient	79
8.5	Near-surface temperatures at five elevations in TSE-5 test cylinder during thermal transient	80
8.6	Comparison of calculated (pretest) and measured surface-temperature transients for TSE-5	80
8.7	Variation of inner-surface heat transfer coefficient with metal surface temperature for TSE-5	81
8.8	COD output during TSE-5, indicating three major initiation-arrest events	82
8.9	Section of TSE-5 test cylinder removed for study of crack profile and fracture surfaces	83
8.10	Cross section of TSE-5 final flaw near midlength of test cylinder	84
8.11	Fracture surface (near midlength of test cylinder) of TSE-5 final long axial flaw	85
8.12	Measurements of crack depth during and after TSE-5	85
8.13	Critical-crack-depth curves from posttest analysis of TSE-5 (original K_{Ic} data)	86
8.14	K_I vs time for several crack depths (TSE-5 posttest analysis)	87

Figure		Page
8.15	K_I vs a/w for several times in the TSE-5 transient (posttest analysis)	88
8.16	K_{Ic} and K_{Ia} values deduced from TSE-5	89
8.17	Critical-crack-depth curves from posttest analysis of TSE-5 using TSE-5 K_{Ic} data	90
8.18	Small-specimen fracture-toughness data for TSE-5 and TSE-6 test-cylinder prolongation, showing upper bound of K_{Ic} data	92
8.19	Comparison of TSE-5 K_{Ic} and K_{Ia} values with lower-bound K_J and mean K_{Ia} small-specimen data	94
8.20	Idealization of final arrested crack front of TSE-5 for purposes of three-dimensional finite-element analysis	95
8.21	Calculated COD vs a/w for TSE-5	97
8.22	COD output (gages 4 and 6) vs time for second crack jump during TSE-5	99
8.23	Post-TSE-5 view of a cross crack and a portion of the primary (axial) flaw at a depth of 8 mm	100
8.24	Secondary cracking pattern on inner surface of test cylinder following TSE-5	101
8.25	Model used for two-dimensional analysis of secondary cracking effects during TSE-5	103
9.1	Comparison of inner-surface (a/w = 0.0083) quench rate for TSE-5 and TSE-5A	105
9.2	Radial temperature distribution at t = 78 s during TSE-5A	106
9.3	Radial temperature distribution at t = 90 s during TSE-5A	106
9.4	Radial temperature distribution at t = 122 s during TSE-5A	107
9.5	Radial temperature distribution at t = 184 s during TSE-5A	107
9.6	Temperature vs a/w for several times during the TSE-5A transient	108

Figure		Page
9.7	Heat transfer coefficient (fluid film plus surface coating) derived from TSE-5A as a function of cylinder (metal) inner-surface temperature	109
9.8	COD data for TSE-5A	110
9.9	Schematic cross section of TSE-5A test-cylinder wall, showing four-step progression of long axial flaw as deduced from fracture surfaces	111
9.10	TSE-5A fracture surface	112
9.11	Calculated COD at inner surface vs fractional crack depth for TSE-5A	113
9.12	Comparison of COD, UT, and fracture-surface crack-depth measurements for TSE-5A	115
9.13	Lower-bound K_J and mean K_{Ia} curves (based on pretest lab data only) used for K_{Ic} and K_{Ia} in TSE-5A pretest analysis	116
9.14	Critical-crack-depth curves for TSE-5A based on toughness curves in Fig. 9.13	117
9.15	Comparison of K_{Ic} and K_{Ia} values deduced from TSE-5A with laboratory data presented in Fig. 9.13	118
9.16	Posttest critical-crack-depth curves for TSE-5A using modified toughness curves in Fig. 9.15	119
9.17	K_I vs a/w and t for TSE-5A	120
9.18	Comparison of K_I vs a curves for TSE-5A and two PWR postulated severe overcooling accidents	121
10.1	Comparison of TSE-5A and TSE-6 inner-surface (metal) temperatures	123
10.2	TSE-6 measured radial temperature distributions for times at which events took place	124
10.3	TSE-6 measured radial temperature distributions for several times during transient	125
10.4	Final radial profile of TSE-6 flaw near midlength of test cylinder	126
10.5	Photograph of TSE-6 fracture surface	127

Figure		Page
10.6	TSE-6 COD-gage output vs time	128
10.7	TSE-6 COD output vs time for the second initiation-arrest event (gage 4)	128
10.8	TSE-6 posttest critical-crack-depth curves, based on measured temperatures and design toughness curves, with actual events superimposed	130
10.9	Characteristic fracture-mechanics curves for TSE-6 at the time of the first initiation-arrest event (69 s), based on posttest analysis using measured temperatures and design toughness curves	131
10.10	Characteristic fracture-mechanics curves for TSE-6 at the time of the second initiation-arrest event (137 s), based on posttest analysis using measured temperatures and design toughness curves	132
10.11	Comparison of TSE-6 K_{Ic} and K_{Ia} values, TSE-6 K_{Ic} and K_{Ia} design curves (deduced from TSE-5 results), and small-specimen K_J, K_{Ic}, and K_{Ia} data	133
10.12	TSE-6 posttest critical-crack-depth curves, based on measured temperatures and lab small-specimen lower-bound K_J and mean K_{Ia} data, with actual events superimposed	134
10.13	Characteristic fracture-mechanics curves for TSE-6 at time of first initiation-arrest event (69 s), based on posttest analysis using small-specimen fracture-toughness data	135
10.14	Characteristic fracture-mechanics curves for TSE-6 at time of second initiation-arrest event (137 s), based on posttest analysis using small-specimen fracture-toughness data	136
10.15	Comparison of K_I vs a curves for TSE-5A, TSE-6, and two PWR postulated severe overcooling accidents	137
11.1	Comparison of TSE-5 and TSE-6 K_{Ic} and K_{Ia} values with lower-bound K_J and mean K_{Ia} small-specimen data	140
11.2	Comparison of small-specimen and large-specimen K_{Ic} data	141
11.3	Comparison of small-specimen and large-specimen K_{Ia} data	142
11.4	Examples of unbroken ligaments (TSE-5A)	143

Figure		Page
A.1	Thermocouple-thimble components and assembly for measuring radial temperature distribution in test cylinders during thermal-shock experiments	147
A.2	Details of thermocouple thimbles used for TSE-5, TSE-5A, and TSE-6	148
A.3	Comparison of temperatures for cylinder and slab geometries for typical TSE thermal-shock conditions	150
A.4	Tapered thermocouple-thimble components and assembly for measuring radial temperature distribution in TSE-5A test cylinder during thermal-shock experiment	151
A.5	Machining of tapered thermocouple-thimble holes in the TSE-5A test cylinder using the electrical discharge machining process	152
B.1	Details of Ailtech SG and DG-125 quarter-bridge strain gages	153
B.2	Installations of Ailtech COD gages for calibration	154

LIST OF TABLES

Table		Page
1.1	Reference calculational model for HSST thermal-shock program	9
1.2	Test conditions specified for TSE-5, TSE-5A, and TSE-6	14
4.1	Test conditions for TSE-5 pretest analysis	32
4.2	Test conditions for TSE-5A pretest analysis	35
4.3	Test conditions for TSE-6 pretest analysis	38
4.4	Comparison of radius-to-wall thickness ratios for PWR vessels and ORNL thermal-shock test cylinders	39
5.1	Chemical composition for TSE-5, TSE-5A, and TSE-6 test cylinders	45
7.1	Rockwell C hardness of TSC-1 prolongation (TSP-1) at various tempering temperatures	63
7.2	CVN and drop-weight properties of TSP-1	64
8.1	Summary of data corresponding to the events for the long axial flaw (TSE-5)	88
8.2	Crack depths derived from COD data and from direct measurements	98
8.3	Calculated CODs for the TSE-5 primary crack with and without the existence of secondary cracking and with a/w (secondary) = 0.35 and t = 7 min	103
9.1	Estimated crack depths near midlength of test cylinder for TSE-5A	113
9.2	Summary of critical data for TSE-5A	117
10.1	Summary of events for TSE-6	133
B.1	Data pertaining to the COD gages used for TSE-5, TSE-5A, and TSE-6	155
C.1	Tensile properties for TSP-1 tempered for 4 h and air cooled	158
C.2	Tensile properties for TSP-1 tempered at 613°C for 4 h and air cooled	159

Table		Page
C.3	Tensile properties for TSC-1 tempered at 613°C for 4 h and air cooled	160
C.4	Static fracture toughness (K_J) from 1T compact specimens of TSP-1 tempered for 4 h and air cooled	161
C.5	Crack-arrest toughness data (K_{Ia}) for TSP-1 and TSP-3 tempered at 613°C for 4 h and air cooled	162
C.6	Static fracture toughness (K_J) data from 1T and 2T compact specimens of TSP-1 tempered at 613°C for 4 h and air cooled	163
C.7	Static fracture toughness (K_J) data from 1T compact specimens of TSP-3 tempered at 613°C for 4 h and air cooled	164
C.8	Static fracture toughness (K_J) data from 1T compact specimens of TSC-3 tempered at 613°C for 4 h and air cooled	165
C.9	Static fracture toughness (K_J) from 0.394T compact specimens of TSP-1 tempered at 613°C for 4 h and air cooled	166
C.10	Static fracture toughness (K_J) from 1T compact specimens of TSP-2 tempered at 677°C for 4 h and air cooled	167
C.11	Static fracture toughness (K_J) from 1T compact specimens of TSP-2 tempered at 707°C for 4 h and air cooled	168
C.12	Static crack-arrest toughness (K_{Ia}) from wedge-loaded compact specimens of TSP-2 tempered at 677°C for 4 h and air cooled	169
C.13	Static fracture toughness (K_J) from 1T compact specimens of TSC-2 tempered at 679°C for 4 h and air cooled	170

NOMENCLATURE AND ACRONYMS

Nomenclature

a	crack depth
D	diameter of test cylinder
E	Young's modulus
h	surface heat transfer coefficient
J	J integral
K_I	Mode-I stress-intensity factor
K_{Ia}	static crack-arrest toughness
K_{Ic}	static crack-initiation toughness
K_J	static crack-initiation toughness based on J integral up to maximum load ($K_J^2 = EJ$)
k	thermal conductivity
l	length of test cylinder
r	radius of test cylinder
Δr	increment of r measured from inner surface
RTNDT	nil-ductility reference temperature
$RTNDT_o$	initial value (zero fluence) of RTNDT
ΔRTNDT	increase in RTNDT due to radiation damage (fluence > 0)
t	time in thermal transient
T	temperature in wall of test cylinder
w	thickness of test-cylinder wall
α	coefficient of thermal expansion
ν	Poisson's ratio
σ	stress
σ_{ys}	yield strength
ρ	density

Acronyms

BCL	Battelle Columbus Laboratories
CVN	Charpy V-notch
COD	crack-opening displacement
CS	compact specimen

EB	electron-beam
HSST	heavy-section steel technology
ID	inner diameter
IWPS	incipient warm prestressing
LBLOCA	large-break loss-of-coolant accident
LWR	light-water reactor
OD	outer diameter
ORNL	Oak Ridge National Laboratory
PWR	pressurized-water reactor
1T-CS	one-inch-thick (25.4-mm) compact specimen
TSE	thermal-shock experiment
TSC	thermal-shock test cylinder
TSP	thermal-shock test-cylinder prolongation
USNSRDC	United States Naval Ship Research and Development Center
UT	ultrasonic
WPS	warm prestressing

FOREWORD

The work reported here was performed at Oak Ridge National Laboratory (ORNL) under the Heavy-Section Steel Technology (HSST) Program, C. E. Pugh, Program Manager. The program is sponsored by the Office of Nuclear Regulatory Research of the U.S. Nuclear Regulatory Commission (NRC). The technical monitor for the NRC is Milton Vagins.

This report is designated HSST Program Technical Report 78. Prior reports in this series are listed below:

1. S. Yukawa, *Evaluation of Periodic Proof Testing and Warm Prestressing Procedures for Nuclear Reactor Vessels*, HSSTP-TR-1, General Electric Company, Schenectady, N. Y. (July 1, 1969).
2. L. W. Loechel, *The Effect of Testing Variables on the Transition Temperature in Steel*, MCR-69-189, Martin Marietta Corporation, Denver, Colo. (November 20, 1969).
3. P. N. Randall, *Gross Strain Measure of Fracture Toughness of Steels*, HSSTP-TR-3, TRW Systems Group, Redondo Beach, Calif. (November 1, 1969).
4. C. Visser, S. E. Gabrielse, and W. VanBuren, *A Two-Dimensional Elastic-Plastic Analysis of Fracture Test Specimens*, WCAP-7368, Westinghouse Electric Corporation, PWR Systems Division, Pittsburgh, Pa. (October 1969).
5. T. R. Mager and F. O. Thomas, *Evaluation by Linear Elastic Fracture Mechanics of Radiation Damage to Pressure Vessel Steels*, WCAP-7328 (Rev.), Westinghouse Electric Corporation, PWR Systems Division, Pittsburgh, Pa. (October 1969).
6. W. O. Shabbits, W. H. Pryle, and E. T. Wessel, *Heavy-Section Fracture Toughness Properties of A533 Grade B Class 1 Steel Plate and Submerged Arc Weldment*, WCAP-7414, Westinghouse Electric Corporation, PWR Systems Division, Pittsburgh, Pa. (December 1969).
7. F. J. Loss, *Dynamic Tear Test Investigations of the Fracture Toughness of Thick-Section Steel*, NRL-7056, Naval Research Laboratory, Washington, D.C. (May 14, 1970).
8. P. B. Crosley and E. J. Ripling, *Crack Arrest Fracture Toughness of A533 Grade B Class 1 Pressure Vessel Steel*, HSSTP-TR-8, Materials Research Laboratory, Inc., Glenwood, Ill. (March 1970).
9. T. R. Mager, *Post-Irradiation Testing of 2T Compact Tension Specimens*, WCAP-7561, Westinghouse Electric Corporation, PWR Systems Division, Pittsburgh, Pa. (August 1970).
10. T. R. Mager, *Fracture Toughness Characterization Study of A533, Grade B, Class 1 Steel*, WCAP-7578, Westinghouse Electric Corporation, PWR Systems Division, Pittsburgh, Pa. (October 1970).

11. T. R. Mager, *Notch Preparation in Compact Tension Specimens*, WCAP-7579, Westinghouse Electric Corporation, PWR Systems Division, Pittsburgh, Pa. (November 1970).

12. N. Levy and P. V. Marcal, *Three-Dimensional Elastic-Plastic Stress and Strain Analysis for Fracture Mechanics, Phase I: Simple Flawed Specimens*, HSSTP-TR-12, Brown University, Providence, R.I. (December 1970).

13. W. O. Shabbits, *Dynamic Fracture Toughness Properties of Heavy Section A533 Grade B Class 1 Steel Plate*, WCAP-7623, Westinghouse Electric Corporation, PWR Systems Division, Pittsburgh, Pa. (December 1970).

14. P. N. Randall, *Gross Strain Crack Tolerance of A533-B Steel*, HSSTP-TR-14, TRW Systems Group, Redondo Beach, Calif. (May 1, 1971).

15. H. T. Corten and R. H. Sailors, *Relationship Between Material Fracture Toughness Using Fracture Mechanics and Transition Temperature Tests*, T&AM Report 346, University of Illinois, Urbana, Ill. (August 1, 1971).

16. T. R. Mager and V. J. McLoughlin, *The Effect of an Environment of High Temperature Primary Grade Nuclear Reactor Water on the Fatigue Crack Growth Characteristics of A533 Grade B Class 1 Plate and Weldment Material*, WCAP-7776, Westinghouse Electric Corporation, PWR Systems Division, Pittsburgh, Pa. (October 1971).

17. N. Levy and P. V. Marcal, *Three-Dimensional Elastic-Plastic Stress and Strain Analysis for Fracture Mechanics, Phase II: Improved Modelling*, HSSTP-TR-17, Brown University, Providence, R.I. (November 1971).

18. S. C. Grigory, *Tests of 6-in.-Thick Flawed Tensile Specimens, First Technical Summary Report, Longitudinal Specimens Numbers 1 through 7*, HSSTP-TR-18, Southwest Research Institute, San Antonio, Tex. (June 1972).

19. P. N. Randall, *Effects of Strain Gradients on the Gross Strain Crack Tolerance of A533-B Steel*, HSSTP-TR-19, TRW Systems Group, Redondo Beach, Calif. (June 15, 1972).

20. S. C. Grigory, *Tests of 6-Inch-Thick Flawed Tensile Specimens, Second Technical Summary Report, Transverse Specimens Numbers 8 through 10, Welded Specimens Numbers 11 through 13*, HSSTP-TR-20, Southwest Research Institute, San Antonio, Tex. (June 1972).

21. L. A. James and J. A. Williams, *Heavy Section Steel Technology Program Technical Report No. 21, The Effect of Temperature and Neutron Irradiation Upon the Fatigue-Crack Propagation Behavior of ASTM A533 Grade B, Class 1 Steel*, HEDL-TME 72-132, Hanford Engineering Development Laboratory, Richland, Wash. (September 1972).

22. S. C. Grigory, *Tests of 6-Inch-Thick Flawed Tensile Specimens, Third Technical Summary Report, Longitudinal Specimens Numbers 14 through 16, Unflawed Specimen Number 17*, HSSTP-TR-22, Southwest Research Institute, San Antonio, Tex. (October 1972).

23. S. C. Grigory, *Tests of 6-Inch Thick Tensile Specimens, Fourth Technical Summary Report, Tests of 1-Inch-Thick Flawed Tensile Specimens for Size Effect Evaluation*, HSSTP-TR-23, Southwest Research Institute, San Antonio, Tex. (June 1973).

24. S. P. Ying and S. C. Grigory, *Tests of 6-Inch-Thick Tensile Specimens, Fifth Technical Summary Report, Acoustic Emission Monitoring of One-Inch and Six-Inch-Thick Tensile Specimens*, HSSTP-TR-24, Southwest Research Institute, San Antonio, Tex. (November 1972).

25. R. W. Derby, J. G. Merkle, G. C. Robinson, G. D. Whitman, and F. J. Witt, *Test of 6-Inch-Thick Pressure Vessels. Series 1: Intermediate Test Vessels V-1 and V-2*, ORNL-4895, Oak Ridge Natl. Lab., Oak Ridge, Tenn. (February 1974).

26. W. J. Stelzman and R. G. Berggren, *Radiation Strengthening and Embrittlement in Heavy Section Steel Plates and Welds*, ORNL-4871, Oak Ridge Natl. Lab., Oak Ridge, Tenn. (June 1973).

27. P. B. Crosley and E. J. Ripling, *Crack Arrest in an Increasing K-Field*, HSSTP-TR-27, Materials Research Laboratory, Inc., Glenwood, Ill. (January 1973).

28. P. V. Marcal, P. M. Stuart, and R. S. Bettes, *Elastic-Plastic Behavior of a Longitudinal Semi-Elliptic Crack in a Thick Pressure Vessel*, HSSTP-TR-28, Brown University, Providence, R.I. (June 1973).

29. W. J. Stelzman, R. G. Berggren, and T. N. Jones, *ORNL Characterization of Heavy-Section Steel Technology Program Plates 01, 02 and 03*, NUREG/CR-4092 (ORNL/TM-9491), Oak Ridge Natl. Lab., Oak Ridge, Tenn. (in preparation).

30. Canceled.

31. J. A. Williams, *The Irradiation and Temperature Dependence of Tensile and Fracture Properties of ASTM A533, Grade B, Class 1 Steel Plate and Weldment*, HEDL-TME 73-75, Hanford Engineering Development Laboratory, Richland, Wash. (August 1973).

32. J. M. Steichen and J. A. Williams, *High Strain Rate Tensile Properties of Irradiated ASTM A533 Grade B Class 1 Pressure Vessel Steel*, Hanford Engineering Development Laboratory, Richland, Wash. (July 1973).

33. P. C. Riccardella and J. L. Swedlow, *A Combined Analytical-Experimental Fracture Study of the Two Leading Theories of Elastic-Plastic Fracture (J-Integral and Equivalent Energy)*, WCAP-8224, Westinghouse Electric Corporation, Pittsburgh, Pa. (October 1973).

34. R. J. Podlasek and R. J. Eiber, *Final Report on Investigation of Mode III Crack Extension in Reactor Piping*, Battelle Columbus Laboratories, Columbus, Ohio (December 14, 1973).

35. T. R. Mager, J. D. Landes, D. M. Moon, and V. J. McLaughlin, *Interim Report on the Effect of Low Frequencies on the Fatigue Crack Growth Characteristics of A533 Grade B Class 1 Plate in an Environment of High-Temperature Primary Grade Nuclear Reactor Water*, WCAP-8256, Westinghouse Electric Corporation, Pittsburgh, Pa. (December 1973).

36. J. A. Williams, *The Irradiated Fracture Toughness of ASTM A533, Grade B, Class 1 Steel Measured with a Four-Inch-Thick Compact Tension Specimen*, HEDL-TME 75-10, Hanford Engineering Development Laboratory, Richland, Wash. (January 1975).

37. R. H. Bryan, J. G. Merkle, M. N. Raftenberg, G. C. Robinson, and J. E. Smith, *Test of 6-Inch-Thick Pressure Vessels. Series 2: Intermediate Test Vessels V-3, V-4, and V-6*, ORNL-5059, Oak Ridge Natl. Lab., Oak Ridge, Tenn. (November 1975).

38. T. R. Mager, S. E. Yanichko, and L. R. Singer, *Fracture Toughness Characterization of HSST Intermediate Pressure Vessel Material*, WCAP-8456, Westinghouse Electric Corporation, Pittsburgh, Pa. (December 1974).

39. J. G. Merkle, G. D. Whitman, and R. H. Bryan, *An Evaluation of the HSST Program Intermediate Pressure Vessel Tests in Terms of Light-Water-Reactor Pressure Vessel Safety*, ORNL/TM-5090, Oak Ridge Natl. Lab., Oak Ridge, Tenn. (November 1975).

40. J. G. Merkle, G. C. Robinson, P. P. Holz, J. E. Smith, and R. H. Bryan, *Test of 6-In.-Thick Pressure Vessels. Series 3: Intermediate Test Vessel V-7*, ORNL/NUREG-1, Oak Ridge Natl. Lab., Oak Ridge, Tenn. (August 1976).

41. J. A. Davidson, L. J. Ceschini, R. P. Shogan, and G. V. Rao, *The Irradiated Dynamic Fracture Toughness of ASTM A533, Grade B, Class 1 Steel Plate and Submerged Arc Weldment*, WCAP-8775, Westinghouse Electric Corporation, Pittsburgh, Pa. (October 1976).

42. R. D. Cheverton, *Pressure Vessel Fracture Studies Pertaining to PWR LOCA-ECC Thermal Shock: Experiments TSE-1 and TSE-2*, ORNL/NUREG/TM-31, Oak Ridge Natl. Lab., Oak Ridge, Tenn. (September 1976).

43. J. G. Merkle, G. C. Robinson, P. P. Holz, and J. E. Smith, *Test of 6-In.-Thick Pressure Vessels. Series 4: Intermediate Test Vessels V-5 and V-9 with Inside Nozzle Corner Cracks*, ORNL/NUREG-7, Oak Ridge Natl. Lab., Oak Ridge, Tenn. (August 1977).

44. J. A. Williams, *The Ductile Fracture Toughness of Heavy Section Steel Plate*, Hanford Engineering Development Laboratory, Richland, Wash., NUREG/CR-0859 (September 1979).

45. R. H. Bryan, T. M. Cate, P. P. Holz, T. A. King, J. G. Merkle, G. C. Robinson, G. C. Smith, J. E. Smith, and G. D. Whitman, *Test of 6-in.-Thick Pressure Vessels. Series 3: Intermediate Test Vessel V-7A Under Sustained Loading*, ORNL/NUREG-9, Oak Ridge Natl. Lab., Oak Ridge, Tenn. (February 1978).

46. R. D. Cheverton and S. E. Bolt, *Pressure Vessel Fracture Studies Pertaining to a PWR LOCA-ECC Thermal Shock: Experiments TSE-3 and TSE-4 and Update of TSE-1 and TSE-2 Analysis*, ORNL/NUREG-22, Oak Ridge Natl. Lab., Oak Ridge, Tenn. (December 1977).

47. D. A. Canonico, *Significance of Reheat Cracks to the Integrity of Pressure Vessels for Light-Water Reactors*, ORNL/NUREG-15, Oak Ridge Natl. Lab., Oak Ridge, Tenn. (July 1977).

48. G. C. Smith and P. P. Holz, *Repair Weld Induced Residual Stresses in Thick-Walled Steel Pressure Vessels*, NUREG/CR-0093 (ORNL/NUREG/TM-153), Oak Ridge Natl. Lab., Oak Ridge, Tenn. (June 1978).

49. P. P. Holz and S. W. Wismer, *Half-Bead (Temper) Repair Welding for HSST Vessels*, NUREG/CR-0113 (ORNL/NUREG/TM-177), Oak Ridge Natl. Lab., Oak Ridge, Tenn. (June 1978).

50. G. C. Smith, P. P. Holz, and W. J. Stelzman, *Crack Extension and Arrest Tests of Axially Flawed Steel Model Pressure Vessels*, NUREG/CR-0126 (ORNL/NUREG/TM-196), Oak Ridge Natl. Lab., Oak Ridge, Tenn. (October 1978).

51. R. H. Bryan, P. P. Holz, J. G. Merkle, G. C. Smith, J. E. Smith, and W. J. Stelzman, *Test of 6-in.-Thick Pressure Vessels. Series 3: Intermediate Test Vessel V-7B*, NUREG/CR-0309 (ORNL/NUREG-38), Oak Ridge Natl. Lab., Oak Ridge, Tenn. (October 1978).

52. R. D. Cheverton, S. K. Iskander, and S. E. Bolt, *Applicability of LEFM to the Analysis of PWR Vessels Under LOCA-ECC Thermal Shock Conditions*, NUREG/CR-0107 (ORNL/NUREG-40), Oak Ridge Natl. Lab., Oak Ridge, Tenn. (October 1978).

53. R. H. Bryan, D. A. Canonico, P. P. Holz, S. K. Iskander, J. G. Merkle, J. E. Smith, and W. J. Stelzman, *Test of 6-in.-Thick Pressure Vessels, Series 3: Intermediate Test Vessel V-8*, NUREG/CR-0675 (ORNL/NUREG-58), Oak Ridge Natl. Lab., Oak Ridge, Tenn. (December 1979).

54. R. D. Cheverton and S. K. Iskander, *Application of Static and Dynamic Crack Arrest Theory to TSE-4*, NUREG/CR-0767 (ORNL/NUREG-57), Oak Ridge Natl. Lab., Oak Ridge, Tenn. (June 1979).

55. J. A. Williams, *Tensile Properties of Irradiated and Unirradiated Welds of A533 Steel Plate and A508 Forgings*, NUREG/CR-1158 (ORNL/Sub-79/50917/2), Hanford Engineering Development Laboratory, Richland, Wash. (July 1979).

56. K. W. Carlson and J. A. Williams, *The Effect of Crack Length and Side Grooves on the Ductile Fracture Toughness Properties of ASTM A533 Steel*, NUREG/CR-1171 (ORNL/Sub-79/50917/3), Hanford Engineering Development Laboratory, Richland, Wash. (October 1979).

57. P. P. Holz, *Flaw Preparations for HSST Program Vessel Fracture Mechanics Testing; Mechanical-Cyclic Pumping and Electron-Beam Weld-Hydrogen Charge Cracking Schemes*, NUREG/CR-1274 (ORNL/NUREG/TM-369), Oak Ridge Natl. Lab., Oak Ridge, Tenn. (May 1980).

58. S. K. Iskander, *Two Finite Element Techniques for Computing Mode I Stress Intensity Factors in Two- or Three-Dimensional Problems*, NUREG/CR-1499 (ORNL/NUREG/CSD/TM-14), Computer Sciences Div., Union Carbide Corp. Nuclear Div., Oak Ridge, Tenn. (February 1981).

59. P. B. Crosley and E. J. Ripling, *Development of a Standard Test for Measuring K_{Ia} with a Modified Compact Specimen*, NUREG/CR-2294 (ORNL/Sub-81/7755/1), Materials Research Laboratory, Glenwood, Ill. (August 1981).

60. S. N. Atluri, B. R. Bass, J. W. Bryson, and K. Kathiresan, *NOZ-FLAW: A Finite Element Program for Direct Evaluation of Stress Intensity Factors for Pressure Vessel Nozzle-Corner Flaws*, NUREG/CR-1843, (ORNL/NUREG/CSD/TM-18), Computer Sciences Div., Oak Ridge Gaseous Diffusion Plant, Oak Ridge, Tenn. (March 1981).

61. A. Shukla, W. L. Fourney, and G. R. Irwin, *Study of Energy Loss and Its Mechanisms in Homalite 100 During Crack Propagation and Arrest*, NUREG/CR-2150 (ORNL/Sub-7778/1), University of Maryland, College Park, Md. (August 1981).

62. S. K. Iskander, R. D. Cheverton, and D. G. Ball, *OCA-1, A Code for Calculating the Behavior of Flaws on the Inner Surface of a Pressure Vessel Subjected to Temperature and Pressure Transients*, NUREG/CR-2113 (ORNL/NUREG-84), Oak Ridge Natl. Lab., Oak Ridge, Tenn. (August 1981).

63. R. J. Sanford, R. Chona, W. L. Fourney, and G. R. Irwin, *A Photoelastic Study of the Influence of Non-Singular Stresses in Fracture Test Specimens*, NUREG/CR-2179 (ORNL/Sub-7778/2), University of Maryland, College Park, Md. (August 1981).

64. B. R. Bass, S. N. Atluri, J. W. Bryson, and K. Kathiresan, *OR-FLAW: A Finite Element Program for Direct Evaluation of K-Factors for User-Defined Flaws in Plate, Cylinders, and Pressure-Vessel Nozzle Corners*, NUREG/CR-2494 (ORNL/CSD/TM-165) Oak Ridge Natl. Lab., Oak Ridge, Tenn. (April 1982).

65. B. R. Bass and J. W. Bryson, *ORMGEN-3D: A Finite Element Mesh Generator for 3-Dimensional Crack Geometries*, NUREG/CR-2997, Vol. 1 (ORNL/TM-8527/V1), Oak Ridge Natl. Lab., Oak Ridge, Tenn. (December 1982).

66. B. R. Bass and J. W. Bryson, *ORVIRT: A Finite Element Program for Energy Release Rate Calculations for 2-Dimensional and 3-Dimensional Crack Models*, NUREG/CR-2997, Vol. 2 (ORNL/TM-8527/V2), Oak Ridge Natl. Lab., Oak Ridge, Tenn. (February 1983).

67. R. D. Cheverton, S. K. Iskander, and D. G. Ball, *PWR Pressure Vessel Integrity During Overcooling Accidents: A Parametric Analysis*, NUREG/CR-2895 (ORNL/TM-7931), Oak Ridge Natl. Lab., Oak Ridge, Tenn. (February 1983).

68. D. G. Ball, R. D. Cheverton, J. B. Drake, and S. K. Iskander, *OCA-II, A Code for Calculating Behavior of 2-D and 3-D Surface Flaws in a Pressure Vessel Subjected to Temperature and Pressure Transients*, NUREG/CR-3491 (ORNL-5934), Oak Ridge Natl. Lab., Oak Ridge, Tenn. (February 1984).

69. A. Sauter, R. D. Cheverton, and S. K. Iskander, *Modification of OCA-I for Application to a Reactor Pressure Vessel with Cladding on the Inner Surface*, NUREG/CR-3155 (ORNL/TM-8649), Oak Ridge Natl. Lab., Oak Ridge, Tenn. (May 1983).

70. R. D. Cheverton and D. G. Ball, *OCA-P, A Deterministic and Probabilistic Fracture-Mechanics Code for Application to Pressure Vessels*, NUREG/CR-3618 (ORNL-5991), Oak Ridge Natl. Lab., Oak Ridge, Tenn. (May 1984).

71. J. G. Merkle, *An Examination of the Size Effects and Data Scatter Observed in Small Specimen Cleavage Fracture Toughness Testing*, NUREG/CR-3672 (ORNL/TM-9088), Oak Ridge Natl. Lab., Oak Ridge, Tenn. (April 1984).

72. C. E. Pugh et al., *Heavy-Section Steel Technology Program — Five-Year Plan FY 1983–1987*, NUREG/CR-3595 (ORNL/TM-9008), Oak Ridge Natl. Lab., Oak Ridge, Tenn. (April 1984).

73. D. G. Ball, B. R. Bass, J. W. Bryson, R. D. Cheverton, and J. B. Drake, *Stress Intensity Factor Influence Coefficients for Surface Flaws in Pressure Vessels*, NUREG/CR-3723 (ORNL/ CSD/TM-216), Oak Ridge National Laboratory, Oak Ridge, Tenn. (February 1985).

74. W. R. Corwin, R. G. Berggren, and R. K. Nanstad, *Charpy Toughness and Tensile Properties of Neutron Irradiated Stainless Steel Submerged-Arc Weld Cladding Overlay*, NUREG/CR-3927 (ORNL/TM-9309), Oak Ridge National Laboratory, Oak Ridge, Tenn. (September 1984).

75. C. W. Schwartz, R. Chona, W. L. Fourney, and G. R. Irwin, *SAMCR: A Two-Dimensional Dynamic Finite Element Code for the Stress Analysis of Moving CRacks*, NUREG/CR-3891 (ORNL/Sub/79-7778/3), University of Maryland, College Park, Md. (November 1984).

76. W. R. Corwin, G. C. Robinson, R. K. Nanstad, J. G. Merkle, R. G. Berggren, G. M. Goodwin, R. L. Swain, and T. D. Owings, *Effects of Stainless Steel Weld Overlay Cladding on the Structural Integrity of Flawed Steel Plates in Bending, Series 1*, NUREG/CR-4015, ORNL/TM-9390, Oak Ridge Natl. Lab., Oak Ridge, Tenn., April 1985.

77. R. H. Bryan, B. R. Bass, S. E. Bolt, J. W. Bryson, D. P. Edmonds, R. W. McCulloch, J. G. Merkle, R. K. Nanstad, G. C. Robinson, K. R. Thoms, and G. D. Whitman, *Pressurized-Thermal-Shock Test of 6-in.-Thick Pressure Vessels. PTSE-1: Investigation of Warm Prestressing and Upper-Shelf Arrest*, NUREG/CR-4106 (ORNL-6135), Oak Ridge Natl. Lab., Oak Ridge, Tenn. (May 1985).

ACKNOWLEDGMENTS

The authors wish to acknowledge contributions made by D. A. Canonico, W. J. Stelzman, and P. P. Holz, former members of the Heavy-Section Steel Technology (HSST) Program at the Oak Ridge National Laboratory; E. K. Lynn, former Nuclear Regulatory Commission (NRC) technical monitor, and Milton Vagins, present NRC technical monitor for the HSST Program; and G. D. Whitman, Manager of the HSST Program at the time of these studies.

PRESSURE VESSEL FRACTURE STUDIES PERTAINING TO THE PWR THERMAL-SHOCK ISSUE: EXPERIMENTS TSE-5, TSE-5A, AND TSE-6

R. D. Cheverton S. E. Bolt
D. G. Ball* S. K. Iskander*
R. K. Nanstad

ABSTRACT

Thermal-shock experiments TSE-5, TSE-5A, and TSE-6 were conducted for the purpose of investigating the behavior of surface flaws under pressurized-water-reactor (PWR) overcooling-accident conditions. These experiments were the fifth, sixth, and seventh in a series of thermal-shock experiments conducted with large steel cylinders (A 508 class-2 chemistry; 991-mm OD by 76- and 152-mm wall by 1.2-m length) as a part of the Heavy-Section Steel Technology (HSST) Program for this purpose.

For each of these experiments, the initial flaw was on the inner surface and extended the full length of the cylinder. The thermal shock was applied to the inner surface only, and this was accomplished by effectively dunking the test cylinder, initially at ~93°C, into a large volume of liquid nitrogen.

Results of the experiments have confirmed that (1) linear-elastic fracture-mechanics is valid for thermal-shock loading; (2) crack arrest will take place in accordance with recently developed crack-arrest concepts; (3) crack-arrest toughness values for rising and falling K_I fields are the same; (4) warm prestressing is effective in preventing crack initiation; (5) thermal shock alone cannot drive a flaw all the way through the wall; (6) dynamic effects for PWR-vessel thermal-shock loading conditions are negligible; (7) in the absence of cladding and under severe thermal-shock loading conditions, finite-length flaws will extend on the surface to become very long; and (8) there can be very large scatter in small-specimen fracture-toughness data.

---

1. INTRODUCTION AND SUMMARY

TSE-5, TSE-5A, and TSE-6 were the fifth, sixth, and seventh in a series of thermal-shock experiments conducted with heavy-walled steel cylinders under the auspices of the Heavy-Section Steel Technology (HSST)

---

*Computing and Telecommunications Division.

Program, which is sponsored by the U.S. Nuclear Regulatory Commission. The purpose of these experiments was to investigate the behavior of surface flaws under thermal-shock loading conditions similar to those that in principle would be encountered during certain pressurized-water reactor (PWR) postulated accidents, such as a large-break loss-of-coolant accident (LBLOCA). The first four experiments[1] were concerned with the behavior of shallow flaws [fractional crack depths $(a/w) < 0.2$], while TSE-5, TSE-5A, and TSE-6 were designed specifically for the purpose of investigating the behavior of deep flaws $(a/w > 0.4)$.

Results from a continuing analysis[2-7] of PWR postulated transients have indicated that PWR vessels containing low concentrations of impurities (primarily copper) are not likely to experience propagation of pre-existing flaws. However, vessels with relatively high concentrations of copper experience a greater radiation-induced reduction in fracture toughness and as a result may experience deep penetration of pre-existing flaws during a severe thermal transient. Many of the PWR vessels in operation today contain high enough concentrations of copper to be of concern; thus, the integrity of PWR vessels during postulated overcooling accidents must be examined very carefully.

A problem with regard to performing a fracture-mechanics analysis for thermal-shock loading conditions is that several fracture-mechanics-related features are involved that had not been adequately examined experimentally (e.g., equal biaxial stresses, steep gradients in stresses and toughness through the wall, variations in these parameters with time, crack arrest in a rising K_I field, warm prestressing, and others that will be mentioned later). Therefore, experimental investigations into the behavior of flaws under severe thermal-shock loading conditions were appropriate.

The most severe thermal shock postulated for a PWR is the result of the LBLOCA. During this transient, emergency core coolant at a rather low temperature (~20°C) is injected into the pressure vessel through main coolant lines and passes over the inner surface of the vessel wall, as illustrated schematically in Fig. 1.1. Initially, the wall is at a relatively high temperature (~290°C), and, thus, contact between the emergency core coolant and the wall results in a severe thermal shock. As shown in Fig. 1.2, this rapid quenching of the inner surface results in rather steep positive temperature gradients through the wall and, thus, high tensile stresses in the inner portion of the wall. The reduction in temperature and the high fast-neutron fluence that accumulates over many years of reactor operation tend to reduce the fracture toughness (K_{Ic}) of the vessel material. Because of the positive gradient in temperature, the attenuation of the fluence, and the sensitivity of fracture toughness to temperature and fluence, there is a net positive gradient in toughness in the vessel wall.

If there is a flaw on the inner surface of the vessel wall, the high, thermally induced tensile stress will result in an appreciable stress-intensity factor (K_I) at the tip of the flaw. The combined effect of high stress-intensity factor and low fracture toughness may result in propagation of the flaw. However, the steep positive gradient in toughness tends to provide a mechanism for arresting the crack. Figure 1.2 illustrates these features for the case of a high-copper vessel with a long, axially oriented flaw.

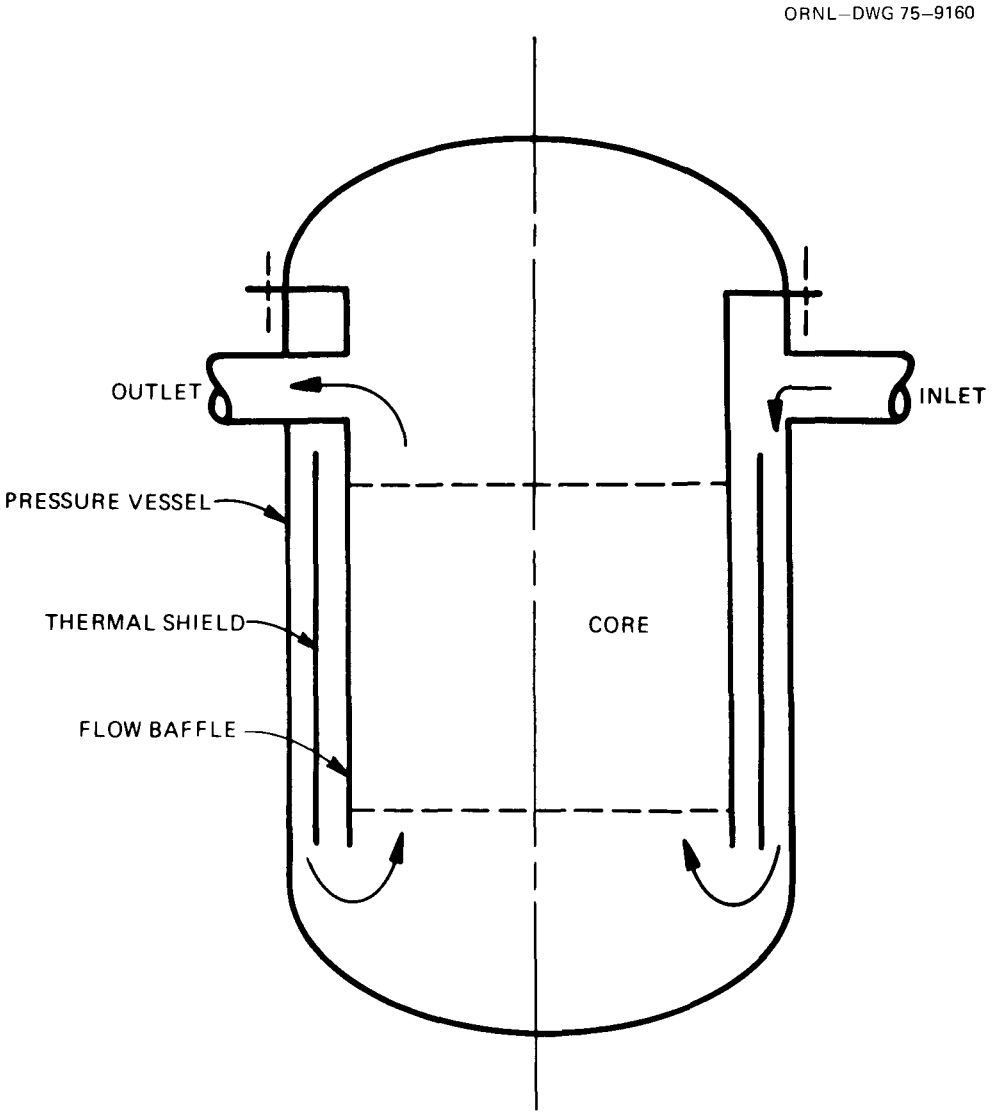

Fig. 1.1. Schematic cross section of PWR vessel showing path of coolant.

Figure 1.2 corresponds to a specific time in the thermal transient and shows that for certain times in the transient, both shallow and deep flaws that extend a considerable distance on the surface can initiate (incipient propagation). The deep flaw may be the result of an earlier initiation-arrest event, and at the time represented by Fig. 1.2, will jump a distance equal to ~10% of the wall thickness. The shallow flaw, which is much more likely to exist as an initial flaw, will jump a much greater distance (~30% of the wall thickness) before arresting. Thus, the experimental investigation of flaw-propagation behavior must include long, as well as relatively short, crack jumps. TSE-5 and TSE-5A were intended to include short jumps only, while a long crack jump was to be included in TSE-6.

ORNL–DWG 85–4396 ETD

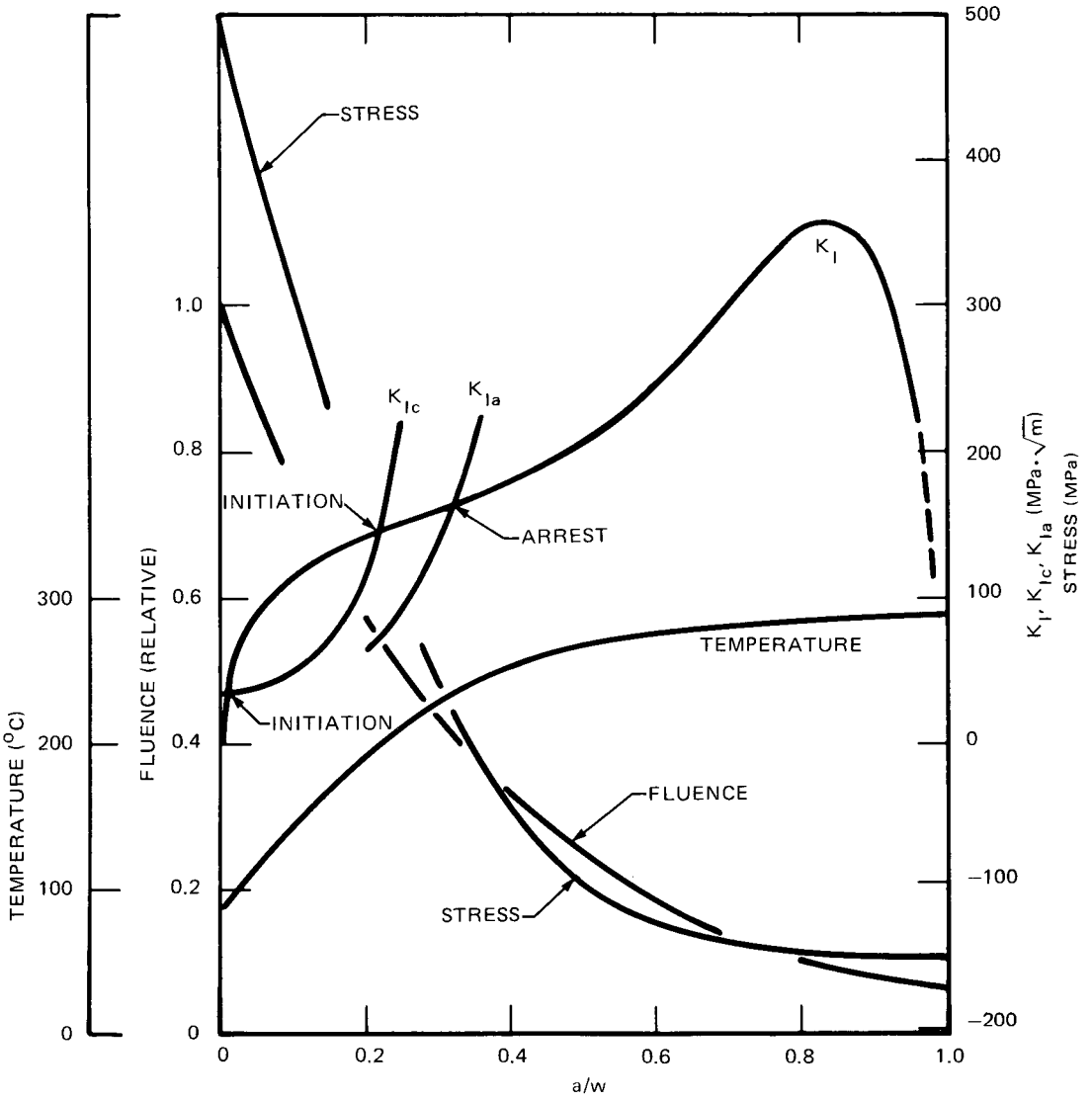

Fig. 1.2. Typical instantaneous temperature, stress, fluence, stress-intensity factor, and fracture-toughness distributions through wall of PWR vessel during LBLOCA (long axial flaw; "high" copper, nickel, and fluence; t = 4 min).

The calculated behavior of a flaw during a transient can be portrayed by plotting the crack depths corresponding to initiation and arrest events ($K_I = K_{Ic}$ and $K_I = K_{Ia}$) and other conditions of interest as a function of the times in the transient at which they occur or exist. Curves of this type are referred to as critical-crack-depth curves and are illustrated in Fig. 1.3 for the case described in Fig. 1.2.

The dashed lines labeled a and b in Fig. 1.3 show possible sequences of events corresponding to three different initial flaw depths. Flaws with $a/w \simeq 0.01$ and 0.10 would initiate at ~1.5 min and would arrest at $a/w \simeq 0.15$, while both a slightly shallower flaw and a deeper flaw

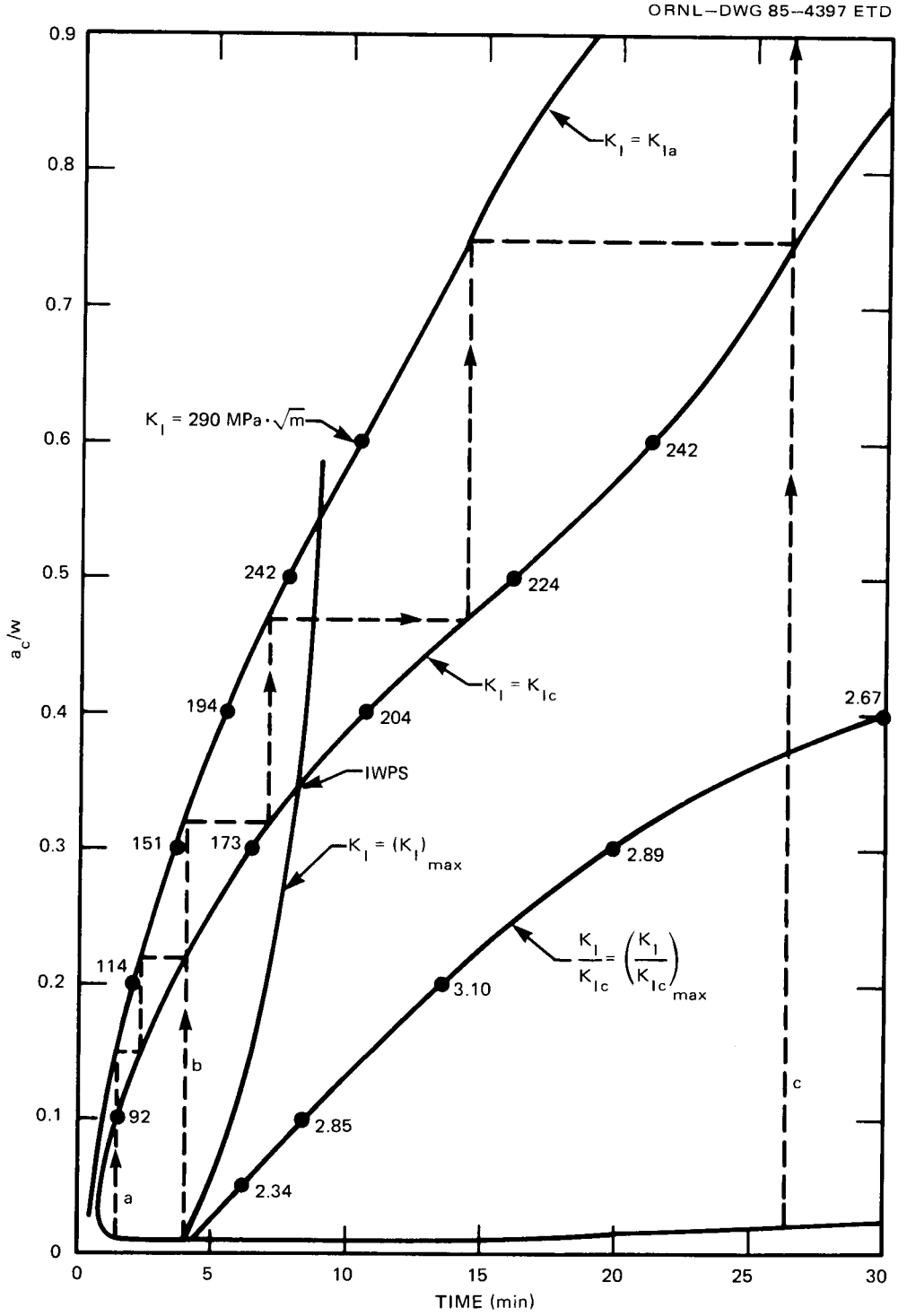

Fig. 1.3. Critical-crack-depth curves for LBLOCA (conditions same as for Fig. 1.2).

($a/w \simeq 0.01$ and 0.22) would initiate later at ~4.0 min and would arrest at $a/w \simeq 0.32$. Moments later, the flaws would reinitiate and arrest. As indicated by the dashed lines, this process would continue until the crack penetrated at least 90% of the wall. Complete penetration presumably would be prevented by the steep negative gradient in K_I for $a/w > 0.9$ (see Fig. 1.2).

A phenomenon referred to as warm prestressing may prevent reinitiation at depths less than the final arrest depth indicated by Figs. 1.2 and 1.3. This particular warm prestressing phenomenon can be described in the following way: according to Irwin[8] and recent experimental results,[9] it appears that a flaw will not initiate when K_I is decreasing with time even though $K_I \gtrsim K_{Ic}$. As shown in Fig. 1.4, K_I for a given crack depth first increases and then decreases with time during a LBLOCA,

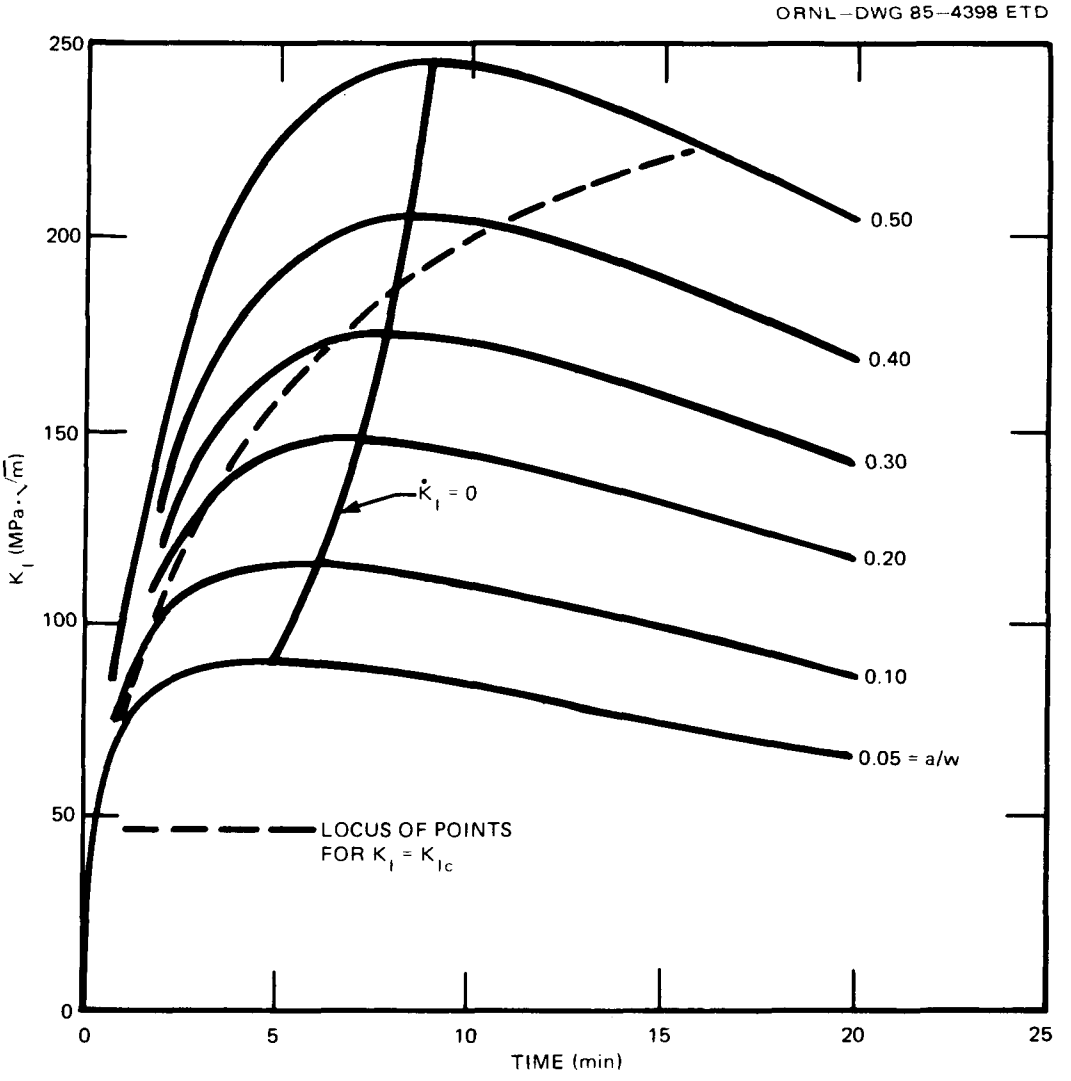

Fig. 1.4. Stress-intensity factor vs time for LBLOCA (conditions same as for Fig. 1.2).

but K_{Ic} decreases as long as the temperature continues to decrease. Thus, it is possible that for some crack depths K_I will be decreasing with time when K_I first becomes equal to K_{Ic}. This situation is depicted in Fig. 1.3 by plotting the times for each of the different crack depths at which K_I reaches its maximum value. This curve is referred to in Fig. 1.3 as $K_I = (K_I)_{max}$. For times less than those indicated by this curve, K_I is always increasing with time, but for greater times K_I is always decreasing with time. Thus, for the case represented in Fig. 1.3, if warm prestressing is effective, crack propagation would be limited to $a/w \simeq 0.47$. A somewhat deeper final arrest point ($a/w = 0.5$) would be obtained if the final initiation point fell just below the incipient warm prestress point.

Another quantity of interest with regard to warm prestressing is the calculated maximum value of K_I/K_{Ic} for cracks that presumably would not initiate because K_I is decreasing with time. The curve in Fig. 1.3 labeled $(K_I/K_{Ic})_{max}$ indicates the times at which $(K_I/K_{Ic})_{max}$ is achieved for various crack depths, and for several of the crack depths, values of $(K_I/K_{Ic})_{max}$ are indicated. The value corresponding to incipient warm prestressing is ~2.8, and values for deeper cracks are less. In an experiment designed to demonstrate warm prestressing, it would be desirable to achieve $(K_I/K_{Ic})_{max} \simeq 2.8$.

A sensitivity study was conducted as part of the thermal-shock program to determine for a LBLOCA the effect of reasonable ranges in emergency core coolant temperature, maximum fast-neutron fluence, and the initial value of the nil-ductility reference temperature (RTNDT). The results of this study, which are reported in Ref. 7, indicate that for most cases the maximum penetration of the wall would be ≤50%, provided that warm prestressing, as described above, is effective.

The warm prestressing phenomenon has been investigated[9] experimentally in connection with the thermal-shock program, using notched beams under load-temperature conditions that simulated to some extent those calculated for a LBLOCA. As mentioned above, these experiments indicated that initiation would not take place while K_I is decreasing with time even though $K_I \gtrsim K_{Ic}$. However, warm prestressing is another facet of fracture mechanics that must be thoroughly investigated under thermal-shock loading conditions in a large test cylinder. An objective of TSE-5 and TSE-5A was to demonstrate warm prestressing under such conditions.

The analysis of the LBLOCA was performed using linear-elastic fracture mechanics, without consideration for the existence of upper-shelf properties and without regard for the proximity of the crack tip to the back surface. The validity of this approach depends to some extent on the maximum calculated values of K_I corresponding to initiation and arrest events and the final crack depth. According to results of the above sensitivity analysis, warm prestressing presumably would limit the final crack depth to ~50% of the wall, and the maximum K_I value corresponding to initiation and arrest events would be ~240 $MPa \cdot \sqrt{m}$ (Figs. 1.3 and 1.4) and, thus, reach the upper transition region. Therefore, at least for these extreme conditions, it was suspected that the method of analysis might not be appropriate for a LBLOCA, and, with regard to the thermal-

shock experiments, it was considered desirable to achieve a maximum critical K_I value of ~240 MPa•$\sqrt{m}$.

Calculations for the LBLOCA indicate, as mentioned above, that even if the effects of warm prestressing are ignored, a long crack will not completely penetrate the wall but will arrest close to the outside surface because of a steep negative gradient in K_I near the back surface (see Fig. 1.2.) In this case the proximity of the crack front to the outside surface raises questions about the accuracy of the analysis. Furthermore, if warm prestressing is ignored and some liberties are taken with regard to the time at which crack initiation takes place, it is possible that deep penetration of the wall will be the result of a rather long crack jump, as illustrated in Fig. 1.3 by the dashed-line c. Because of this and because there was concern that warm prestressing might not be effective under some circumstances, it appeared prudent to determine experimentally whether a crack would actually arrest very deep in the wall following a long crack jump. TSE-6 was designed for a long crack jump with arrest deep in the wall.

The multiplicity of the initiation-arrest events illustrated in Fig. 1.3 introduced the possibility of anomalous behavior of the crack during propagation. Irwin[8] had suggested that crack-tip blunting may occur as a result of a run-arrest event. This would tend to increase the effective value of K_{Ic} and during an experiment might give a false indication of warm prestressing, if the blunting prevented reinitiation following an arrest event. Irwin made reference to experiments conducted by Ripling, who, in a later discussion[10] with the author, indicated that the observed increase in K_{Ic} was small (<25%) for the particular materials he had tested.

Because of the uniqueness of the multiple initiation-arrest events calculated for the LBLOCA, a similar series of events was to be included in the thermal-shock experiments. The possible blunting effect would be compensated for by making $(K_I/K_{Ic})_{max}$ associated with incipient warm prestressing large enough to offset crack-tip blunting and otherwise permit an acceptable demonstration of warm prestressing.

A situation of interest with regard to crack arrest is illustrated in Fig. 1.5, which is a plot of K_I vs a/w, with time as a parameter, for the LBLOCA case described in Fig. 1.2. Included in this figure are the first three initiation-arrest events described in Fig. 1.3. It is observed that for each of the three events, arrest is predicted to take place in a rising K_I field ($dK_I/da > 0$). There has been some concern that arrest behavior in a rising K_I field might be different from that in a decreasing K_I field, and most available experimental data have been obtained under the latter conditions. In one of the earlier HSST thermal-shock experiments (TSE-4) (Ref. 1), arrest took place when dK_I/da reached zero after having been positive. It appeared that further investigations were warranted; thus, one of the objectives of subsequent thermal-shock experiments was to demonstrate arrest in a rising K_I field.

The LBLOCA analyses that were conducted as a part of the HSST thermal-shock program were based on a reference calculational model that in many respects represents a typical present-generation 1000-MW(e) PWR. Characteristics of the reference calculational model are summarized in Table 1.1, and various analyses are discussed in Refs. 1 and 7. Although finite-length flaws have been considered to some extent, most of the

Table 1.1. Reference calculational model for HSST thermal-shock program

Vessel dimensions, m	
Outside diameter	4.8
Wall thickness	0.22
Cladding[a]	0.0
Neutron fluence (E > 1 MeV), neutrons/cm^2	$4 \times 10^{19} \exp(-0.0094\ \Delta r)$[b,c]
Thermal shock (LBLOCA)	
Coolant temperature (not a function of time), °C	21[d]
Heat transfer coefficient (not a function of time), W•m^{-2}•°C^{-1}	1700
Wall temperature (initial), °C	288
Pressure (gage)	0
Fracture toughness	
K_{Ic} (source)	*ASME Code*, Sect. XI,
K_{Ia} (source)	Appendix A and Ref. 11
RTNDT (unirradiated), °C	−18[e]
ΔRTNDT vs fluence and copper concentration (source)	= f(Cu,P,F) (Ref. 12)[f] = f(Cu,Ni,F) (Ref. 13)[g]
Copper and nickel concentrations,[h] wt %	
Copper	0.25
Nickel	1.0
Residual stresses	Assumed zero

[a]Neither thermal nor stress effects of cladding were included because these two effects tend to compensate for each other.

[b]Δr is the radial distance into the vessel wall measured from the inner surface (mm).

[c]A range of 2 to 6 × 10^{19} neutrons/cm^2 for Δr = 0 was used in the sensitivity analysis.

[d]A range of 21 to 54°C was used in the sensitivity analysis.

[e]A range of −40 to +4°C was used in the sensitivity analysis.

[f]Used for sensitivity studies [Cu = wt % copper, P = wt % phosphorus, F = fast-neutron fluence (neutrons/cm^2)].

[g]Used for analysis represented by Figs. 1.2 and 1.3.

$$\Delta RTNDT = 0.56\ (38 + 470\ Cu + 350\ Cu\ Ni)\ (F \times 10^{-19})^{0.27},\ °C$$

where Cu = wt % copper,
Ni = wt % nickel,
F = fast-neutron fluence (neutrons/cm^2).

[h]A range of values used in sensitivity analysis.

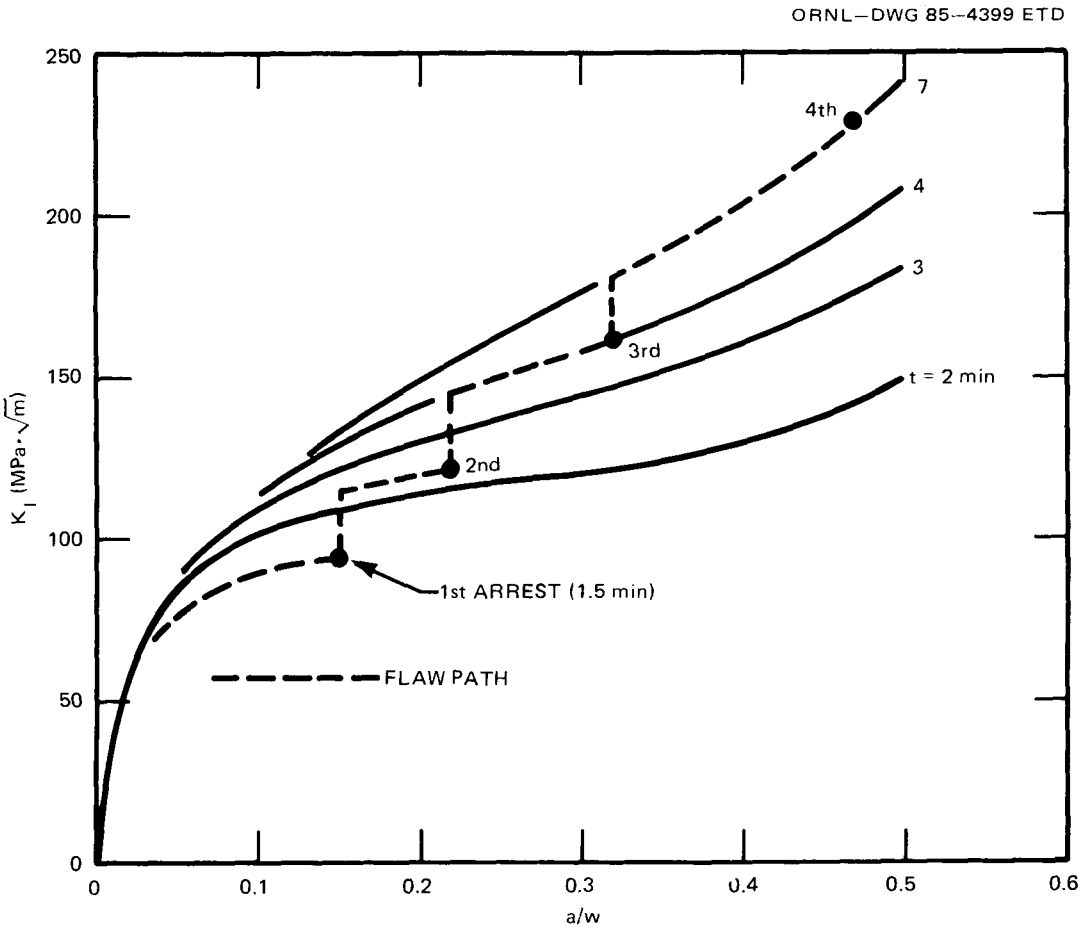

Fig. 1.5. K_I vs a/w for LBLOCA (conditions same as for Fig. 1.2).

calculations were made for long axial and, to a lesser extent, continuous circumferential flaws, both of which are represented by two-dimensional models. The two-dimensional axial model tends to be conservative because it does not include the effect of end restraints (heads) or the axial gradient in toughness (fluence), and both the two-dimensional axial and circumferential models tend to be conservative from the point of view that long flaws are not likely to exist. On the other hand, the analysis of short flaws indicates that under severe thermal-shock loading conditions, such flaws may grow in length to effectively become long flaws. Thus, there was a need to include long flaws in the thermal-shock experiments.

Another point in favor of using the two-dimensional model is that it is readily amenable to accurate analysis. This is particularly important with regard to the interpretation of experimental results, and for this reason, too, long flaws were particularly appropriate for the thermal-shock experiments.

Analysis of the two-dimensional reference calculational model indicated that as long flaws penetrate the wall beyond a/w = 0.1, the net

bending moment associated with the thermal stress tends to open the crack and, thus, enhances K_I, compared with an analysis that does not include the bending. The bending is illustrated in Figs. 1.6 and 1.7 for the axial and circumferential flaws, respectively. The effect on K_I is shown in Fig. 1.8, which compares the results of calculations that do and do not include the bending effect for the two long flaws. It is apparent that the bending effect contributes to the deep penetration of a flaw and that the effect is substantially greater for the axial flaw than for the circumferential flaw. Thus, it appears that the axial crack has a greater potential for penetrating deep into the wall.

For the preceding reasons the thermal-shock program has been oriented toward the two-dimensional axial flaw. The initial flaws for TSE-5, TSE-5A, and TSE-6 extended the full length of the test cylinders, and the cylinders were of sufficient length and the loading conditions were such that the two-dimensional analytical model could be used for calculating K_I with sufficient accuracy.

ORNL–DWG 75–4133R

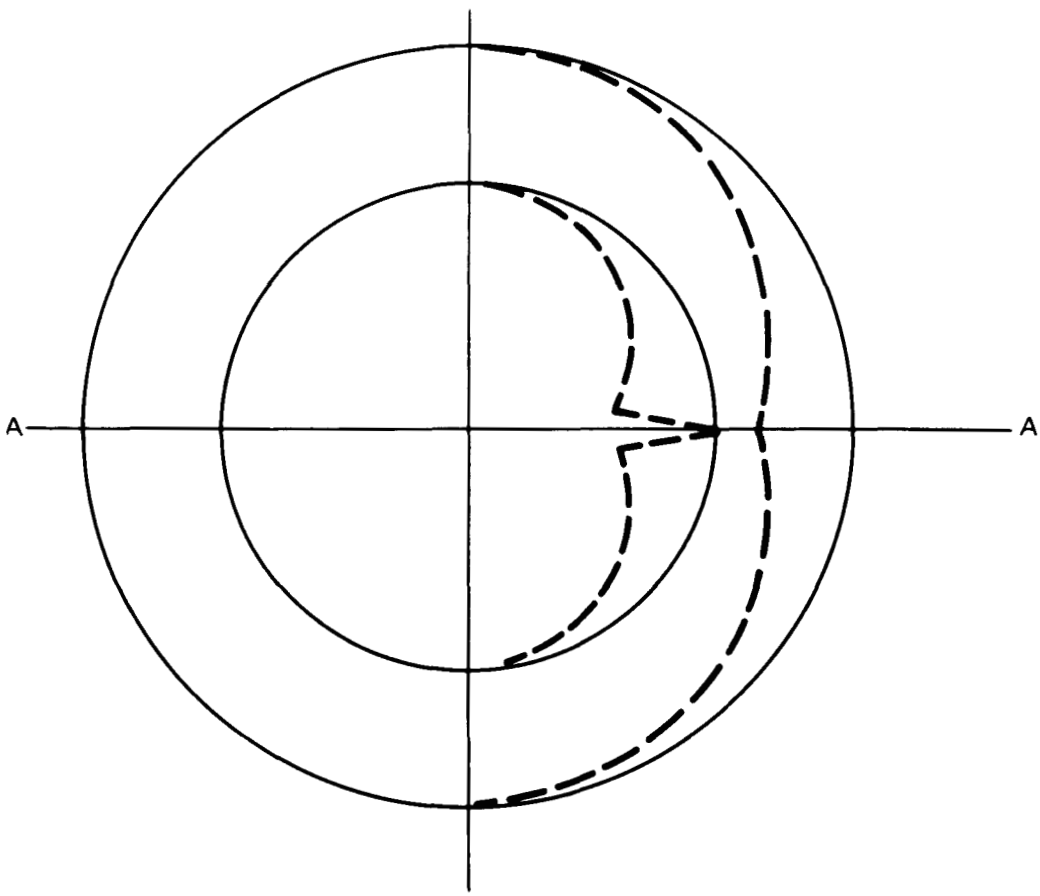

Fig. 1.6. Thermal-shock-induced bending of the wall of a cylinder containing a long axial flaw.

ORNL-DWG 75-9159R

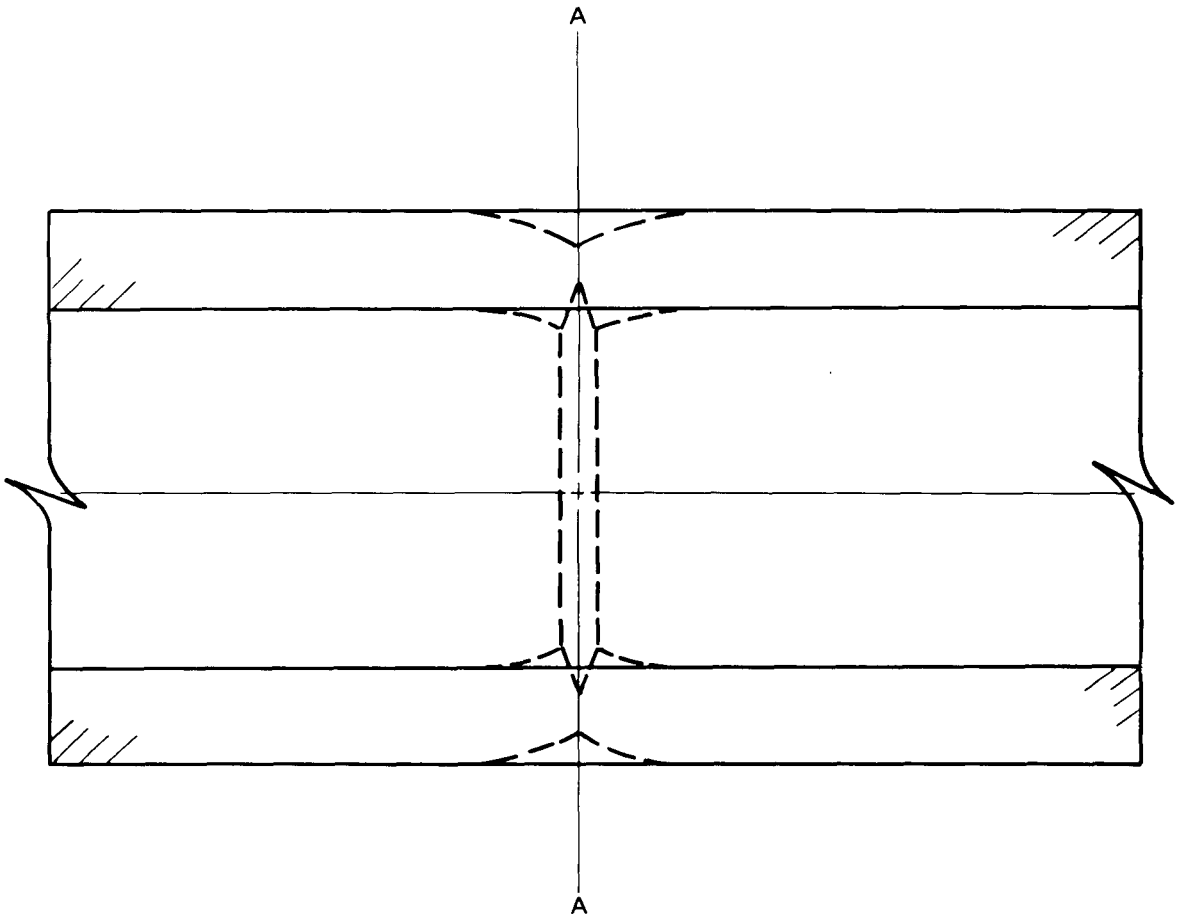

Fig. 1.7. Thermal-shock-induced bending of the wall of a cylinder containing a continuous circumferential flaw.

The bending effect in a cylinder wall under thermal-shock loading conditions is a function of the flexibility of the wall or the diameter-to-wall-thickness ratio (D/w); increasing this ratio increases the flexibility and, thus, increases the bending effect. Other than to influence the value of K_I, the bending presumably has no unique effect on crack behavior. Even so, it was desirable to have a substantial bending effect in TSE-5, TSE-5A, and TSE-6, and from a practical point of view, it was necessary in order to obtain the desired crack propagation. In the first four thermal-shock experiments (TSE-1, TSE-2, TSE-3, and TSE-4) the value of D/w was so small that there was very little bending effect. For this reason it was not possible in those experiments to demonstrate deep penetration, multiple events, arrest in a rising K_I field, or warm prestressing. However, with the larger cylinders specified for TSE-5, TSE-5A, and TSE-6, and with appropriate material properties and loading conditions, these things could be done, at least in principle.

In the earlier thermal-shock experiments a modified reactor-grade A 508 class-2 chemistry material was used for the test cylinders. The

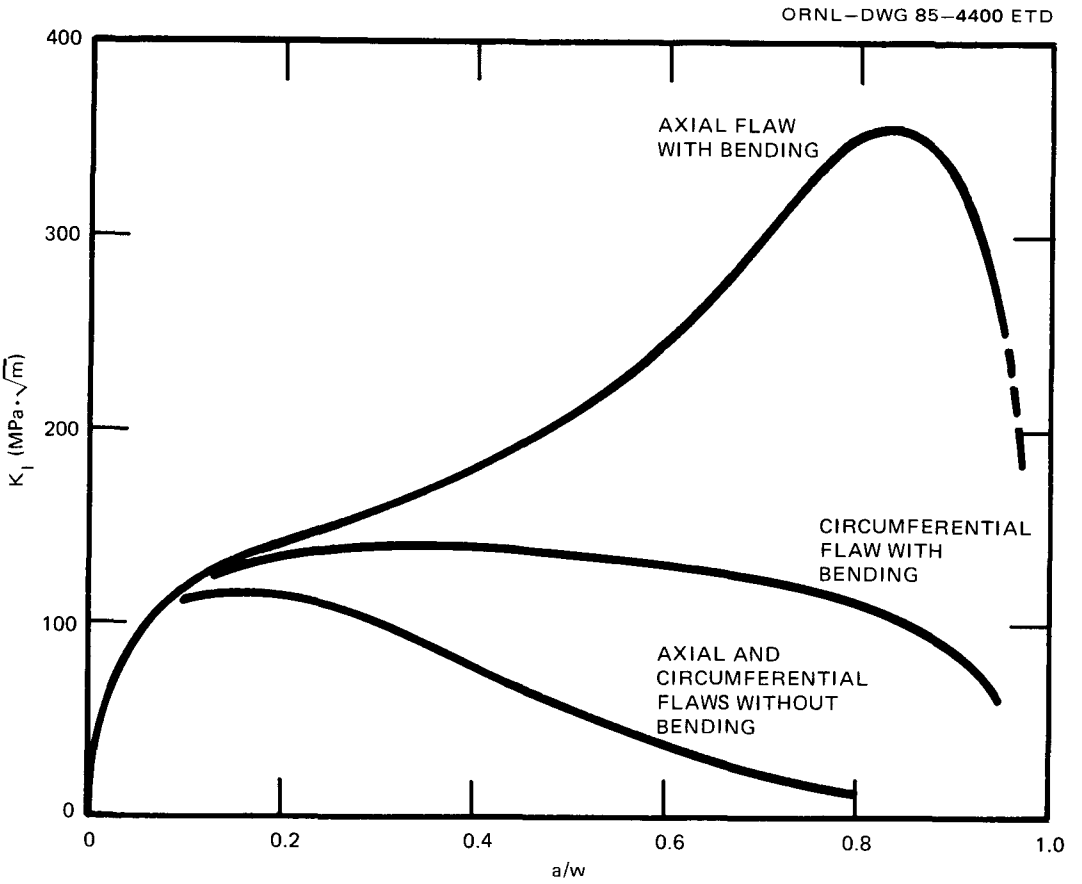

Fig. 1.8. K_I vs a/w for long axial and continuous circumferential flaws with and without the bending effect included (conditions same as for Fig. 1.2).

modification consisted of a quench-only heat treatment, as opposed to tempering at about 700°C, and provided to some extent the toughness properties that would exist in high-copper PWR vessels after many years of exposure to radiation. This suited the purpose for those experiments, but at the same time, the material was somewhat unique. For TSE-5 and TSE-5A there was a desire to use the same type of material with a conventional heat treatment.

The higher toughness associated with the "conventional" heat treatment and the test objectives required a more severe thermal shock than that used for the earlier experiments. Much earlier in the thermal-shock program[14] (prior to TSE-1), an experiment similar to TSE-5 was proposed, and liquid nitrogen was considered for the quench medium. At that time there did not appear to be a reasonable way of coping with film boiling, which tends to insulate the test specimen from the liquid nitrogen and prevents a rapid quench. More recently, a possible method for suppressing film boiling was suggested by the French,[15] and several years of a modest development effort[16–22] at Oak Ridge National Laboratory (ORNL) resulted in its practical application to TSE-5, TSE-5A, and TSE-6. The method consists of applying a thin layer of insulating material to the

surface that otherwise comes in contact with the liquid nitrogen. By this means the temperature of the surface in contact with the liquid nitrogen is very quickly reduced to the point where transitional nucleate boiling is established. The net gain in overall heat transfer coefficient is substantial and sufficient.

The maximum effectiveness of the coating is limited to an initial test-cylinder temperature of ~130°C. An initial temperature of ~95°C was found to be adequate for TSE-5, TSE-5A, and TSE-6 and was sufficiently removed from the uncertain limiting condition.

A summary of test conditions for TSE-5, TSE-5A, and TSE-6 is presented in Table 1.2, and the test facility is illustrated in Fig. 1.9. As indicated by Fig. 1.9, the TSE-5, TSE-5A, and TSE-6 thermal shocks were achieved by effectively dunking the test specimen in a tank of liquid nitrogen after heating the test cylinders to the desired initial temperature. Only the inner surface was exposed to the liquid nitrogen, and this was done in such a way as to produce a very uniform and severe quench.

Table 1.2. Test conditions specified for TSE-5, TSE-5A, and TSE-6

	Thermal-shock experiment		
	TSE-5	TSE-5A	TSE-6
Test-cylinder designation	TSC-1	TSC-2	TSC-3
Test-cylinder dimensions, m			
Outside diameter	0.991	0.991	0.991
Inside diameter	0.682	0.682	0.838
Length	1.22	1.22	1.22
Test-cylinder material	A 508, class-2 chemistry		
Test-cylinder heat treatment	Tempered at 613°C for 4 h	Tempered at 679°C for 4 h	Tempered at 613°C for 4 h
Flaw	Long axial sharp crack, a = 15 mm	Long axial sharp crack, a = 11 m	Long axial sharp crack, a = 7.6 mm
Temperatures, °C			
Wall (initial)	93	93	93
Sink	−196	−196	−196
Coolant	Liquid nitrogen	Liquid nitrogen	Liquid nitrogen
Flow conditions	Natural convection	Natural convection	Natural convection
Coating on quenched surface	Rubber cement (3M-NF34)	Rubber cement (3M-34 and 3M-NF34)	Rubber cement (3M-34 and 3M-NF34)
Coating surface density, g/m^2	350	270	241

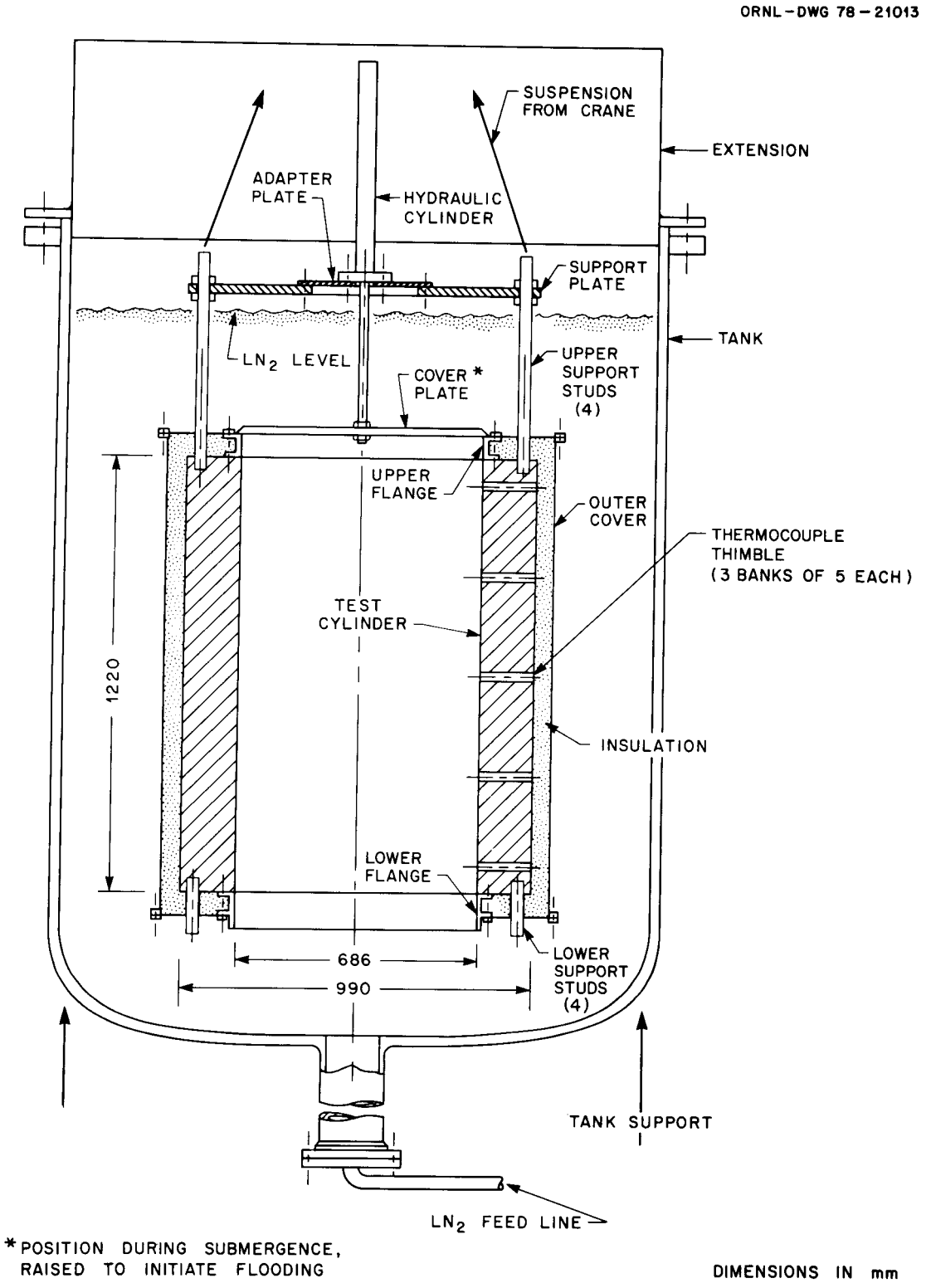

Fig. 1.9. Liquid-nitrogen thermal-shock test facility.

During the design phase of TSE-5, it was decided that a toughness-vs-temperature curve similar to that obtained for HSST plate 02 (Ref. 23) would be appropriate, and it was assumed that the flaw would behave in accordance with a mean curve through the lab toughness-vs-temperature data. A material characterization program, using the TSE-5 test-cylinder prolongation as an appropriate source of material, was undertaken to determine the precise tempering temperature; eventually a tempering temperature of 613°C was selected.

The final pretest analysis for TSE-5 indicated that three initiation-arrest events would take place and that a fourth initiation would be prevented by warm prestressing. The final crack depth would be in the range of a/w = 0.5 to 0.7, and the first two arrest events would take place in a rising K_I field.

During TSE-5 there were three initiation-arrest events, and the final fractional crack depth near midlength was ~0.8. Calculated K_I values for the first two initiation events agreed well with the design toughness curve, but the corresponding value for the third initiation event, which took place at a substantially higher temperature, was much less than expected on the basis of pretest material-characterization studies. Because of this apparent discrepancy, additional material-characterization studies were conducted, and they indicated that the material had not been adequately characterized prior to TSE-5. The additional testing of the material revealed greater scatter in fracture toughness (±50%) with lower lower-bound values.

As a result of the lower-than-expected fracture toughness associated with TSE-5, conditions for arrest in a rising K_I field were not achieved, and warm prestressing was not demonstrated satisfactorily. However, in addition to achieving multiple events with deep penetration, an unexpected long crack jump occurred. It appears that the second initiation event was delayed somewhat by relatively high effective toughness, resulting in the long crack jump. The existence of this long jump permitted an analytical assessment of dynamic effects, and the results indicated that dynamic effects were negligible.

Another unexpected event during TSE-5 was the extensive propagation of a very short circumferentially oriented crack, which originated in the electron-beam weld that was used to generate the long axial flaw. The small cross crack was not intentional, but its propagation was a convincing demonstration of the ability of a short flaw to extend in length to effectively become a long flaw and tended to justify our concern over the behavior of long flaws during severe thermal shock.

Because some of the objectives of TSE-5 were not met and because it appeared that they could be met by simply increasing the effective toughness of the material, another attempt was made to achieve the objectives of TSE-5, and the experiment was referred to as TSE-5A. In preparation for TSE-5A, a very extensive material-characterization program was conducted for the purpose of obtaining appropriate K_J and mean K_{Ia} curves. The tempering temperature finally selected was 679°C.

The final pretest analysis for TSE-5A, using the actual TSE-5 thermal transient and the above lab toughness data, indicated that four initiation-arrest events would take place and that a fifth initiation event would be prevented by warm prestressing. The final crack depth (a/w) would be in the range of 0.45 to 0.65, and the corresponding range

in $(K_I/K_{Ic})_{max}$ would be 2.2 to 1.7. Furthermore, the first two arrest events would take place in a rising K_I field. Following TSE-5A, a more precise analysis, using the actual thermal transient and the same toughness curves as before, indicated essentially the same behavior with a calculated final crack depth of 0.54 and a corresponding value of $(K_I/K_{Ic})_{max}$ of 2.0.

During TSE-5A there were four initiation-arrest events, warm prestressing prevented a fifth initiation event, and the final crack depth was 0.54. A final analysis of TSE-5A, based on experimental results, indicated that $(K_I/K_{Ic})_{max}$ for the final crack depth was 2.3, providing a very convincing demonstration of warm prestressing. The first arrest event took place in a rising K_I field.

TSE-6 was designed to demonstrate that, under severe thermal-shock loading conditions only, and following a long crack jump, a long axial flaw could not fully penetrate the wall but, rather, in accordance with calculations, would arrest deep in the wall. To achieve the long crack jump, it was necessary to reduce the wall thickness to one-half that used for TSE-5 and TSE-5A (for increased wall flexibility) and to use the relatively low fracture toughness associated with TSE-5. During TSE-6, there were two initiation-arrest events, the second constituting a long crack jump with arrest taking place deep in the wall as predicted. The first event involved a relatively short crack advance with arrest in a steeply rising K_I field.

To briefly summarize, it can be stated that nearly all of the objectives of TSE-5, TSE-5A, and TSE-6 were met, and there were a few bonus events and revelations as well. Specific pertinent accomplishments are listed below:

1. a series of initiation-arrest events with deep penetration of the wall in good agreement with "predictions" (TSE-5, TSE-5A, TSE-6);
2. warm prestressing with $\dot{K}_I < 0$ (TSE-5A);
3. arrest in a rising K_I field (TSE-5A, TSE-6);
4. long crack jump without significant dynamic effects at arrest (TSE-5, TSE-6).;
5. extensive surface extension of an initially very short and shallow flaw in agreement with calculations (TSE-5);
6. demonstration of inability of flaw to penetrate outer surface after long crack jump (TSE-6);
7. "discovery" of large scatter in small-specimen K_J data (material-characterization studies for TSE-5);
8. "discovery" of ability of arrested long flaw to exhibit unusually high fracture toughness (TSE-5, TSE-6); and
9. confirmation that for critical values of $K_I \leq 150$ MPa$\cdot\sqrt{m}$, linear-elastic fracture mechanics is appropriate for severe thermal-shock loading conditions associated with LBLOCA.

It was not possible during the thermal-shock experiments to achieve critical values of $K_I > 150$ MPa$\cdot\sqrt{m}$. The significance of not being able to achieve the desired maximum value of ~250 MPa$\cdot\sqrt{m}$ was, of necessity, relegated to a later experiment[24] that would combine both pressure and thermal-shock loading to achieve larger values of K_I.

References

1. R. D. Cheverton and S. E. Bolt, *Pressure Vessel Fracture Studies Pertaining to a PWR LOCA-ECC Thermal Shock: Experiments TSE-3 and TSE-4 and Update of TSE-1 and TSE-2 Analysis*, ORNL/NUREG-22, Union Carbide Corp. Nuclear Div., Oak Ridge Natl. Lab., December 1977.

2. C. B. Buchalet and W. H. Bamford, *Methods of Fracture Mechanics Analysis of Nuclear Reactor Vessels Under Severe Thermal Transients*, ASME Paper 75-WA/PVR-3, American Society of Mechanical Engineers, 1975.

3. A. S. Kobayashi et al., "Surface Flaw in a Thermally Shocked Hollow Cylinder," in *Transactions of the 3rd International Conference on Structural Mechanics in Reactor Technology*, London, Sept. 1–5, 1975, Vol. 3, Part G-H, Paper G4/3, North-Holland Publishing Company, Amsterdam, 1975.

4. D. J. Ayres and W. F. Siddal, Jr., *Finite Element Analysis of Structural Integrity of a Reactor Pressure Vessel During Emergency Core Cooling*, Report NP-18198, Combustion Engineering Inc., January 1970.

5. T. R. Mager, T. A. Meyer, and M. Galliani, "Fracture Mechanics Evaluation of the Trino Vercellese Reactor Vessel Following a Postulated Main Coolant Pipe Break," in *Transactions of the 3rd International Conference on Structural Mechanics in Reactor Technology*, London, Sept. 1–5, 1975, Vol. 3, Part G-H, Paper G5/4, North-Holland Publishing Company, Amsterdam, 1975.

6. J. Reynen, *Surface Cracks in Cylinders During Thermal Shock*, paper presented at the ASME Pressure Vessel and Piping Conference, Mexico City, Mexico, Sept. 19–24, 1976.

7. R. D. Cheverton, S. K. Iskander, and S. E. Bolt, *Applicability of LEFM to the Analysis of PWR Vessels Under LOCA-ECC Thermal Shock Conditions*, ORNL/NUREG-40, Union Carbide Corp. Nuclear Div., Oak Ridge Natl. Lab., October 1978.

8. G. R. Irwin et al., University of Maryland, College Park, personal communication to R. D. Cheverton, Oak Ridge Natl. Lab., Oak Ridge, Tenn.

9. F. J. Loss, A. A. Gray, Jr., and J. R. Hawthorne, *Significance of Warm Prestress to Crack Initiation During Thermal Shock*, NRL/NUREG 8165, Naval Research Laboratory, Washington, D.C., September 1977.

10. E. J. Ripling, Materials Research Laboratory, Inc., Chicago, personal communication to R. D. Cheverton, Oak Ridge Natl. Lab., Oak Ridge, Tenn.

11. T. U. Marston, ed., *Flaw Evaluation Procedures: ASME Section XI*, EPRI NP-719-SR, Electric Power Research Institute, Palo Alto, Calif., 1978.

12. U.S. Nuclear Regulatory Commission, "Effects of Residual Elements on Predicted Radiation Damage to Reactor Pressure Vessel Materials," *Reg. Guide 1.99*, Rev. 1, Sept. 16, 1976.

13. P. N. Randall, U.S. Nuclear Regulatory Commission, Washington, D.C., personal communication to R. D. Cheverton, Oak Ridge National Laboratory, Oak Ridge, Tenn., April 1982.

14. R. D. Cheverton, "Thermal Shock Investigations," pp. 87–89 in *Quarterly Progress Report on Reactor Safety Programs Sponsored by the Division of RSR for April–June 1974*, ORNL-TM-4655, Vol. II, Union Carbide Corp. Nuclear Div., Oak Ridge Natl. Lab.

15. J. J. Doyen, Framatome, Paris, personal communication to R. D. Cheverton, Oak Ridge National Laboratory, Oak Ridge, Tenn., June 1976.

16. R. D. Cheverton, "Thermal Shock Investigations," pp. 62–64 in *Heavy-Section Steel Technology Program Quart. Prog. Rep. for October–December 1976*, ORNL/NUREG/TM-94, Union Carbide Corp. Nuclear Div., Oak Ridge Natl. Lab.

17. R. D. Cheverton, "Thermal Shock Investigations," pp. 88–97 in *Heavy-Section Steel Technology Program Quart. Prog. Rep. for January–March 1977*, ORNL/NUREG/TM-120, Union Carbide Corp. Nuclear Div., Oak Ridge Natl. Lab.

18. R. D. Cheverton, "Thermal Shock Investigations," pp. 69–86 in *Heavy-Section Steel Technology Program Quart. Prog. Rep. for April–June 1977*, ORNL/NUREG/TM-147, Union Carbide Corp. Nuclear Div., Oak Ridge Natl. Lab.

19. R. D. Cheverton, "Thermal Shock Investigations," pp. 109–12 in *Heavy-Section Steel Technology Program Quart. Prog. Rep. for July–September 1977*, ORNL/NUREG/TM-166, Union Carbide Corp. Nuclear Div., Oak Ridge Natl. Lab.

20. R. D. Cheverton, "Thermal Shock Investigations," pp. 63–73 in *Heavy-Section Steel Technology Program Quart. Prog. Rep. for October–December 1977*, ORNL/NUREG/TM-194, Union Carbide Corp. Nuclear Div., Oak Ridge Natl. Lab.

21. R. D. Cheverton, "Thermal Shock Investigations," pp. 33–38 in *Heavy-Section Steel Technology Program Quart. Prog. Rep. for January–March 1978*, ORNL/NUREG/TM-209, Union Carbide Corp. Nuclear Div., Oak Ridge Natl. Lab.

22. R. D. Cheverton, "Thermal Shock Investigations," pp. 50–56 in *Heavy-Section Steel Technology Program Quart. Prog. Rep. for April–June 1978*, ORNL/NUREG/TM-239, Union Carbide Corp. Nuclear Div., Oak Ridge Natl. Lab.

23. W. O. Shabbits, W. H. Pryle, and E. T. Wessel, *Heavy-Section Steel Technology Program Technical Report No. 6, Heavy Section Fracture Toughness Properties of A533 Grade B Class 1 Steel Plate and Submerged-Arc Weldment*, USAEC Report WCAP-7414, Westinghouse Electric Corporation, December 1969.

24. R. H. Bryan et al., *Pressurized-Thermal-Shock Test of 6-in.-Thick Pressure Vessels. PTSE-1: Investigation of Warm Prestressing and Upper-Shelf Arrest*, NUREG/CR-4106 (ORNL-6135), Martin Marietta Energy Systems, Inc., Oak Ridge Natl. Lab., May 1985.

2. PURPOSE AND SCOPE OF TSE-5, TSE-5A, AND TSE-6

The purpose of TSE-5 was to examine the behavior of a long axial surface flaw under a set of conditions that would result in essentially the same type of flaw behavior as that calculated for a PWR large-break loss-of-coolant accident (LBLOCA), assuming "high" concentrations of copper and nickel and a fast-neutron fluence corresponding to the end of plant life. The calculated behavior for the LBLOCA is summarized graphically in Figs. 1.2—1.5. Considering these results and the intended purpose of TSE-5, the scope of TSE-5 included (1) a series of initiation-arrest events involving both shallow and deep flaws, (2) termination of the series of events by warm prestressing deep in the wall ($0.4 \leq a/w \leq 0.7$), and (3) arrest in a rising K_I field. A long crack jump was to be relegated to a later experiment.

As mentioned in Chap. 1, some of the specific objectives of TSE-5 were not met, and some of the results that were obtained indicated new trends that needed to be investigated further. Thus, an additional experiment, TSE-5A, was planned, the purpose and scope of which were essentially the same as for TSE-5.

Analysis of the LBLOCA indicates that if warm prestressing were not effective, a long axial flaw would penetrate deep into the wall ($a/w \simeq 0.9$) but would not go all the way through. Furthermore, if crack initiation did not take place until fairly late in the transient, a long crack jump could precede the deep arrest event and might introduce dynamic effects that, contrary to the static analysis, would allow the flaw to penetrate the wall. TSE-6 was designed to confirm the inability of a long axial crack to penetrate the wall following a long crack jump.

The basic analytic tool used for calculating the behavior of flaws, when plasticity effects are not large, is linear-elastic fracture mechanics. Thus, a specific purpose of the thermal-shock program has been to examine the validity of linear-elastic fracture mechanics for analyzing surface flaws in thick-walled cylinders subjected to severe thermal-shock loading conditions.

Linear-elastic fracture mechanics makes use of two basic variables: the crack-tip stress-intensity factor and the material fracture toughness. The primary question regarding the validity of linear-elastic fracture mechanics for thermal-shock loading has been whether K_{Ic} and K_{Ia}, as measured in the lab with small specimens, agree well with critical values of K_I corresponding to initiation and arrest events occurring during the thermal-shock experiments. An accurate comparison of these data requires that K_I for the flaws in the thermal-shock test cylinder be accurately known and that appropriate lab data be available. Thus, the scope of the thermal-shock program has also included (1) developing accurate methods for calculating K_I for flaws in the test cylinder and (2) obtaining K_{Ic} and K_{Ia} data for the test-cylinder material. This latter effort also included a determination of appropriate tempering temperatures to obtain the desired toughness curves for the experiments.

3. METHODS OF ANALYSIS FOR CALCULATING K_I FOR TWO- AND THREE-DIMENSIONAL INNER-SURFACE FLAWS

Details of the methods developed for calculating the Mode I stress-intensity factor, K_I, for the thermal-shock program are discussed in Refs. 1–4. It suffices to say here that for the two-dimensional surface flaws strain-energy release-rate techniques were used and for three-dimensional flaws stress and displacement techniques were used. The stresses and displacements required for the calculations of K_I for both flaw geometries were obtained using a finite-element code[2] developed specifically for this purpose. A typical finite-element mesh for the long, axial, two-dimensional flaw is shown in Fig. 3.1.

The two-dimensional mesh shown in Fig. 3.1 is the result of numerous mesh convergence studies that were conducted in an effort to obtain adequate accuracy in K_I without excessive computer costs. Eventually, as described in Refs. 3 and 4, influence coefficients were derived and used in conjunction with superposition techniques to calculate K_I for the two-dimensional flaws. This permitted a substantial investment in very accurate influence coefficients because subsequent calculations of K_I values would be almost trivial. It is believed that the calculation of K_I for a given set of two-dimensional conditions for the thermal-shock test cylinders is accurate within ±5%. Of course, the overall accuracy of the calculated value of K_I depends on a number of experimental factors, including the accuracy of the measurement of temperatures and crack depth and the extent to which the problem deviates from two-dimensional conditions.

The most recent version of the fracture-mechanics codes described in Refs. 3 and 4 is a code referred to as OCA-P.[5] This code was used for the most recent posttest analyses for TSE-5, TSE-5A, and TSE-6.

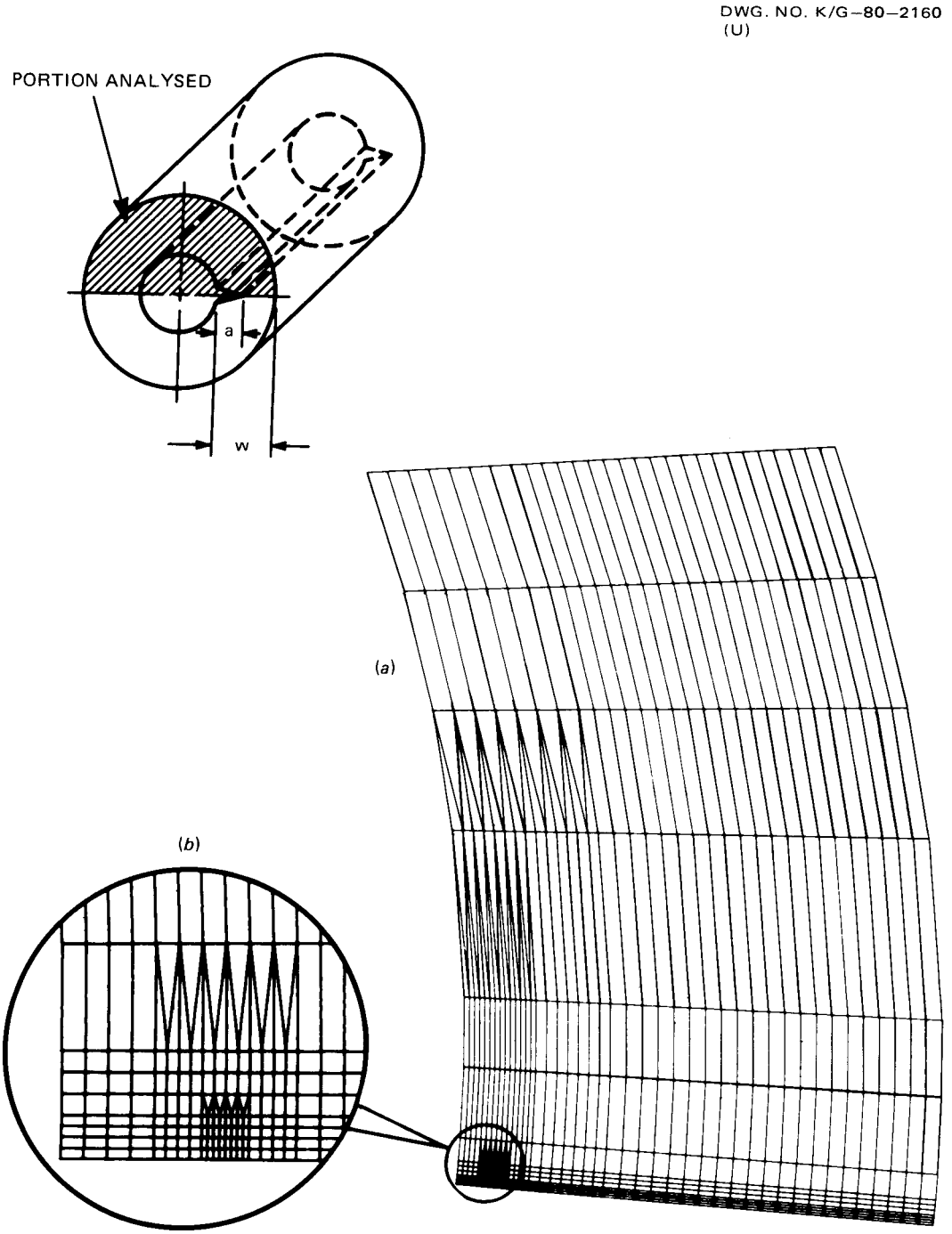

Fig. 3.1. A typical finite-element mesh used for calculating K_I via the energy-release-rate method.

References

1. S. K. Iskander, *The Calculation of Stress Intensity Factors in Thick Cylinders Subjected to Transient Temperature Gradients by the Finite Element Method*, K/CSD/TM-2, Union Carbide Corp. Nuclear Div., Oak Ridge Natl. Lab., 1976.

2. S. K. Iskander, *Two Finite-Element Techniques for Computing Mode I Stress Intensity Factors in Two- and Three-Dimensional Problems*, ORNL/NUREG/CSD/TM-14, Union Carbide Corp. Nuclear Div., Oak Ridge Natl. Lab., February 1981.

3. S. K. Iskander, R. D. Cheverton, and D. G. Ball, *OCA-I, A Code for Calculating the Behavior of Flaws on the Inner Surface of a Pressure Vessel Subjected to Temperature and Pressure Transients*, ORNL/NUREG-84, Union Carbide Corp. Nuclear Div., Oak Ridge Natl. Lab., August 1981.

4. D. G. Ball et al., *OCA-II, A Code for Calculating the Behavior of 2-D and 3-D Surface Flaws in a Pressure Vessel Subjected to Temperature and Pressure Transients*, NUREG/CR-3491 (ORNL-5934), Union Carbide Corp. Nuclear Div., Oak Ridge Natl. Lab., February 1984.

5. R. D. Cheverton and D. G. Ball, *OCA-P, A Deterministic and Probabilistic Fracture-Mechanics Code for Application to Pressure Vessels*, NUREG/CR-3618 (ORNL-5991), Martin Marietta Energy Systems, Inc., Oak Ridge Natl. Lab., May 1984.

4. PRETEST ANALYSIS AND SPECIFICATION OF TEST CONDITIONS

4.1 Preliminary Selection of Test Conditions

4.1.1 Test-cylinder dimensions

As discussed in Chap. 1 and Ref. 1, the ratio of wall thickness to diameter for the PWR vessels is small enough that local bending of the wall contributes significantly to K_I for long deep flaws. From a practical point of view, the diameter of a test cylinder must be much smaller than that for a PWR vessel. Thus, to retain the same degree of wall flexibility, the test-cylinder wall thickness must also be much smaller. However, there are conflicting requirements because reducing the wall thickness reduces the severity of the thermal shock and also reduces the radial distance that a flaw can propagate without being affected by the proximity of the outside surface of the cylinder. Corten[2] suggested that the effect would be negligible if $(w - a)/r_y > 10$, where $(w - a)$ is the uncracked ligament and r_y is the radius of the plastic zone at the tip of the crack. Assuming maximum flaw depths of interest for TSE-5 and TSE-5A to be ~65% of the wall thickness ($a/w = 0.65$), the wall thickness required to satisfy Corten's suggestion was ~150 mm and was calculated as follows:

$$w = \frac{10 \times r_y}{(1 - 0.65)} \simeq 150 \text{ mm} ,$$

where[3]

$$r_y \simeq \left(\frac{1}{6\pi} \frac{K_{Ic}}{\sigma_{ys}}\right)^2 = 5.3 \text{ mm} ,$$

and where

$$\left.\begin{aligned} K_{Ic} &= 165 \text{ MPa}\cdot\sqrt{m} \\ \sigma_{ys} &= 520 \text{ MPa} \end{aligned}\right\} \quad \text{assumed consistent values for TSE-5.}$$

Selection of a wall thickness on the basis of thermal-shock severity considerations is much more complicated but evolved from a preliminary parametric analysis that included both the heat transfer and fracture mechanics for the proposed experiment. The results indicated that a 150-mm wall thickness would be satisfactory.

Studies[1] conducted early in the thermal-shock program indicated that an outside diameter of ~1 m in conjunction with a 150-mm wall thickness

would provide adequate flexibility of the wall for deep penetration ($a/w > 0.5$) of a long axial flaw and that for times of interest, dK_I/da would be positive throughout most of the inner half of the wall. The effect of bending on K_I for a long axial flaw (two-dimensional model) and for these dimensions and a typical thermal shock is illustrated in Fig. 4.1, which compares K_I vs a/w curves calculated with and without the bending effect included. As indicated, the bending effect is substantial for $a/w > 0.1$, and the slope of the curve is positive for $0 \leq a/w \leq 0.5$. Aside from other considerations to be discussed later, these conditions were considered to be acceptable for TSE-5.

The length of the test cylinder needed to be great enough so that a two-dimensional analysis of a long axial flaw would be acceptable. Initially, the appropriate length was estimated using the thin-shell relation[4]

$$\ell \geq 2\pi \left[\frac{r^2 w^2}{3(1-\nu^2)}\right]^{1/4} = 1.2 \text{ m} ,$$

where

ℓ = required minimum length of test cylinder,
r = radius of test cylinder = 420 mm,
w = wall thickness = 152 mm,
ν = Poisson's ratio = 0.3.

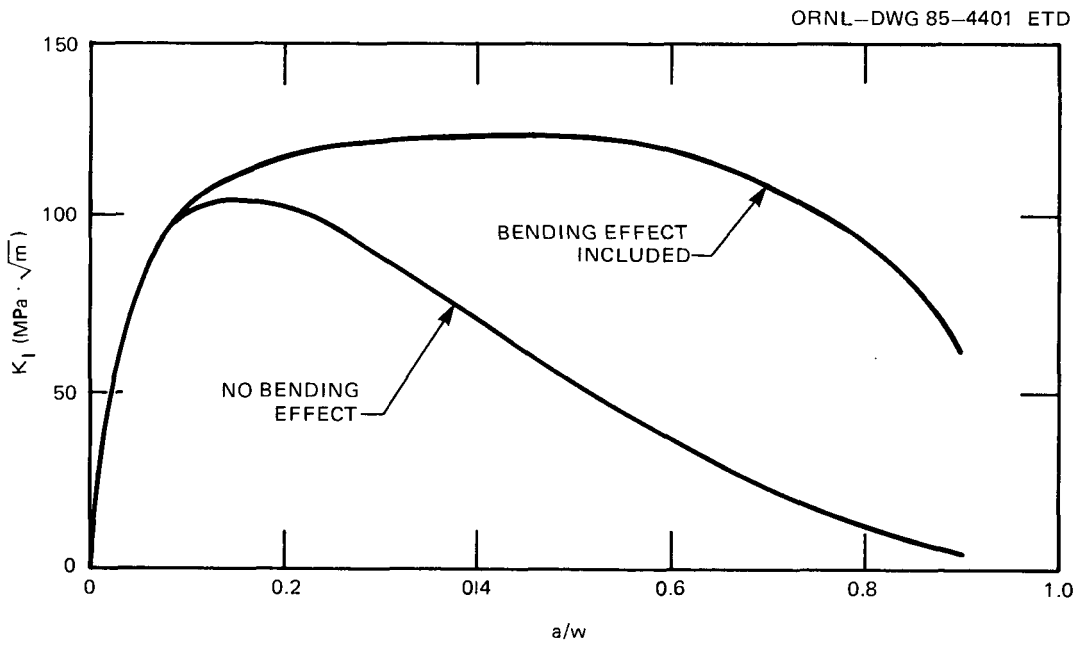

Fig. 4.1. K_I vs a/w for long axial flaw with and without wall bending included in analysis (typical TSE-5 conditions with t = 3.5 min).

Eventually, a three-dimensional analysis was performed that confirmed the acceptability of this particular length, and the results are summarized in Fig. 4.2. The three-dimensional calculations were made for cylinder lengths of 686 mm, 914 mm, 1220 mm, and infinity (two-dimensional model), assuming a full-length, uniform-depth axial flaw with a fractional depth (a/w) of 0.5 and considering a specific time in a typical thermal transient. The results in Fig. 4.2 are presented in terms of $[K_I - K_I(\ell = \infty)]/K_I(\ell = \infty)$ vs axial position. As indicated, all three finite lengths considered resulted in high values near midlength relative to the two-dimensional model (10 to 15%) and much lower values near the ends. Only the 1220-mm length resulted in a reasonably flat region over a substantial length of the cylinder. For this cylinder length, K_I was within 10% of the two-dimensional value over a length of 860 mm or 70% of the length of the cylinder. This was considered to be acceptable.

It was recognized that the relatively low values of K_I near the ends of the test cylinder would result in less crack penetration near the ends than elsewhere (as experienced in previous thermal-shock experiments)[5] and that for very deep cracks this nonuniformity in crack depth could affect the K_I value for the central (deepest) portion of the crack. However, for the reason discussed below, no attempt was made to effectively eliminate this possibly significant variation by extending the length of the cylinder beyond 1220 mm.

The test-cylinder length also influences the axial uniformity of heat removal from the inner surface of the test specimen during the thermal-shock transient. Liquid nitrogen removes heat from the inner

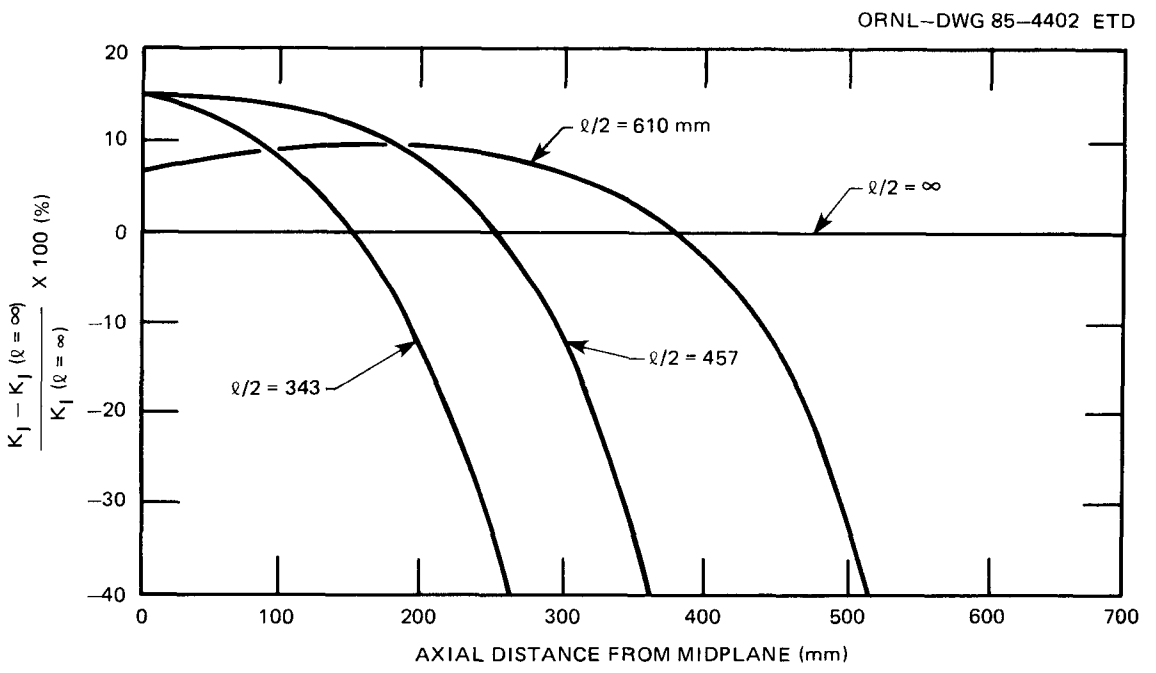

Fig. 4.2. K_I (normalized) for long axial flaw in finite-length cylinder (990-mm OD by 152-mm wall) vs axial distance from midlength of cylinder for $\ell/2$ = 343, 457, 610, and ∞ (TSE-5 loading, a/w = 0.5).

surface by boiling, and because the bulk liquid is at the saturation temperature, the vapor rises in the form of bubbles without condensing. Therefore, the vapor fraction increases with increasing height in the cylinder and, thus, with increasing cylinder length. This is beneficial from the standpoint of increasing the natural convection flow rate, but it can decrease the heat flux in the upper region of the cylinder if the vapor density becomes excessive. This tendency for axial asymmetry is also a function of quench rate (heat removal rate) and characteristics of the inner-surface coating that is used to suppress film boiling. The problem is quite complicated. However, after a considerable coating development effort, the results of heat transfer experiments with the full-size test cylinder finally indicated that the 1.22-m length could result in symmetrical heat removal, a condition necessary for preserving the two-dimensional nature of the experiment.

4.1.2 Test-cylinder material

Typical light-water reactor pressure-vessel material was specified for TSE-5, and this specification included the heat treatment as well as the chemistry. The choices of material were A 533 grade B class 1 and A 508 class 2 steels.

In earlier thermal-shock experiments[1,5] A 508 with class-2 chemistry and a quench-only heat treatment were specified. This heat treatment reduced the fracture toughness, simulating to some extent the effects of radiation damage, but at the same time resulted in a rather unique material. It was decided that for TSE-5 a normal tempering heat treatment would be more appropriate, provided that an adequately severe thermal shock could be achieved by practical means.

The toughness curve (K_{Ic} vs temperature) selected for the preliminary design analysis of TSE-5 was an average curve for HSST plate 02 (Ref. 6). It was assumed that the test cylinder would behave in accordance with average rather than lower-bound toughness values, and it was believed that the plate 02 properties could be achieved for the TSE-5 test cylinder by appropriate selection of tempering conditions. To include a consistent K_{Ia} vs temperature curve in a more advanced stage of the design analysis, the K_{Ic} and K_{Ia} curves in Sect. XI, Appendix A of the *ASME Code*[7] were used with RTNDT = −34°C. The K_{Ic} curve so obtained is essentially the same as the average HSST plate 02 curve used earlier (Fig. 4.3 referred to as TSE-5 design curve elsewhere in report). The low value of RTNDT was required in the *Code* equations because those equations represent lower-bound rather than average-toughness values, and RTNDT for plate 02 was approximately −18°C. On the basis of pretest material-characterization studies, it appeared that a tempering temperature of 613°C was appropriate, even though this temperature was recognized as being low relative to the usual tempering temperature for class 2 material. This situation is discussed further in Chap. 7.

The fracture toughness desired for TSE-5A was about the same as that specified for TSE-5. However, the results of TSE-5 and post-TSE-5 material-characterization studies indicated that the fracture toughness of the TSE-5 test cylinder was considerably less than specified. Thus, a higher tempering temperature was required for TSE-5A, and the value

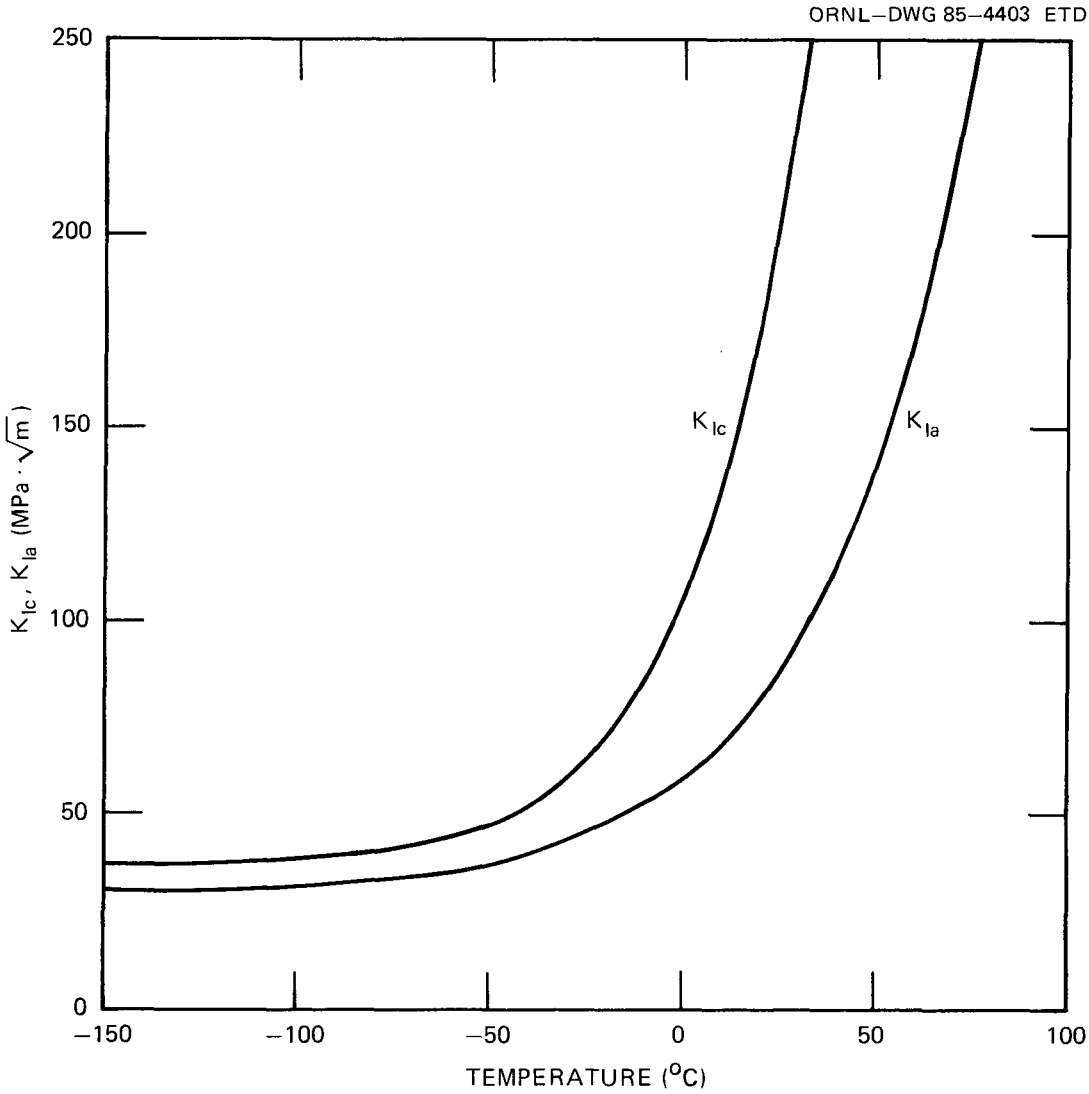

Fig. 4.3. K_{Ic} and K_{Ia} curves used in pretest analysis of TSE-5 (ASME Sect. XI curves with RTNDT = –34°C).

finally selected was 679°C. The corresponding lower-bound K_J and mean K_{Ia} curves obtained for this material using small compact specimens (see Chap. 7) and used in the pretest analysis of TSE-5A are shown in Fig. 4.4.

The fracture toughness required for TSE-6 was the same as the actual toughness for the TSE-5 test cylinder, and, thus, a tempering temperature of 613°C was specified. The toughness curves used for the pretest analysis were based on K_{Ic} and K_{Ia} values deduced from TSE-5 and are shown in Fig. 4.5 (refer to Chap. 8 for a discussion of the TSE-5 data).

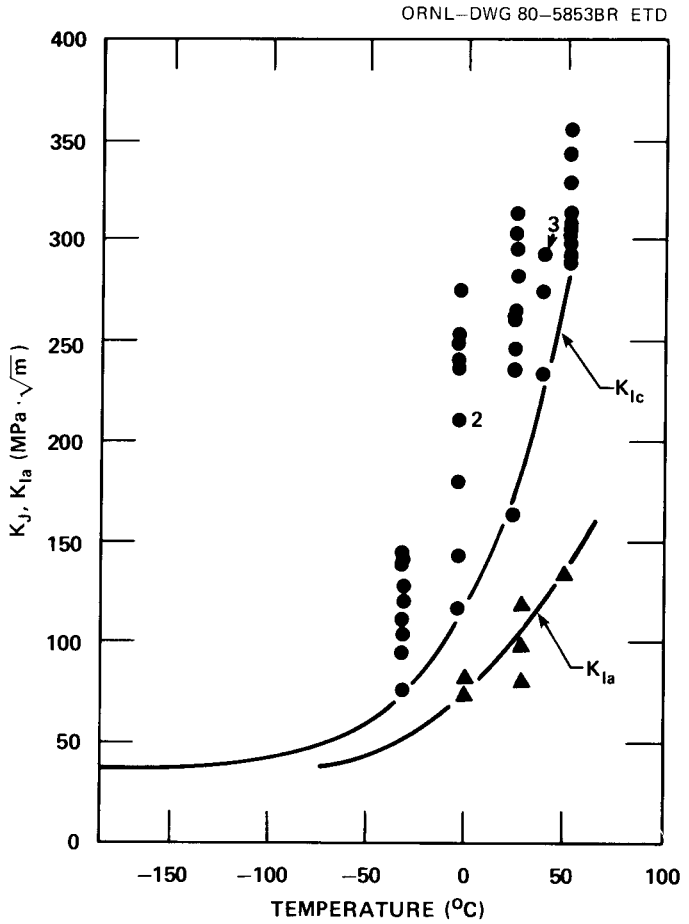

Fig. 4.4. Lower-bound K_J and mean K_{Ia} curves derived from small-specimen data and used in TSE-5A pretest analysis.

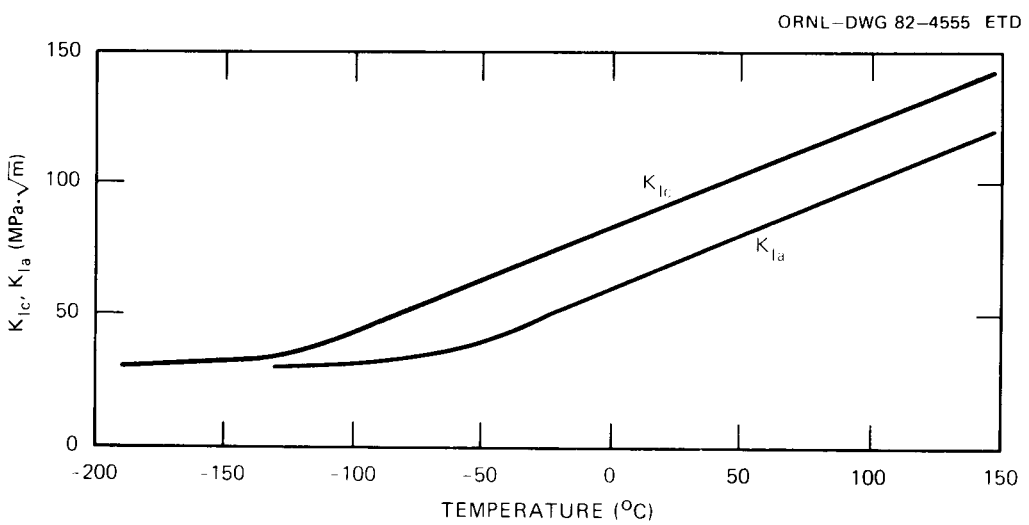

Fig. 4.5. K_{Ic} and K_{Ia} curves deduced from TSE-5 and used in TSE-6 pretest analysis.

4.1.3 Influence of existing forgings on specification of test-cylinder characteristics

At the time TSE-5 was being planned, there were economic and schedule-related reasons for wanting to use a 992-mm-OD × 152-mm-wall × 1.22-m-length A 508 class-2 chemistry test cylinder. Three rough-cut forgings and their prolongations from which test cylinders of these dimensions could be machined and metallurgically characterized were on hand. The preliminary analysis indicated that these forgings would be suitable, and the above dimensions were eventually specified for the final design of TSE-5 and TSE-5A. The TSE-6 test cylinder was the same except it had a thinner wall.

4.1.4 Severity of thermal shock

The objectives of TSE-5, TSE-5A, and TSE-6 required a thermal shock more severe than that used in the earlier thermal-shock experiments.[5] In these earlier experiments an alcohol-water mixture at high velocity and a temperature of −24°C were used for the thermal-shock medium, and the initial temperature of the test specimen was 288°C. The required thermal shocks for TSE-5, TSE-5A, and TSE-6 were achieved using (1) liquid nitrogen as the heat sink (−197°C), (2) a special surface coating to enhance the liquid-nitrogen fluid-film heat transfer coefficient, and (3) a test-cylinder initial temperature of ~93°C. Details regarding the specific thermal-shock technique are discussed in Chap. 6.

4.2 Final Pretest Analysis

4.2.1 TSE-5

Test conditions assumed for the final pretest analysis of TSE-5 are listed in Table 4.1, and the results of the analysis are presented in Figs. 4.6 and 4.7. Figure 4.6 shows a set of critical-crack-depth curves that indicates the expected behavior of the long axial flaw during TSE-5. It includes the initiation curve ($K_I = K_{Ic}$), the arrest curve ($K_I = K_{Ia}$), the warm prestress curve [$K_I = (K_I)_{max}$], and the maximum K-ratio curve [$K_I/K_{Ic} = (K_I/K_{Ic})_{max}$]. Also included in Fig. 4.6 are temperatures corresponding to several points along the initiation curve and several values of $(K_I/K_{Ic})_{max}$ along the maximum K-ratio curve.

The dashed lines in Fig. 4.6 represent the possible behavior of the flaw during TSE-5, assuming $(a/w)_{initial} = 0.10$. If warm prestressing were not effective and if the crack front remained reasonably uniform in depth (retained its two-dimensional nature), it is apparent that the flaw would penetrate ~90% of the wall. However, if warm prestressing were effective, the maximum penetration might be limited to ~56%. Deeper penetration could result, even with warm prestressing effective, if the dashed curve happened to hit the $K_I = K_{Ic}$ curve just below the point of incipient warm prestressing, in which case the penetration would be ~70%. The least penetration would occur when the dashed line hit the $K_I = K_{Ic}$

Table 4.1. Test conditions for TSE-5 pretest analysis

Test cylinder	TSC-1
Test-cylinder dimensions, m	
Outside diameter	0.991
Inside diameter	0.686
Wall thickness	0.152
Length	1.22
Test-cylinder material	A 508 class-2 chemistry
Test-cylinder heat treatment	Tempered at 613°C for 4 h
K_{Ic} and K_{Ia} curves used in TSE-5 final design analyses	ASME Sect. XI, Appendix A RTNDT = −34°C
Flaw (initial)	Long axial sharp crack, a = 15 mm
Temperatures, °C	
Wall (initial)	93
Sink	−196
Fluid-film heat transfer coefficient	h_f vs T curve based on liquid-nigrogen development studies

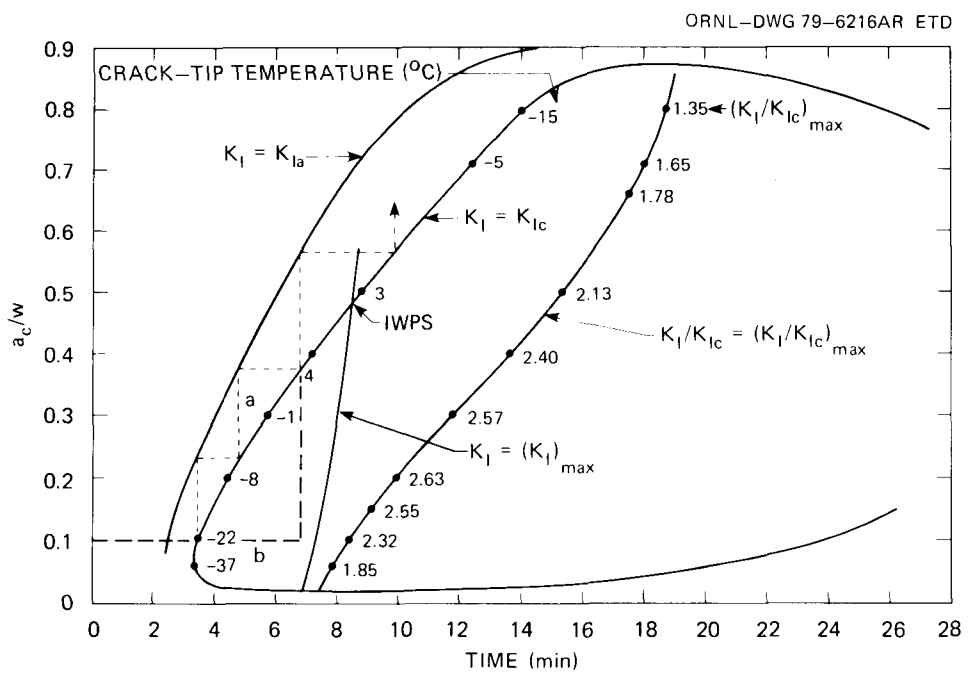

Fig. 4.6. Critical-crack-depth curves for pretest analysis of TSE-5.

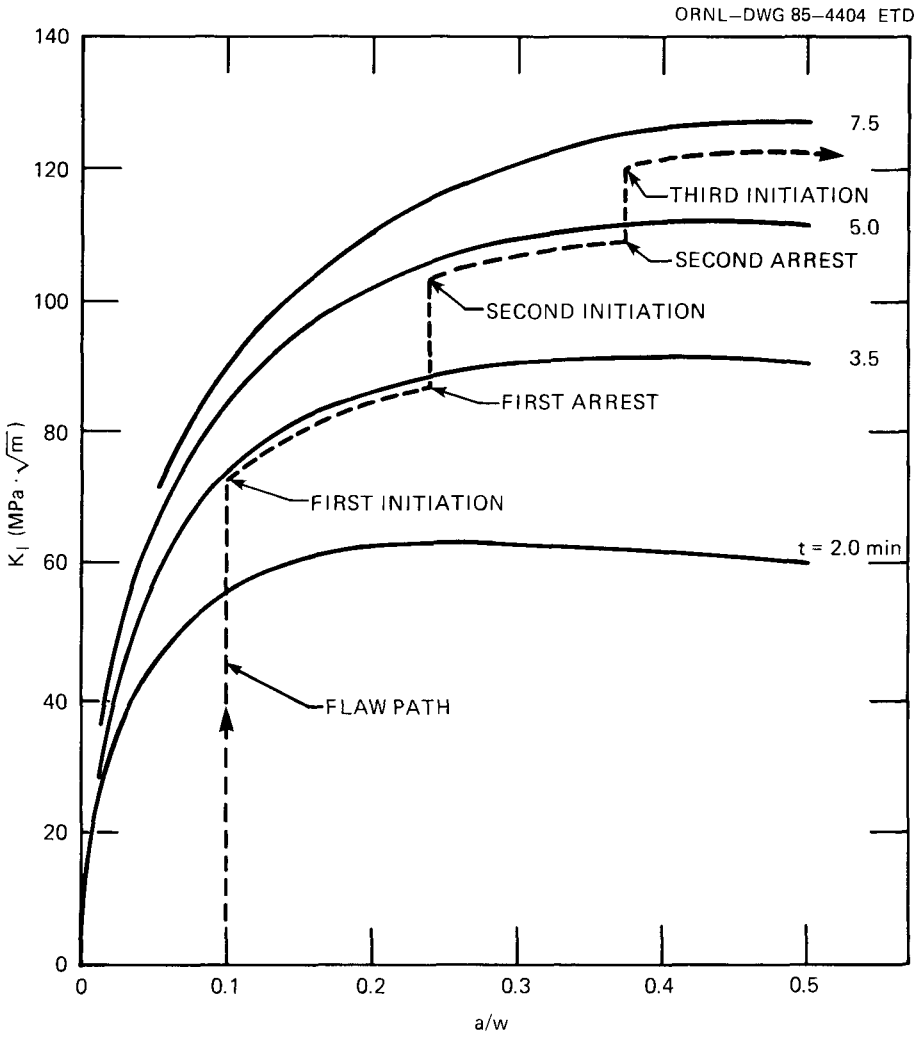

Fig. 4.7. K_I vs a/w for TSE-5 design conditions.

curve just above incipient warm prestressing. For this case the penetration would be limited to ~50%. Thus, the nominal range of predicted final crack depth for TSE-5 was 50 to 70%.

In Fig. 4.6 the area circumscribed by the $K_I = K_{Ic}$ curve and the $K_I = (K_I)_{max}$ curve represents a zone in which flaws with higher-than-anticipated effective toughness could initiate. The result of the higher toughness could be an increase in the crack-jump distance, as illustrated in Fig. 4.6, assuming an initial flaw depth (a/w) of 0.1 and taking the dashed-line path b as opposed to a. In this hypothetical case, crack initiation would be delayed from t = 3.4 min to 6.8 min, and the crack would extend in a single jump from a/w = 0.1 to 0.56 instead of to a/w = 0.23.

It is also of interest to note in Fig. 4.6 that a long crack jump can also be obtained with a very shallow, sharp flaw, that is, with flaw depths represented by the lower portion of the $K_I = K_{Ic}$ curve. Because

of the inadvertent inclusion of such a flaw in TSE-5, this is an important observation.

The $(K_I/K_{Ic})_{max}$ curve in Fig. 4.6 represents a measure of the degree of assurance that K_I will actually become equal to K_{Ic} during the experiment. It is important that this condition exist for the experiment to be successful; that is, initiation of flaws with depths less than that corresponding to incipient warm prestressing must take place. Furthermore, to adequately demonstrate warm prestressing, there must be no doubt that the actual value of $(K_I/K_{Ic})_{max}$ for the final flaw depth is greater than unity. Thus, the nominal calculated value of $(K_I/K_{Ic})_{max}$ must be large enough to accommodate all reasonable uncertainties in this ratio and, thus, result in $(K_I/K_{Ic})_{max} > 1$. For the TSE-5 initial flaw, the nominal calculated value of $(K_I/K_{Ic})_{max}$ was ~2.3, and for the deepest final flaw (a/w = 0.7) it was 1.7. These values were considered to be adequate for TSE-5.

Figure 4.7 is a plot of K_I vs a/w for several values of time in the transient. This type of plot is used to determine whether arrest will take place in a rising K_I field. The predicted path (K_I vs a/w and t) for the first three initiation-arrest events is shown with the dashed lines and is based on data taken from Fig. 4.6. As indicated, the first two initiation-arrest events take place with positive values of $dK_I/d(a/w)$, while the third arrest event takes place with a negative value of $dK_I/d(a/w)$. Thus, the predicted behavior for the first two arrest events is consistent with the objective of demonstrating arrest in a rising K_I field.

It is observed in Fig. 4.7 that the K_I values corresponding to initiation and arrest events are in the range of 70 to 130 MPa$\cdot\sqrt{m}$. As mentioned in Chap. 1, it was hoped that a maximum critical K_I value near 250 MPa$\cdot\sqrt{m}$ could be achieved. With this exception, the results of the final pretest analysis indicated that all of the objectives for TSE-5 could be met.

4.2.2 TSE-5A

Because the scope of TSE-5A was the same as that for TSE-5, the pretest calculated behavior of the long axial flaw for the two experiments was similar. However, there were differences in the assumed thermal transients, toughness curves, and initial flaw depths, and these differences resulted in somewhat different calculated behaviors for the flaws.

Test conditions assumed and/or specified for TSE-5A are shown in Table 4.2 and include a thermal transient equal to that actually achieved during TSE-5 (more severe than used in the TSE-5 pretest analysis), toughness curves based on very extensive material-characterization studies (lower-bound K_J and mean K_{Ia}), and an initial crack depth (a/w) equal to 0.075 as compared with 0.10 for TSE-5.

Results of the final pretest analysis for TSE-5A are shown in Fig. 4.8. As indicated by this set of critical-crack-depth curves, the flaw would penetrate deeper than 90% of the wall without warm prestressing but only 45 to 65% with warm prestressing. The range of $(K_I/K_{Ic})_{max}$ for the latter range of final crack depths is 2.2 to 1.7, and, thus, presumably

Table 4.2. Test conditions for TSE-5A pretest analysis

Test cylinder	TSC-2
Test-cylinder dimensions, m	
Outside diameter	0.991
Inside diameter	0.686
Wall thickness	0.152
Length	1.22
Test-cylinder material	A 508 class-2 chemistry
Test-cylinder heat treatment	Tempered at 679°C for 4 h
K_{Ic} and K_{Ia} curves used in design	Lower-bound K_J and mean K_{Ia} data from ORNL and BCL TSE-5A material-characterization studies (see Fig. 4.4)
Flaw (initial)	Long axial sharp crack, a = 11 mm
Temperatures, °C	
Wall (initial)	93
Sink	−196
Fluid-film heat transfer coefficient	h_f vs T curve from TSE-5

an adequate demonstration of warm prestressing could be achieved. Assuming warm prestressing to be effective, there would be four initiation-arrest events, and the longest crack jump ($\Delta a/w$) would be the last and equal to 0.20.

Figure 4.8 includes a curve referred to as $K_I = (K_I)_{max(a/w)}$, which represents the crack depth for which $dK_I/da = 0$ for different times in the transient. If arrest takes place at a depth less than that corresponding to the $K_I = (K_I)_{max(a/w)}$ curve, it will do so in a rising K_I field. Thus, according to the pretest analysis, the first two arrest events would take place in a rising K_I field.

Another point of interest illustrated in Fig 4.8 is that the K_I values corresponding to initiation and arrest events cover a range from ~70 to 140 MPa•$\sqrt{m}$, that is, the lower to midtransition region. This range is similar to that calculated for some PWR large-break loss-of-coolant accident cases, but the maximum value is still less than desired (250 MPa•$\sqrt{m}$). With this exception, the results of the final pretest analysis indicated that the objectives of TSE-5A could be met.

4.2.3 TSE-6

A long crack jump with arrest deep in the wall was specified for TSE-6. To achieve this without the initial flaw having to be very shallow or blunted, it was necessary to use a thinner wall (76 mm) for TSE-6

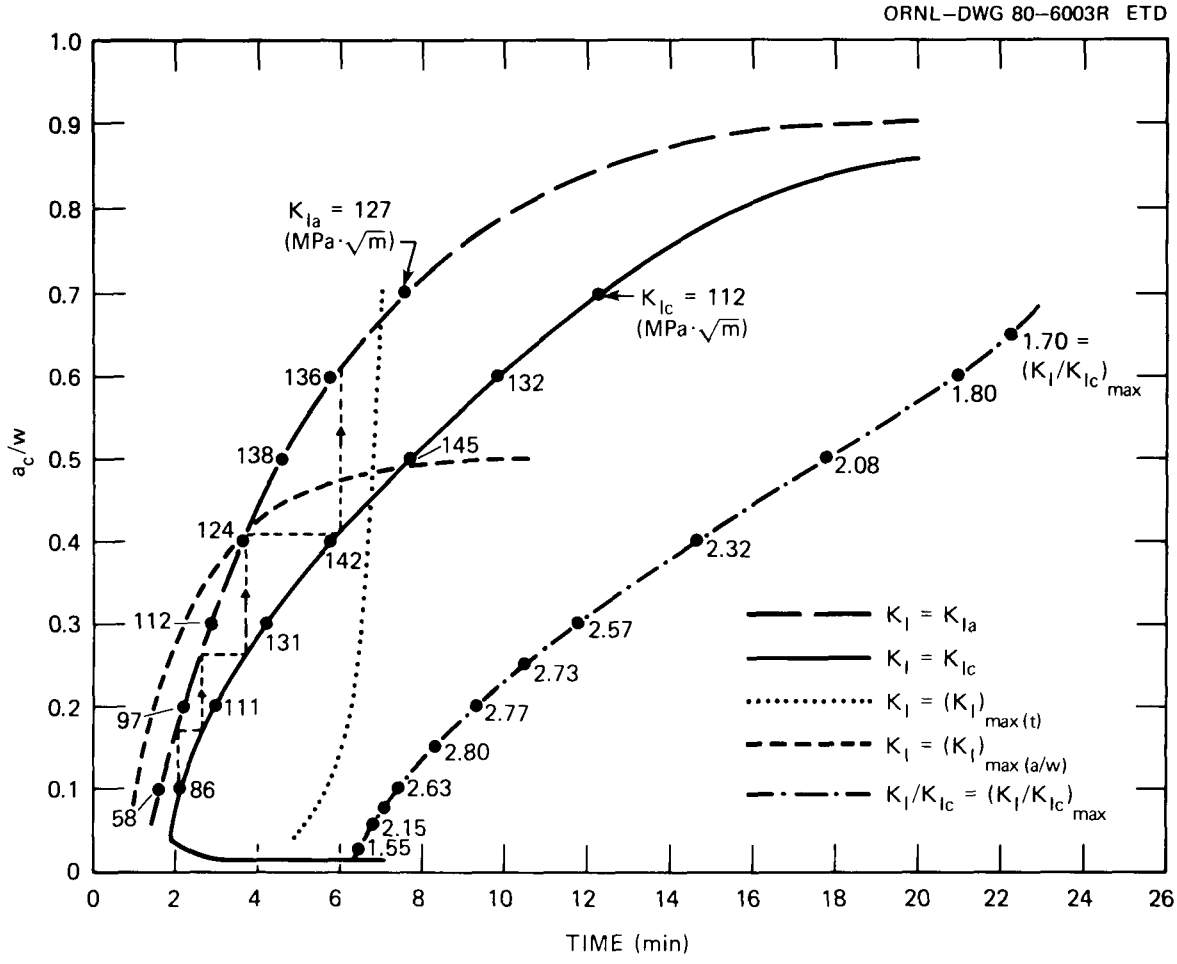

Fig. 4.8. Pretest critical-crack-depth curves for TSE-5A assuming TSE-5 thermal transient and TSE-5A lower-bound K_{IJ} and mean K_{Ia} curves.

than that used for the TSE-5 and TSE-5A test cylinders (152 mm) and to use the same low fracture-toughness properties actually obtained for the TSE-5 test cylinder (see Table 4.3 for test conditions used in pretest analysis). This combination resulted in a set of calculated critical-crack-depth curves with nearly vertical sections of the initiation and arrest curves (Fig. 4.9). The dashed lines in Fig. 4.9 represent the expected behavior of the flaw and indicate a single long crack jump from a/w = 0.1 (initial flaw) to a/w = 0.95. Reinitiation would not be likely because of warm prestressing or $(K_I/K_{Ic})_{max} < 1$. For the initial flaw, $(K_I/K_{Ic})_{wps} = 1.36$, which was large enough to ensure initiation prior to warm prestressing. Furthermore, K_I values all along the initiation and arrest curves were below upper-shelf toughness values.

The expected inability of the flaw to completely penetrate the wall under thermal-shock loading conditions only is illustrated in Fig. 4.10,

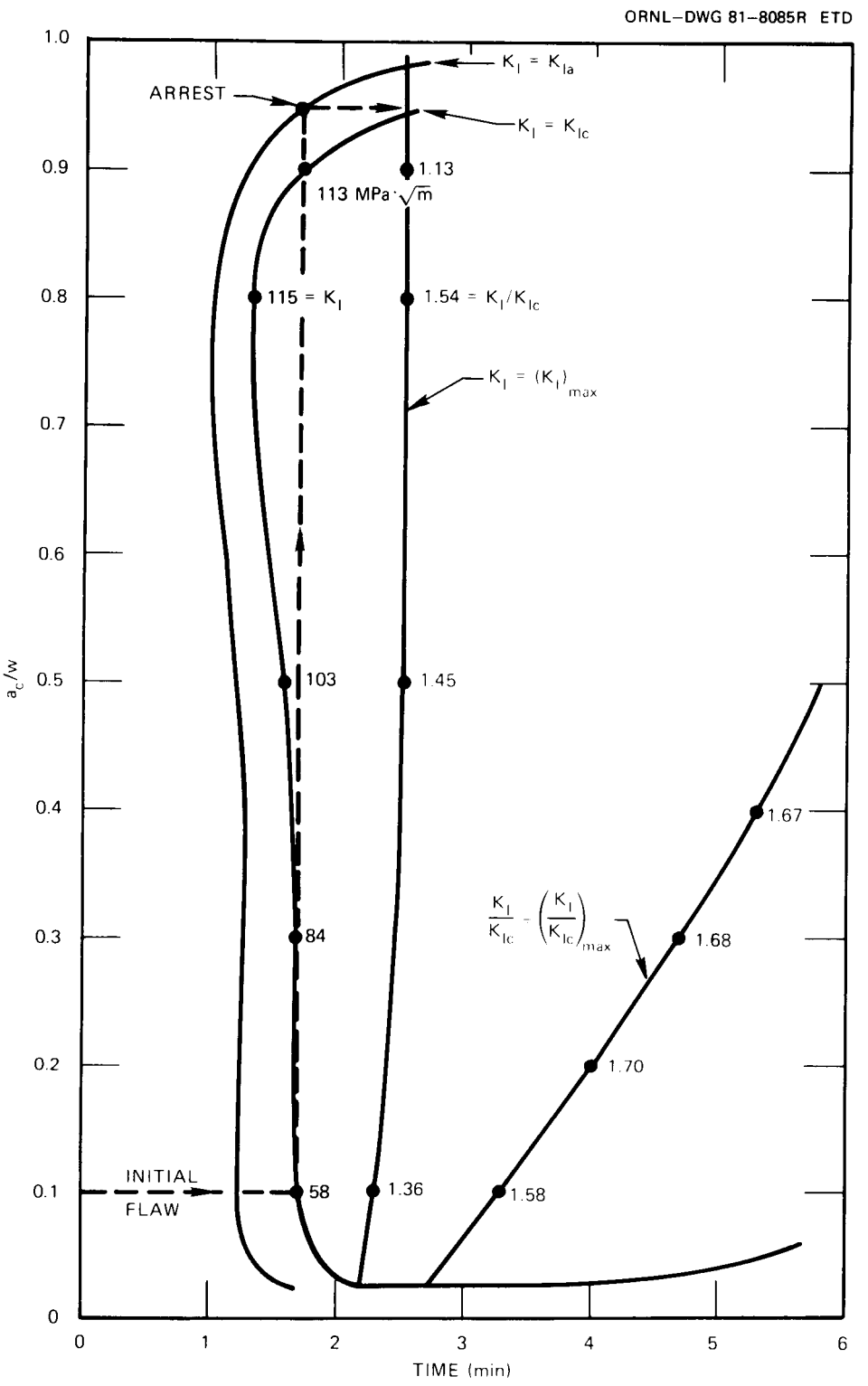

Fig. 4.9. Pretest critical-crack-depth curves for TSE-6.

Table 4.3. Test conditions for TSE-6 pretest analysis

Test cylinder	TSC-3
Test-cylinder dimensions, m	
Outside diameter	0.991
Inside diameter	0.838
Wall thickness	0.076
Length	1.22
Test-cylinder material	A 508 class-2 chemistry
Test-cylinder heat treatment	Tempered at 613°C for 4 h
K_{Ic} and K_{Ia} curves used in design	Toughness curves deduced from TSE-5 (see Fig. 4.5)
Flaw (initial)	Long axial sharp crack, a = 7.6 mm
Temperatures, °C	
Wall (initial)	93
Sink	−196
Fluid-film heat transfer coefficient	h_f vs T_s deduced from TSE-5A

which is a plot of K_I and K_{Ia} vs a/w at approximately the predicted time of crack propagation ($t \approx 1.7$ min). This figure shows the tendency for a steep negative gradient in K_I near the outside surface, with K_I dropping below K_{Ia}. This tendency for linear-elastic fracture mechanics to predict that K_I will approach zero is the result of (1) a limited extent of crack-surface rotation associated with the net thermal bending moment, (2) the resistance of the cylinder wall to bending, and (3) a compressive load on the free-body remaining ligament (see Fig. 4.11). As the crack tip approaches the back surface, the crack-surface rotation and the compressive load approach their maximum values, while the bending moment at the ligament approaches zero. The result is a substantial compressive-stress component in the ligament, and, thus, presumably the crack could not completely penetrate the wall.

The resistance of the wall to bending decreases with an increase in the ratio of cylinder radius to wall thickness (r/w). As shown in Table 4.4, the ratio is much larger for a typical PWR vessel than it is for the thermal-shock test cylinders. Thus, there is a greater tendency for deep propagation of a flaw in the PWR vessels than in the test cylinders. However, a linear-elastic fracture-mechanics analysis of the PWR vessel indicates that for this case, too, a long axial flaw could not fully penetrate the wall under thermal-shock loading only (see Chap. 1). Thus, if during TSE-6 the flaw did not breach the wall, this would be considered an adequate demonstration.

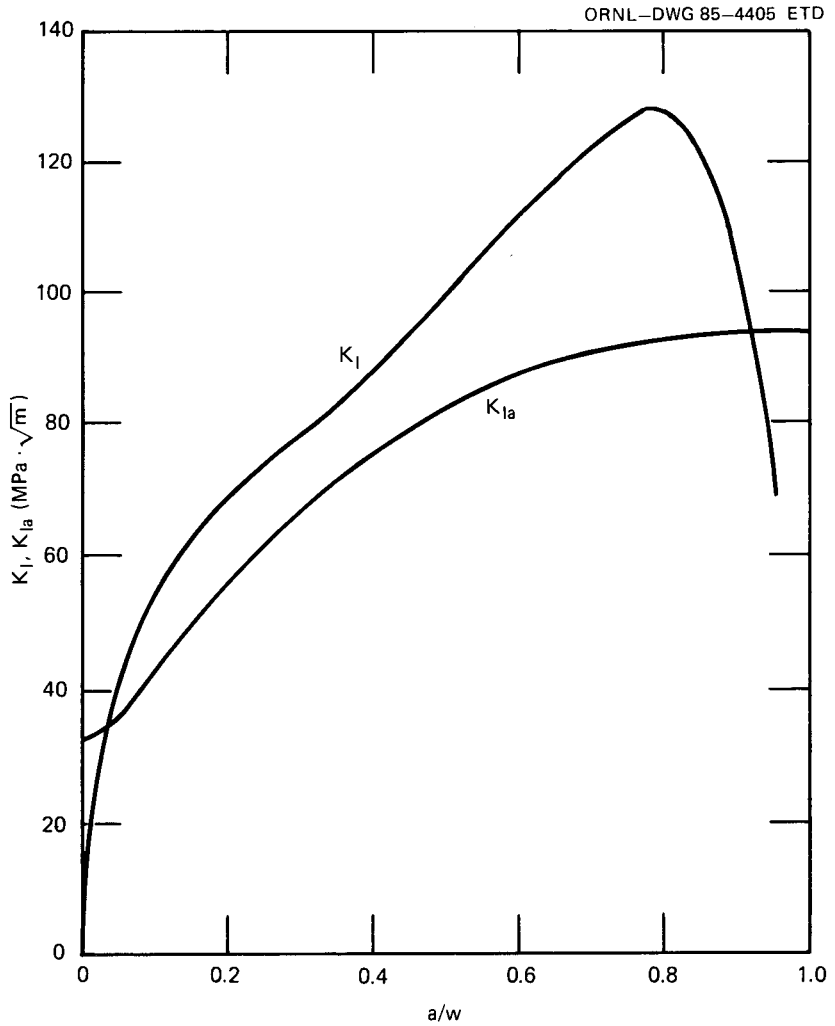

Fig. 4.10. K_I and K_{Ia} vs a/w for TSE-6 at t = 1.5 min (pretest analysis).

Table 4.4. Comparison of radius-to-wall thickness ratios for PWR vessels and ORNL thermal-shock test cylinders

Cylinder	r_i/w^a
PWR vessel	2180/216 = 10
Test cylinders	
TSE-6	419/76 = 5.5
TSE-5, TSE-5A	346/152 = 2.3
TSE-1, TSE-2, TSE-3, TSE-4	114/152 = 0.8

[a]Inside radius (r_i)/wall thickness (w), dimensions in millimeters.

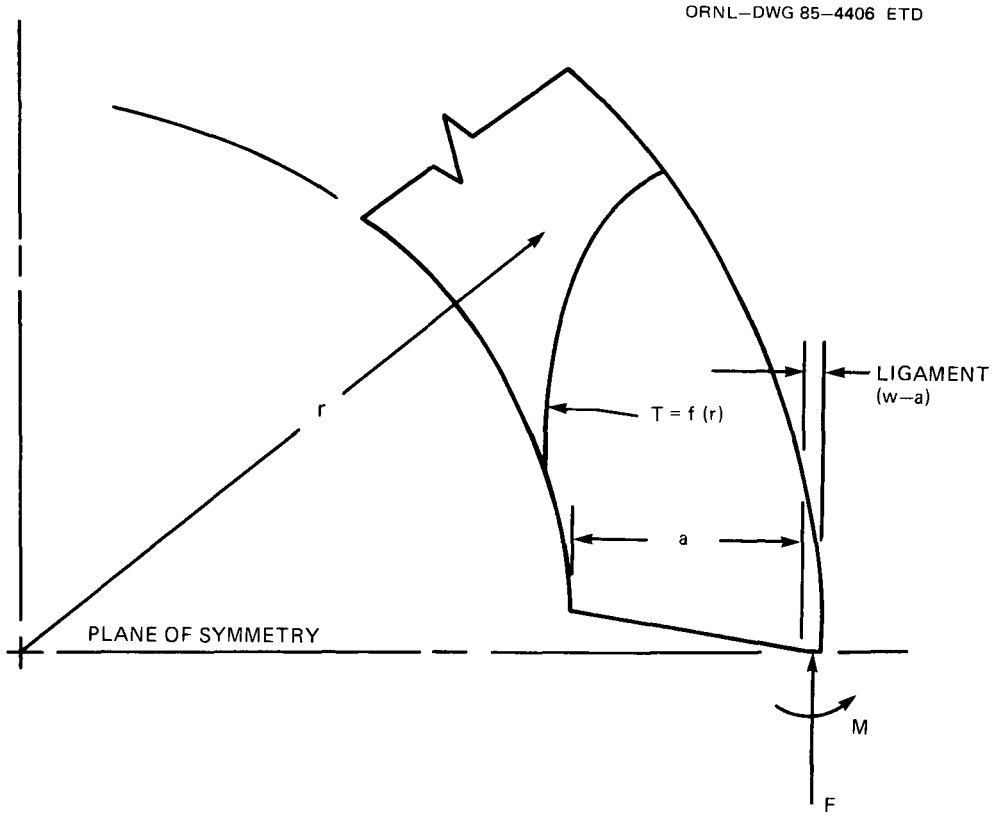

Fig. 4.11. Compressive force and bending moment applied to ligament beyond tip of deep inner-surface long axial flaw during thermal shock to inner surface.

References

1. R. D. Cheverton, *Pressure Vessel Fracture Studies Pertaining to a PWR LOCA-ECC Thermal Shock: Experiments TSE-1 and TSE-2*, ORNL/TM-31, Union Carbide Corp. Nuclear Div., Oak Ridge Natl. Lab., September 1976.

2. H. Corten, University of Illinois (consultant to HSSTP), personal communication to R. D. Cheverton, Oak Ridge Natl. Lab., Oak Ridge, Tenn., September 1974.

3. G. R. Irwin, "Linear Fracture Mechanics, Fracture Transition, and Fracture Control," *Eng. Fract. Mech.*, 1(2), 241–57 (August 1968).

4. S. Timoshenko, *Theory of Plates and Shells*, McGraw-Hill, New York, 1970, p. 397.

5. R. D. Cheverton and S. E. Bolt, *Pressure Vessel Fracture Studies Pertaining to a PWR LOCA-ECC Thermal Shock: Experiments TSE-3 and TSE-4 and Update of TSE-1 and TSE-2 Analysis*, ORNL/NUREG-22, Union Carbide Corp. Nuclear Div., Oak Ridge Natl. Lab., December 1977.

6. W. O. Shabbits et al., *Heavy-Section Steel Technology Program Technical Report No. 6, Heavy-Section Fracture Toughness Properties of A533 Grade B Class 1 Steel Plate and Submerged-Arc Weldment*, WCAP-7414, Westinghouse Electric Corporation, Pittsburgh, Pa., December 1969.

7. T. U. Marston, ed., *Flaw Evaluation Procedures, ASME Section XI, Background and Application of ASME Section XI, Appendix A, Special Report*, EPRI NP-719-SR, American Society of Mechanical Engineers, New York, Electric Power Research Institute, Palo Alto, Calif., August 1978.

5. TEST-CYLINDER FABRICATION DETAILS AND ASSEMBLY

5.1 Test-Cylinder Configuration and Dimensions

Dimensional details for the test cylinders used for TSE-5, TSE-5A, and TSE-6 are shown in Fig. 5.1, and the rationale for selecting the particular dimensions for the test cylinders is discussed in Chap. 4. The complete test-cylinder assembly, including instrumentation attached thereto, is discussed in Chap. 6.

5.2 Test-Cylinder Fabrication and Heat Treatment

The three test cylinders used for TSE-5, TSE-5A, and TSE-6 and prolongations of these cylinders that were used for characterizing the material were taken from the same forging (Fig. 5.2). Prior to heat treating, the original, single, long forging was rough machined and divided into three cylinders, each having sufficient length for a test cylinder and its prolongation. The heat treatment applied before shipment of the oversized cylinders to ORNL consisted of normalizing at 930°C for 8 h, austenitizing at 860°C for 9 h, and quenching in water at ~10°C. After the test cylinders and prolongations were received at ORNL, the test cylinders were machined to final dimensions and were then subjected to a tempering heat treatment. For TSE-5 and TSE-6, the tempering temperature was 613°C, and for TSE-5A it was 679°C. The hold time at these temperatures was 4 h, and subsequent cooling was in room-temperature air.

As indicated in Fig. 5.2, the test cylinders were oversized for the initial portion of the heat treatment. This was done for two reasons: (1) the quench-in-water treatment results in very high residual compressive stresses near the surface (Fig. 5.3) and (2) the gradient in quench rate normal to the surface results in a significant gradient in fracture toughness, even after tempering[1] (Fig. 5.4). Both of these conditions were undesirable for the thermal-shock experiments and were essentially eliminated by removing appropriate amounts of material from the cylindrical and end surfaces, following the quench-in-water treatment. Residual stresses were measured in the prolongations prior to the thermal-shock experiments to confirm that they were negligible once the final radial dimensions for the test cylinder were achieved. Also, Charpy specimens were used to confirm the absence of significant radial gradients in fracture toughness.

5.3 Test-Cylinder Material

The type of material specified for the test cylinders was SA 508 with class-2 chemistry. The actual chemistry is shown in Table 5.1.

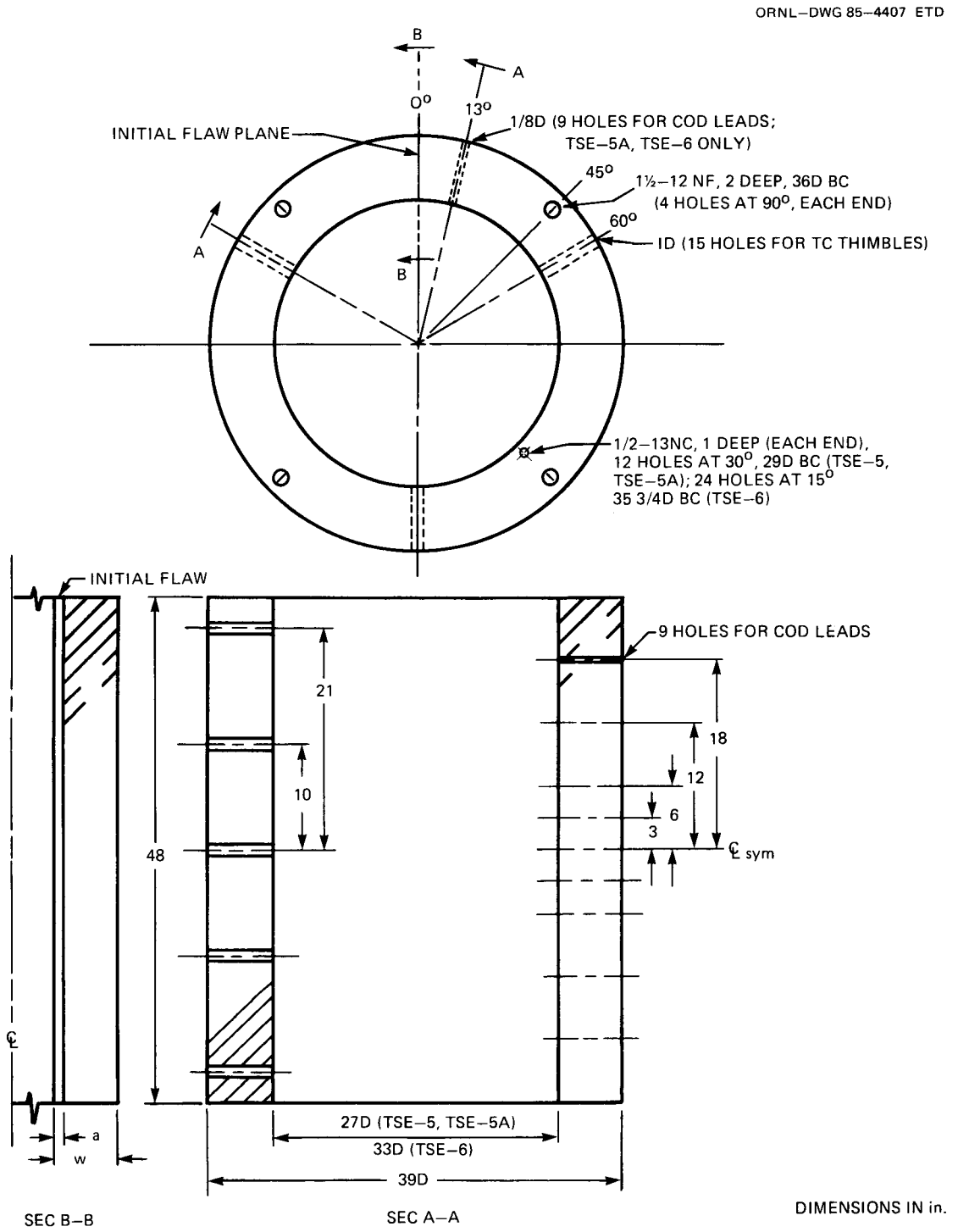

Fig. 5.1. Dimensional details for TSE-5, TSE-5A, and TSE-6 test cylinders.

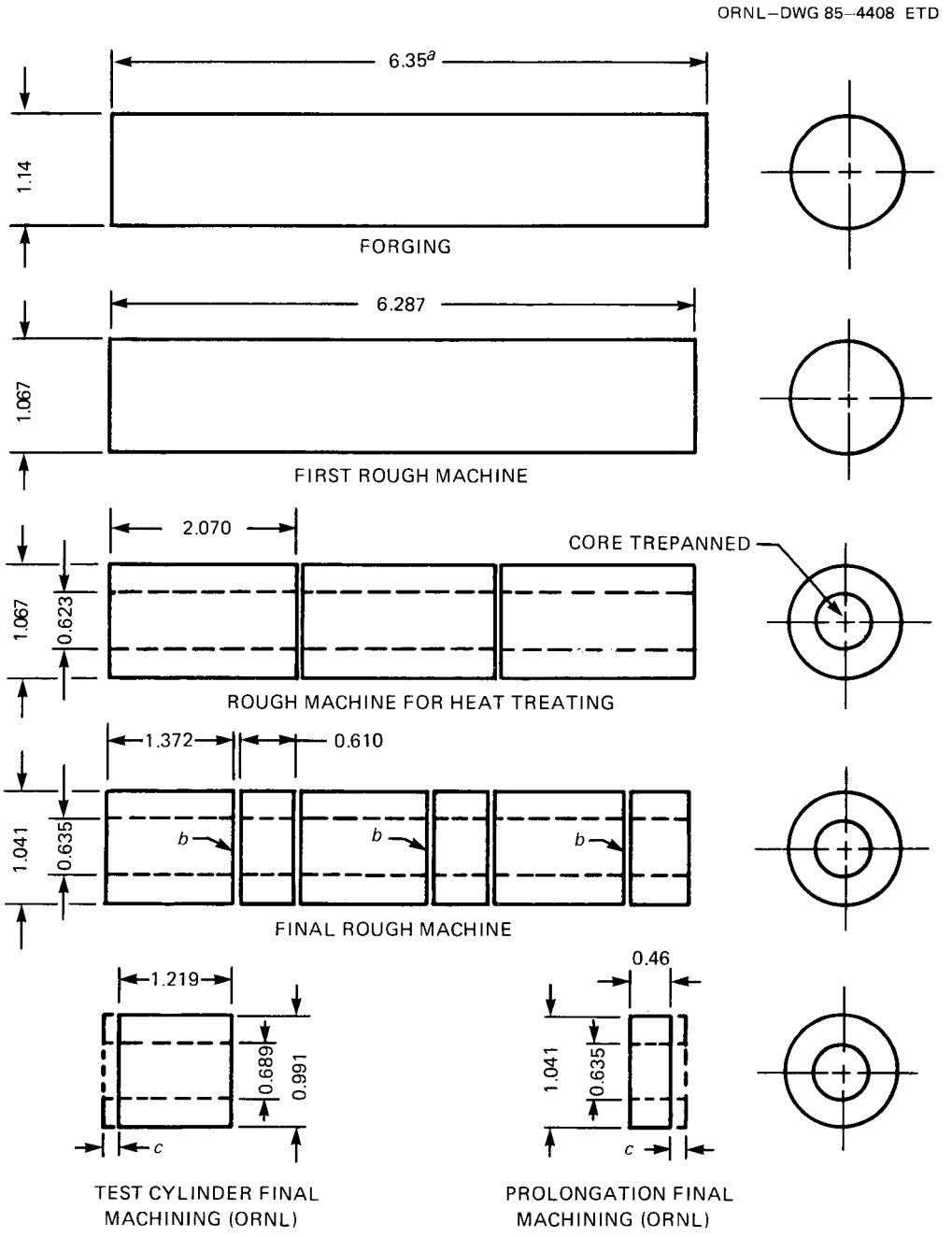

[a]DIMENSIONS IN m
[b]THESE ADJACENT SURFACES MARKED "ADJ FACES"
[c]EXCESS (~0.15) REMOVED FROM THIS END FOR EACH TEST CYLINDER AND PROLONGATION

Fig. 5.2. Steps in fabrication of TSE-5, TSE-5A, and TSE-6 test cylinders and prolongations.

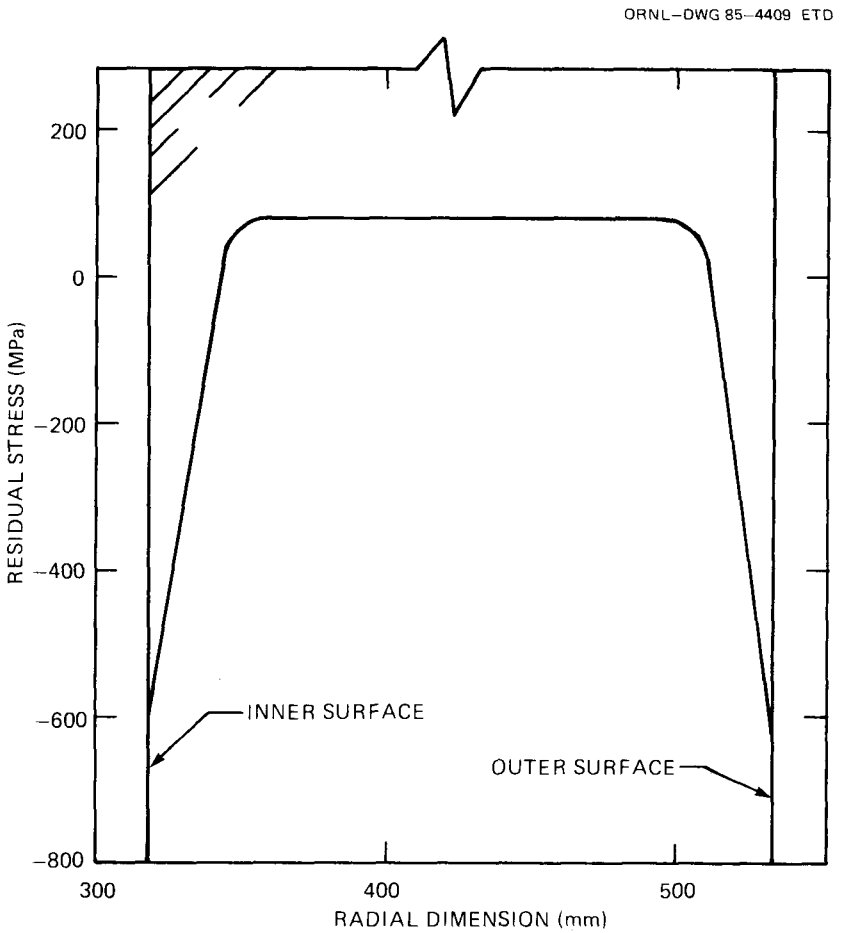

Fig. 5.3. Approximate residual stresses in test-cylinder wall as a result of quench-only heat treatment.

Table 5.1. Chemical composition for TSE-5, TSE-5A, and TSE-6 test cylinders

	Composition (wt %)								
	C	Mn	P	S	Si	Cr	Ni	Mo	V
Heat analysis[a]	0.23	0.77	0.008	0.006	0.27	0.39	0.81	0.63	0.63
Check analysis									
Top	0.23	0.79	0.009	0.006	0.28	0.41	0.82	0.63	0.63
Bottom	0.18	0.76	0.007	0.004	0.29	0.40	0.79	0.63	0.03
ASME specification SA 508 class 2[b]	0.27	0.50 / 1.00	0.012	0.015	0.15 / 0.40	0.25 / 0.45	0.50 / 1.00	0.55 / 0.70	0.05

[a]National Forge Heat 41-5655.

[b]Single values are maximum.

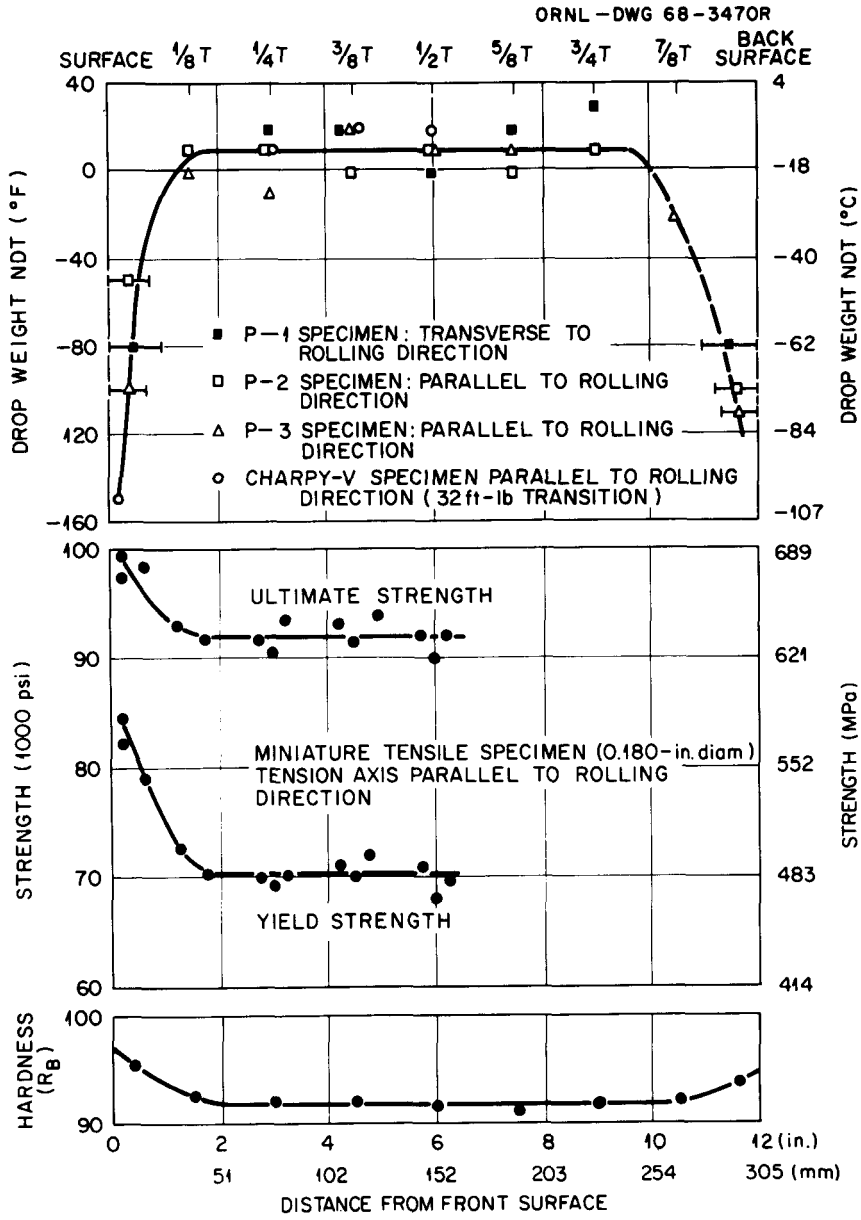

Fig. 5.4. Variation with depth in plate of representative mechanical properties for central region of a 3.05-m × 6.10-m × 305-mm plate of ASTM A 533 grade B class 1 steel.

5.4 Generation of Initial Flaw

The initial flaws for TSE-5, TSE-5A, and TSE-6 were sharp, uniform-depth cracks that were oriented in the longitudinal (axial) direction and extended the full length of the test cylinder (Fig. 5.1). Each flaw was generated by means of the electron-beam (EB)-weld technique, which is discussed in detail in Refs. 2 and 3. A typical setup of a test cylinder in the EB-weld vacuum box is shown in Fig. 5.5.

ORNL PHOTO 7426–79R

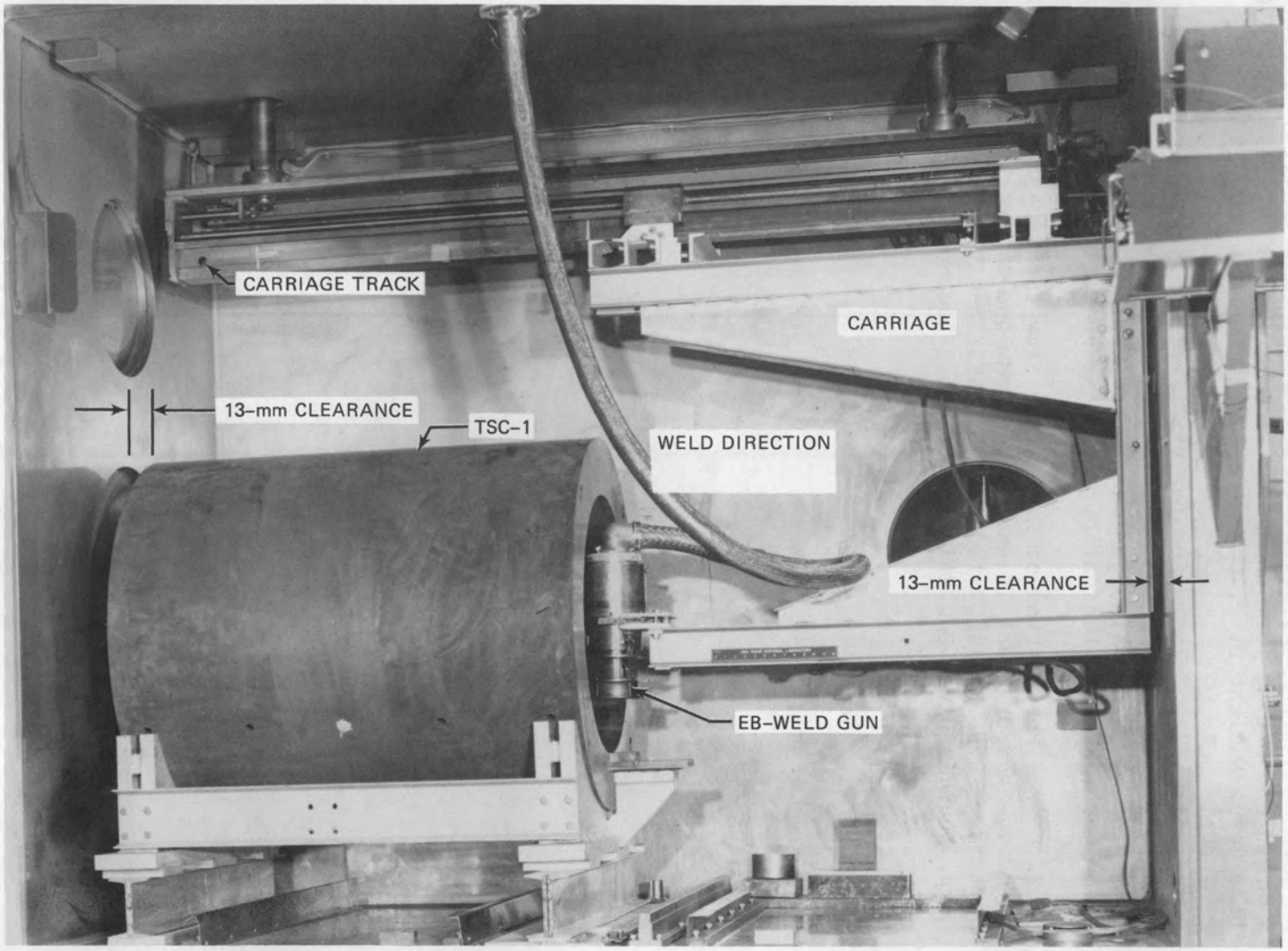

Fig. 5.5. Typical setup of test cylinder in EB-weld vacuum box in preparation for generation of axial flaw.

References

1. D. A. Canonico et al., *Assessment of Materials Technology of Pressure Vessels and Piping for Coal Conversion Systems*, ORNL-5238, Union Carbide Corp. Nuclear Div., Oak Ridge Natl. Lab., August 1978.

2. P. P. Holz, *Flaw Preparation for HSST Program Vessel Fracture Mechanics Testing; Mechanical-Cyclic Pumping and Electron-Beam Weld-Hydrogen Charge Cracking Schemes*, NUREG/CR-1274 (ORNL/NUREG/TM-369), Union Carbide Corp. Nuclear Div., Oak Ridge Natl. Lab., May 1980.

3. P. P. Holz, "Preparation of Long Axial Flaw for TSE-5A," pp. 35–37 in *Heavy-Section Steel Technology Program Quart. Prog. Rep. July–September 1980*, NUREG/CR-1806 (ORNL/NUREG/TM-419), Union Carbide Corp. Nuclear Div., Oak Ridge Natl. Lab., December 1980.

6. EXPERIMENTAL TECHNIQUE, EQUIPMENT, AND INSTRUMENTATION

6.1 Technique for Achieving Thermal Shock

The required severe thermal shock for TSE-5, TSE-5A, and TSE-6 was achieved by heating the test specimen to a specified elevated temperature (~93°C) and then exposing the inner surface of the test cylinder to liquid nitrogen. Required high heat transfer rates were achieved by applying a thin coating of rubber cement to the inner surface.[1-10] The presence of this coating suppresses film boiling, which has a rather low heat transfer coefficient, and promotes nucleate boiling, which has a relatively high heat transfer coefficient. The heat transfer coefficient so obtained is a function of surface temperature (Fig. 6.1), and, within limits, the desired h vs temperature curve can be achieved through proper selection of coating thickness and the surface density of nucleation sites on the coating. Removal of nitrogen vapor from the vicinity of the surface was assisted by natural convection of the coolant through the central cavity of the cylinder.

Quenching of the test cylinder in liquid nitrogen was accomplished by effectively dunking the test cylinder in a large tank containing ~4500 L of liquid nitrogen. A schematic of the test facility is shown in Fig. 6.2, and a photograph of a test-cylinder assembly being lowered into the tank is shown in Fig. 6.3.

The outer surface and ends of the test cylinder were insulated to prevent significant heat removal from these surfaces during the thermal-shock experiment and also during the heating operation that preceded the dunk. Granular material (Vermiculite) was used for the insulation, and as shown in Fig. 6.2 it filled the annular space between the test cylinder and a surrounding lightweight steel jacket. A slight overpressure of nitrogen gas was applied to the annular space during the experiment to prevent in-leakage of cold nitrogen.

The actual dunking operation consisted of lowering the test specimen with the building overhead crane to a submerged position in the tank. During this operation, a top cover plate (Fig. 6.2) sealed the upper opening in the test cylinder and thereby trapped a gas bubble within the cavity. The bubble was fed from an external source of nitrogen gas to compensate for decreasing gas temperatures and increasing head (pressure) as the test-cylinder assembly was lowered into the liquid nitrogen. By this means, the liquid nitrogen was kept out of the test-cylinder cavity until the cylinder was fully submerged. Upon suddenly raising the top cover plate (with a pneumatic cylinder), the cavity flooded rapidly, and a natural-convection loop was established up through the central cavity and down around the exterior of the test-cylinder assembly. Nitrogen vapor escaped through the top of the tank, and liquid nitrogen makeup was provided as required through an opening in the bottom of the tank. Using this procedure and technique, it was possible to obtain a very uniform quench over the inner surface.

Prior to each of the three thermal-shock experiments (TSE-5, TSE-5A, and TSE-6) the respective test cylinders, unflawed, were subjected to a

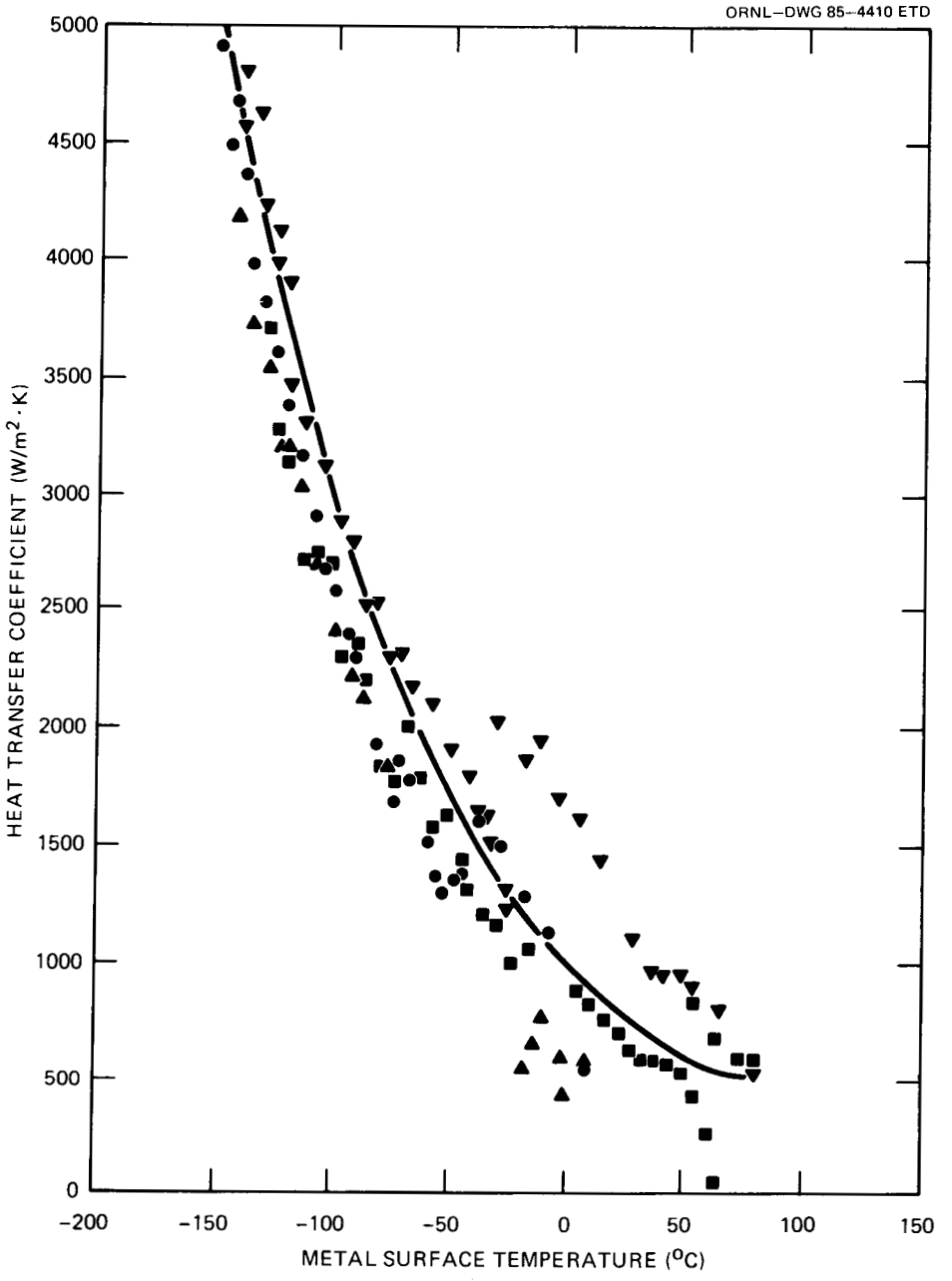

Fig. 6.1. Heat transfer coefficients deduced from thermal-shock experiments conducted as a part of surface-coating development effort.

thermal shock in the test facility to check on the adequacy of the inner-surface coating in terms of providing the desired temperature distributions in the wall. For these tests the cylinders were equipped with a full array of thermocouples for measuring the temperature distributions in the wall, and they were in the quench-only heat-treated condition to prevent yielding at the inner surface.

Following these tests, the coating was removed from the inner surface of the cylinder, and the cylinder was given an appropriate tempering

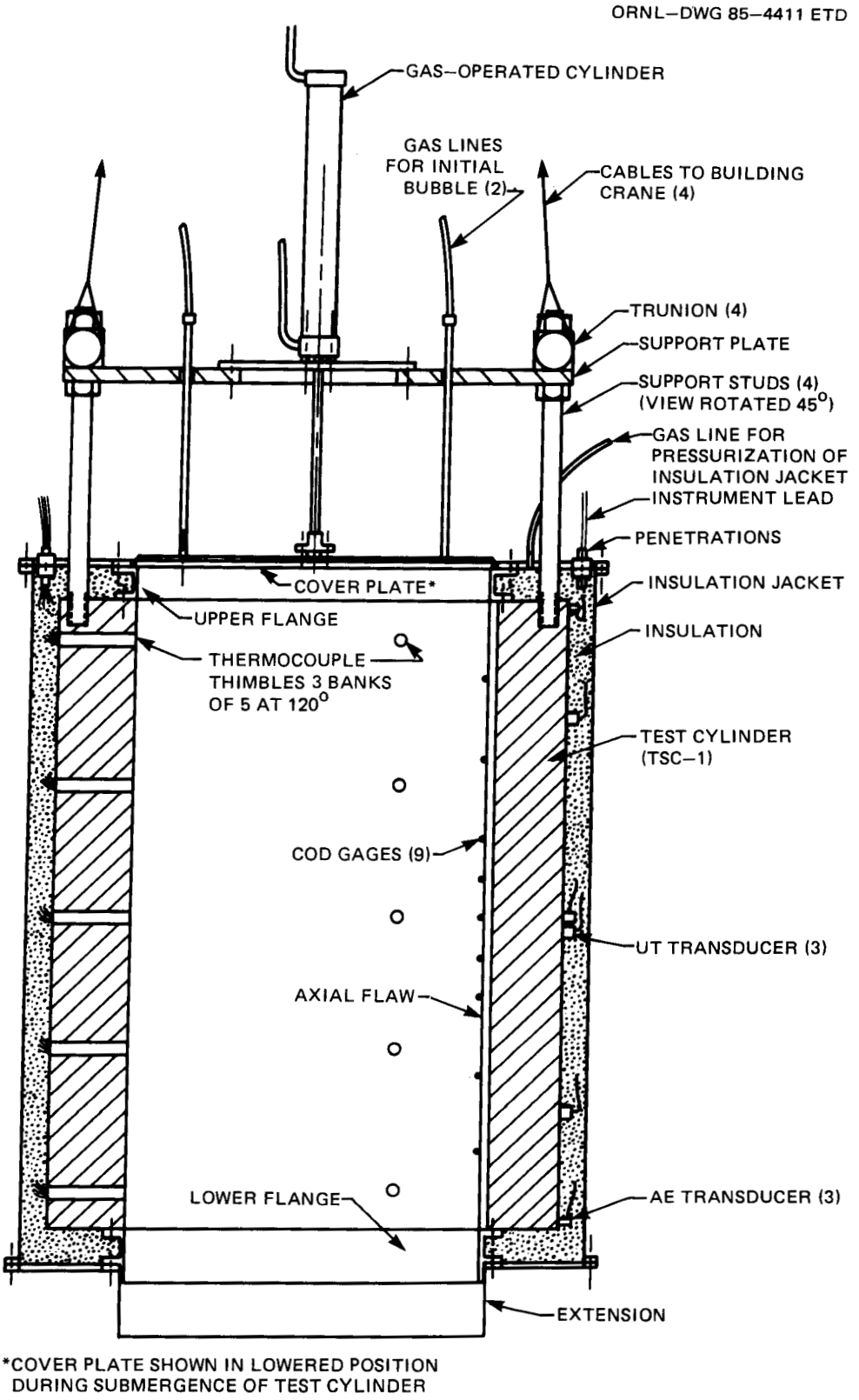

Fig. 6.2. Test-cylinder assembly for TSE-5.

ORNL PHOTO 7165–79A

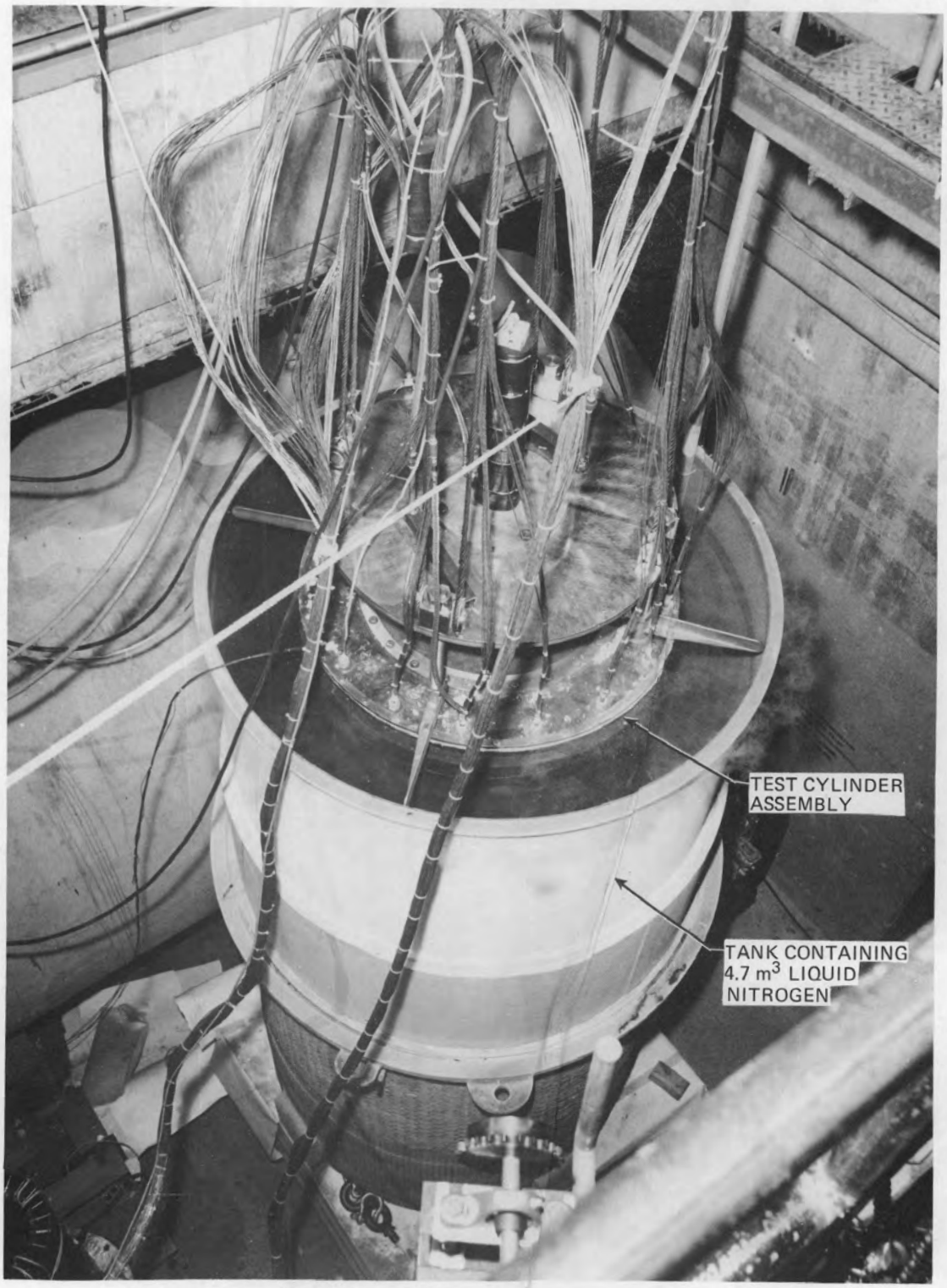

Fig. 6.3. HSST thermal-shock test facility, showing test-cylinder assembly just prior to its submergence in liquid nitrogen.

heat treatment. When the new inner-surface coating was then applied, adjustments in the coating were made, if necessary, based on the results of the previous experiment.

6.2 Heating of Test Cylinder Prior to Thermal Shock

Prior to dunking the test cylinder in the liquid nitrogen, the cylinder was heated slowly over a 24-h period to its desired initial temperature (~93°C). This was done after the inner-surface coating was applied and with the test cylinder completely assembled with the outer insulating jacket, the pneumatically operated top cover plate, and all instrumentation. Heat was applied to the inner surface by means of a forced-air bayonet-type heater that entered the central cavity through the bottom end, as shown schematically in Fig. 6.4. The heating rate was such that the temperature difference through the wall did not exceed 15°C, thus limiting the thermal stress to ~25 MPa. To protect the rubber-cement coating, the temperature of the outer surface of the heater and of the circulating air was not allowed to exceed 150°C.

At the completion of the heating operation, the test-cylinder assembly was lifted off of the heater and immediately transferred to the liquid nitrogen tank. The heater station was located adjacent to the liquid nitrogen tank to minimize transfer time and the length of the instrumentation cables. All instrumentation and other leads were permanently connected prior to heating the cylinder.

6.3 Data Acquisition

Experimental data collected from the TSE-5, TSE-5A, and TSE-6 test cylinders during the thermal-shock experiments included (1) temperature distributions through the wall, (2) crack-opening displacement (COD) at the inner surface of the test cylinder, (3) crack-opening rate during a crack jump, (4) crack depth, and (5) indications of crack-initiation and arrest events, all as a function of time in the thermal-shock transient. The measured temperature distributions were used as thermal-loading inputs to the posttest fracture-mechanics analysis. Knowing the times at which initiation-arrest events took place and the corresponding crack depths, it was then possible to determine K_I values corresponding to the initiation and arrest events.

Temperature gradients in the wall of the test cylinder were measured at 15 different locations around and along the length of the test cylinder to check on the spatial uniformity of quenching. At each of the 15 locations, 10 (TSE-6) or 12 (TSE-5 and TSE-5A) thermocouples, incorporated in a special thermocouple thimble, were used to measure the temperatures and temperature gradient in the wall. The 180 thermocouples were scanned at the rate of 10^4 s^{-1}, and complete sets of output were recorded on tape every 2 s for the duration of the experiment. Locations of the thermocouple thimbles are shown in Figs. 6.5–6.7, and design details of the thimbles are given in Appendix A.

ORNL–DWG 85–4412 ETD

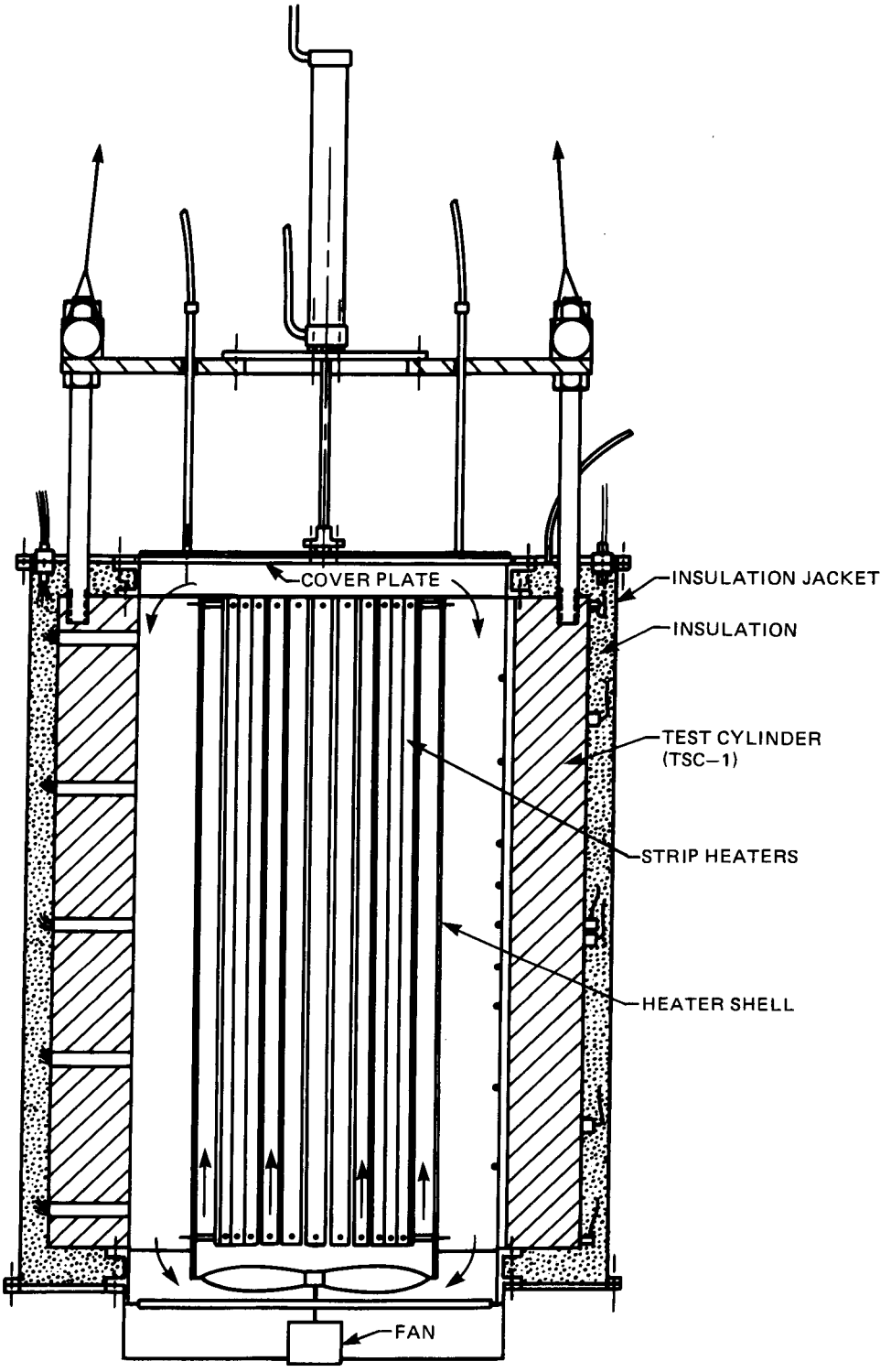

Fig. 6.4. Test-cylinder assembly positioned on heater.

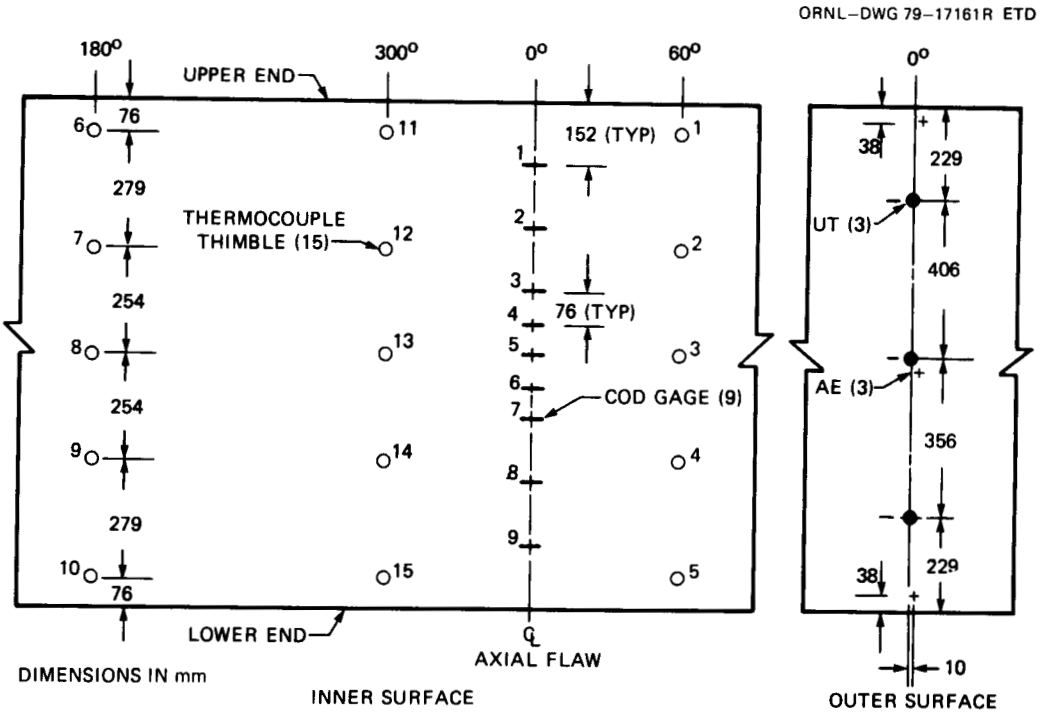

Fig. 6.5. Developed views of TSE-5 test cylinder showing locations of instrumentation.

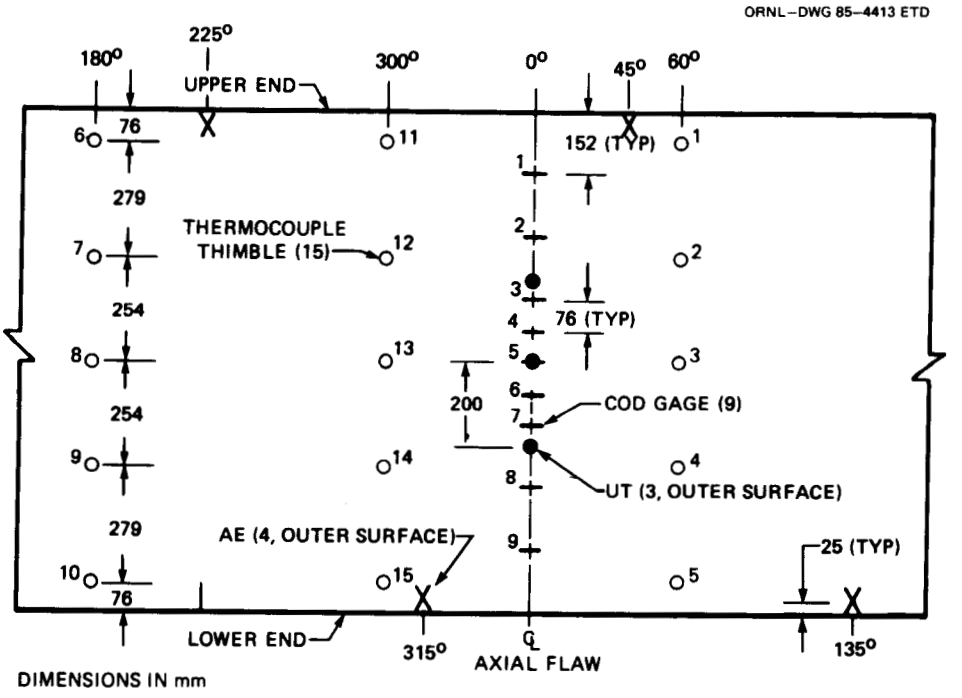

Fig. 6.6. Developed view of inner surface of TSE-5A test cylinder showing locations of instrumentation.

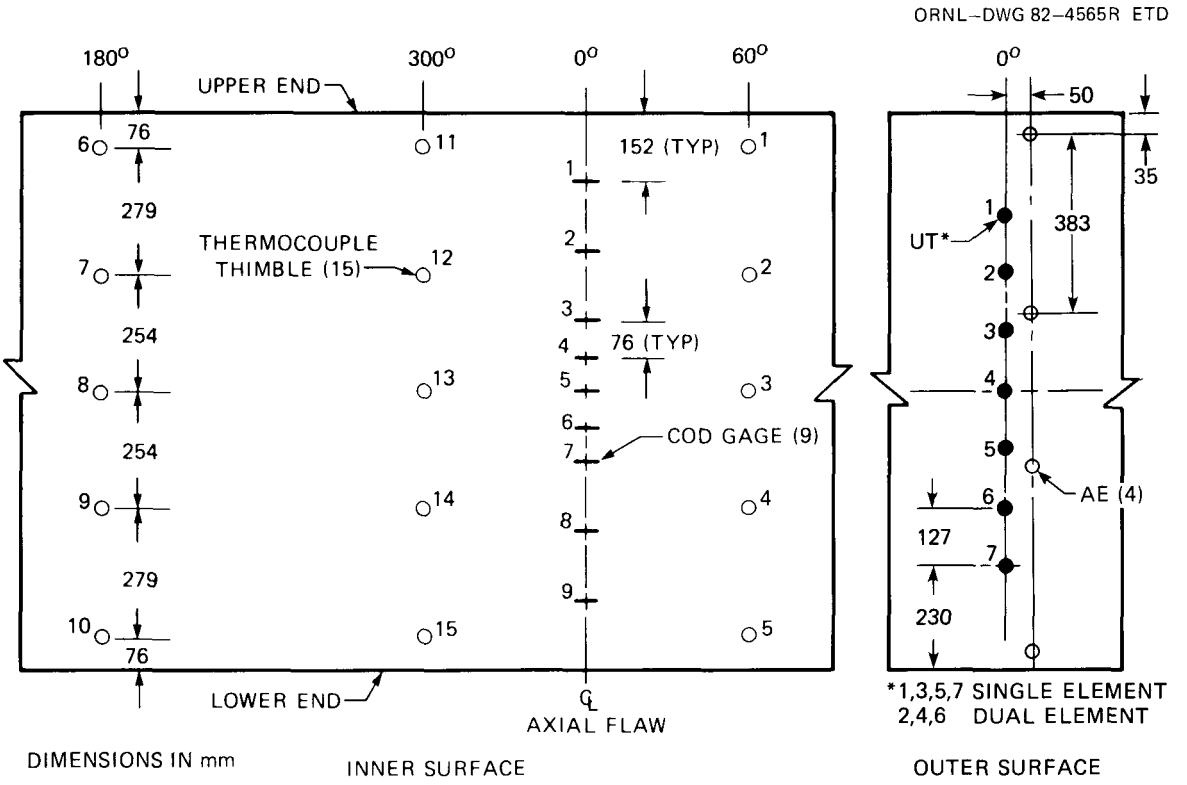

Fig. 6.7. Developed views of TSE-6 test cylinder showing locations of instrumentation.

Crack-opening displacement was measured at nine locations along the length of the flaw with weldable strain gages that straddled the flaw as shown in Figs. 6.2, 6.5–6.8. The output from six of these gages was recorded continuously on chart recorders so that an initiation-arrest event, which was indicated by a step change in output, would be recognized immediately. Output from these six and one additional gage was recorded on tape along with the temperatures mentioned above. The other two gages (3 and 5) were used for measuring COD rate following crack initiation. Output from these gages was recorded with fast-phenomena instrumentation. This information was used to estimate crack speed during a run-arrest event. Details pertaining to the COD gages are included in Appendix B.

Ultrasonic (UT) instrumentation was used to measure crack depth before, during, and after the experiments. Before and after the experiments, measurements were made all along the length of a test cylinder; the UT crystal was applied to the outer surface directly opposite the flaw so that the crystal looked directly at the tip of the flaw along a radial line. During the experiments, several axial locations were monitored continuously by crystals that were permanently attached to the outer surface. Output from these UT crystals was displayed on a scope during the thermal-shock experiments and was also recorded on tape. Locations of the permanently installed crystals are shown in Figs. 6.5–6.7 and 6.9.

ORNL PHOTO 7546–79A

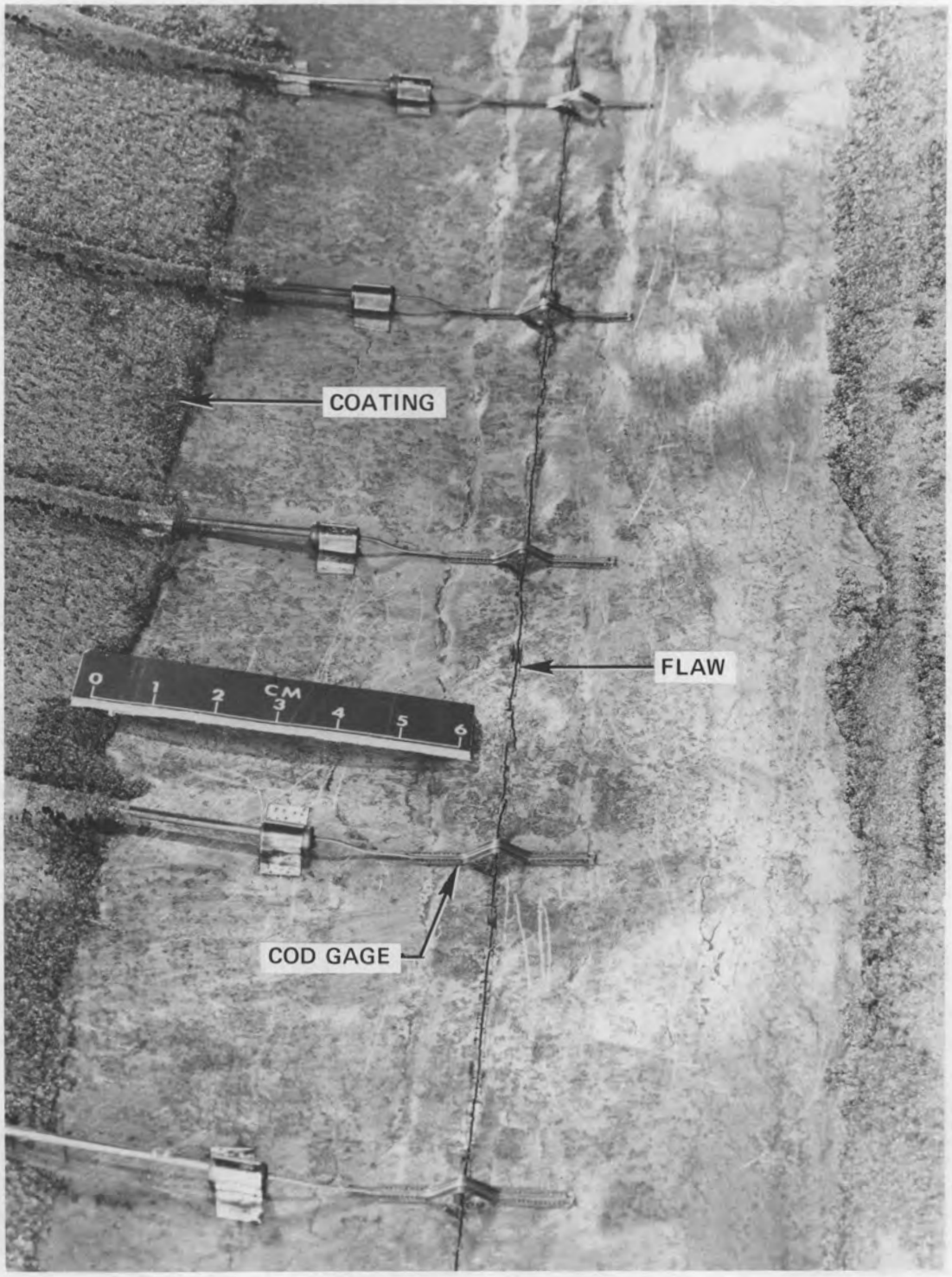

Fig. 6.8. Typical COD gage installation for TSE-5, TSE-5A, and TSE-6. Buckled condition of gages is result of crack closing following large opening.

ORNL PHOTO 7966–81A

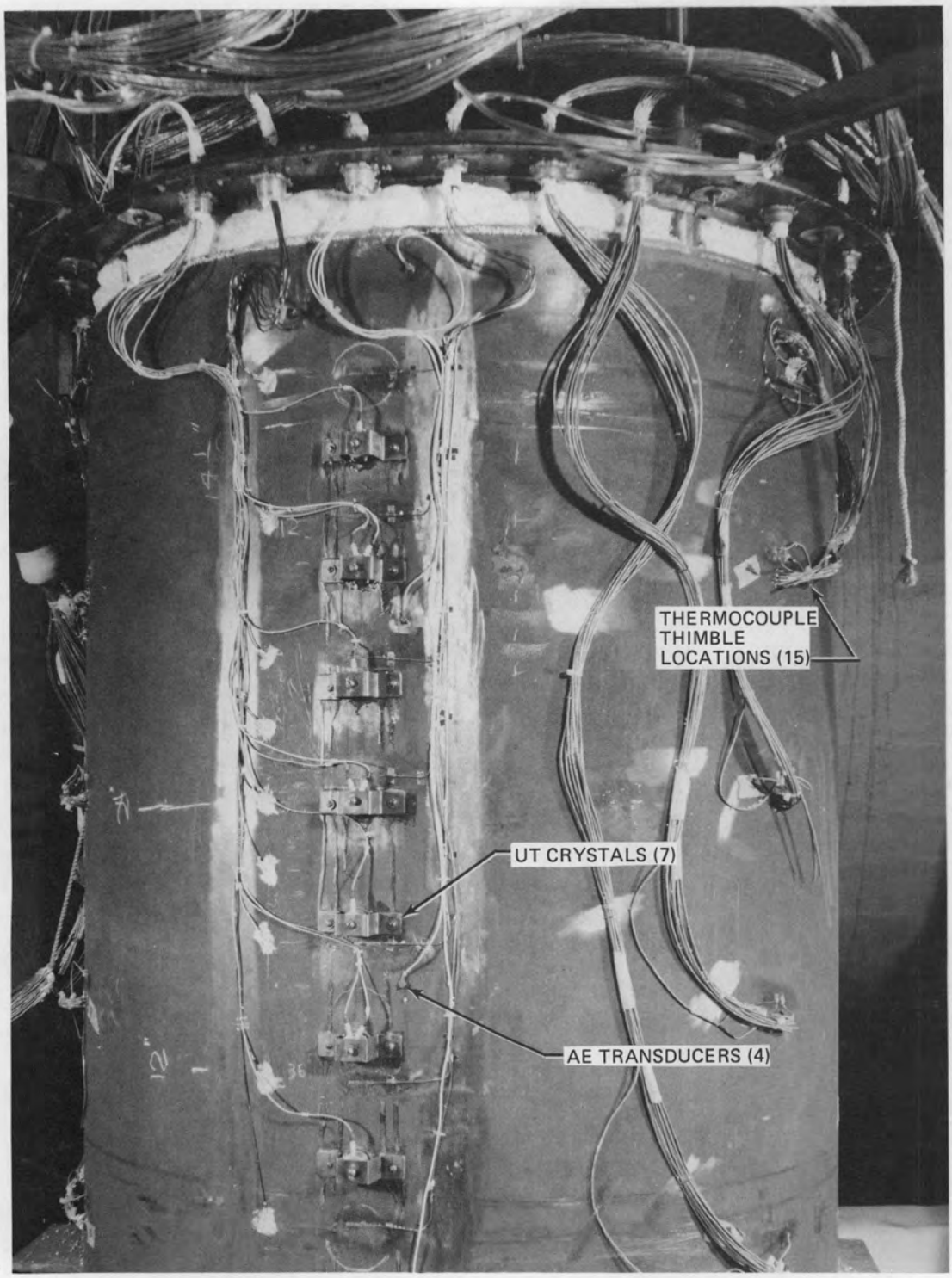

Fig. 6.9. Exterior surface of TSE-6 test cylinder showing locations of UT and acoustic-emission instrumentation.

Crack depth was also estimated using the measured COD data in conjunction with the posttest calculated relation between COD and crack depth, and crack velocity was estimated in a similar manner using the measured COD rate rather than COD.

An attempt was made to use acoustic-emission instrumentation as another event indicator. For TSE-5, three transducers were cemented to the outer surface of the test cylinder directly opposite the crack front (Fig. 6.5). TSE-5A made use of four transducers located at 90° intervals, alternating top and bottom and straddling the flaw plane (Fig. 6.6). For TSE-6, four transducers extending from top to bottom of the cylinder were located on a line offset from the flaw plane by a small amount (Figs. 6.7 and 6.8). Data were recorded continuously during the experiments on charts and tape. Unfortunately, for a variety of reasons, including malfunctioning of the acoustic-emission instrumentation, essentially no usable data were obtained. Thus, the acoustic-emission results are not discussed in this report.

References

1. R. D. Cheverton and S. E. Bolt, "Thermal Shock Investigations," pp. 62–64 in *Heavy-Section Steel Technology Program Quart. Prog. Rep. October–December 1976*, ORNL/NUREG/TM-94, Union Carbide Corp. Nuclear Div., Oak Ridge Natl. Lab.

2. R. D. Cheverton and S. E. Bolt., "Thermal Shock Investigations," pp. 88–97 in *Heavy-Section Steel Technology Program Quart. Prog. Rep. January–March 1977*, ORNL/NUREG/TM-120, Union Carbide Corp. Nuclear Div., Oak Ridge Natl. Lab.

3. R. D. Cheverton and S. E. Bolt, "Thermal Shock Investigations," pp. 69–86 in *Heavy-Section Steel Technology Program Quart. Prog. Rep. April–June 1977*, ORNL/NUREG/TM-147, Union Carbide Corp. Nuclear Div., Oak Ridge Natl. Lab.

4. R. D. Cheverton and S. E. Bolt, "Thermal Shock Investigations," pp. 109–14 in *Heavy-Section Steel Technology Program Quart. Prog. Rep. July–September 1977*, ORNL/NUREG/TM-166, Union Carbide Corp. Nuclear Div., Oak Ridge Natl. Lab.

5. R. D. Cheverton and S. E. Bolt, "Thermal Shock Investigations," pp. 63–73 in *Heavy-Section Steel Technology Program Quart. Prog. Rep. October–December 1977*, ORNL/NUREG/TM-194, Union Carbide Corp. Nuclear Div., Oak Ridge Natl. Lab.

6. R. D. Cheverton, S. E. Bolt and S. K. Iskander, "Thermal Shock Investigations," pp. 33–38 in *Heavy-Section Steel Technology Program Quart. Prog. Rep. January–March 1978*, NUREG/CR-0106 (ORNL/NUREG/TM-209), Union Carbide Corp. Nuclear Div., Oak Ridge Natl. Lab.

7. R. D. Cheverton, "Thermal Shock," pp. 50–56 in *Heavy-Section Steel Technology Program Quart. Prog. Rep. April–June 1978*, NUREG/CR-0310 (ORNL/NUREG/TM-239), Union Carbide Corp. Nuclear Div., Oak Ridge Natl. Lab.

8. R. D. Cheverton, "Thermal Shock Investigations," pp. 84–86 in *Heavy-Section Steel Technology Program Quart. Prog. Rep. July–September 1978*, NUREG/CR-0476 (ORNL/NUREG/TM-275), Union Carbide Corp. Nuclear Div., Oak Ridge Natl. Lab.

9. R. D. Cheverton and S. E. Bolt, "Thermal Shock Investigations," pp. 90–91 in *Heavy-Section Steel Technology Program Quart. Prog. Rep. January–March 1979*, NUREG/CR-0818 (ORNL/NUREG/TM-324), Union Carbide Corp. Nuclear Div., Oak Ridge Natl. Lab.

10. R. D. Cheverton, "Thermal Shock Investigations," pp. 63–67 in *Heavy-Section Steel Technology Program Quart. Prog. Rep. April–June 1979*, NUREG/CR-0980 (ORNL/NUREG/TM-347), Union Carbide Corp. Nuclear Div., Oak Ridge Natl. Lab.

7. CHARACTERIZATION OF TEST-CYLINDER MATERIAL

As indicated in Chap. 5, a prolongation from each of the three test cylinders was used as a source of material for characterizing the test cylinders. The material properties measured included the tensile properties, hardness, Charpy V-notch (CVN) impact data, drop-weight NDT (Ref. 1), and fracture toughness, which included K_{Ic} (Ref. 2), K_J (Ref. 3), and K_{Ia} (Ref. 4). Values of K_J were calculated using the relation $K_J^2 = EJ$ (Ref. 3), where the J integral, J, was based on the energy to maximum load, and E = Young's modulus.

Most of the material property data were obtained as a function of tempering temperature to determine the appropriate tempering temperature for each thermal-shock experiment. The prolongations (TSP-1, TSP-2, TSP-3) from each of the test cylinders (TSC-1, TSC-2, TSC-3) were cut into sections before tempering so that different tempering treatments could be considered. The test cylinders for TSE-5 and TSE-6 (TSC-1, TSC-3) were tempered at the same temperature, and thus the material-characterization studies performed for each of these cylinders apply to both. In all cases the tempering temperature was maintained for 4 h, and this was followed by cooling at room temperature.

The material-characterization studies for each test cylinder are discussed briefly in the remainder of this section, and additional related information, primarily tables of materials property data, is included in Appendix C.

7.1 TSE-5 and TSE-6

Tensile data from TSP-1, corresponding to different tempering temperatures, are plotted in Fig. 7.1, and hardness data are included in Table 7.1 (see Fig. 7.2 for explanation of specimen orientation). These data indicate an increase in strength with increasing tempering temperature up to ~600°C, with a steep decline thereafter. The data also indicate that the yield strength at temperatures of interest (≤100°C) would be no less than 550 MPa for tempering temperatures ≤680°C. This was a point of interest because the maximum unperturbed thermal stress for the experiments was expected to be ~550 MPa, and it was preferred that the yield strength be at least this high.

Following TSE-5, tensile properties were obtained for the TSC-1 actual tempering temperature (613°C), using both TSP-1 and TSC-1 material. These data are plotted in Fig. 7.3 as a function of test temperature.

Pretest hardness, CVN, and fracture-toughness data as a function of tempering temperature are presented in Table 7.2 and Figs. 7.4 and 7.5. The orientations for the CVN and drop-weight specimens are indicated in Fig. 7.2, and the orientation for the compact specimens (CS) is shown in Fig. 7.6. As indicated by the CVN and drop-weight data in Table 7.2 and Fig. 7.4, there is a slight decrease in toughness with increasing tempering temperature up to ~600°C and then an abrupt increase, the same trend observed in the tensile data.

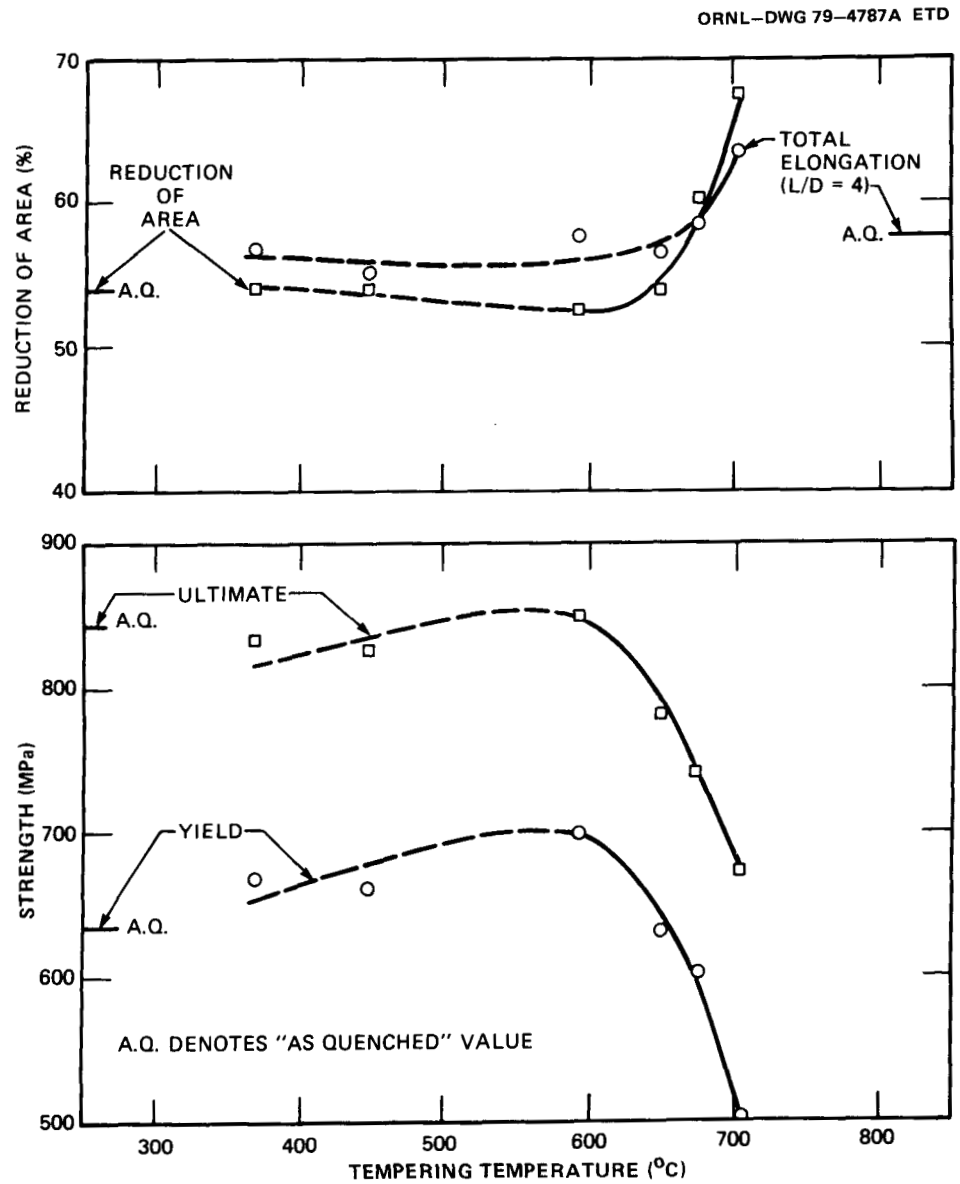

Fig. 7.1. Effect of tempering temperature on the room-temperature tensile properties of TSP-1 after tempering for 4 h and cooling in air.

The fracture-toughness design curve in Fig. 7.5 represents the ASME Sect. XI lower-bound K_{Ic} curve[5] corresponding to a nil-ductility reference temperature[6] (RTNDT) of −34°C. Based on an evaluation of the K_{Ic} data that were used to obtain the ASME Sect. XI lower-bound K_{Ic} curve, this value of RTNDT translates to about −10°C, if the design of the experiment were based on average rather than lower-bound toughness, and it was. With reference to Table 7.2, it is apparent that to achieve RTNDT = −10°C would require a tempering temperature in excess of 700°C.

Table 7.1. Rockwell C hardness of TSC-1 prolongation (TSP-1) at various tempering temperatures

Tempering[a] temperature (°C)	Hardness[b]
As quenched	23.9
704	12.2
677	20.7
649	22.4
593	26.1
448	24.2
371	24.1

[a]Held at temperature for 4 h, then cooled in air.

[b]Average of six measurements.

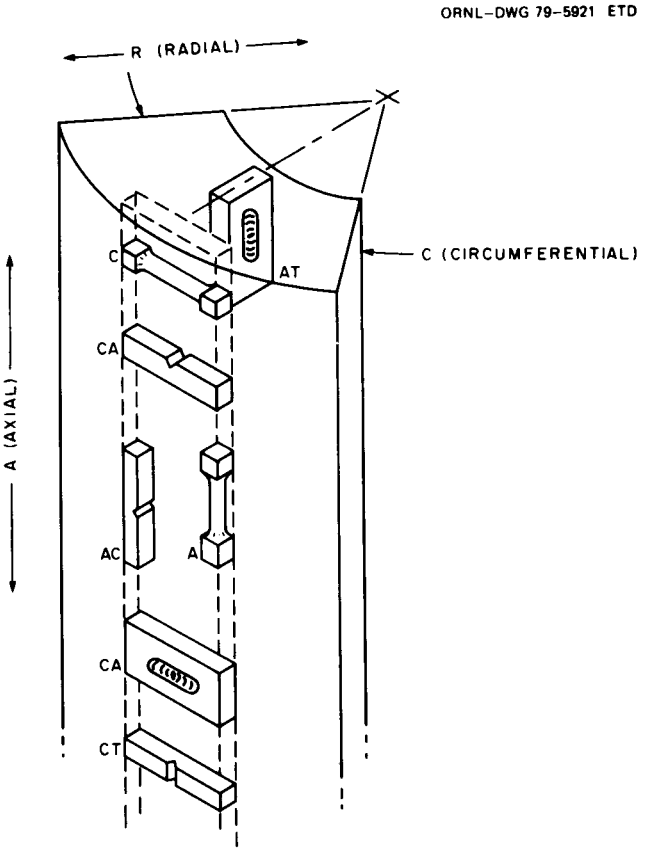

Fig. 7.2. Specimen orientation notation for tensile, CVN, and drop-weight specimens.

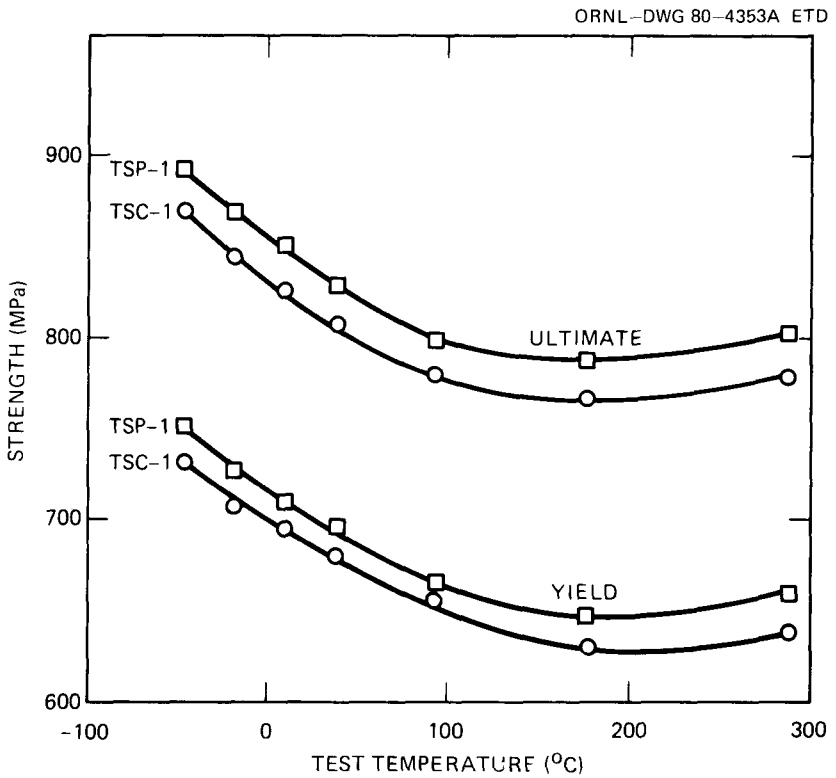

Fig. 7.3. Tensile properties at the quarter-thickness depth in the 152-mm-thick wall of TSC-1 and TSP-1 after tempering at 613°C.

Table 7.2. CVN and drop-weight properties of TSP-1

Tempering[a] temperature	Temperature (°C)					Upper-shelf energy (J)
	68-J (50 ft-lb) Energy[b]	0.89-mm (35-mil) Lateral expansion	50% Shear	Drop-weight[c] NDT	RTNDT	
As quenched	96	88	79	24	36[d]	108
371	85	85	77	18	52[d]	102
449	102	91	82	29	69[d]	99
593	102	91	88	29	69[d]	98
649	66	54	60	24	33[d]	102
677	35	32	41	0	2[d]	118
704	−9	−1	24	−6	−6	153

[a]Held at temperature for 4 h, then cooled in air.

[b]CT-oriented specimens.

[c]AT-oriented specimens.

[d]Controlled by Charpy values.

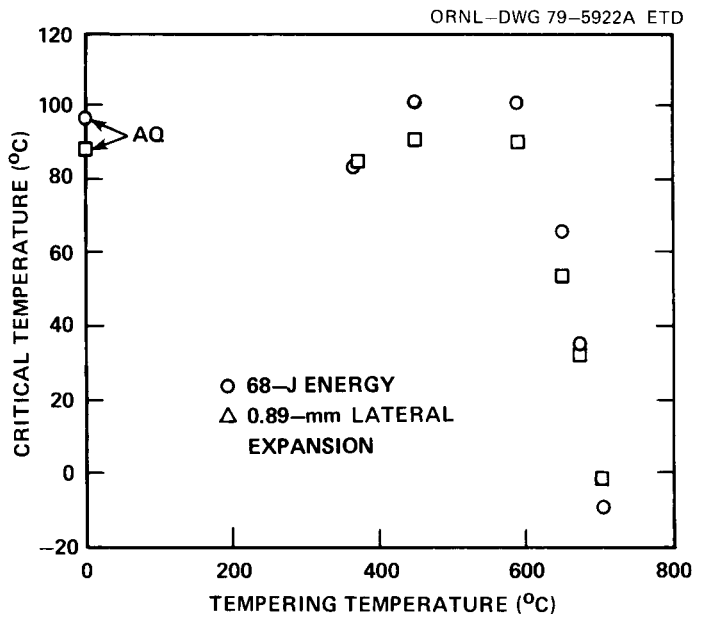

Fig. 7.4. CVN energy and lateral expansion for TSP-1 after tempering for 4 h and cooling in air.

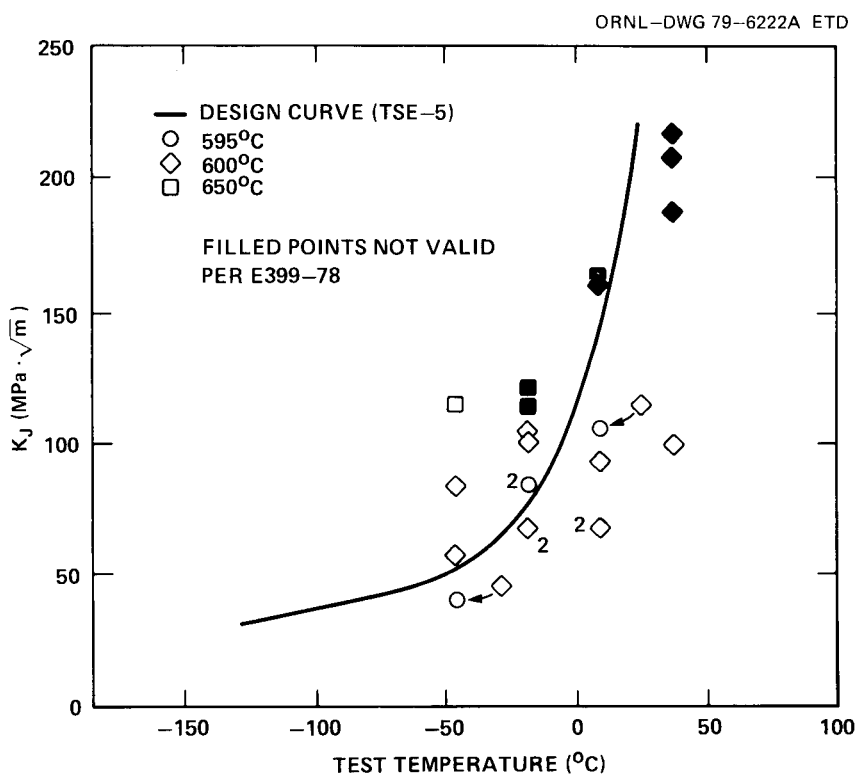

Fig. 7.5. K_J data from 1T compact specimens of TSP-1 after tempering at 595, 600, and 650°C.

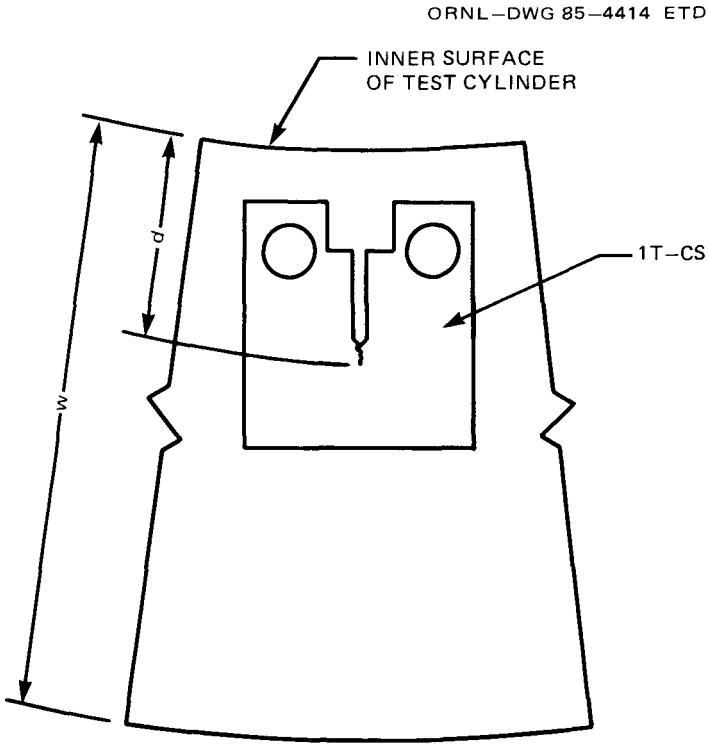

Fig. 7.6. Orientation of compact specimens.

Because of the peculiar trends indicated in Figs. 7.1 and 7.4, there was a tendency to disregard the RTNDT data and rely more on the 1T* compact-specimen data for selecting an appropriate tempering temperature for TSC-1. Furthermore, because all of the invalid specimens represented by Fig. 7.5 experienced very little ductile tearing (<0.25 mm) before cleavage fracture, all data points in Fig. 7.5 were considered essentially valid. Based on this approach and believing that the design of the experiment should be based on a mean K_{Ic} curve, a tempering temperature of 613°C was selected for the TSE-5 test cylinder, even though the corresponding indicated value of RTNDT from Table 7.2 was ~66°C.

Once the tempering temperature was selected, static crack-arrest data were obtained using wedge-loaded, compact, crack-arrest specimens (25 × 150 × 150 mm), and the orientation of these specimens, relative to the test cylinder, was the same as that for the K_J compact specimens (see Fig. 7.6). The K_{Ia} measurements were made by Battelle Columbus Laboratories (BCL), and the data obtained by BCL[7] are presented in Fig. 7.7.

Following TSE-5, it was apparent that the fracture toughness of the test-cylinder material above 0°C was substantially less than expected. Suspecting that the pretest data were insufficient in number because of the indicated large scatter in K_J data and that the flaw in the test cylinder behaved in accordance with the lower bound rather than the mean,

*Standard compact-tension specimen[2] with a thickness, T, of 25.4 mm. Other values of T mentioned in this report are 50.8 mm (2T-CS) and 10.0 mm (0.394T-CS).

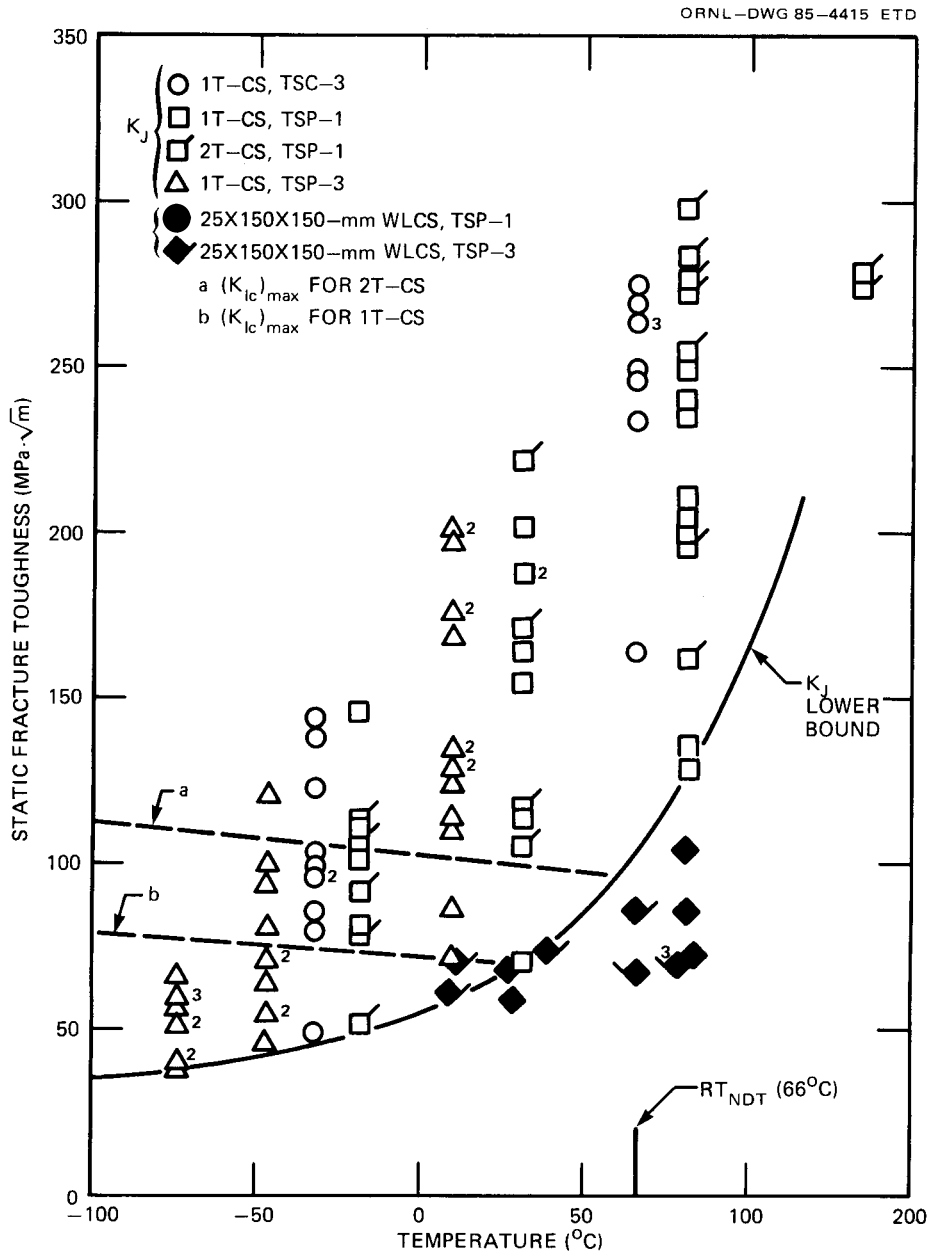

Fig. 7.7. K_J and K_{Ia} data for TSP-1, TSP-3, and TSC-3, each tempered at 613°C.

a relatively large number of additional compact specimens was tested, including 2T and 0.394T, as well as 1T specimens. The 1T and 2T-CS data are included in Fig. 7.7, and the 0.394T compact-specimen data are presented in Fig. 7.8.

Figure 7.7 shows large scatter in the K_J data (ratio of upper-to-lower bound ≈3) extending over the full range of temperatures (−80 to +80°C). The scatter for the 1T and 2T specimens is about the same, and both of these specimen sizes yielded about the same lower bound. There

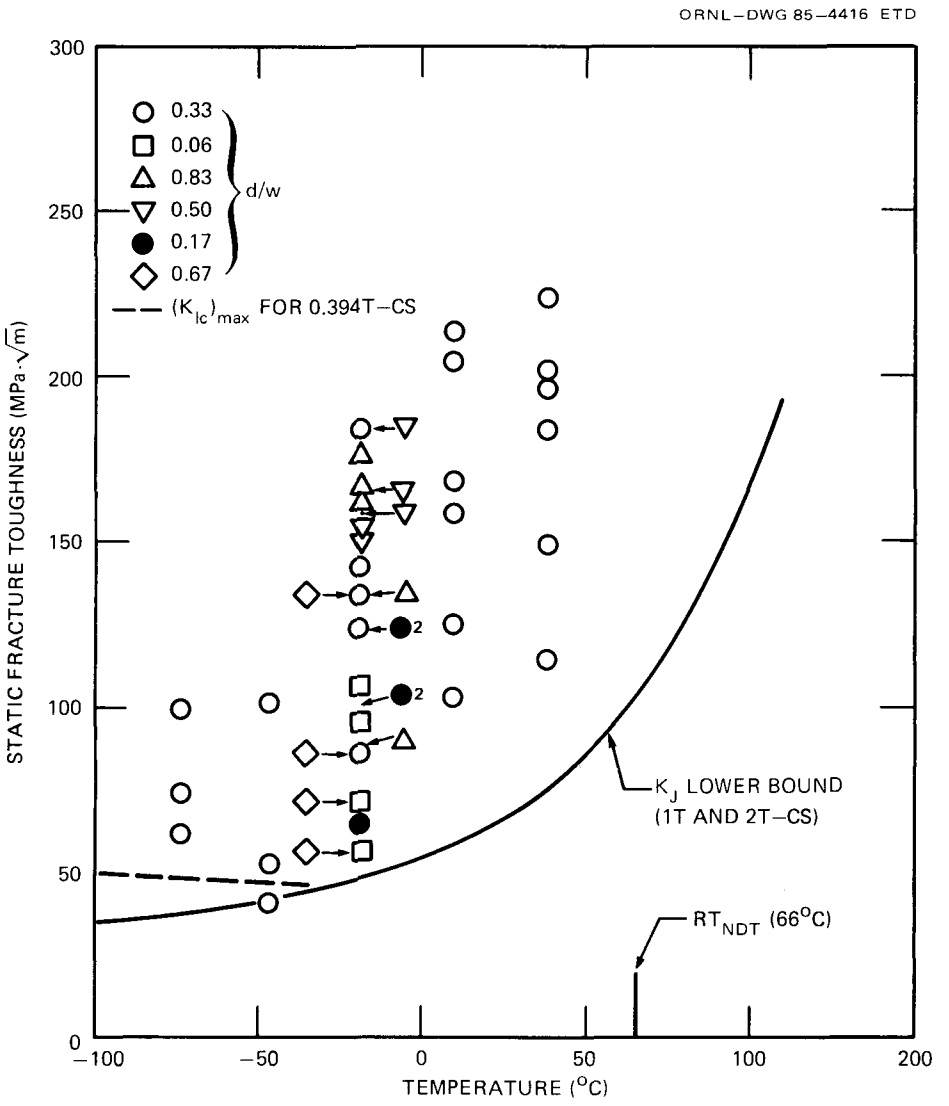

Fig. 7.8. K_J data from 0.394T compact specimens of TSP-1 after tempering at 613°C.

is also rather large scatter in the relatively few valid data points (valid in accordance with ASTM Standard E399-78).[2] As discussed in greater detail in Chap. 8, the flaw in the TSE-5 test cylinder tended to behave more in accordance with the lower bound than the mean of the K_J data because the lower bound is more representative of truly valid data.

Figure 7.8 indicates that (1) the scatter in the K_J data obtained from the 0.394T compact specimens is somewhat greater than that for the 1T and 2T specimens and (2) for temperatures less than 0°C, the lower bound of the 0.394T data coincides with that for the 1T and 2T data. Also, as indicated by the data corresponding to a test temperature of –18°C, there was no significant gradient in toughness through the wall of the cylinder.

Although a tempering temperature of 613°C was not appropriate for the intended purpose of TSE-5, it was for TSE-6, and since the two test cylinders came from the same heat of material, only one overlapping test temperature was used for the TSP-3 pretest K_J data. The remainder of the pretest TSE-6 K_J data were obtained at lower temperatures, consistent with the requirements for TSE-6.

Following TSE-6, the test cylinder, TSC-3, was used as a source of material for further characterization studies. K_J data were obtained with 1T compact specimens at temperatures of −32 and 66°C, and CVN data were obtained over a temperature range of −73 to 149°C at depth locations (d/w) of 0.08 and 0.42. The K_J data for TSC-3 and also the K_J and BCL K_{Ia} (Ref. 8) data for TSP-3 are included in Fig. 7.7, while the CVN data are presented in Figs. 7.9 and 7.10. As indicated in these latter two

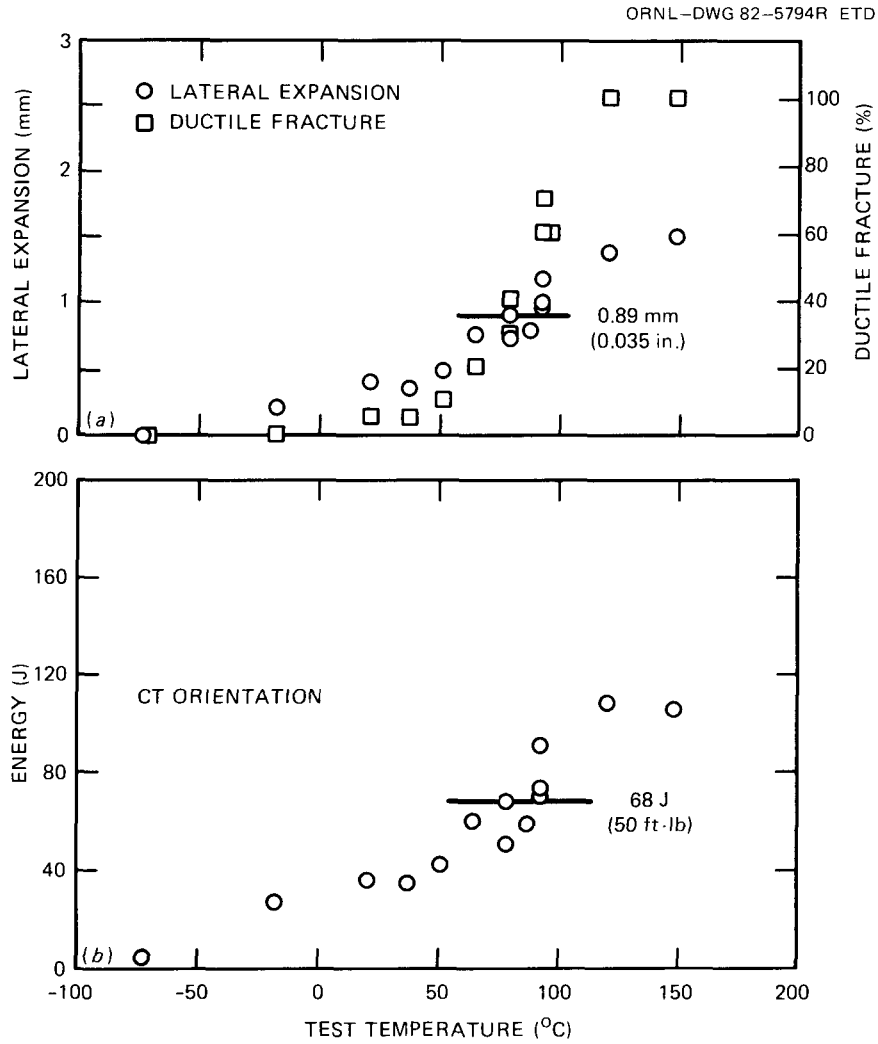

Fig. 7.9. CVN data for TSC-3 (tempered at 613°C) at a depth location (d/w) = 0.08. (*a*) Fracture appearance and lateral expansion and (*b*) impact energy.

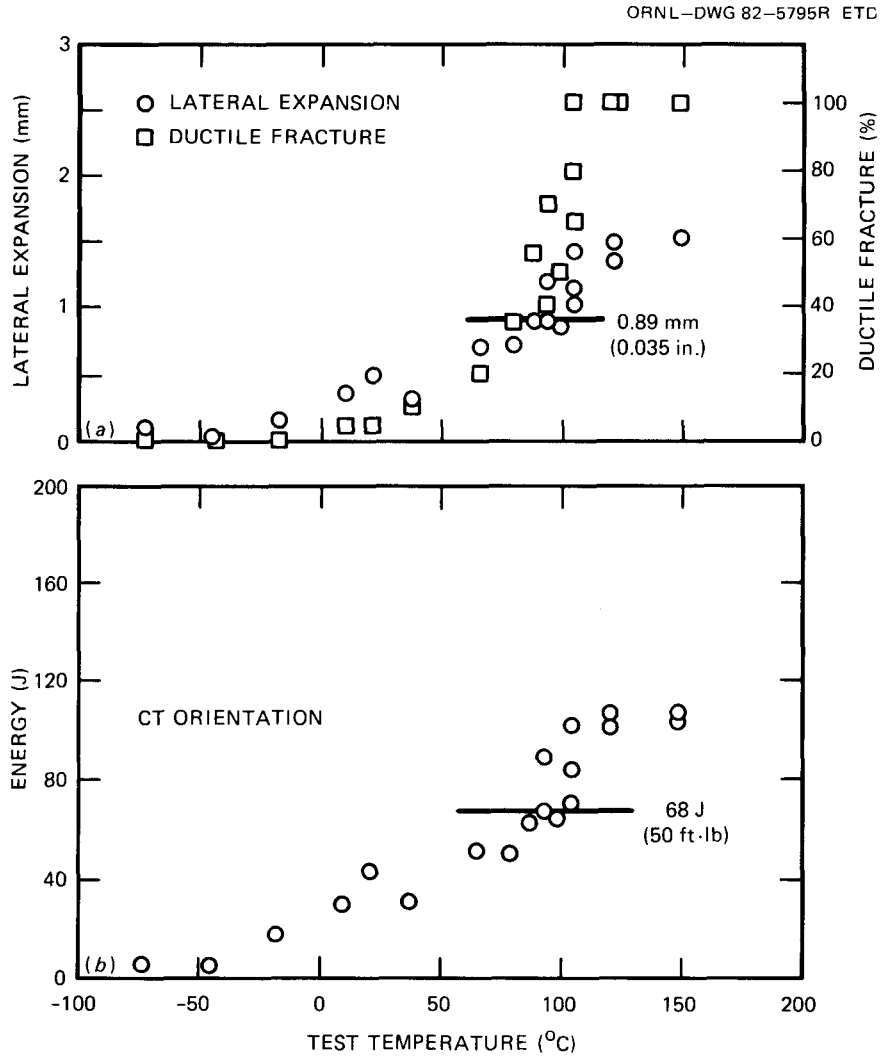

Fig. 7.10. CVN data for TSC-3 (tempered at 613°C) at a depth location (d/w) = 0.42. (*a*) Fracture appearance and lateral expansion and (*b*) impact energy.

figures, the lowest temperature at which the 68-J and 0.89-mm lateral expansion criteria in Ref. 6 are satisfied is ~100°C. Thus, in accordance with Ref. 6, RTNDT ≈ 67°C, which is in good agreement with the value obtained for TSP-1.

An examination of all the data in Figs. 7.3 and 7.7–7.10 indicates that (1) there are no significant differences between TSP-1, TSP-3, and TSC-3; (2) a rather large number of compact specimens (>10 at any one test temperature) is required to define the lower-bound K_J curve in the transition region, even if the specimen is capable of measuring a valid value (K_{Ic}); and (3) the scatter in K_{Ia} data points appears to be less than that in the K_J data, although the number of data points may be too small for an accurate comparison.

7.2 TSE-5A

The fracture-toughness curves specified for TSE-5A corresponded to the ASME Sect. XI K_{Ic} and K_{Ia} curves[5] with RTNDT = −18°C. Furthermore, considering the results of TSE-5, it was believed that the TSE-5A flaw would behave more in accordance with the lower bound of the small-specimen K_J data than the mean.

Based on the results of the TSE-5 materials-characterization studies, trial tempering temperatures of 677 and 707°C were selected for TSE-5A, and only 1T compact specimens were used for obtaining the K_J data. Although 1T compact specimens were not expected to yield valid (K_{Ic}) values [in accordance with the size requirements in ASTM E399-78 (Ref. 2)], it was believed that their lower-bound values would be adequate for selecting an appropriate tempering temperature.

In addition to using standard 1T compact specimens and standard loading conditions, 20% side-grooved specimens with standard loading conditions and standard specimens with spring loading were used in an effort to reduce the scatter in data. ORNL performed the standard K_J tests, BCL tested the side-grooved specimens,[9] and the United States Naval Ship Research and Development Center (USNSRDC) conducted the spring-loaded tests.[10] BCL also obtained all of the K_{Ia} data.[11,12]

The ORNL K_J data for the two tempering temperatures are shown in Figs. 7.11 and 7.12, and the BCL and USNSRDC data are included in Fig. 7.11. As indicated in Fig. 7.11, it is not apparent that side grooving or spring loading had any significant effect on the scatter or lower bound of the K_J data. It was not really expected that spring loading would have an effect because very few of the standard tests resulted in fracture after maximum load.[13]

The design toughness curves for TSE-5A are also included in Figs. 7.11 and 7.12. As indicated, if one assumes that K_{Ic} values would be somewhat less than the lower bound of the K_J data, a tempering temperature of ~677°C would be about right, and 707°C would be too high. Based on this information, a tempering temperature of 679°C was specified.

The K_J data at the higher tempering temperature were obtained from four different radial positions in the wall of TSP-2. This provided another opportunity to check on radial gradients in fracture toughness, and as indicated in Fig. 7.12 (by perhaps too few data points) there is no apparent gradient. This is consistent with the indications obtained for TSP-1 with the larger number of 0.394T compact specimens (see Fig. 7.8).

Following TSE-5A, the test cylinder (TSC-2) was used as a source of material for 1T compact specimens. The K_J data obtained from these specimens are included with and are consistent with the TSP-2 data in Fig. 7.11.

The K_{Ia} data in Fig. 7.11 appear to be divided into two groups, and in fact, they are divided by the size of the crack-arrest specimen and by the location, within TSP-2, of the material from which the specimens were made. A separate study by Rosenfield et al.[8] tends to rule out specimen size as a factor in the difference shown in Fig. 7.11. Thus, it appears that inhomogeneities may have existed in TSP-2. However, this was not

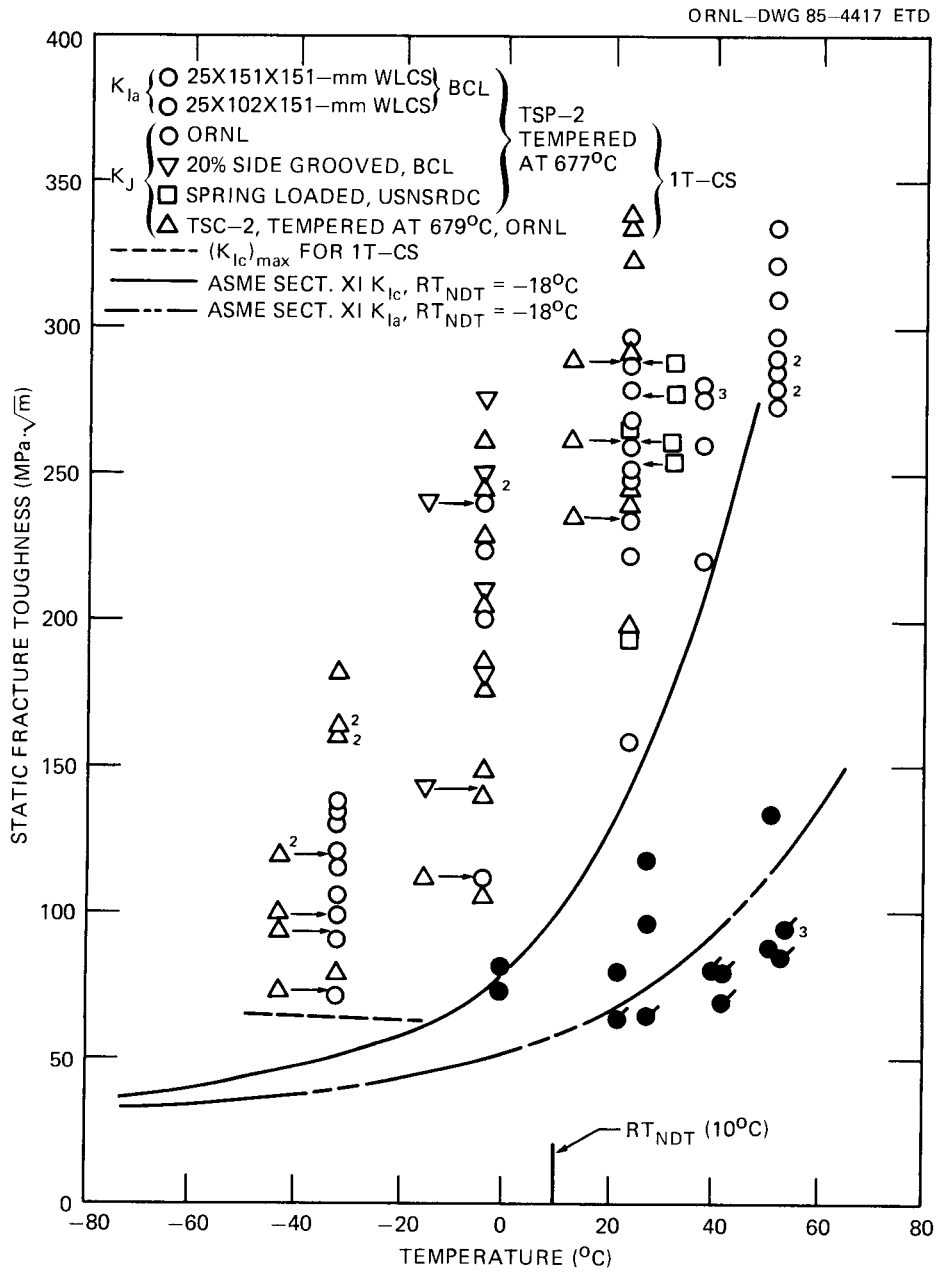

Fig. 7.11. K_J and K_{Ia} data for TSP-2 tempered at 677°C and TSC-2 (tempered at 679°C).

apparent in any of the K_J data; for this reason, it is believed that significant inhomogeneities did not actually exist.

It is of interest to note at this point that the several values of K_{Ic} and K_{Ia} deduced from TSE-5A fell very close to the design curves in Fig. 7.11. These results are discussed in detail in Chap. 8.

Because of the large scatter in small-specimen K_J data, we were prompted to determine if the same scatter existed in CVN data. The results of extensive CVN testing for TSP-2 are shown in Fig. 7.13. It is

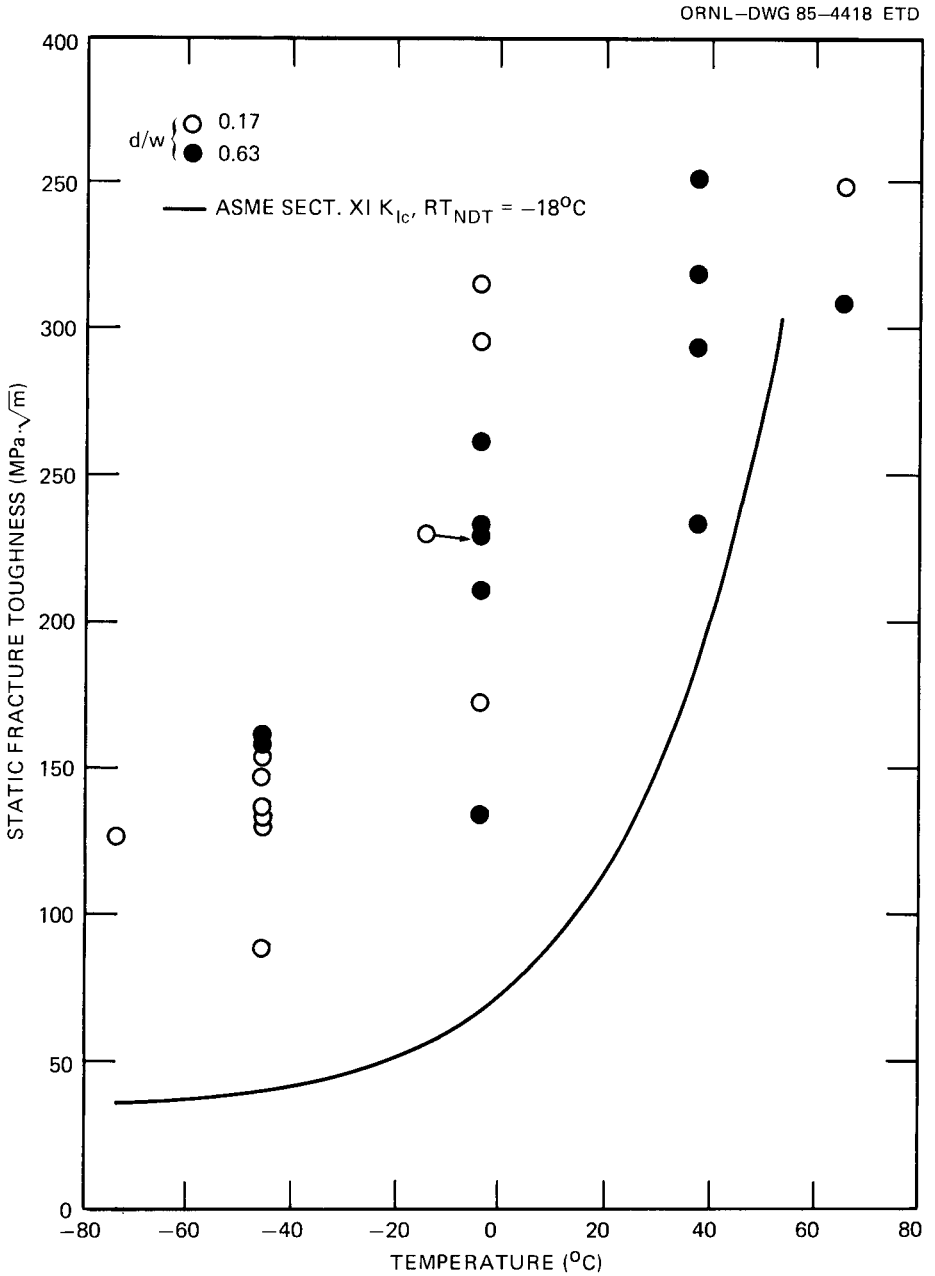

Fig. 7.12. K_J data from 1T compact specimens of TSP-2 tempered at 707°C.

apparent that the scatter is about the same as that for the K_J data. Following TSE-5A, CVN data were also obtained for the test cylinder (TSC-2), and these data are included with the TSP-2 data in Fig. 7.14. As indicated, the two sets of data are consistent, indicating once again that the test cylinders and their prolongations have the same properties.

The drop-weight NDT for TSP-2 tempered at 677°C for 4 h was determined, using P-3 drop-weight specimens[1] with a CA orientation (see Fig. 7.2), to be 10°C. At a temperature 33°C higher (43°C), the CVN energy

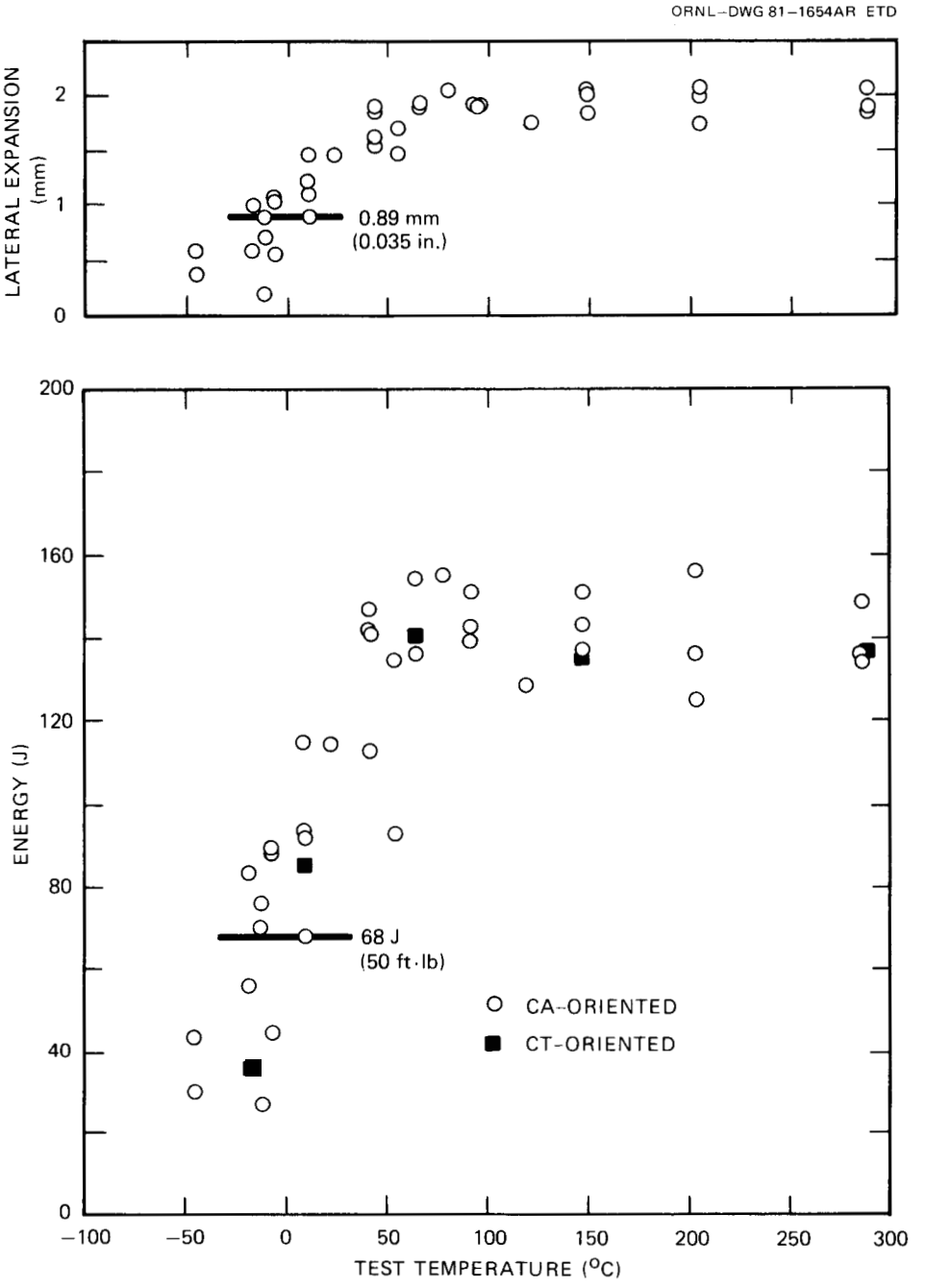

Fig. 7.13. CVN properties for TSP-2 after tempering at 677°C.

and lateral expansion were greater than 68 J and 0.89 mm, respectively, as indicated in Fig. 7.13. Thus, in accordance with Ref. 6, RTNDT is 10°C. This is only slightly higher than the value measured for TSP-1 using an AT-oriented specimen and the same tempering temperature (see Table 7.2).

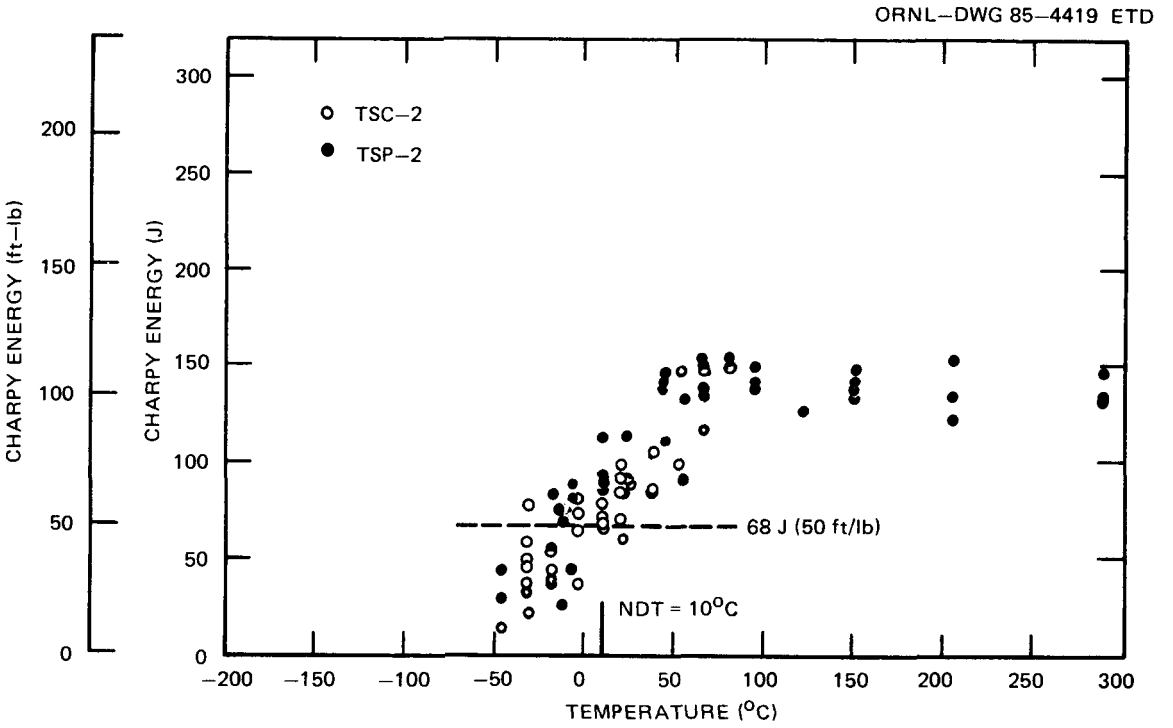

Fig. 7.14. CVN data for TSP-2 (tempered at 677°C) and for TSC-2 (tempered at 679°C).

References

1. "Standard Method for Conducting Drop-Weight Test to Determine Nil-Ductility Transition Temperature of Ferritic Steels," *1983 Annual Book of ASTM Standards*, Sect. 3, Vol. 03.01, American Society for Testing and Materials, Designation E208-81, Philadelphia, Pa., 1983.

2. "Plane Strain Fracture Toughness of Metallic Materials," ASTM E399-78, *Annual Book of ASTM Standards, Part 31*, American Society for Testing and Materials, Philadelphia, Pa., 1978.

3. J. G. Merkle and H. T. Corten, "A J-Integral Analysis for the Compact Specimen, Considering Axial Force as Well as Bending Effects," *ASME Journal of Pressure Vessel Technology* 96, 286–92, (November 1974).

4. A. R. Rosenfield et al., *Critical Experiments, Measurements and Analyses to Establish a Crack-Arrest Methodology for Nuclear Pressure Vessel Steels*, NUREG/CR-1887 (BMI-2071), January 1981.

5. T. U. Marston ed., *Flaw Evaluation Procedures, ASME Section XI, Background and Application of ASME Section XI, Appendix A, Special Report*, EPRI NP-719-SR, Electric Power Research Institute, (August 1978).

6. *ASME Code*, Section XI, Division 1, Subsection NB-2331.

7. A. R. Rosenfield et al., *Critical Experiments, Measurements, and Analyses to Establish a Crack-Arrest Methodology for Nuclear-Pressure-Vessel Steels, Progress Report for June–December 1979*, NUREG/CR-1555 (BMI-2064), R5, June 1980.

8. A. R. Rosenfield et al., "BCL HSST Support Program," pp. 8–35 in *Heavy-Section Steel Technology Program Quart. Prog. Rep. January–March 1982*, NUREG/CR-2751, Vol. 1 (ORNL/TM-8369/V1), Union Carbide Corp. Nuclear Div., Oak Ridge Natl. Lab.

9. A. R. Rosenfield and D. K. Shetty, "Lower-Bound Toughness of a Reactor Vessel Steel," *Eng. Fract. Mech.* 14, 883–42, 1981.

10. M. Vassilaros, U. S. Naval Ship Research and Development Center, Washington, D.C., letter to D. A. Canonico, Oak Ridge Natl. Lab., Oak Ridge, Tenn., March 1981.

11. A. R. Rosenfield et al., Appendix B in *Critical Experiments, Measurements and Analyses to Establish a Crack-Arrest Methodology for Nuclear Pressure Vessel Steels*, NUREG/CR-1887 (BMI-2071), January 1981.

12. A. R. Rosenfield et al., "BCL HSST Support Program," pp. 7–39 in *Heavy-Section Steel Technology Program Quart. Prog. Rep. July–September 1982*, NUREG/CR-2751, Vol. 3 (ORNL/TM-8369/V3), Union Carbide Corp. Nuclear Div., Oak Ridge Natl. Lab.

13. R. D. Cheverton and S. K. Iskander, "Thermal-Shock Investigations," pp. 87–93 in *Heavy Section Steel Technology Program Quart. Prog. Rep. January–March 1981*, NUREG/CR-2141/V1 (ORNL/TM-7822) Union Carbide Corp. Nuclear Div., Oak Ridge Natl. Lab.

8. TSE-5 RESULTS

8.1 Heat Transfer

During TSE-5, the initial long axial flaw in the test cylinder experienced three major initiation-arrest events. The measured radial temperature distributions in the wall of the test cylinder corresponding to the times of these events are shown in Figs. 8.1–8.3, and temperatures for additional times are included in Fig. 8.4.

Each of the data points on the curves in Figs. 8.1–8.3 represents the average of 15 measurements obtained from the 15 thermocouple thimbles described in Chap. 6. The axial and azimuthal variations in the indicated temperatures close to the inner surface were only ±6°C at the time of the three events. Near-surface measured temperatures as a function of time in the transient for all five thermocouple thimbles in one axial plane are shown in Fig. 8.5, and the good agreement among thimbles is apparent. As illustrated in Fig. 8.6, the transient was somewhat more severe than nominally specified, and it was also more severe than anticipated on the basis of the pre-TSE-5 thermal-hydraulic experiment. However, this had little bearing on the outcome of TSE-5.

The inner-surface thermal conductance, which includes both the fluid-film and rubber-cement-coating conductances, was obtained as a function of surface (metal) temperature for the thermal-shock experiments, using the measured inner-surface temperature as a boundary condition in a one-dimensional (radial) transient thermal analysis. A trial and error solution in the form of a computer code[1] was performed to obtain the appropriate surface conductance for each of many small successive time steps. The results for TSE-5 are shown in Fig. 8.7.

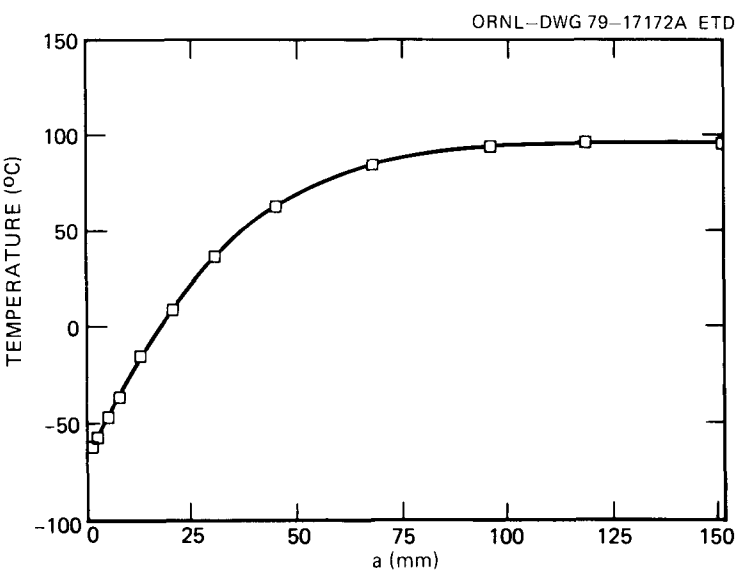

Fig. 8.1. Radial temperature distribution at t = 106 s during TSE-5.

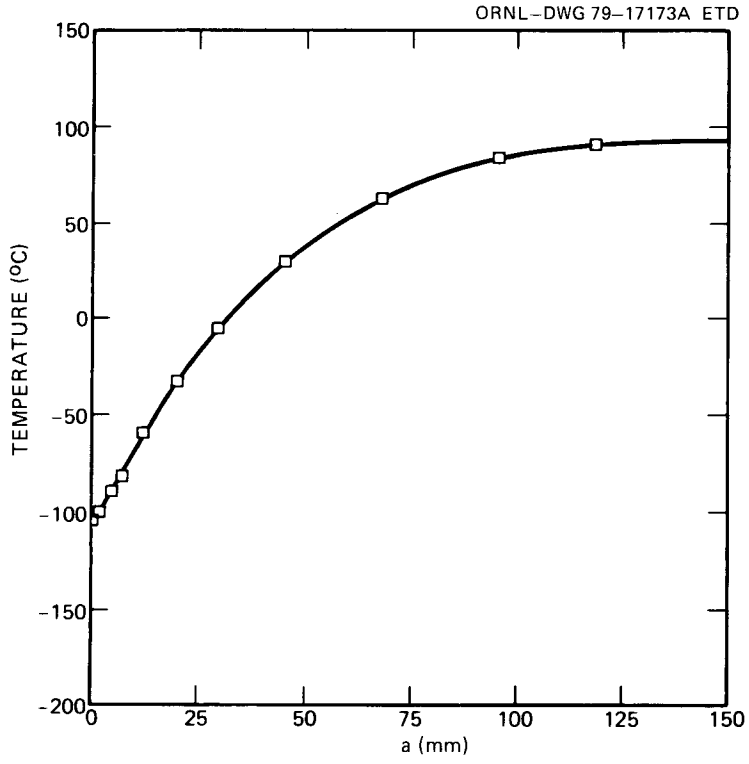

Fig. 8.2. Radial temperature distribution at t = 178 s during TSE-5.

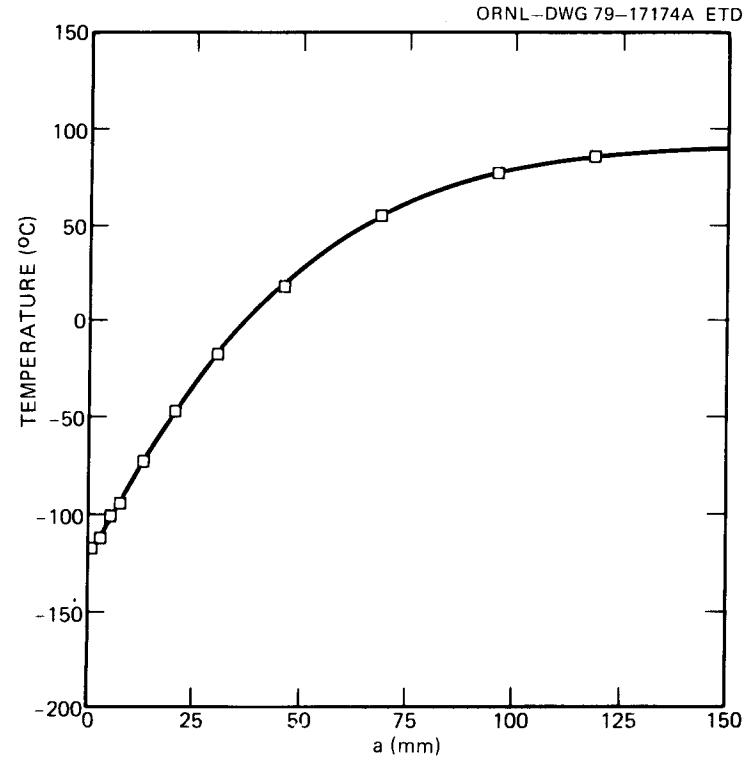

Fig. 8.3. Radial temperature distribution at t = 206 s during TSE-5.

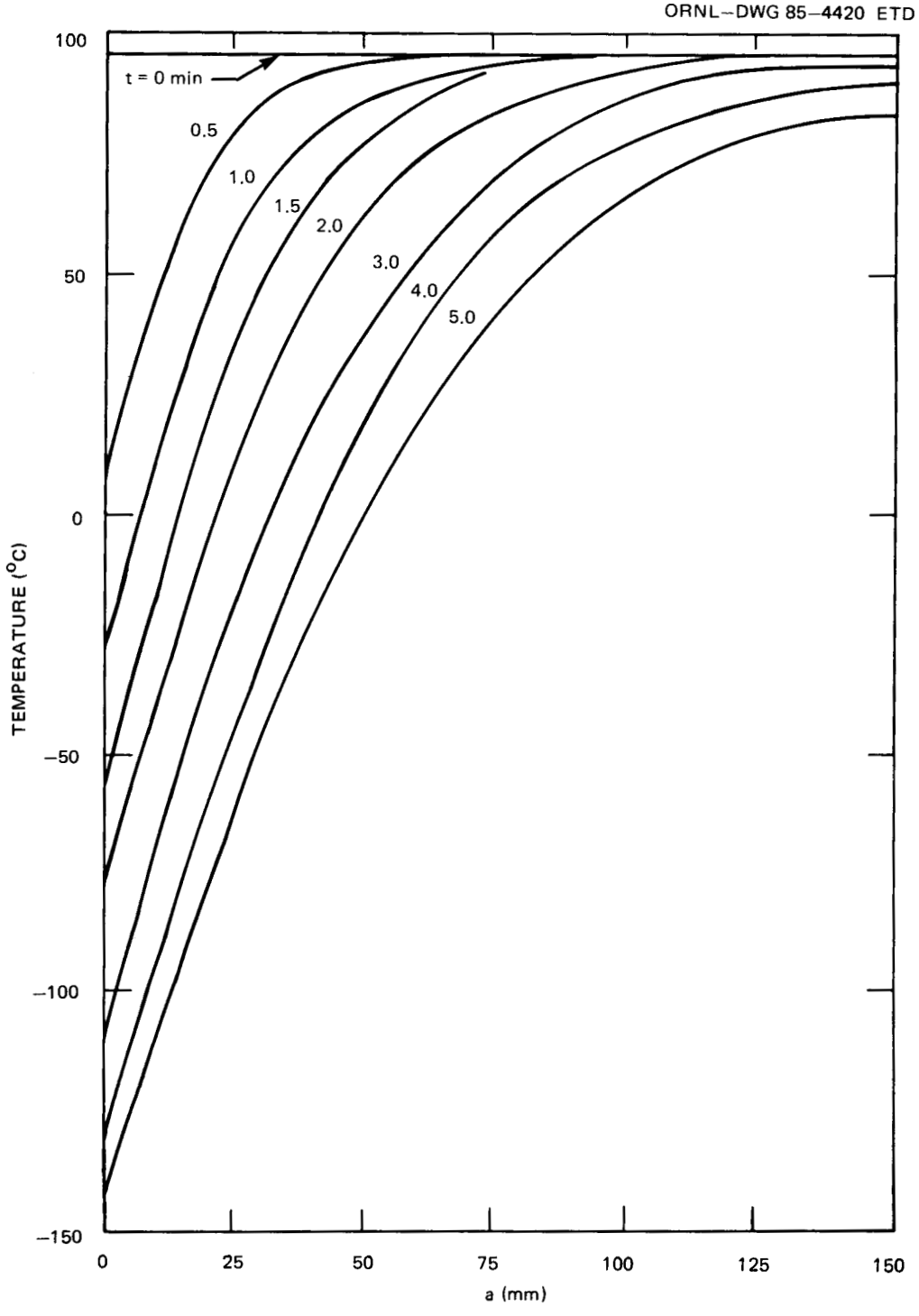

Fig. 8.4. Temperature vs a/w for several times in the TSE-5 transient.

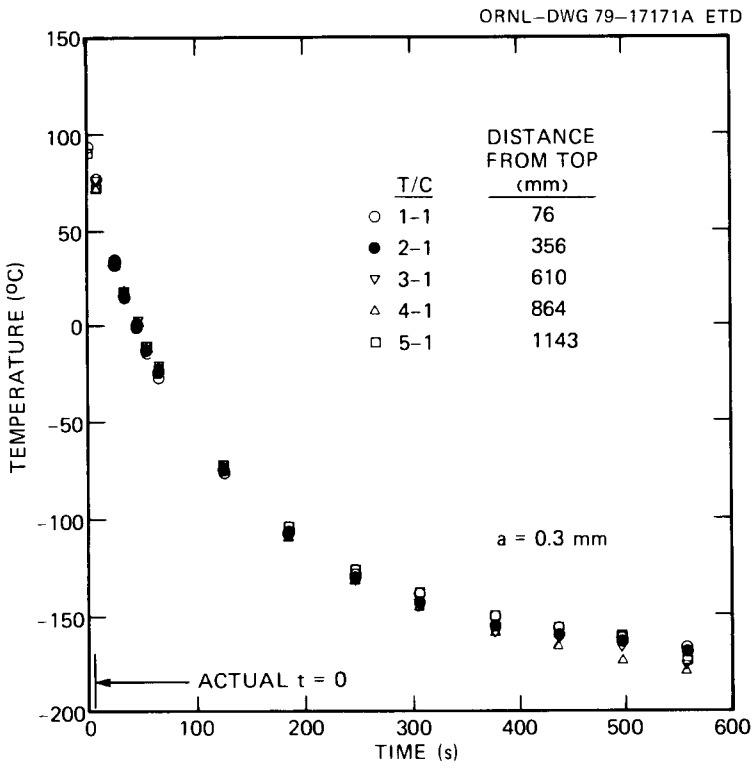

Fig. 8.5. Near-surface temperatures at five elevations in TSE-5 test cylinder during thermal transient.

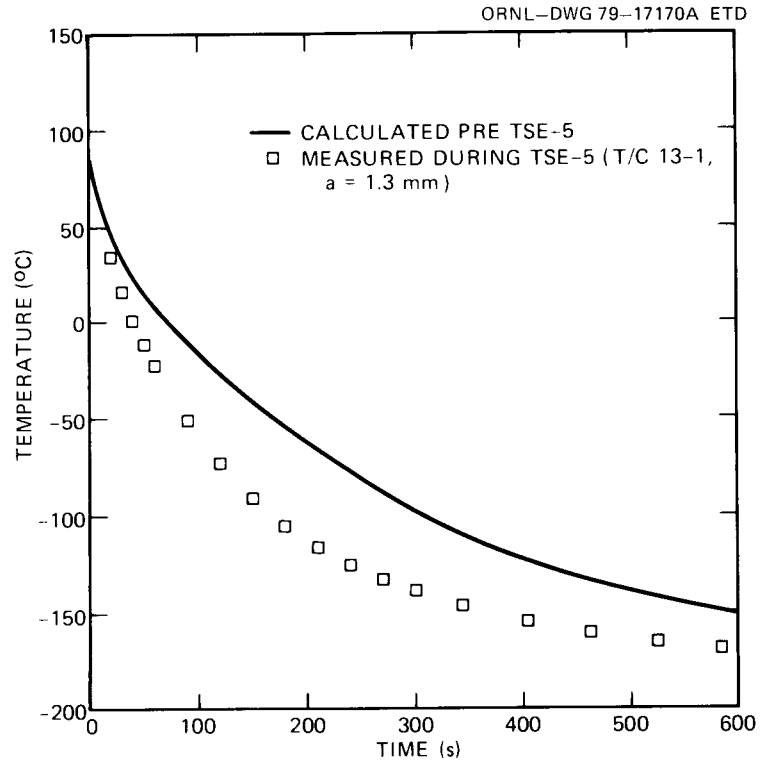

Fig. 8.6. Comparison of calculated (pretest) and measured surface-temperature transients for TSE-5.

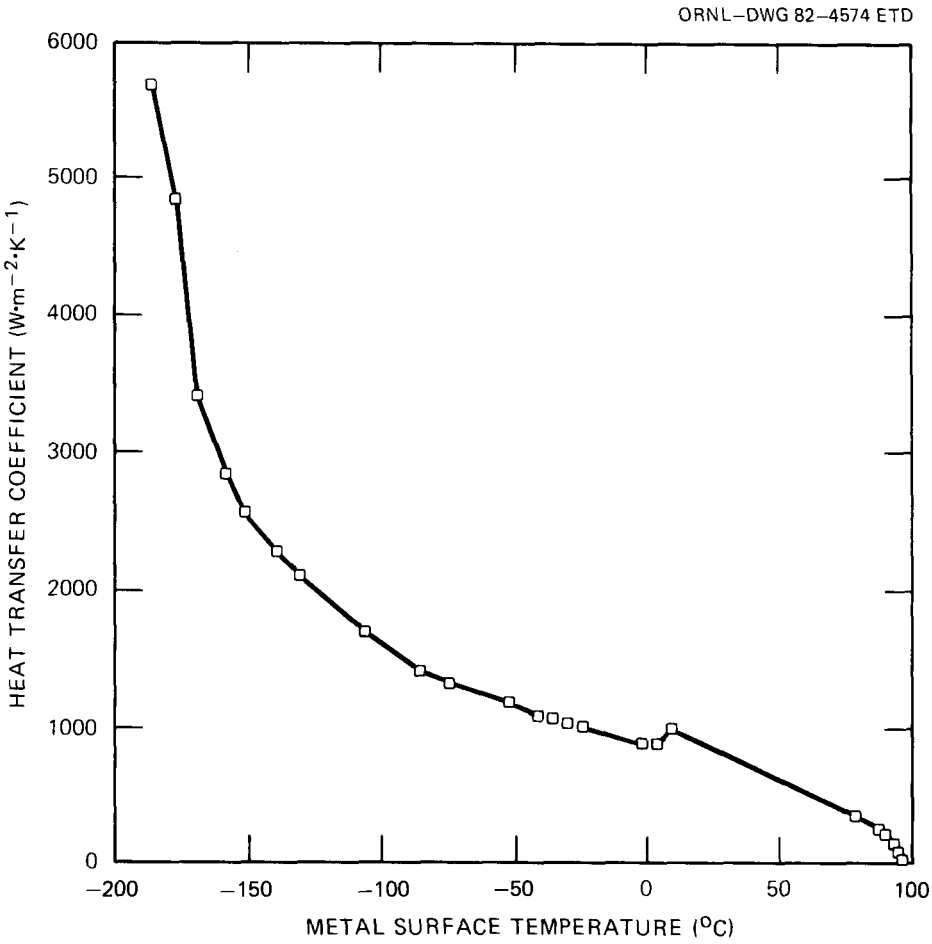

Fig. 8.7. Variation of inner-surface heat transfer coefficient with metal surface temperature for TSE-5.

8.2 Events During TSE-5

In addition to the three initiation-arrest events associated with the long axial flaw, there were one or more initiation-arrest events associated with a cross crack that initially resided in the EB weld that was used to generate the axial flaw. It appears that this latter cracking (referred to as secondary cracking) had no significant influence on the behavior of the primary (axial) flaw, and thus the events associated with the primary flaw will be discussed separately. The secondary cracking is discussed in Sect. 8.6.

The trace of the COD-gage output (Fig. 8.8) illustrates graphically the primary-flaw events that took place during TSE-5. As indicated, initiation-arrest events took place at 1.75, 2.95, and 3.42 min, with all gages* indicating each of these events. Four of the seven gages survived

*Gages 4 and 6 were recorded elsewhere.

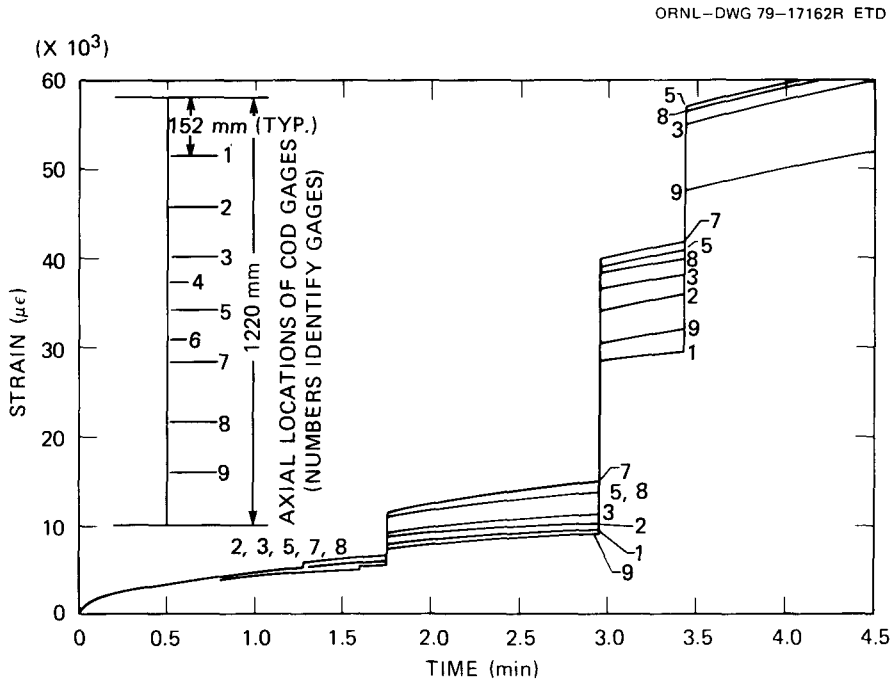

Fig. 8.8. COD output during TSE-5, indicating three major initiation-arrest events.

the 3.42-min event and indicated no further events during the remainder of the 30-min test. Prior to the event at 1.75 min, a few relatively small events took place but were not indicated by all gages.

8.3 Crack Depths

Estimates of crack depth prior to the test and at the time of each of the three events were obtained from three UT transducers secured to the outer surface of the test cylinder directly opposite the tip of the flaw. Once the test was completed and the outer-surface insulation was removed, UT instrumentation was used to obtain a detailed description of the final crack depth. Finally, a pie-shaped section of the cylinder wall containing the primary flaw was removed from the cylinder and was cut into several lengths to expose cross sections of the flaw at several positions along the length of the cylinder (Fig. 8.9). Once the cross sections were examined, the fracture in each block was completed under mechanical loading conditions at cryogenic temperatures to reveal the fracture surfaces. The cross sections and fracture surfaces revealed the initial crack depth, first crack-arrest depth, and final crack depth, but the second arrested crack depth was not discernible. A typical cross section and fracture surface are shown in Figs. 8.10 and 8.11, and all depth measurements are shown in Fig. 8.12.

The data in Fig. 8.12 show good agreement between crack-depth measurements and indicate that crack penetration in the central portion of

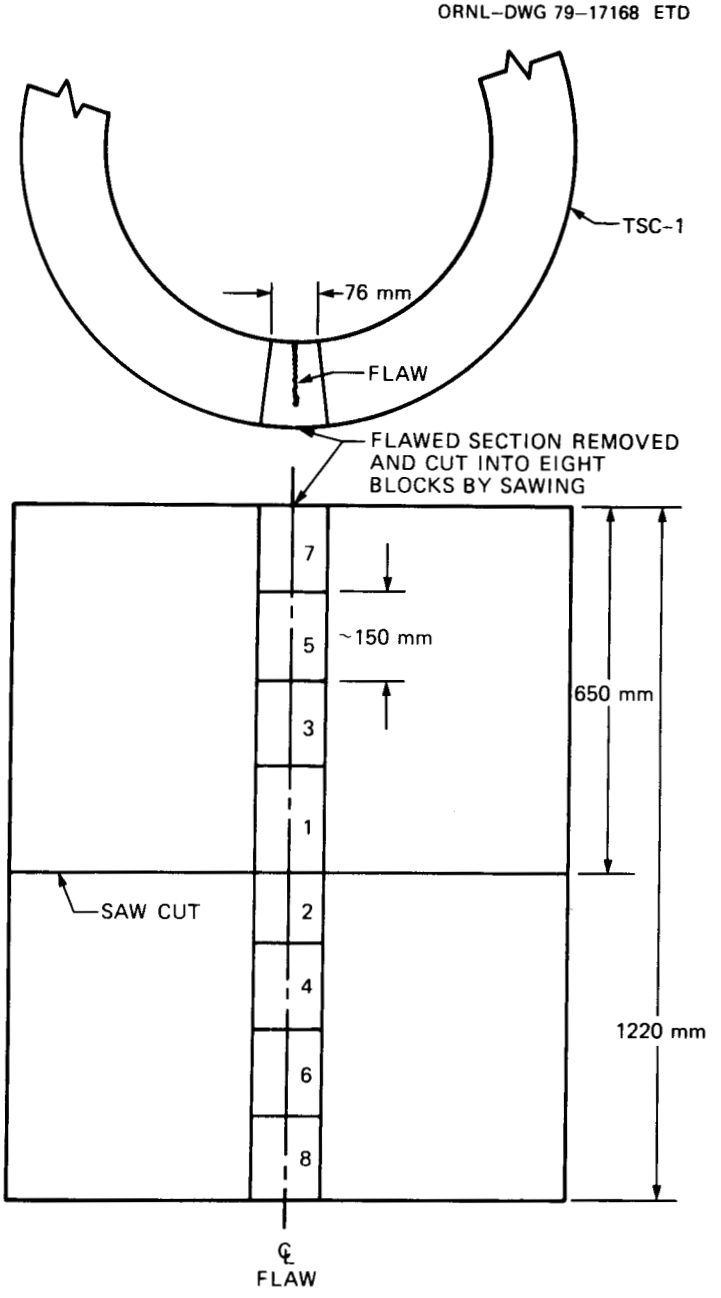

Fig. 8.9. Section of TSE-5 test cylinder removed for study of crack profile and fracture surfaces.

M&C PHOTO Y164626

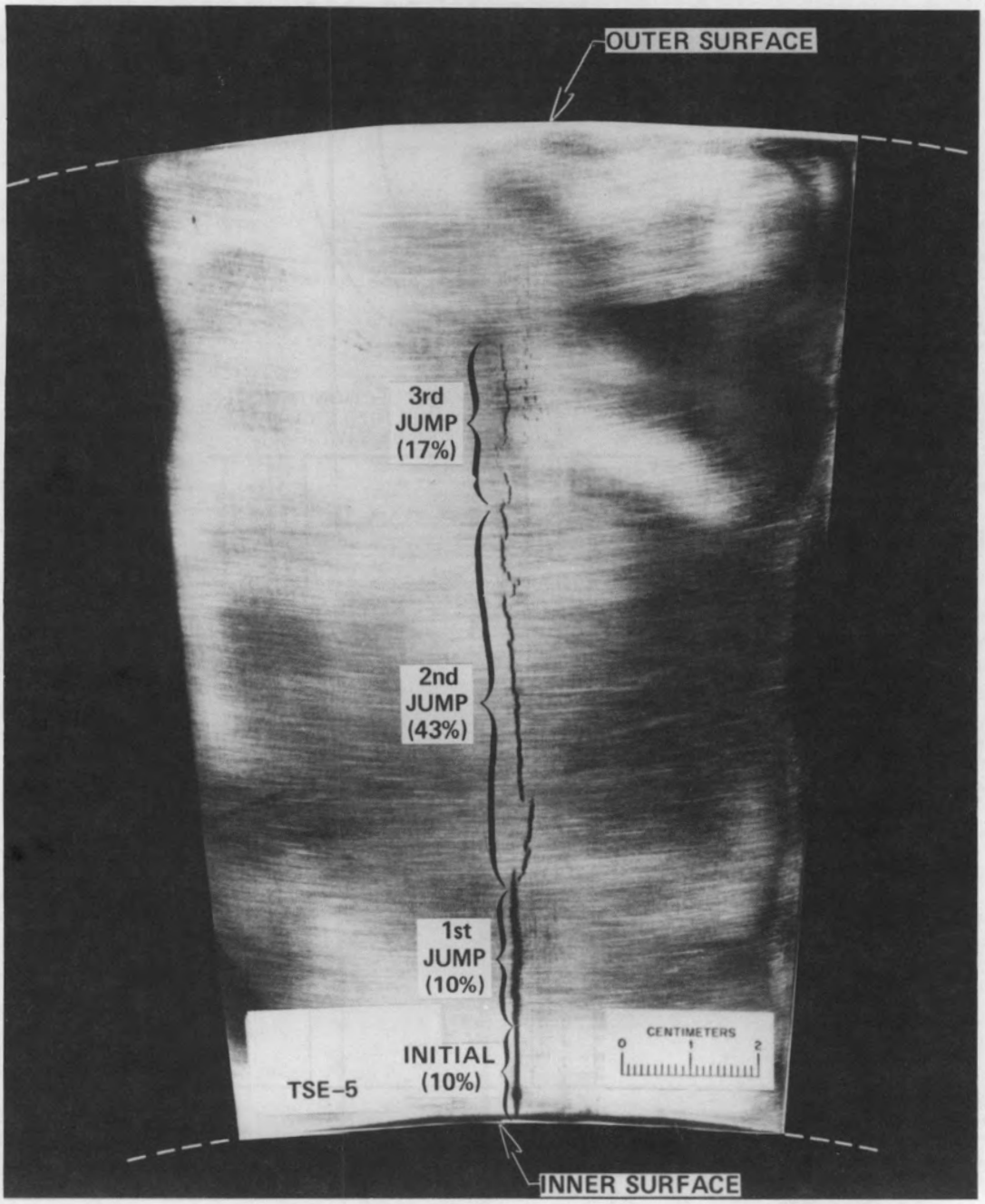

Fig. 8.10. Cross section of TSE-5 final flaw near midlength of test cylinder.

ORNL PHOTO 0057–80

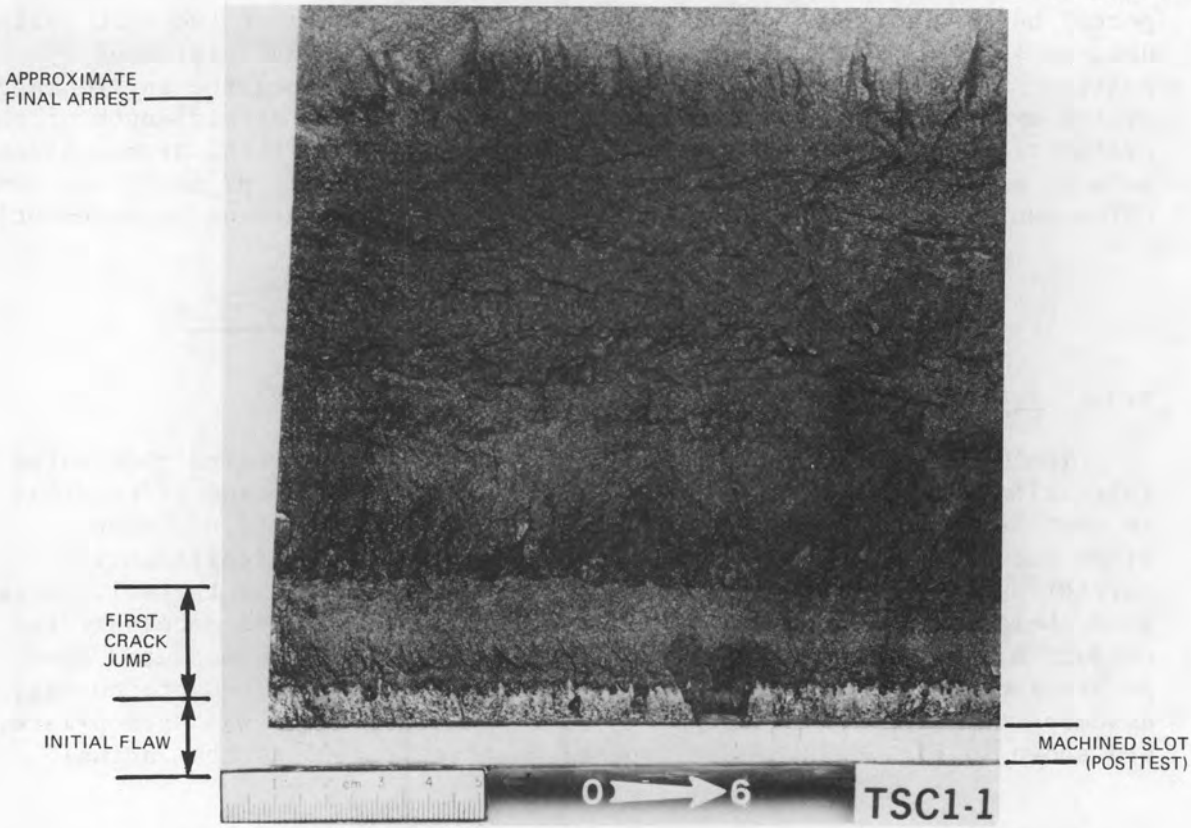

Fig. 8.11. Fracture surface (near midlength of test cylinder) of TSE-5 final long axial flaw.

ORNL–DWG 79–17163 ETD

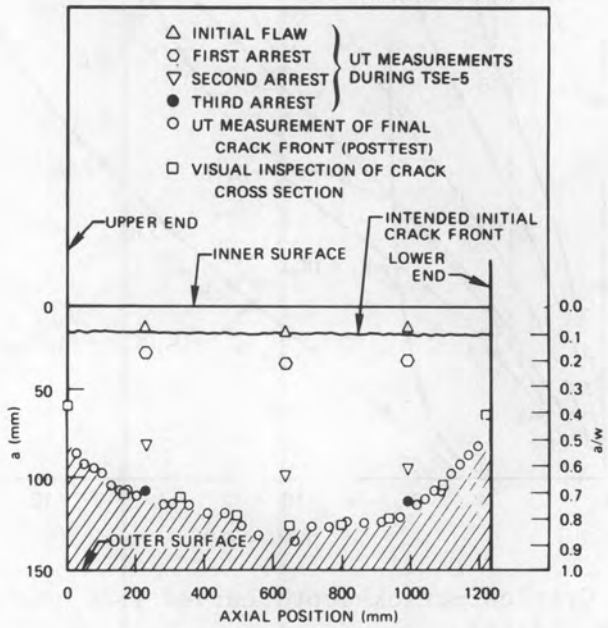

Fig. 8.12. Measurements of crack depth during and after TSE-5.

the test cylinder was greater than near the ends. This behavior was expected because of the variation in K_I along the length of the test cylinder, as shown in Fig. 4.2. The initial crack depth, as determined by posttest fracture-surface measurements was uniform along the entire length of the cylinder and was equal to 15 mm (a/w = 0.10). At midlength of the cylinder, the crack depths for the first, second, and third arrest events were 30 mm (a/w = 0.20) (fracture-surface measurement), 97 mm (a/w = 0.63) (UT measurement), and 122 mm (a/w = 0.80) (fracture-surface measurement).

8.4 Fracture-Mechanics Analysis of Primary Flaw

8.4.1 Posttest analysis based on design toughness curve

The TSE-5 pretest fracture-mechanics analysis indicated that three initiation-arrest events would take place during TSE-5, and indeed that is what happened. However, a comparison of the estimated and actual times for the events shows that the latter times were significantly earlier due in part to the greater severity of the actual thermal shock. Thus, before additional comparisons could be made, it was necessary to conduct a posttest fracture-mechanics analysis using the measured temperature distributions. The corresponding critical-crack-depth curves, assuming that the TSE-5-design K_{Ic} vs temperature curve was appropriate, are shown in Fig. 8.13. Superimposed on these curves is the "actual"

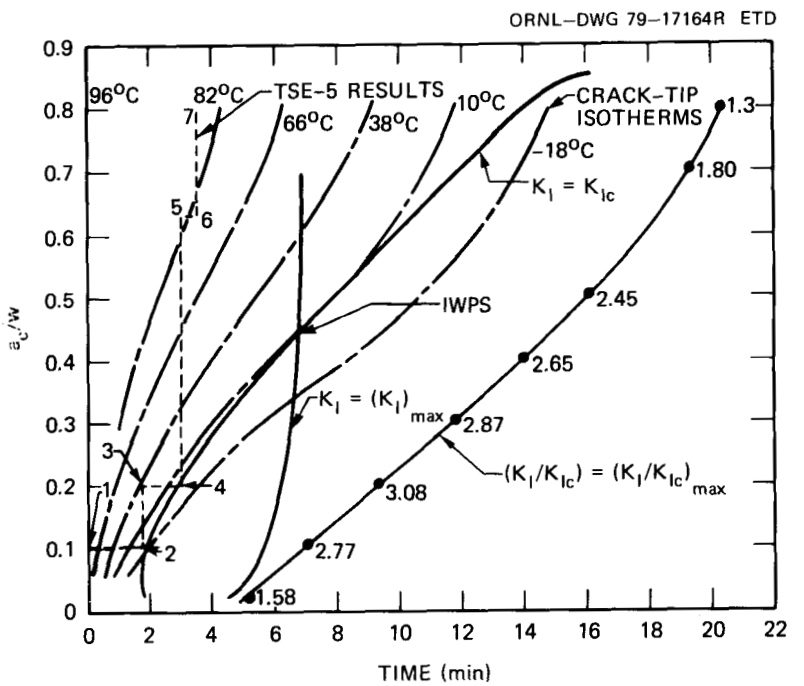

Fig. 8.13. Critical-crack-depth curves from posttest analysis of TSE-5 (original K_{Ic} data).

path of events, using the measured midlength crack-arrest depths. As indicated, the first two initiation events agree well with the calculations, but the very long second crack jump [$\Delta(a/w) \cong 0.4$] resulted in arrest at a much greater depth and temperature than expected. Thus, the toughness at the higher temperature had to be much less than indicated by the design-toughness curve.

8.4.2 K_{Ic} and K_{Ia} values deduced from TSE-5

The calculated K_I vs time and K_I vs a/w curves for the actual thermal shock are shown in Figs. 8.14 and 8.15 with the initiation-arrest events superimposed. As indicated in these figures, the K_I values corresponding to the three initiation-arrest events are 79, 111, and 115 MPa•$\sqrt{m}$ for the initiation events and 86, 104, and 92 MPa•$\sqrt{m}$ for the arrest events. Corresponding temperatures obtained from Figs. 8.1–8.3 are –9, –3, and 79°C for the initiation events and 36, 82, and 89°C for the arrest events. All of these data are summarized in Table 8.1.

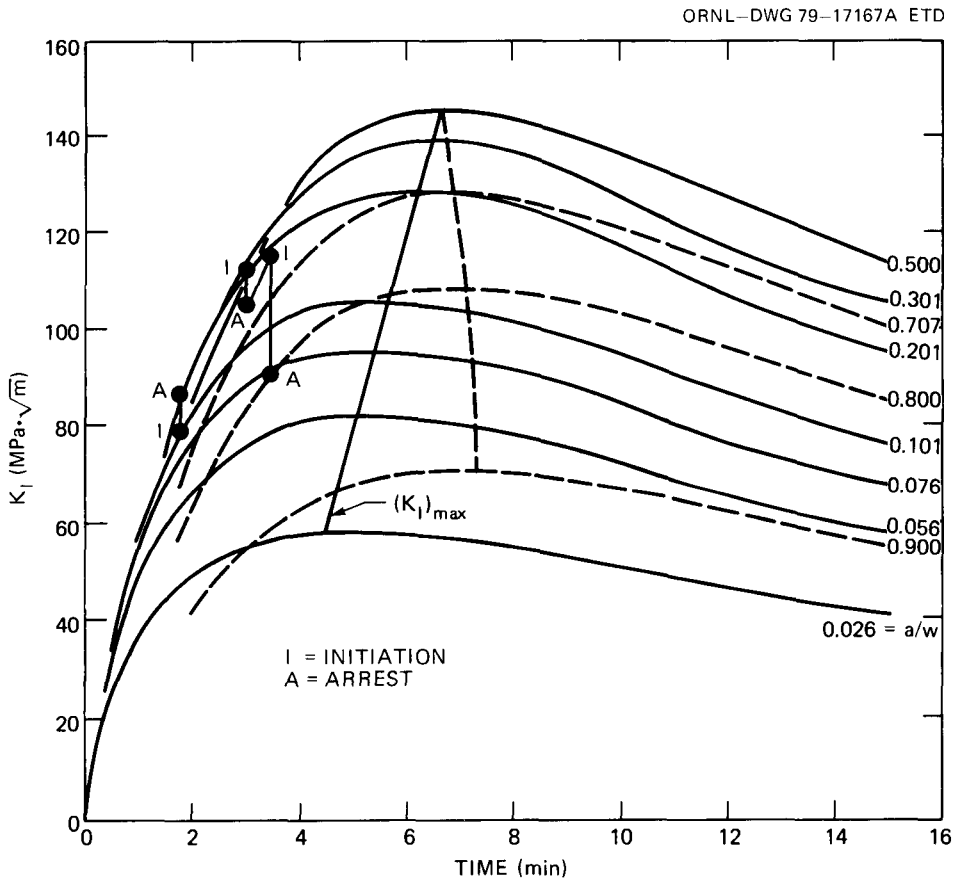

Fig. 8.14. K_I vs time for several crack depths (TSE-5 posttest analysis).

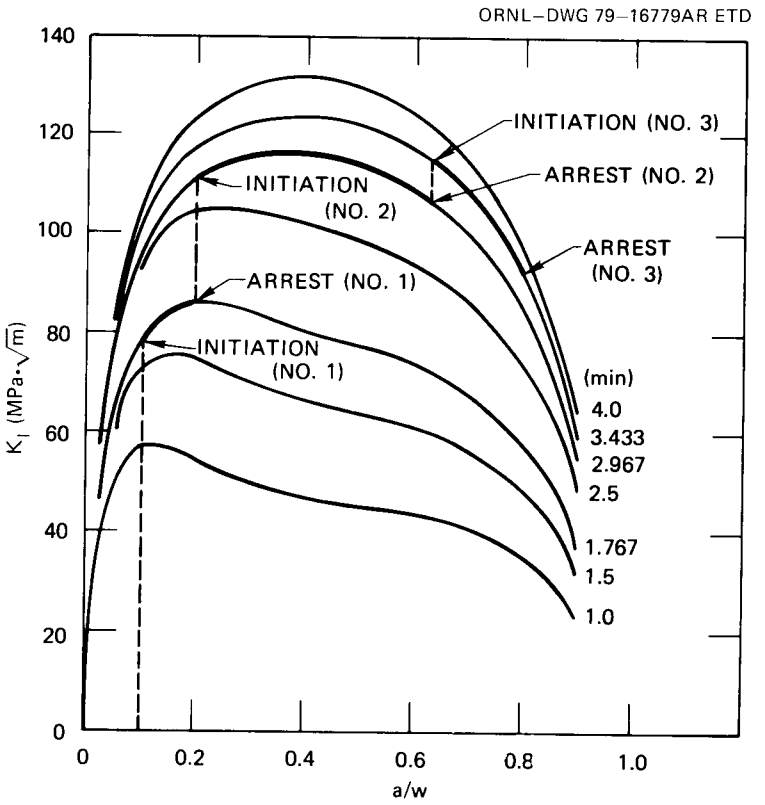

Fig. 8.15. K_I vs a/w for several times in the TSE-5 transient (posttest analysis).

Table 8.1. Summary of data corresponding to the events for the long axial flaw (TSE-5)

Parameters	Initiation-arrest event		
	1	2	3
Time, s	105	177	205
Crack depth,[a] a/w			
Initiation	0.10	0.20	0.63
Arrest	0.20	0.63	0.80
Temperature, °C			
Initiation	−9	−3	79
Arrest	36	82	89
K_{Ic}, MPa•$\sqrt{m}$	79	111	115
K_{Ia}, MPa•$\sqrt{m}$	86	104	92
Duration of experiment, min	30		

[a]Maximum depth (midlength of test cylinder).

8.4.3 Posttest analysis based on K_{Ic} and K_{Ia} curves deduced from TSE-5

A comparison of the K_{Ic} and K_{Ia} values deduced from TSE-5 and the TSE-5 design curve for K_{Ic} vs temperature is shown in Fig. 8.16. It is apparent from this comparison that the material toughness for temperatures above 0°C was considerably less than specified. Assuming that a more realistic K_{Ic} curve over the temperature range of interest is a straight line drawn through the first and third initiation values (dashed line) and that an appropriate K_{Ia} curve could be obtained by shifting this K_{Ic} curve 56°C, another posttest calculation was made. The corresponding set of critical-crack-depth curves is shown in Fig. 8.17 with

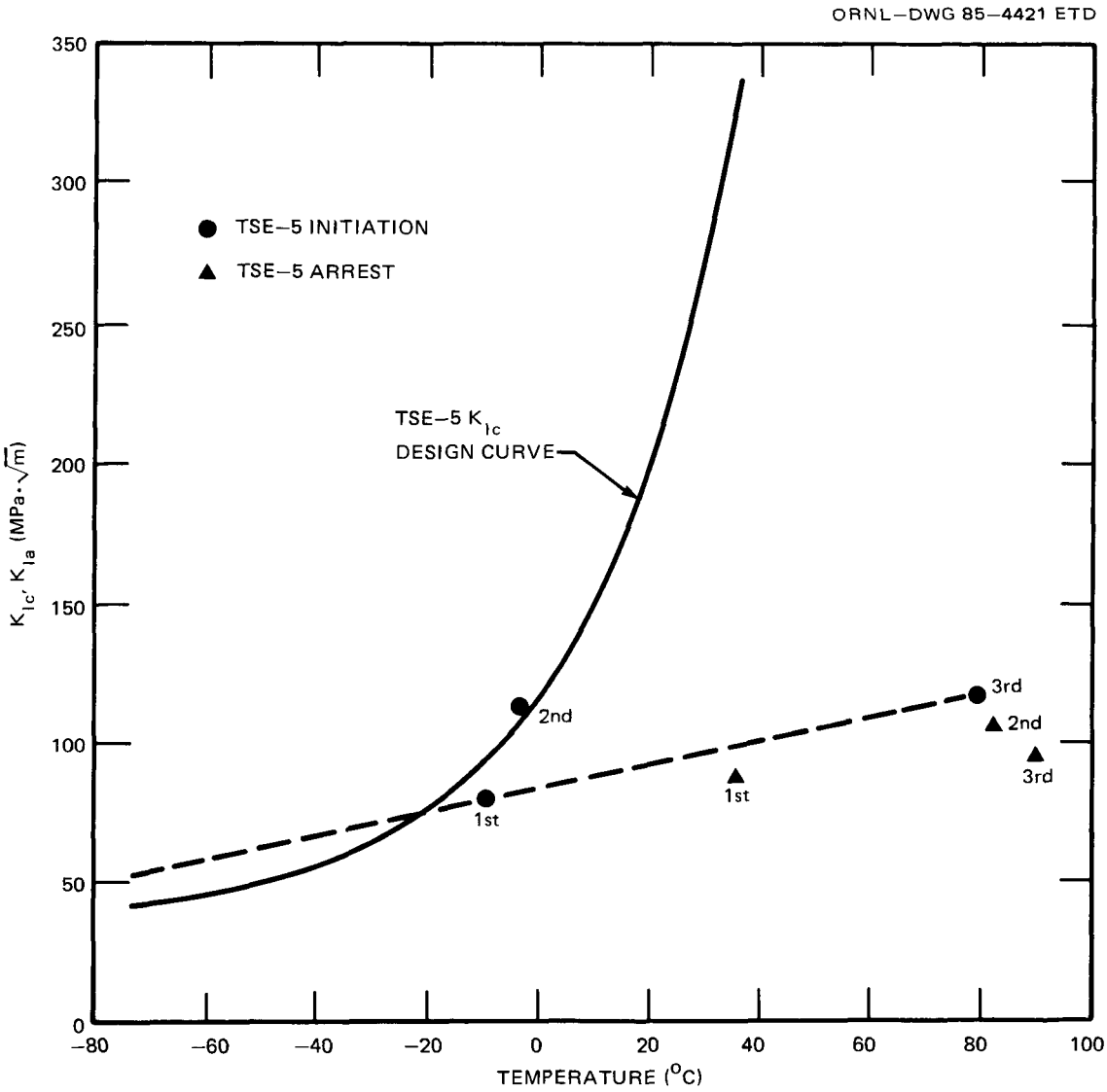

Fig. 8.16. K_{Ic} and K_{Ia} values deduced from TSE-5.

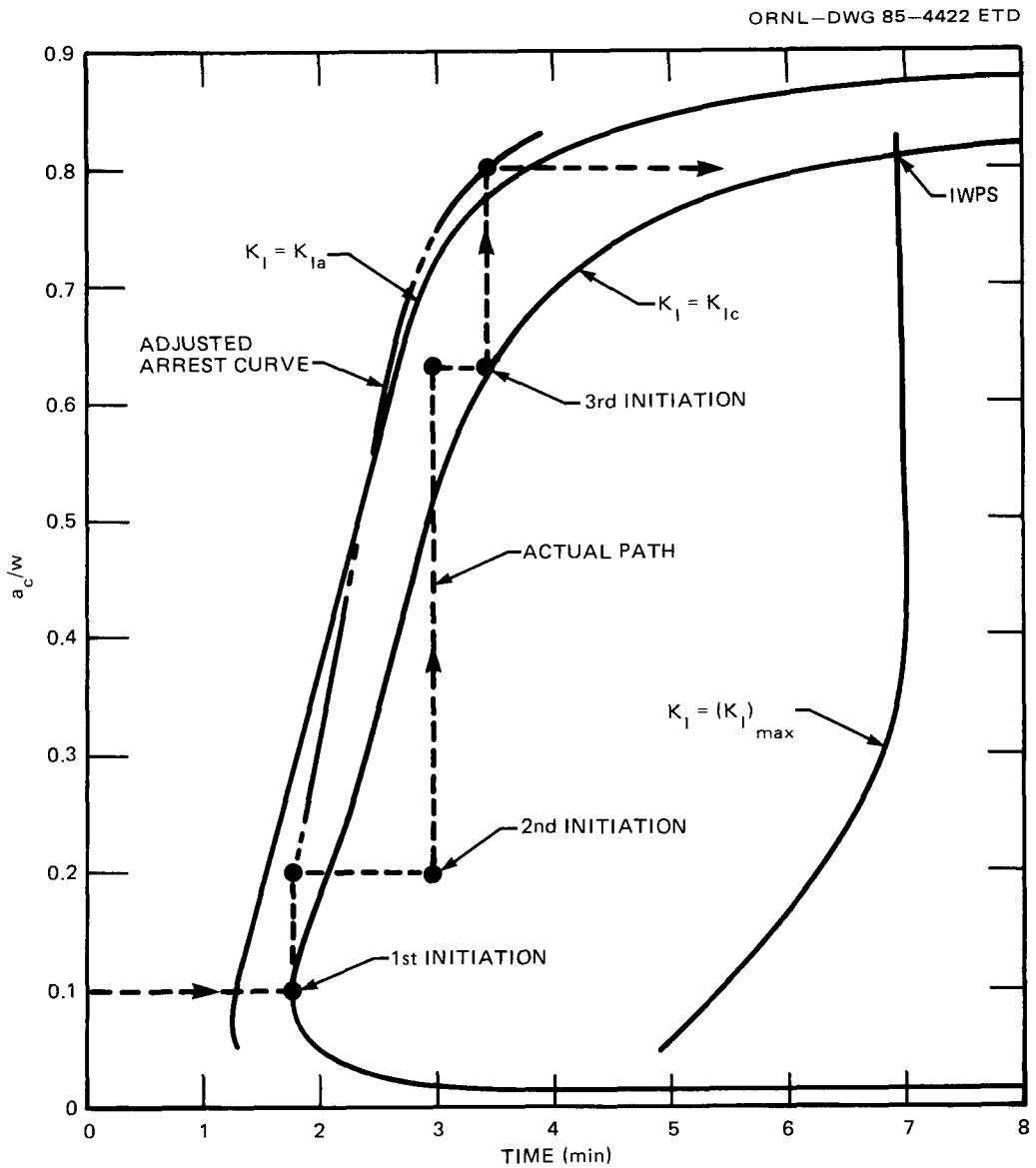

Fig. 8.17. Critical-crack-depth curves from posttest analysis of TSE-5 using TSE-5 K_{Ic} data.

the path of actual events superimposed (detailed digital output for this case is included in Appendix D). It is observed in Fig. 8.17 that the second initiation event falls far to the right of the initiation curve, indicating that the effective toughness for that event was greater than would be expected. (This situation would be expected to result in a long crack jump, and, as indicated, that is what happened.) It may be that the effective toughness was high as a result of crack-tip blunting due to the preceding arrest event, but this was not observed for the third initiation event. Another possible explanation is a radial variation in toughness that is not associated with unusual crack-tip conditions. However, such a gradient presumably would affect arrest behavior as well,

but it is observed in Fig. 8.16 and implied by Fig. 8.17 that the arrest toughness for the first arrest event was not relatively high.

The indicated relatively high toughness associated with the second initiation event might also be explained by the existence of low-toughness sites, as suggested by Landes.[2] If the density of these sites is such that a crack front may or may not coincide with a low-toughness site and if the effective toughness of these sites varies substantially, there can be considerable variation in the effective toughness from one initiation event to another, and the lowest-toughness sites will establish a lower bound for K_{Ic}, provided the local toughness is not less than K_{Ia}. Furthermore, the arrest toughness would not be influenced by the low-toughness sites because presumably arrest takes place in accordance with the relatively high toughness of the bulk of the material. It might be expected that a structure such as the TSE-5 test cylinder with a very long flaw (1.22 m) would behave in accordance with lower-bound toughness because of the likelihood of the long crack front coinciding with a lower-bound toughness low-toughness site. However, this may not always be the case and if not would explain what happened during TSE-5.

8.4.4 Evidence of large scatter in lab K_J data

The apparent discrepancy between the specified and actual toughness curves for TSE-5 prompted additional material-characterization studies. They were carried out on the TSE-5 and TSE-6 test-cylinder prolongation material following TSE-5 in preparation for TSE-6. The results of all K_J and K_{Ia} measurements are shown in Fig. 8.18 (same data as that in Fig. 7.7). It is observed that the upward scatter in the K_J data relative to the lower bound is quite large (as much as 300%), while the scatter in the smaller sampling of lab K_{Ia} values is much less.

The lower-bound K_J curve in Fig. 8.18 represents the lower bound of some valid (K_{Ic}) data at temperatures below ~30°C and the lower bound of nonvalid data above that temperature. Thus, at temperatures above ~30°C a valid lower-bound curve could be somewhat lower. Of course, any lower-bound curve is only the lower bound of a particular set of data and does not preclude the existence of even lower data points, valid or otherwise. With this in mind, it is of interest to compare the three K_{Ic} values deduced from TSE-5 with the lower-bound K_J curve and the upper-bound K_{Ic} curve in Fig. 8.18, and such a comparison is made in Fig. 8.19. It is apparent that the first two K_{Ic} values are well above the lower-bound K_J curve (55 and 109%), while the third value is slightly less than the lower bound. It is also observed that the first K_{Ic} value is midway between the small-specimen K_{Ic} scatter bands, while the second value is close to the upper bound. Thus, even a very large specimen (1.22-m-long crack front) can exhibit large scatter in K_{Ic} data, at least when arrest and reinitiation events are involved.

A comment should also be made about rather special and not well-defined conditions that exist at the tip of the initial flaw. As mentioned in Sect. 5.4, the initial flaw was generated by means of the EB-weld process. Cracking of the EB-weld fusion zone to create the initial flaw presumably is the result of high residual tensile stresses in the fusion zone as well as very low fracture toughness, both of which are the

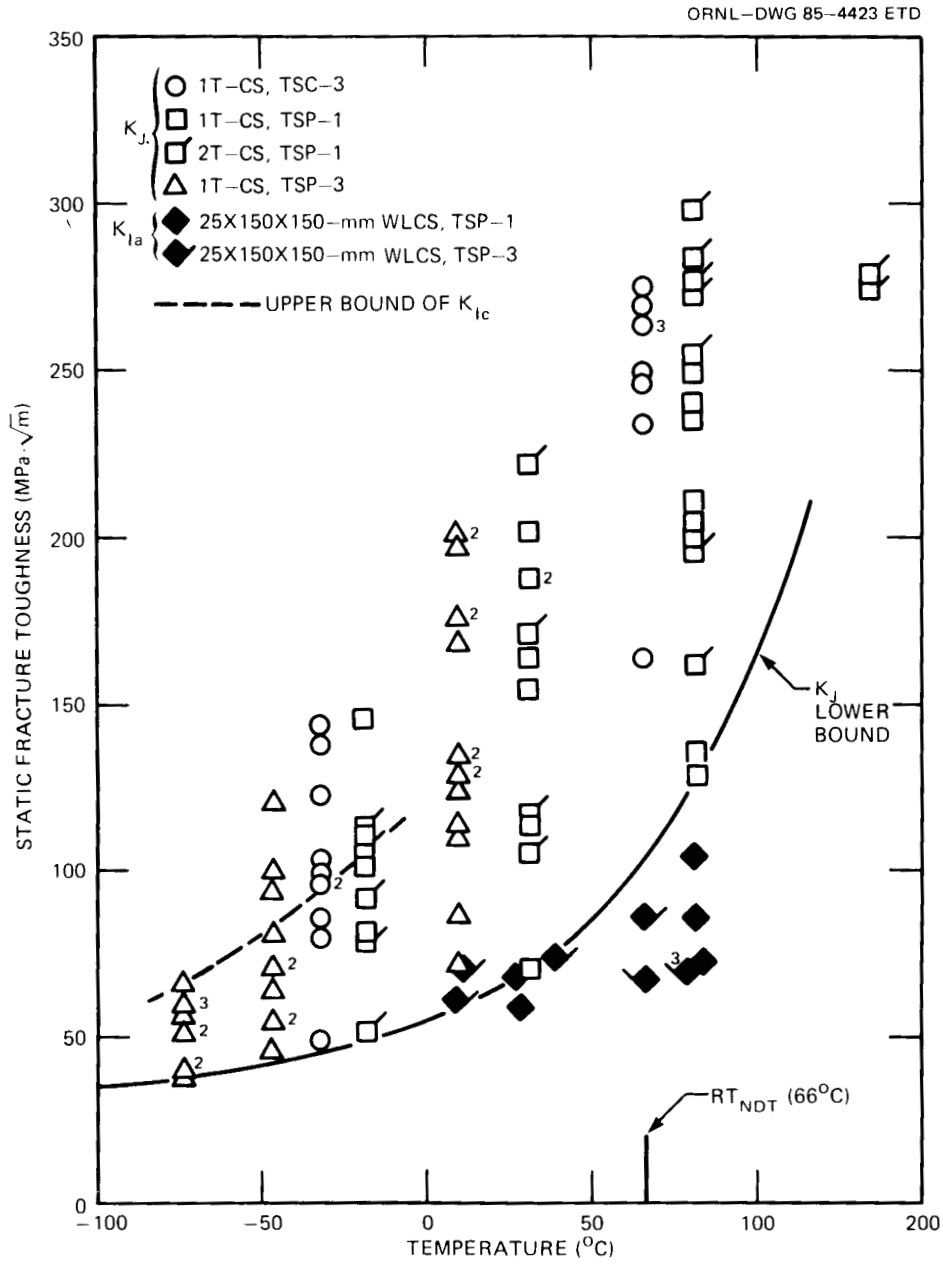

Fig. 8.18. Small-specimen fracture-toughness data for TSE-5 and TSE-6 test-cylinder prolongation, showing upper bound of K_{Ic} data.

result of very rapid quenching of the fusion zone moments after the zone is created. Cracking of the fusion zone, which normally takes place sometime later during hydrogen charging and at room temperature, relieves some of the residual stress, and the crack arrests near the tip of the fusion zone. Thus, the initial flaw has a residual K_I value equal to the room-temperature value of K_{Ia} near the tip of the fusion zone, and the toughness of the material at the tip of the flaw presumably is lower than

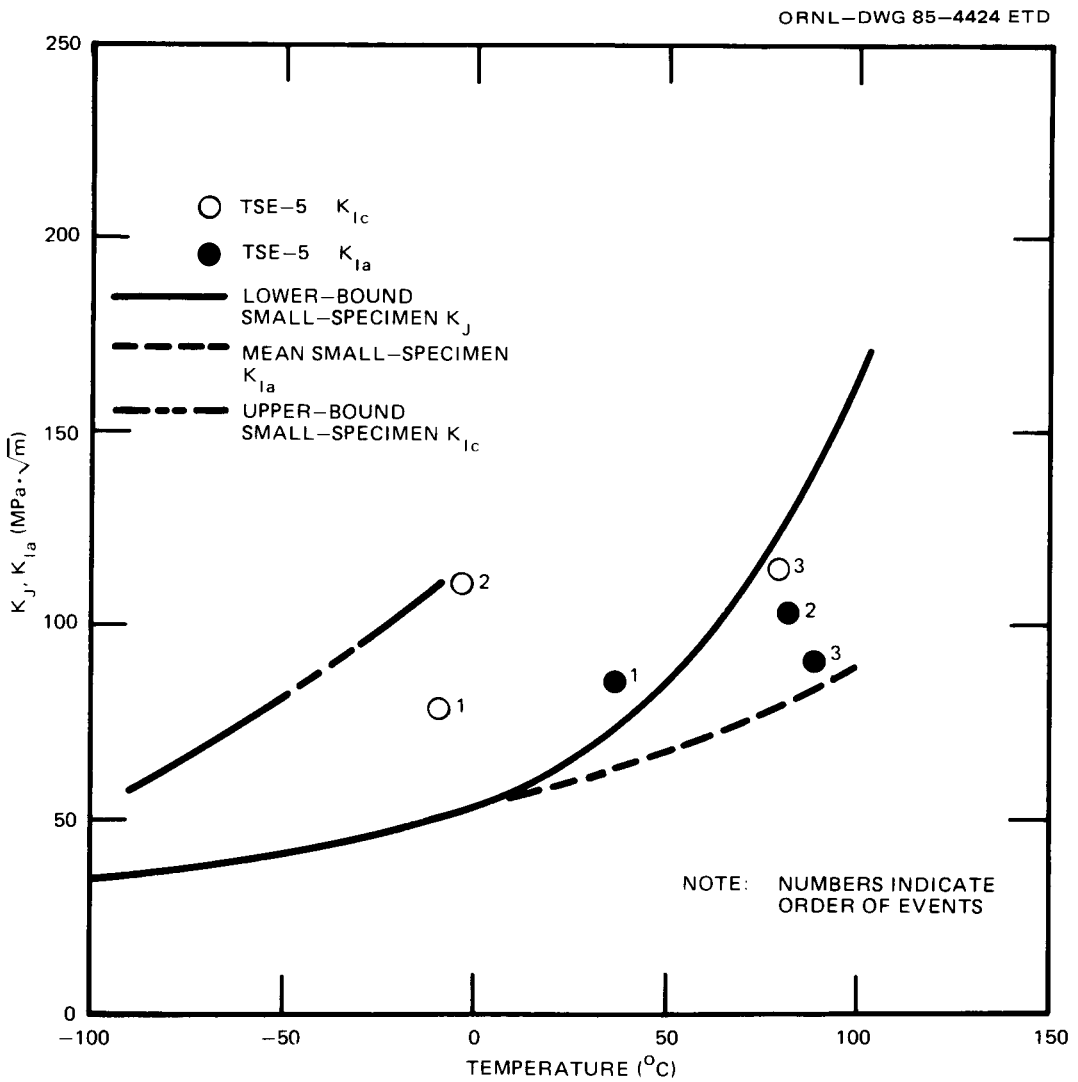

Fig. 8.19. Comparison of TSE-5 K_{Ic} and K_{Ia} values with lower-bound K_J and mean K_{Ia} small-specimen data.

that for the surrounding material. Because of these conditions and presumed very steep gradients in the residual stress and fracture toughness beyond the tip of the flaw, very small "early" crack jumps would be expected during a thermal-shock experiment until the crack tip extends to the edge of this small region. At the time of the first relatively large crack jump the residual K_I value and the deviation in fracture toughness due to the EB weld should be negligible. Furthermore, the extension of the flaw prior to the first major event should also be negligible. Even so, it is of interest to note that, although small, the effect of the residual stress and the extended crack length is a larger K_I value and a higher crack-tip temperature at the time of the first major event than that calculated on the basis of the initial flaw depth and the applied loads.

The average of the lab K_{Ia} values included in Fig. 8.18 is about 20% less than the TSE-5 K_{Ia} values, and the lowest K_J values in the temperature range −20 to 40°C are 28% less than the TSE-5 K_{Ic} curve constructed in Fig. 8.16. It is also observed that, in this temperature range, the smallest lab K_J values are about equal to the lab K_{Ia} values. At a temperature of ~80°C, the K_{Ia} values are somewhat less than those deduced from TSE-5.

8.4.5 Implications of two-dimensional analysis of flaw

The critical K_I values calculated for TSE-5 and included in Table 8.1 and Fig. 8.19 are based on a two-dimensional analysis of the flaw; that is, the flaw was assumed to be uniform in depth and infinitely long, the depth being that at the central portion of the test cylinder. Thus, the calculated K_I values do not reflect the restraining effect of the actual flaw shapes that developed during the experiment, nor do they include the effect of the finite length of the cylinder.

As discussed in Sect. 4.1, the free-end effect results in relatively low values of K_I near the ends of the cylinder for a uniform depth flaw, and this was responsible for less propagation of the flaw near the ends than elsewhere. The resultant flaw shape tends to result in lower K_I values at the deepest point relative to that calculated for a two-dimensional flaw of the same depth. However, the three-dimensional K_I value at midlength of a uniform-depth flaw is somewhat greater than the two-dimensional value. Thus, the effects of the finite length of the cylinder and of the actual flaw shape for the extended flaws tend to compensate near midlength of the cylinder.

As a check on the adequacy of the two-dimensional analysis, a three-dimensional analysis was performed for the final flaw shape in TSE-5, using the temperatures that corresponded to the final arrest event. The flaw was modeled as shown in Fig. 8.20, and the results of the analysis indicated good agreement with the two-dimensional analysis for the central portion of the cylinder. Toward the ends of the cylinder, the three-dimensional K_I values were somewhat higher (<10%), and this, together with the lower toughness (lower temperature) associated with the shallower portion of the crack front, introduced the possibility of a higher critical value of K_I and a corresponding lower value of the temperature than those values included in Table 8.1 and Figs. 8.16 and 8.19, at least for the final crack configuration.

The accuracy of the three-dimensional analysis near the ends of the cylinder was not expected to be better than 10%. Thus, an additional method for estimating the distribution of K_I along the crack front was considered. If the assumption is made that the entire crack front arrests at exactly the same time, it can be concluded that K_I at that instant must decrease toward the ends of the cylinder. This is because at the instant of arrest, $K_I = K_{Ia}$ all along the crack front, and K_{Ia} decreases toward the ends of the cylinder [result of decreasing crack depth (Fig. 8.12) and thus decreasing crack-tip temperature]. If reinitiation takes place shortly after the arrest event, the K_I distribution would be nearly the same as that at arrest. A detailed analysis of this type indicated that the decline in K_I toward the end of the cylinder was quite small (<10%). Thus, it was concluded that the two-dimensional analysis,

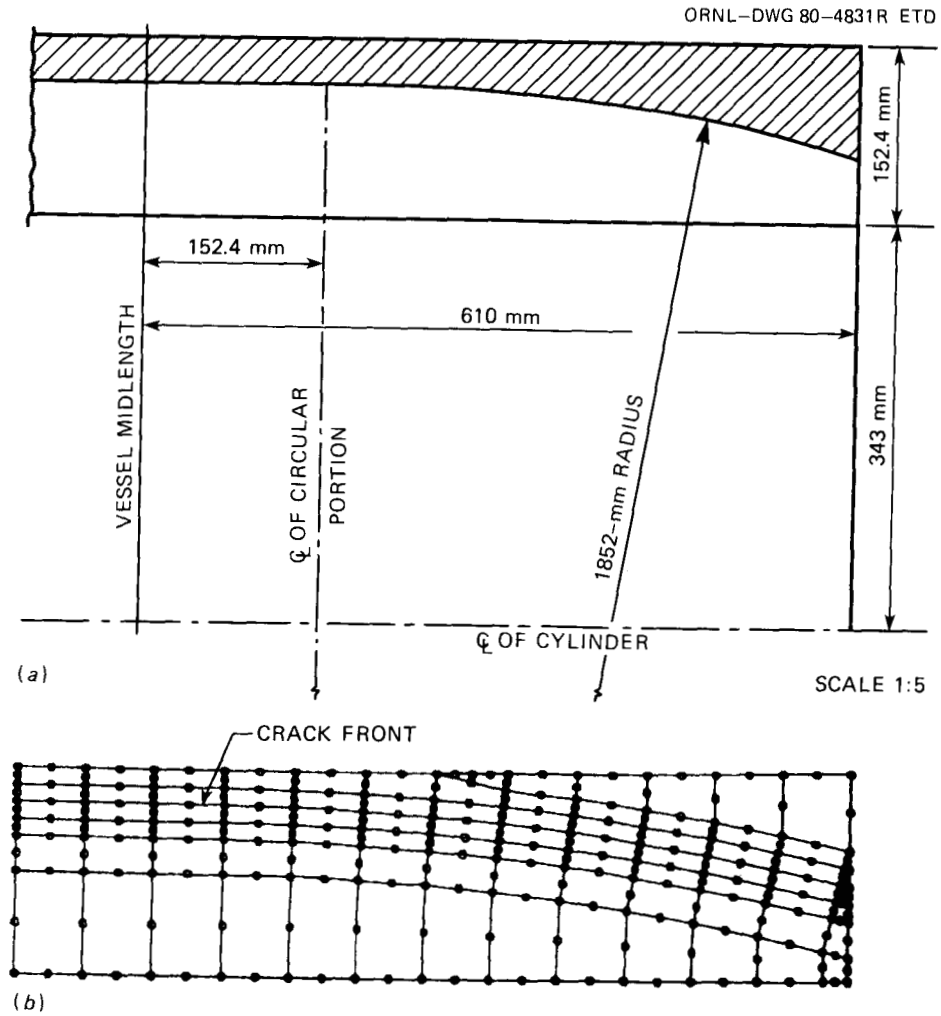

Fig. 8.20. Idealization of final arrested crack front of TSE-5 for purposes of three-dimensional finite-element analysis. (*a*) Partial longitudinal section through vessel wall, and (*b*) finite-element model of cylinder wall used to generate three-dimensional mesh by rotating it about cylinder axis.

using the midsection flaw depth, was appropriate for estimating critical values of K_I corresponding to initiation and arrest events.

8.4.6 Dynamic effects at arrest

The long crack jump that took place during TSE-5 introduced the possibility of dynamic effects that might have resulted in a significantly longer crack jump than that predicted with the usual static analysis. The possible existence of significant dynamic effects can be judged in at least two ways. First, it is assumed on the basis of the results of TSE-4 (Refs. 3 and 4) that the first and third crack jumps were short enough to have not been influenced by dynamic effects. The next step is

to compare the three crack depths at which the three arrest events took place, and this is done simply by adjusting the arrest curve in Fig. 8.17 so that it passes through the first and third arrest points. When this is done, it is apparent that the actual crack jump for the second event is *less* than predicted with the static analysis. Thus, a dynamic effect is not discernible and is presumed to be small.

The second method used to determine if the static analysis was adequate was to simply compare the K_{Ia} values deduced from TSE-5, using a static analysis, with K_{Ia} values measured in the lab. As indicated in Fig. 8.18 and 8.19 and mentioned in Sect. 8.3.4, the lab K_{Ia} values are less than those deduced from TSE-5. Use of the lab K_{Ia} data in an analysis would result in deeper calculated crack-arrest points. Thus, this comparison of lab K_{Ia} data and K_{Ia} values deduced from TSE-5 not only indicates no dynamic effects but also indicates a discrepancy between TSE-5 and lab K_{Ia} data. In this regard, it is of interest to note that dynamic effects in the lab specimen, if unaccounted for in the calculation of the critical value of K_I, tend to result in low estimated values of K_{Ia}; that is, low compared with a situation for which dynamic effects are less.

One other clue to the possible extent of dynamic effects during the second crack jump is derived from knowledge of the crack velocity during the crack jump. As discussed in Sect. 8.5, an attempt was made to measure crack velocity during the second crack jump. It appears that the maximum velocity was ~100 m/s, which is much less than the average velocity for the cracks in lab crack-arrest specimens (>500 m/s). The lower velocity indicates less dynamic effect.

8.4.7 Warm prestressing

With regard to warm prestressing, the results in Fig. 8.17 show that use of the "actual" toughness curve in the posttest analysis results in a much greater crack depth for incipient warm prestressing $[(a/w)_{IWPS} = 0.80]$ than calculated with the design-toughness curve $[(a/w)_{IWPS} = 0.45]$ (see Fig. 8.13), and the corresponding value of $(K_I/K_{Ic})_{max}$ is only 1.16. Thus, although warm prestressing may have prevented a fourth initiation event, conditions were not favorable for a convincing demonstration of warm prestressing during TSE-5.

8.4.8 Arrest in a rising K_I field

The low toughness of the TSE-5 test-cylinder material also prevented a demonstration of arrest in a rising K_I field during TSE-5. This is illustrated in Fig. 8.15, which shows that the first arrest event took place with $dK_I/d(a/w) \cong 0$, and for the second and third arrest events $dK_I/d(a/w)$ was negative.

8.5 Estimate of Crack Depth from COD Data

The COD measurements can be used to obtain estimates of crack depth by calculating the relation between COD and crack depth. This relation

was obtained from the two-dimensional fracture-mechanics analysis of TSE-5, and the results are shown in Fig. 8.21 for times corresponding to the three initiation-arrest events. COD-gage output was converted to actual COD by calibrating typical COD gages in a testing machine. The calibration factor was constant over the full range of the gage, was essentially independent of the temperature range of interest (93 to −196°C), and was equal to 25-mm COD/ε (see Appendix B).

Fractional crack depths (a/w) derived from the COD data and as measured directly are presented in Table 8.2. The COD values used were the averages of gages 5 and 7.

The differences observed in Table 8.2 are probably within the accuracy of the measurements and calculations. However, the general trend of the differences is consistent with the three-dimensional effect that developed as the flaw propagated deeper into the wall, increasing the nonuniformity in crack depth (shallower near the ends). The nonuniformity tends to decrease the COD for a given crack depth, and this effect is not included in the two-dimensional analysis. Thus, a three-dimensional analysis would tend to increase the a/w values derived from the COD measurements above those shown in Table 8.2, the effect increasing with increasing crack depth.

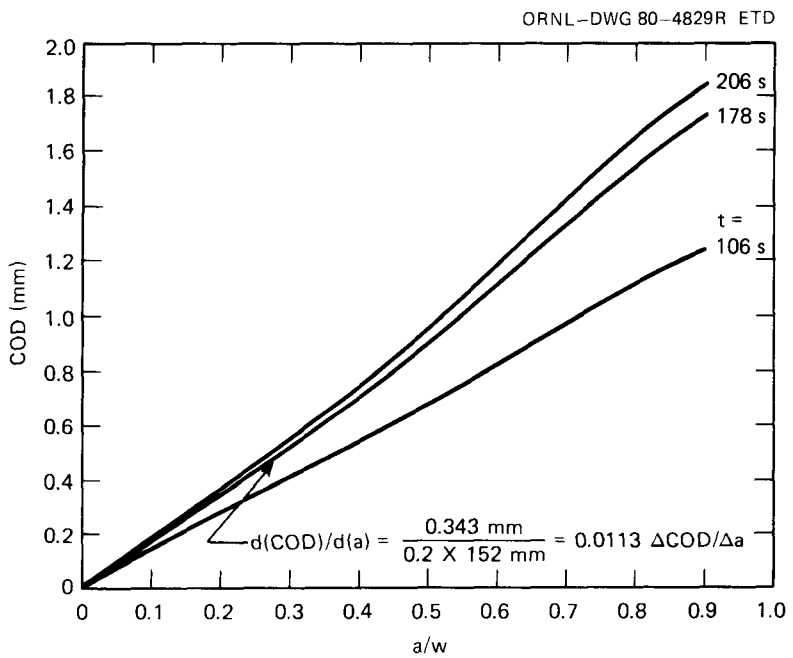

Fig. 8.21. Calculated COD vs a/w for TSE-5.

Table 8.2 Crack depths derived from COD data and from direct measurements

Time (s)	Fractional crack depth (a/w)	
	Direct	COD
106	0.10[a]	0.12
106	0.20[a]	0.21
178	0.20[a]	0.22
178	0.63[b]	0.55
206	0.63[b]	0.55
206	0.80[a]	0.72

[a]Fracture-surface measurement.

[b]UT measurement.

8.6 Crack-Velocity Measurements

An attempt was made to determine crack velocity during TSE-5 by measuring the crack-opening rate at the surface of the test cylinder with two of the nine COD gages. These two gages (gages 4 and 6, Fig. 6.5), located near midlength of the test cylinder, were recorded on fast-phenomena recorders. The effort was developmental in nature and was prompted by future plans for a long crack jump experiment.

Because of difficulties encountered with the fast recorders during TSE-5, only the second crack jump was recorded properly. COD vs time for this event is shown in Fig. 8.22. The slope of the steepest portion of the curve (initial straight-line segment) is

$$\frac{6 \times 4200\ \mu\varepsilon}{2.2 \times 215\ \mu s} = 53.2\ \frac{\varepsilon}{s}\ ,$$

and application of the COD-gage calibration factor (25-mm COD/ε) yielded the maximum COD rate:

$$(\dot{COD})_{max} = 52.3 \times 25 = 1.33\ m/s\ .$$

The slope of the COD vs a/w curve in Fig. 8.21 at a/w ≅ 0.2 is 0.0113 ΔCOD/Δa. Thus, the estimated maximum crack velocity is

$$a_{max} = 1.33\ m/s \times \frac{1}{0.0113} = 118\ m/s\ .$$

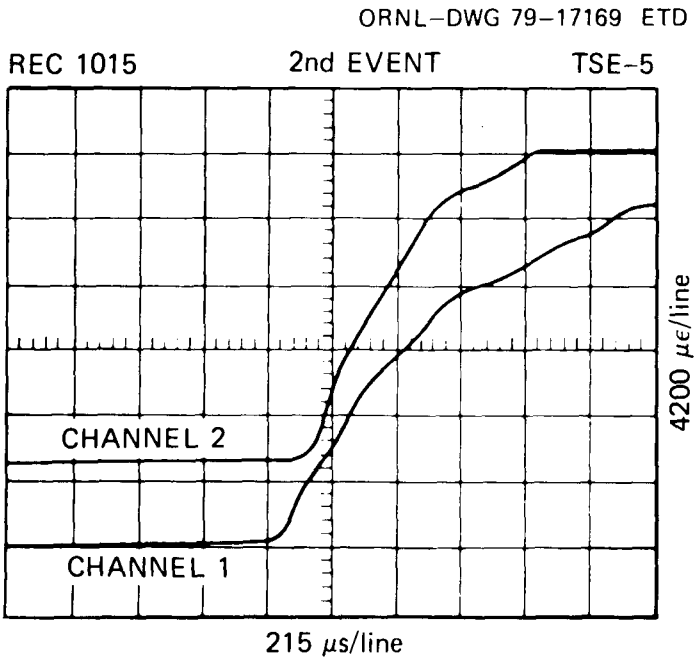

Fig. 8.22. COD output (gages 4 and 6) vs time for second crack jump during TSE-5.

It is of interest to note that this velocity is considerably less than that obtained during the lab K_{Ia} measurements (>500 m/s) for the TSE-5 material.

8.7 Secondary Cracking

As discussed in Sect. 5.4, the long axial flaw was generated by the EB-weld technique, wherein, following the welding process, hydrogen charging of the weld was used to promote cracking of the weld. While developing the technique specifically for TSE-5, it was observed during the hydrogen-charging phase that numerous circumferential cracks (cross cracks), confined in length to about twice the width of the EB-weld fusion zone (~5 mm), formed prior to the formation of the axial flaw. A post-TSE-5 view of a cross crack and a short portion of the axial crack at a depth of ~8 mm in the TSE-5 test cylinder are shown in Fig. 8.23. The abrupt discontinuity in the axial crack at the cross crack indicates that the cross crack developed first and that the axial crack developed in segments, the cross cracks terminating each segment. [Access to the 8-mm depth was gained by machining a narrow slot (~5 mm) to that depth following TSE-5.]

A pre-TSE-5 cursory examination of the cross cracks indicated that they were too small to propagate during TSE-5. However, because of the lower-than-expected fracture toughness, one of the cross cracks did propagate extensively during TSE-5, extending from one of its ends in a circumferential direction and then branching as shown in Fig. 8.24. Many

ORNL PHOTO 6391–80A

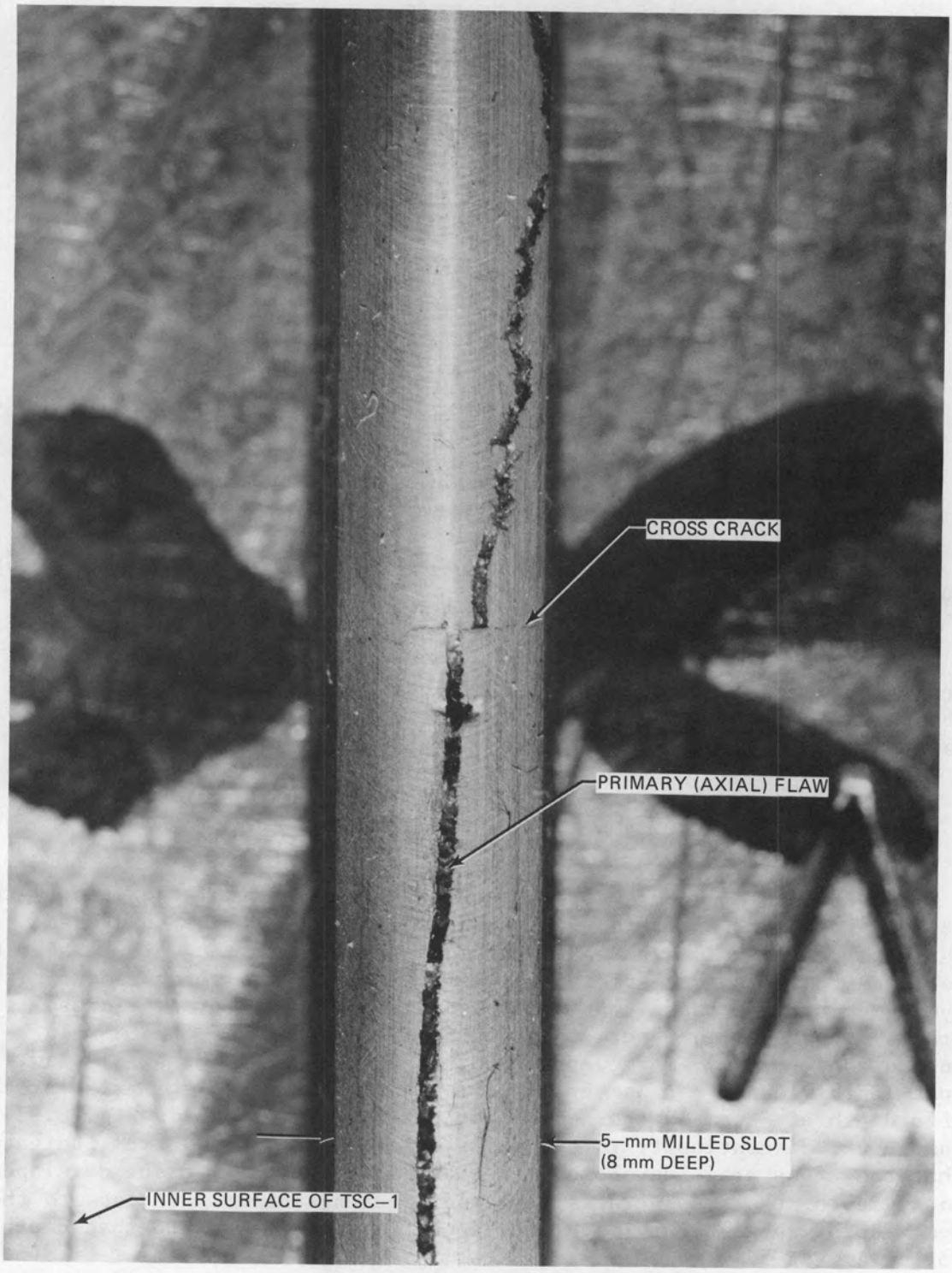

Fig. 8.23. Post-TSE-5 view of a cross crack and a portion of the primary (axial) flaw at a depth of 8 mm.

ORNL-DWG 79-16775R ETD

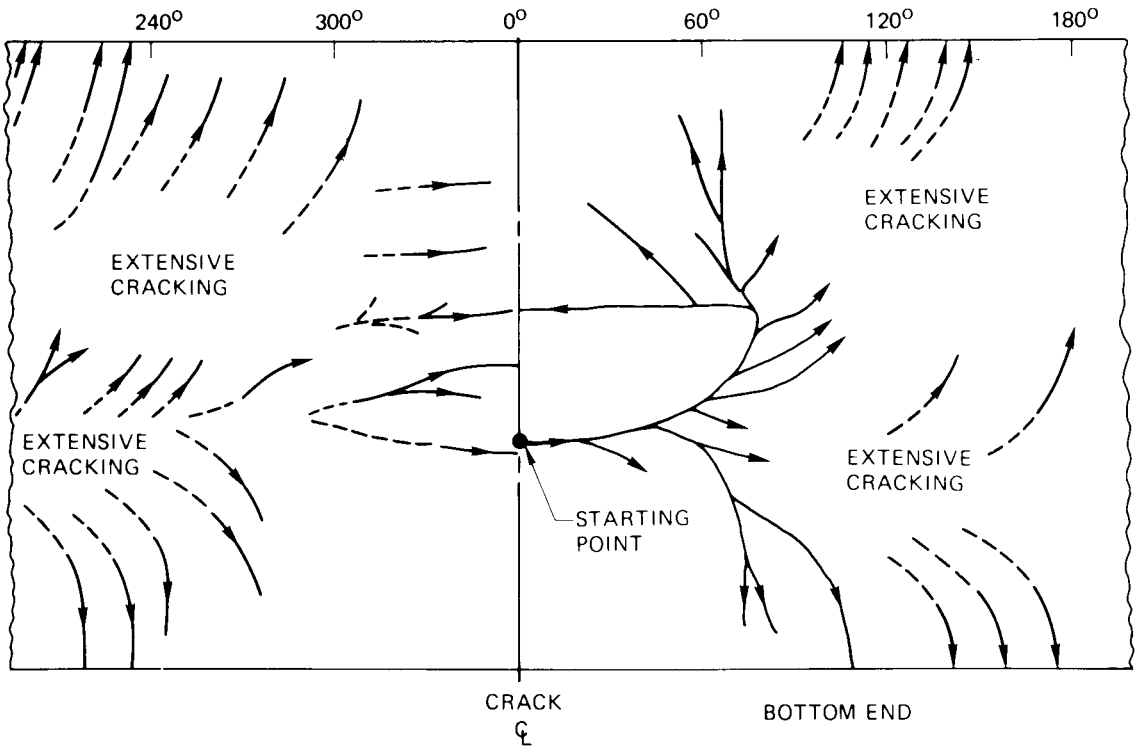

Fig. 8.24. Secondary cracking pattern on inner surface of test cylinder following TSE-5.

of the branches turned in an axial direction and terminated at or near the ends of the cylinder. Several circumferential branches effectively extended ~360°, terminating at or near the long axial (primary) flaw. Thus, TSE-5 demonstrated the ability of a very short crack to grow in length to become a much longer flaw.

The TSE-5 fracture-mechanics analysis (see Fig. 8.17) shows that flaws (both axial and circumferential) with depths as shallow as 1 mm could initiate during TSE-5. The time for initiation of the shallowest flaw would be ~5 min, and the temperature would be about −130°C. These shallow-crack events correspond to the lower portion of the initiation curve in Fig. 8.17, and thus a single, long crack jump might be expected. Long circumferential cracks and finite-length axial cracks would not jump as far as indicated by Fig. 8.17, and indeed the maximum fractional depth of the secondary cracking is only about 0.40.

The timing of secondary-crack propagation relative to primary-crack propagation is important because of the possible effect of the former on the latter. Three pieces of evidence indicate that the secondary cracking took place after propagation of the primary crack was completed. First of all, it is observed in Fig. 8.24 that while the secondary-cracking circumferential branches extend nearly a full 360°, axial branches did not form within the 120° segment centered about the primary axial flaw, even though in an unperturbed field axial flaws are more

likely to propagate deep than are circumferential flaws. This indicates that prior to propagation of the secondary crack, deep penetration of the primary flaw relieved the circumferential stresses locally, thus preventing the formation of axial flaws adjacent to the primary flaw. Deep penetration of the primary axial flaw would not relieve the axial stresses, and thus circumferential flaws could propagate up to the primary flaw.

The second piece of evidence is the observation that the circumferential cracks, with the exception of the initial cross cracks, do not extend across the primary flaw, indicating that the final flaw depth for the primary flaw existed prior to propagation of the secondary cracking.

The third bit of evidence comes from an examination of the fracture surfaces and from the fact that much branching took place. The branching indicates high crack velocity, and the fracture surfaces are very flat; both the high velocity and flat fracture indicate a low fracture temperature (toughness). By contrast, crack velocity for the primary flaw was relatively low, and, with the exception of the fracture surface corresponding to the first crack jump, the fracture surfaces were quite irregular and rough. Thus, it appears that the fracture temperatures for the secondary cracking were much less than those for the primary cracking, and this implies a later time in the transient for propagation of the secondary cracking.

Although it seemed very clear on the basis of these arguments that the secondary cracking occurred after the events associated with the long axial flaw, an analysis was performed to determine the effect that the secondary cracking could have on the long axial flaw if the secondary cracking had taken place earlier. Fracture-mechanics calculations were made with seven and nine secondary axial flaws in addition to the primary flaw. The secondary cracks were spaced about 30° apart (as shown in Fig. 8.25) starting 180° from the primary flaw. The fractional crack depth for these cracks was 0.35, and, for the primary crack, two depths were considered: $a/w = 0.1$ and 0.8. All calculations were made for a time of 7 min in the TSE-5 transient, because the COD for the primary crack was a maximum at this time. The calculational model was two-dimensional finite-element linear-elastic fracture mechanics.

Introduction of the secondary axial cracks tends to relieve the tensile stress in the inner portion of the wall and thus would tend to reduce the primary-crack COD. However, the existence of the secondary cracks also reduces the stiffness of the wall, and this reduction tends to increase the primary-crack COD.

Results of the analysis are shown in Table 8.3. For a primary crack depth (a/w) of 0.1, the introduction of seven secondary cracks decreases the COD by only 3%. For a crack depth of 0.8, the introduction of seven secondary cracks increases the COD by 10%, and the introduction of nine secondary cracks reduces the COD by 5%. Thus, even if the secondary cracking occurred during the propagation period for the primary crack, the effect of the former on the latter would be very small.

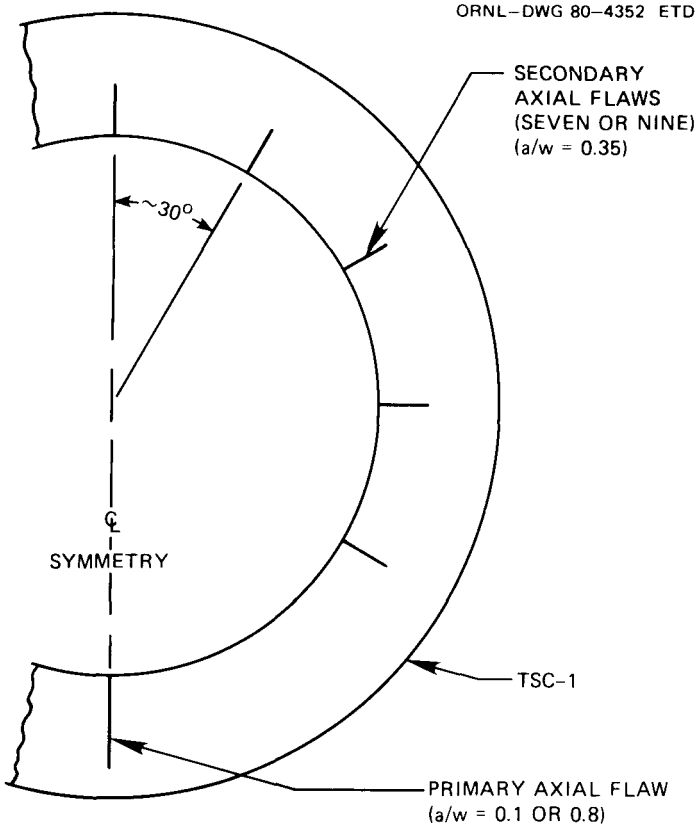

Fig. 8.25. Model used for two-dimensional analysis of secondary cracking effects during TSE-5.

Table 8.3. Calculated CODs for the TSE-5 primary crack with and without the existence of secondary cracking and with a/w (secondary) = 0.35 and t = 7 min

Total number of cracks	Primary-crack depth (a/w)	COD Primary crack (mm)
1	0.1	0.170
8	0.1	0.166
1	0.8	1.91
8	0.8	2.11
10	0.8	1.82

References

1. B. R. Bass, *INCAP: A Finite Element Program for One-Dimensional Nonlinear Inverse Heat Conduction Analysis*, NUREG/CR-0832 (ORNL/NUREG/CSD/TM-8), Union Carbide Corp. Nuclear Div., Oak Ridge Natl. Lab., July 1979.

2. J. D. Landes and D. H. Shaffer, *Statistical Characterization of Fracture in the Transition Region*, Westinghouse Scientific Paper 79-ID3-JINTF-P4, June 8, 1979.

3. R. D. Cheverton, Appendix B in *Pressure Vessel Fracture Studies Pertaining to a PWR LOCA-ECC Thermal Shock: Experiments TSE-3 and TSE-4 and Update of TSE-1 and TSE-2 Analysis*, ORNL/NUREG-22, Union Carbide Corp. Nuclear Div., Oak Ridge Natl. Lab., December 1977.

4. R. D. Cheverton and S. K. Iskander, *Application of Static and Dynamic Crack Arrest Theory to Thermal-Shock Experiment TSE-4*, NUREG/CR-0767 (ORNL/NUREG-57), Union Carbide Corp. Nuclear Div., Oak Ridge Natl. Lab., June 1979.

9. TSE-5A RESULTS

9.1 Heat Transfer

The thermal shock for TSE-5A was intended to be somewhat more severe than that corresponding to TSE-5, and, as shown in Fig. 9.1, the quench rate achieved during TSE-5A was, in fact, somewhat greater than that for TSE-5. Furthermore, the quench was very uniform over the inner surface, and, thus, the thermal two-dimensional nature of the problem was preserved.

Measured temperature distributions through the wall of the TSE-5A test cylinder at times corresponding to the four initiation-arrest events that took place during TSE-5A are shown in Figs. 9.2–9.5, and additional temperature distributions are shown in Fig. 9.6.

A combined heat transfer coefficient for the coolant fluid film and the rubber-cement coating was determined for TSE-5A and is plotted as a function of inner-surface (metal) temperature in Fig. 9.7. The method of

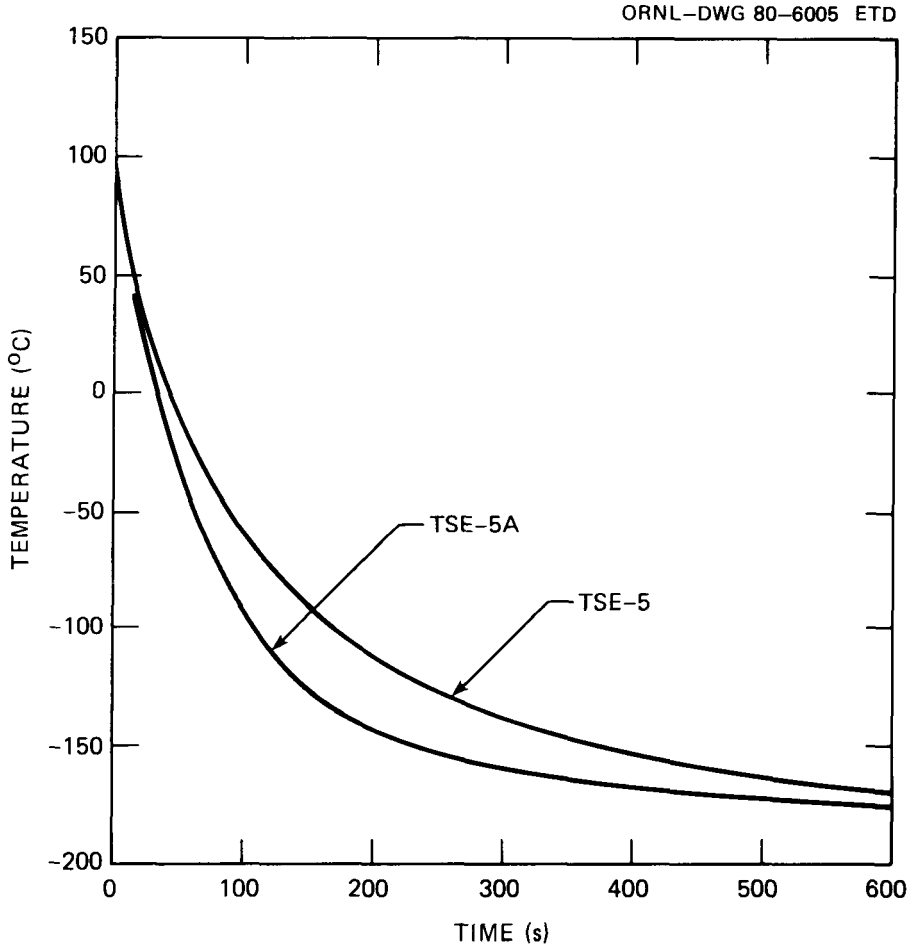

Fig. 9.1. Comparison of inner-surface (a/w = 0.0083) quench rate for TSE-5 and TSE-5A.

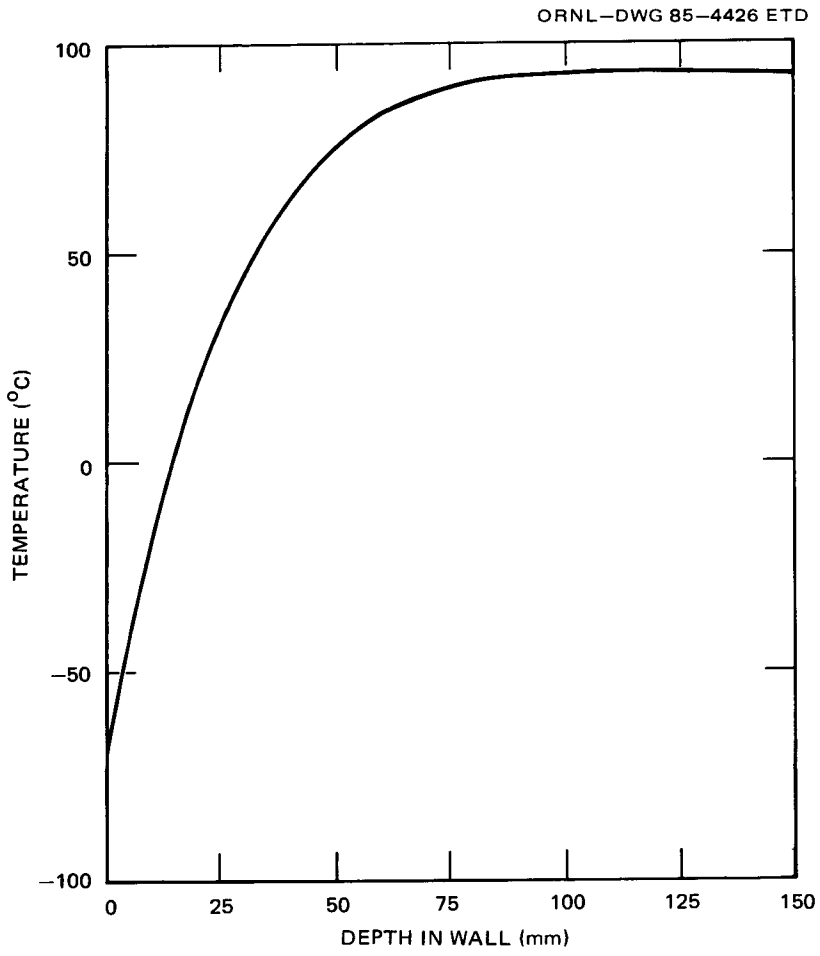

Fig. 9.2. Radial temperature distribution at t = 78 s during TSE-5A.

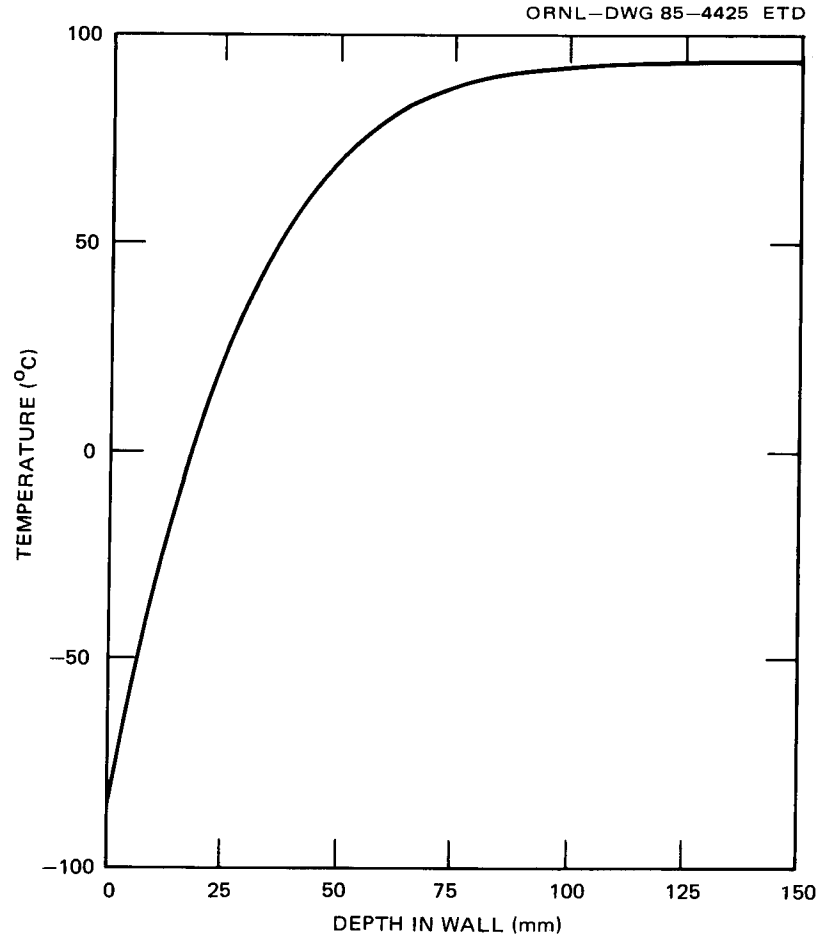

Fig. 9.3. Radial temperature distribution at t = 90 s during TSE-5A.

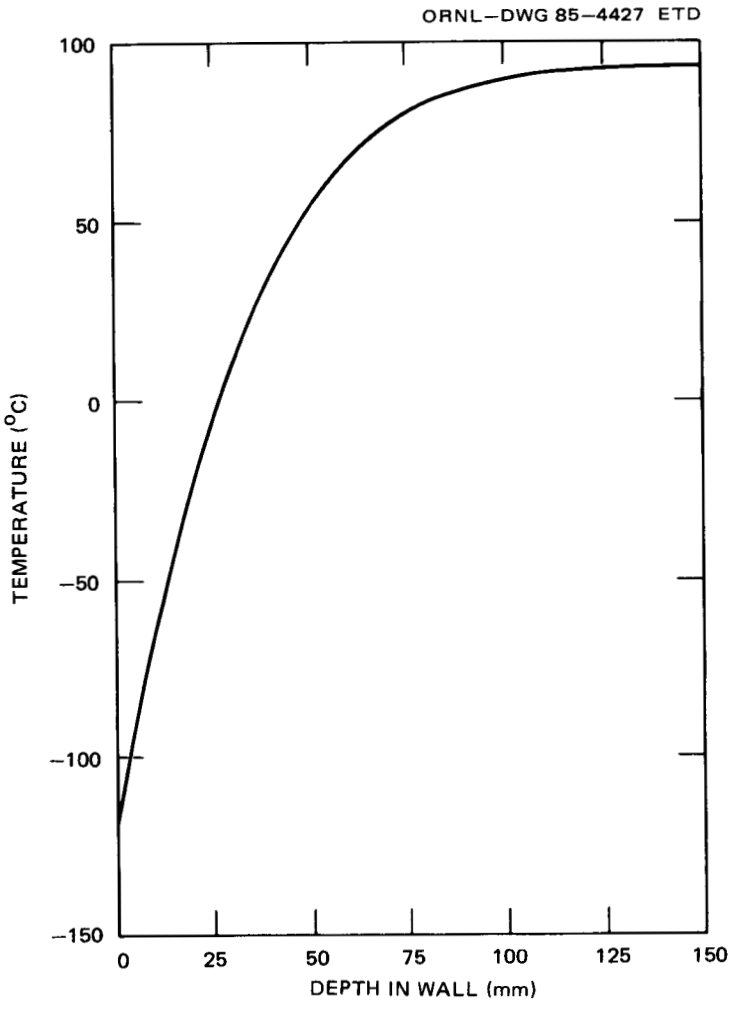

Fig. 9.4. Radial temperature distribution at t = 122 s during TSE-5A.

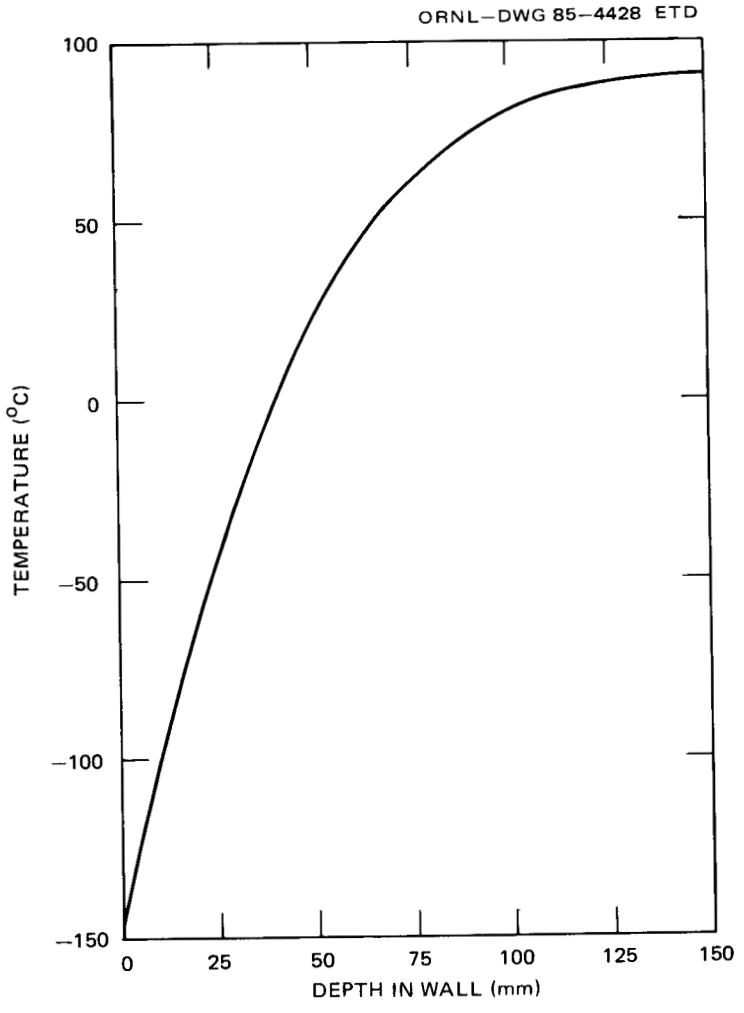

Fig. 9.5. Radial temperature distribution at t = 184 s during TSE-5A.

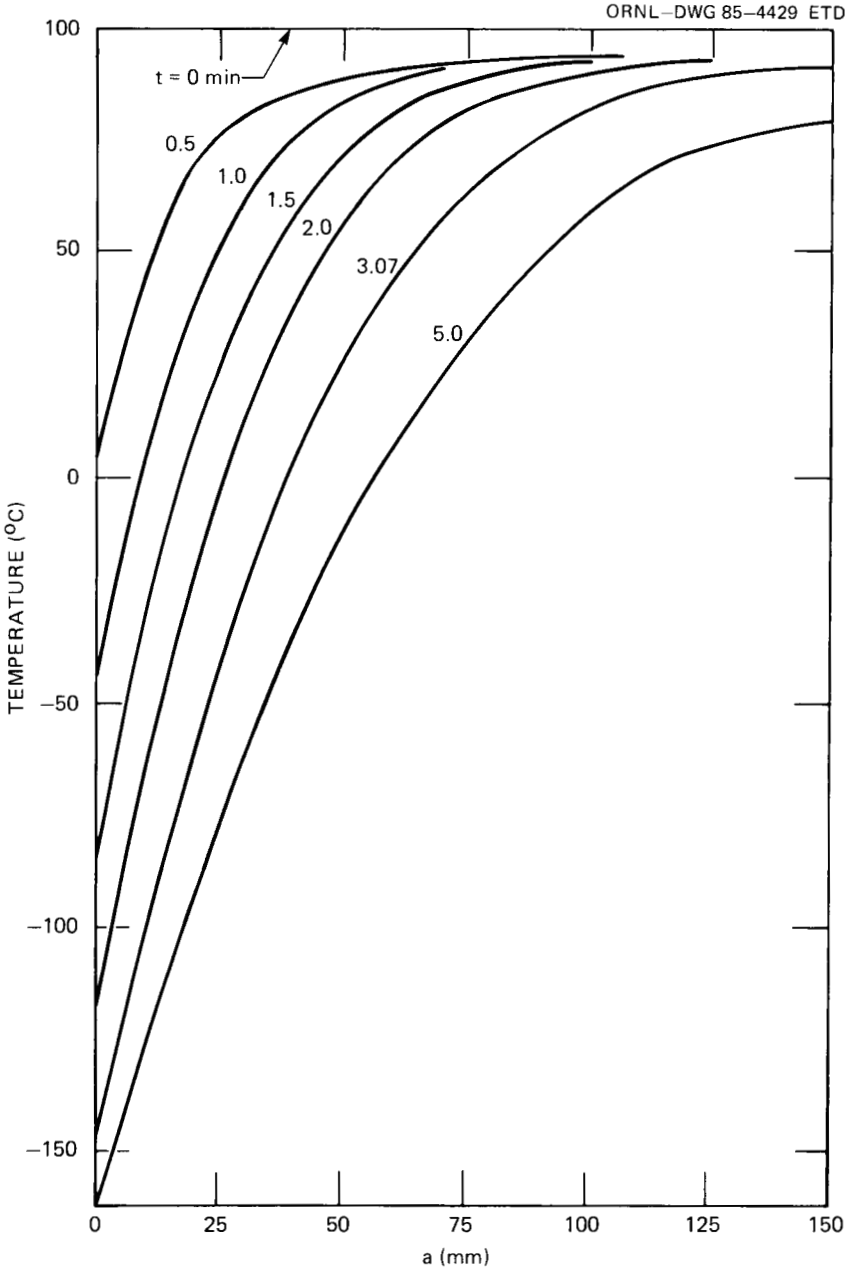

Fig. 9.6. Temperature vs a/w for several times during the TSE-5A transient.

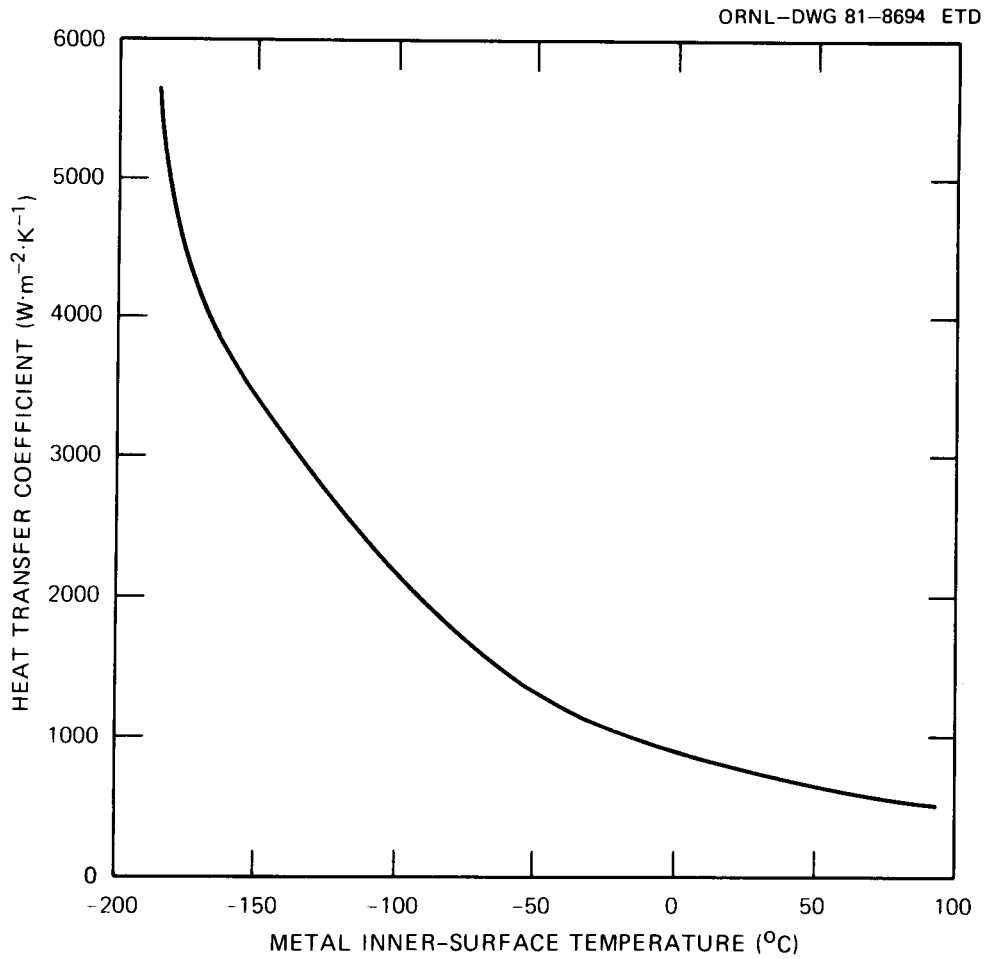

Fig. 9.7. Heat transfer coefficient (fluid film plus surface coating) derived from TSE-5A as a function of cylinder (metal) inner-surface temperature.

obtaining the coefficient from the measured temperatures is discussed in Sect. 8.1.

9.2 Events During TSE-5A

The trace of COD output shown in Fig. 9.8 indicates that four initiation-arrest events took place during TSE-5A and that the times of these events were 78.5, 90.5, 123.0, and 184.5 s. There was an earlier event (74.5 s) that was indicated by a single COD gage and, thus, was very localized. Because the area involved was so small, this first event had no bearing on the overall behavior of the flaw and will not be referred to hereafter.

The first and second major initiation-arrest events during TSE-5A were not identified by all COD gages, indicating that these events also did not extend the full length of the test cylinder. For the first event,

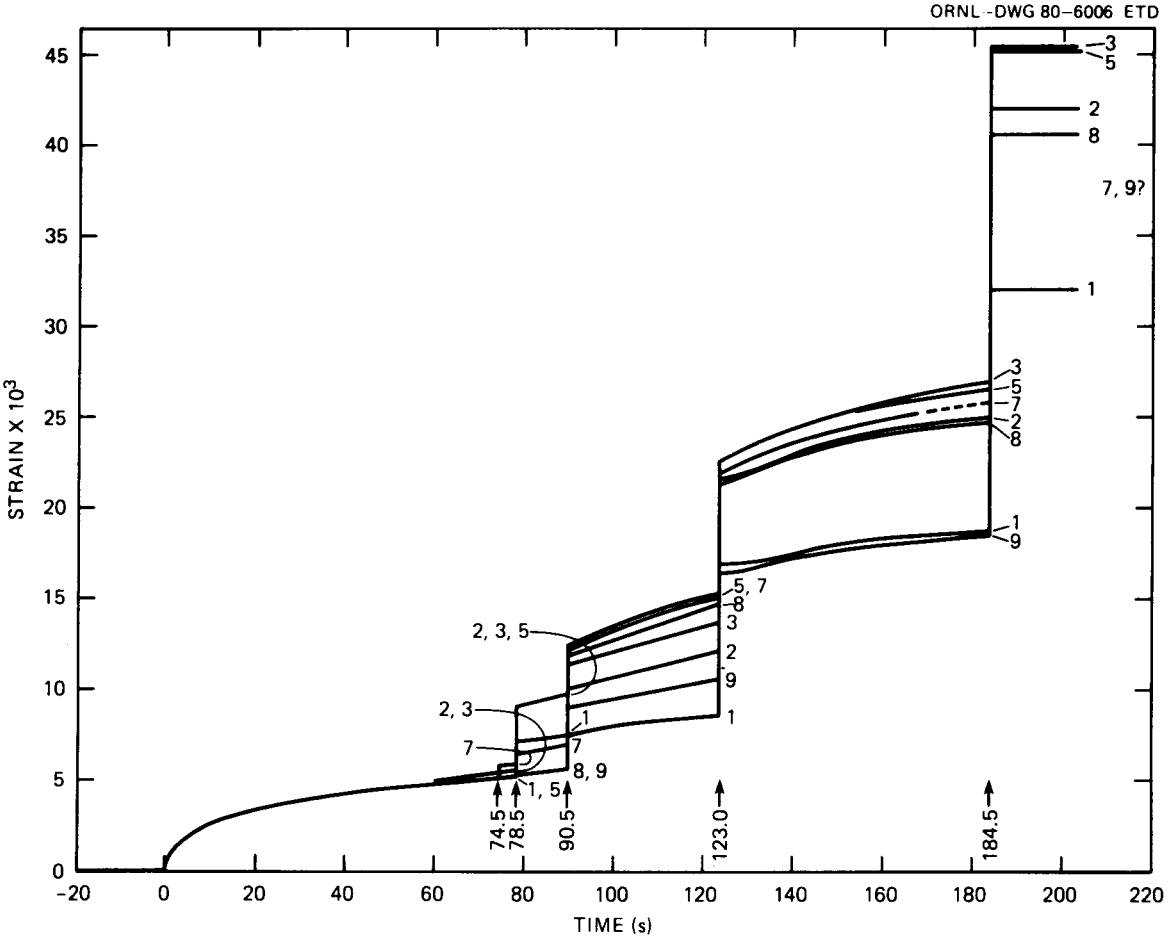

Fig. 9.8. COD data for TSE-5A.

gages 8 and 9 (see Figs. 6.6 and 9.9) gave essentially no response, indicating that the first arrest event covered the upper two-thirds of the cylinder. For the second event, there was essentially no response from gages 1 and 2, indicating that the second arrest event covered only the lower two-thirds of the cylinder. In the central portion of the cylinder, the first and second arrested crack fronts apparently overlapped each other, in which case gages 3, 5, and 7 should have indicated all four events, and they did. A graphic description of this progressive nature of the long axial flaw during TSE-5A is shown in Fig. 9.9.

Evidence of four initiation-arrest events was also obtained from an examination of the TSE-5A fracture surfaces. Following the TSE-5A experiment, a full-length section of the wall containing the flaw was removed from the cylinder and was then divided into eight nearly equal-length subsections (see Fig. 8.9 for a typical cutting pattern). These sections were then cooled in liquid nitrogen and the fractures completed by forcing a wedge into the crack. Each piece was immediately placed in alcohol to prevent discoloration of the surface and was photographed

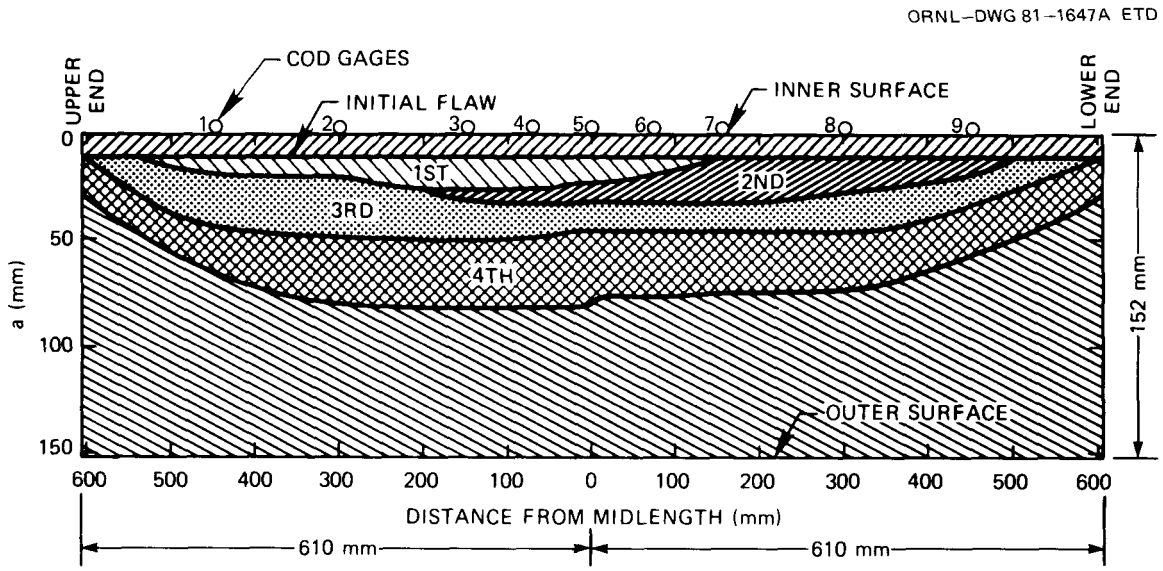

Fig. 9.9. Schematic cross section of TSE-5A test-cylinder wall, showing four-step progression of long axial flaw as deduced from fracture surfaces.

shortly thereafter. A composite photograph of the entire fracture surface is shown in Fig. 9.10 along with an enlarged view of one section. Figure 9.9 was constructed by obtaining measurements of crack depth from photographs of this type.

Figure 9.10 shows a clear indication of an additional event just ahead of the final arrest event. This event was not detected with the COD gages but, rather with the UT instrumentation, as were the four major events. According to an analysis of the UT data, the time between the final arrest event and the preceding arrest event was only 900 μs. This short period of time suggests that the additional event was the result of dynamic effects that created an oscillation in K_I. When K_I dipped down, arrest took place, but immediately thereafter initiation took place as K_I increased. Such oscillations have been observed in lab K_{Ia} tests,[1] and dynamic analyses of the lab specimens indicate such behavior.[2] A dynamic analysis was also attempted for TSE-5A; it did not indicate that a momentary arrest event would take place.[3]

9.3 Crack Depths

Crack depths were determined from the COD and UT data and also from direct observations of the fracture surfaces. The COD data were analyzed in the manner described in Sect. 8.5, and the calculated relation between COD and crack depth for times of interest during TSE-5A is shown in Fig. 9.11. Crack depths based on COD and UT data and obtained from examination of the fracture surfaces are presented in Table 9.1 for the central portion of the test cylinder. As indicated, the agreement is reasonably good.

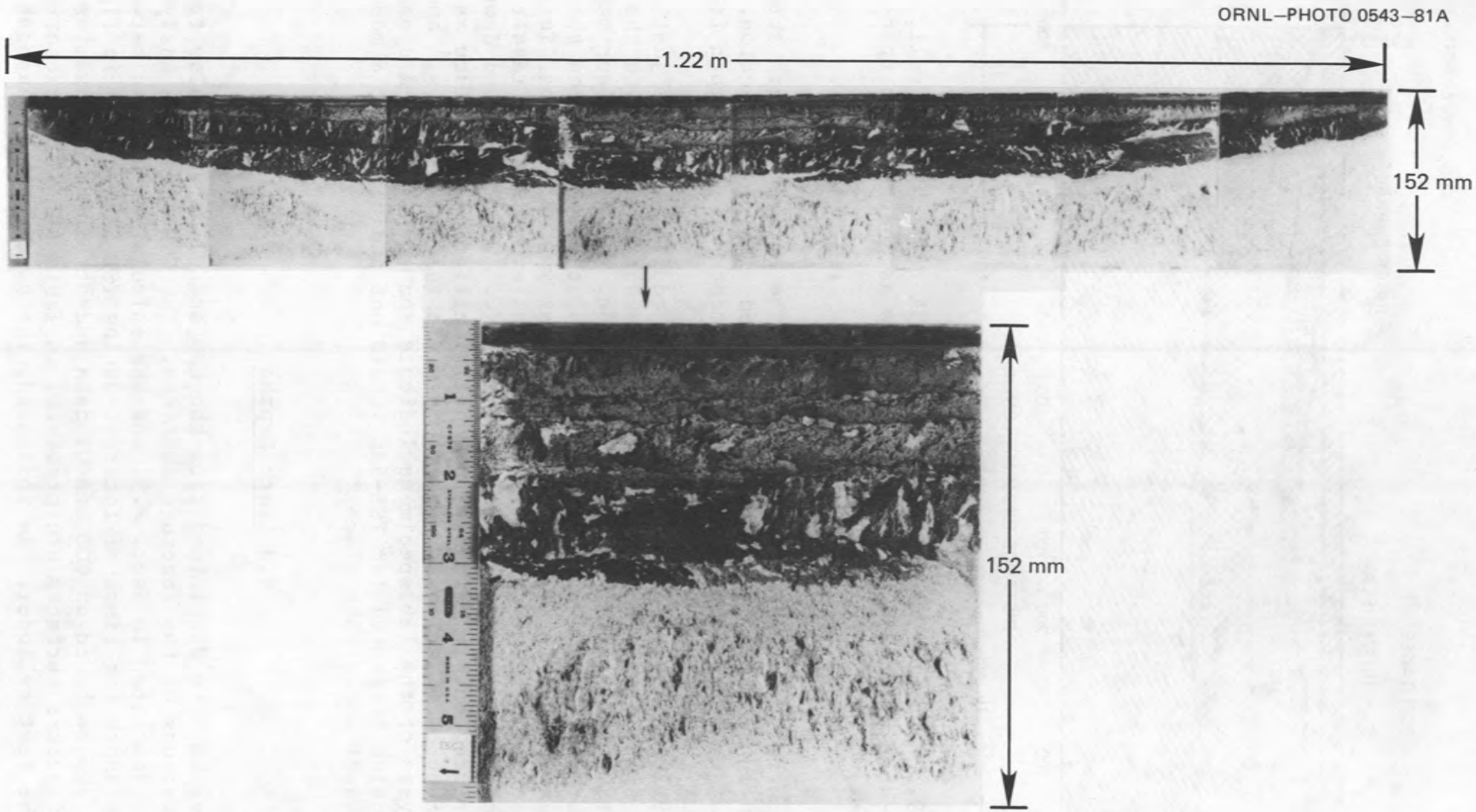

Fig. 9.10. TSE-5A fracture surface.

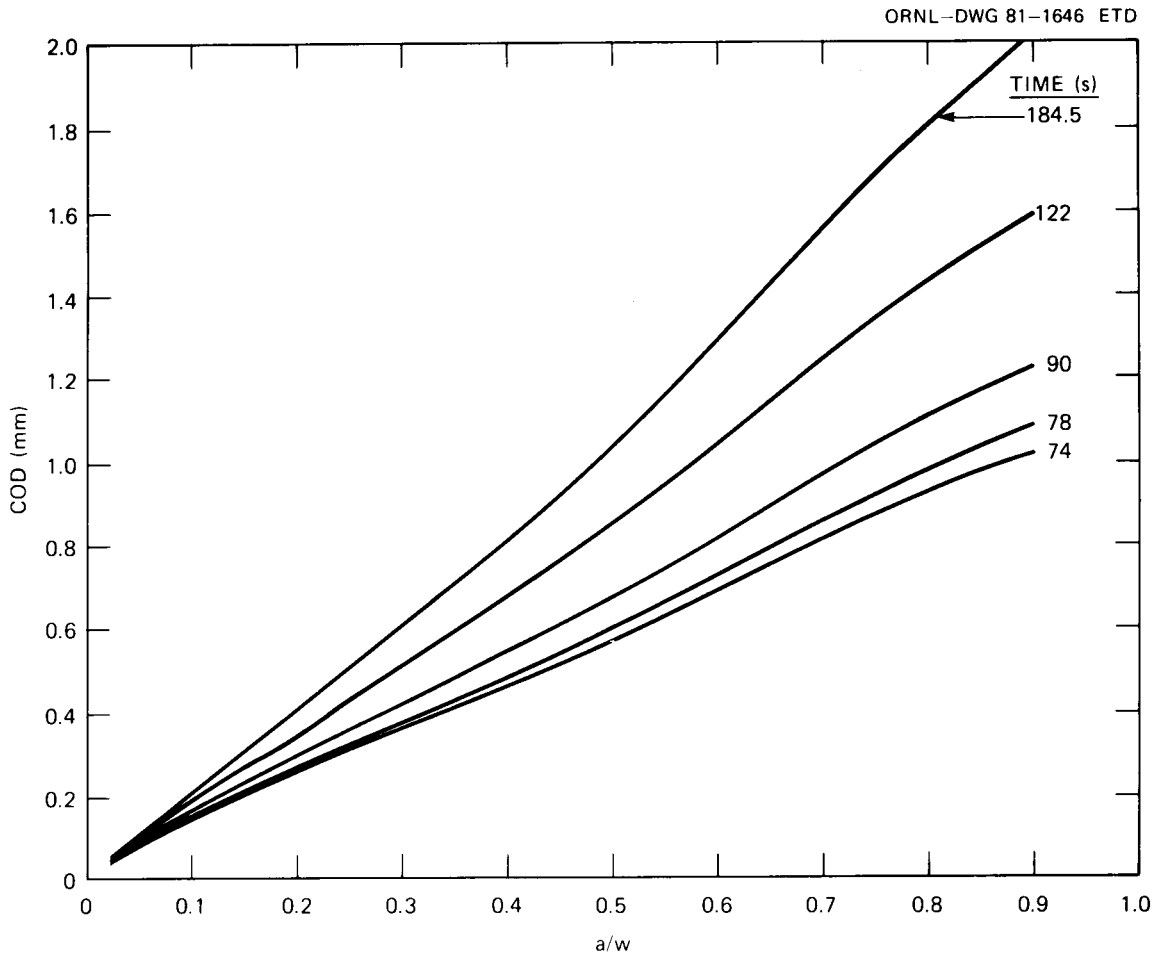

Fig. 9.11. Calculated COD at inner surface vs fractional crack depth for TSE-5A.

Table 9.1. Estimated crack depths near midlength of test cylinder for TSE-5A

Event No.	Event	Time (s)	Crack depth (mm)		
			COD	Fracture surface	UT
1	Initiation	78.5	12	12	11
	Arrest		21	23	17
2	Arrest	90.5	30	30	31
3	Arrest	123.0	48	48	41
4	Arrest	184.5	81	81	81

A comparison of crack depths based on COD and fracture surface appearance for the full length of the test cylinder is shown in Fig. 9.12, and once again the agreement is quite good. Also included in Fig. 9.12 is the final crack depth based on UT measurements made posttest at ~25-mm increments along the length of the cylinder. The agreement in this case is quite good also.

Crack depths determined by means of the COD measurements are generally considered to be more accurate than the UT values. This is because the COD values represent local averages for a possibly irregular crack front, while the UT measurements tend to be very localized, allowing crack-tip irregularities to introduce false readings relative to an effective local average crack depth.

As explained in connection with TSE-5, the tapering off of crack depth near the ends of the test cylinder is the result of end effects that result in lower values of K_I near the ends. End effects, however, do not explain why the first initiation-arrest event was not symmetrical about midlength.

There are several possible explanations for the axial asymmetry associated with the first initiation-arrest event; they involve axial variations in crack sharpness, fracture toughness, and quench rate. Variations in crack sharpness do not seem to be a reasonable explanation because crack initiation undoubtedly is a very localized event, and once initiated, the fast-running crack will be sharp. Also, variations in temperature (quench rate) do not appear to be a reasonable explanation because temperature measurements indicate very little axial variation, and the small variation that did exist corresponds to higher rather than lower temperatures in the upper portion of the cylinder where the first event took place. Thus, the remaining possible explanation is an initial small axial variation in toughness. However, as indicated in Chap. 7, a comparison of fracture-toughness data (1T-CS and CVN) for the test cylinder and prolongation did not reveal significant axial variations.

9.4 Fracture-Mechanics Analysis

9.4.1 Posttest analysis based on design toughness curves

The number of initiation-arrest events taking place during TSE-5A agrees with the pretest analysis (Fig. 4.8), but the times at which the events actually took place were earlier than calculated. This indicated that the thermal shock was more severe than that used for the pretest analysis and/or that the actual material toughness was less than that used in the pretest analysis. As planned (Fig. 9.1), the thermal shock was more severe than that assumed for the pretest analysis (that achieved during TSE-5), and, apparently, the toughness was less than assumed, as discussed below.

The toughness curves used in the pretest analysis are shown in Fig. 9.13. The K_{Ic} curve represents the lower bound of fifty 1T-CS data points, while the K_{Ia} curve is a mean curve through six data points obtained from 25 × 151 × 151-mm, wedge-loaded, crack-arrest specimens (also refer to Fig. 7.11).

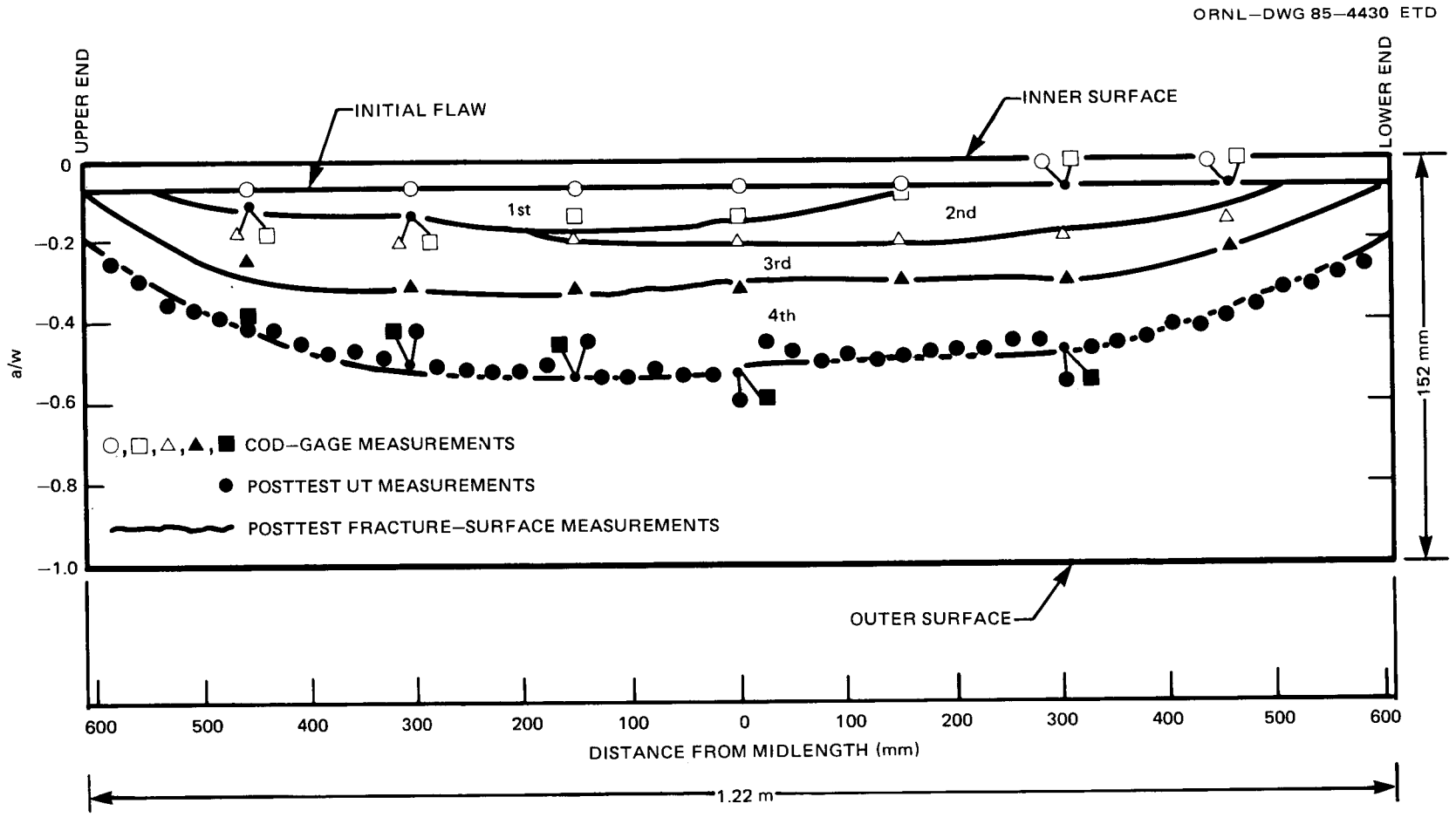

Fig. 9.12. Comparison of COD, UT, and fracture-surface crack-depth measurements for TSE-5A.

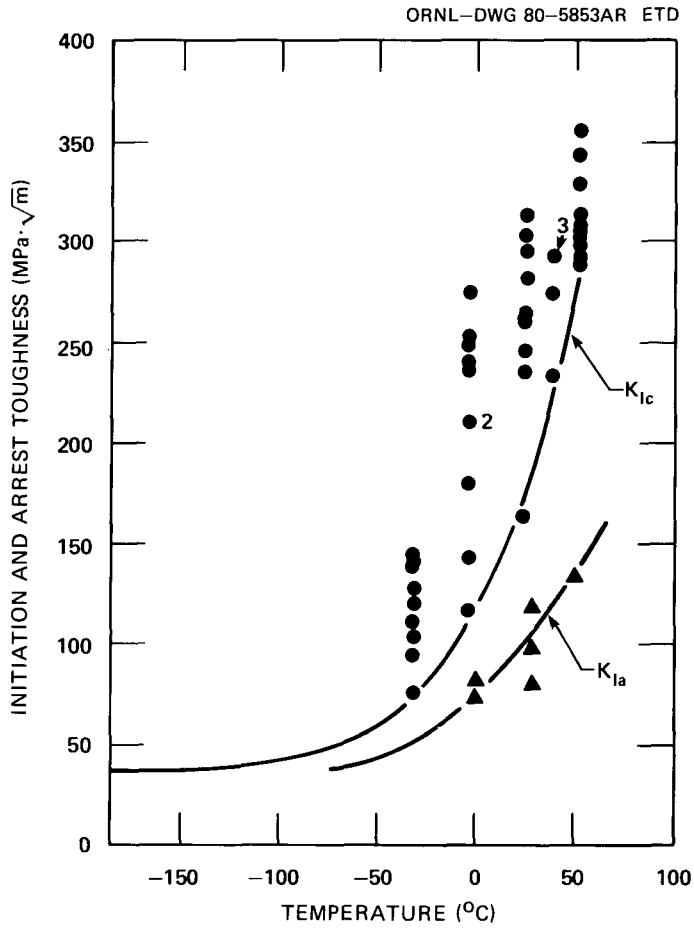

Fig. 9.13. Lower-bound K_J and mean K_{Ia} curves (based on pretest lab data only) used for K_{Ic} and K_{Ia} in TSE-5A pretest analysis.

Posttest analyses of TSE-5A were conducted using the measured test-cylinder temperatures shown in Figs. 9.2–9.6. The results of such an analysis, based on the toughness curves in Fig. 9.13, are shown in Fig. 9.14, which is a set of critical-crack-depth curves that includes the actual path of events. It is observed that the initiation and arrest events fall to the left of their respective initiation and arrest curves, indicating that the actual crack-initiation and crack-arrest toughness values were below the curves in Fig. 9.13.

9.4.2 K_{Ic} and K_{Ia} values deduced from TSE-5A

Critical values of K_I corresponding to the four initiation and arrest events during TSE-5A are shown in Table 9.2, and these values are compared with the experiment-design toughness curves in Fig. 9.15. It is obvious that the K_{Ic} and K_{Ia} values deduced from TSE-5A are substantially less than the values assumed for the design of the experiment on the bases of the lab data. Of course, this was to be expected insofar as crack initiation is concerned because none of the lab initiation data

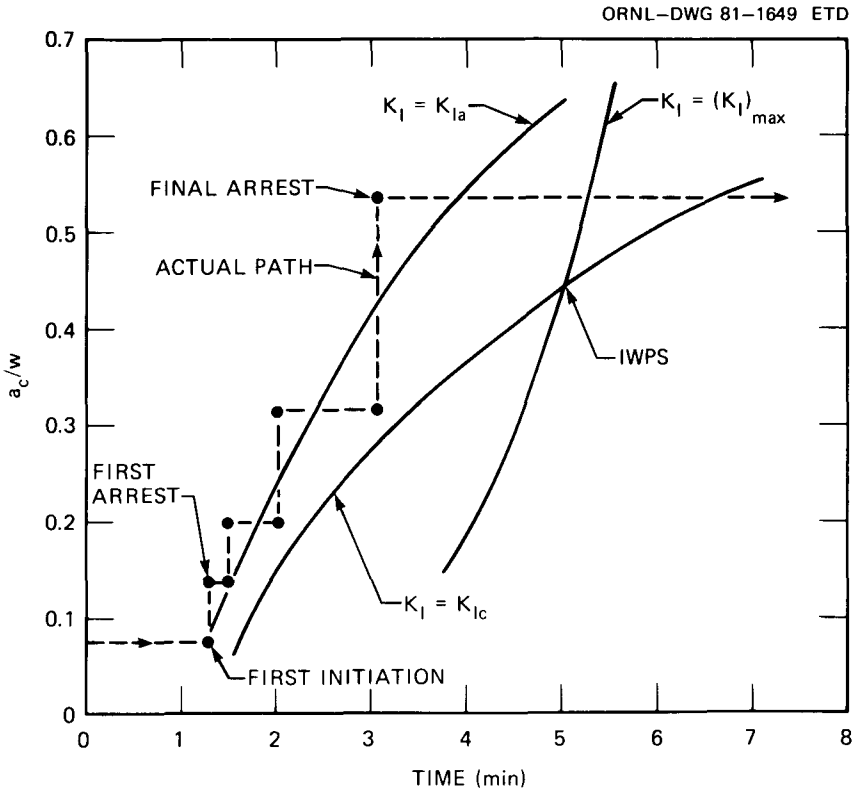

Fig. 9.14. Critical-crack-depth curves for TSE-5A based on toughness curves in Fig. 9.13.

Table 9.2. Summary of critical data for TSE-5A

Time (s)	Event	a/w	K_I (MPa•$\sqrt{m}$)	Temperature (°C)
78.5	1st initiation	0.076	70	−11
90.5	2nd initiation	0.138	85	12
123.0	3rd initiation	0.198	108	13
184.5	4th initiation	0.316	135	21
78.5	1st arrest	0.138	76	22
90.5	2nd arrest	0.198	86	38
123.0	3rd arrest	0.316	107	51
184.5[a]	4th arrest	0.535	130	67

[a]K_I/K_{Ic} reached a maximum value of 2.3 at ~14 min.

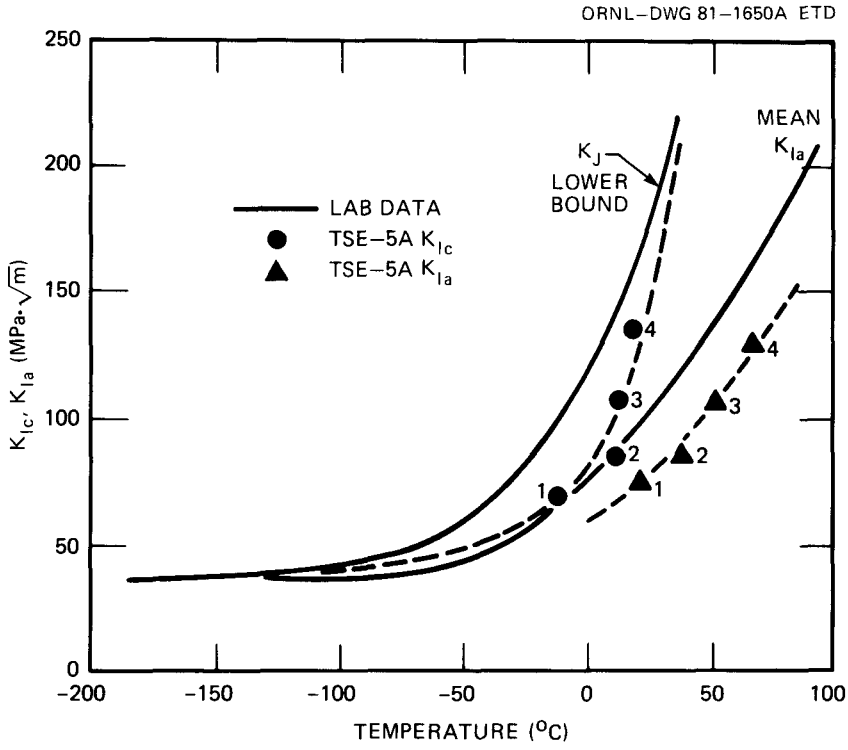

Fig. 9.15. Comparison of K_{Ic} and K_{Ia} values deduced from TSE-5A with laboratory data presented in Fig. 9.13.

points was valid. However, as indicated below, the lab data were adequate for designing the experiment; that is, all objectives of TSE-5A were achieved.

9.4.3 Posttest analysis based on K_{Ic} and K_{Ia} curves deduced from TSE-5A

The dashed curves in Fig. 9.15 represent a best fit of the K_{Ic} and K_{Ia} data points deduced from TSE-5A. These curves were used in a second posttest analysis, and as one would expect, the agreement between actual and "predicted" flaw behavior is much better than when using the solid curves in Fig. 9.15. Results of the second posttest analysis are shown in Fig. 9.16, and a complete set of digital output is included in Appendix E.

9.4.4 Warm prestressing

Figure 9.16 indicates that a fifth crack-initiation event was prevented by warm prestressing, and the maximum value of K_I/K_{Ic} for the final crack depth was 2.3. This maximum value was reached ~9 min after the time of incipient warm prestressing, and the corresponding crack-tip

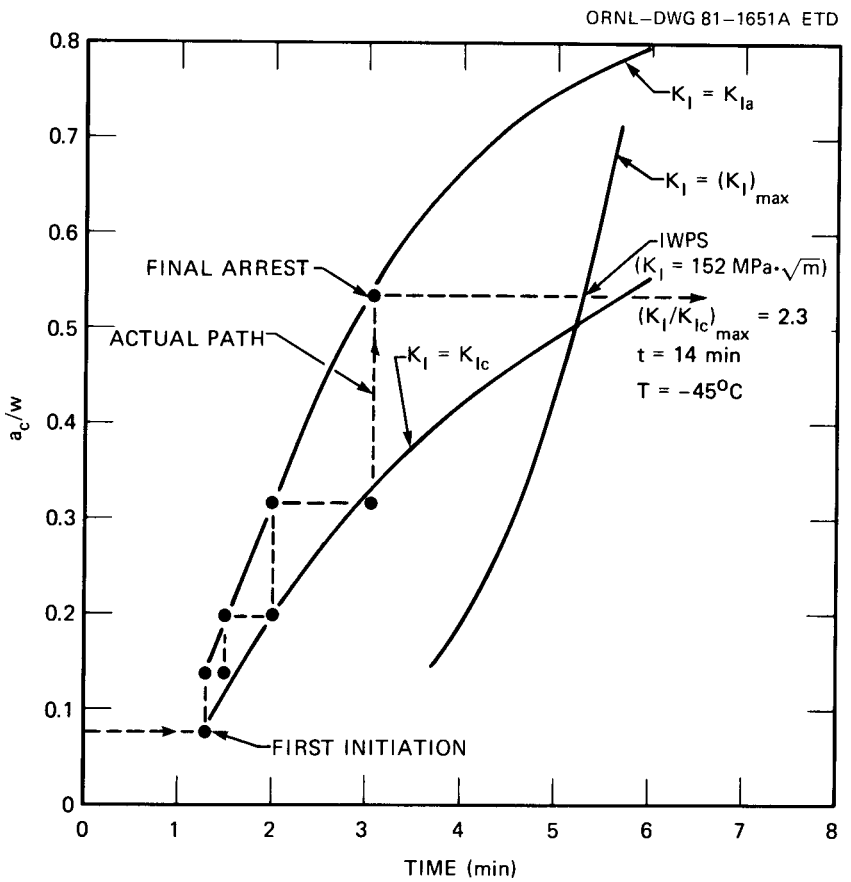

Fig. 9.16. Posttest critical-crack-depth curves for TSE-5A using modified toughness curves in Fig. 9.15.

temperature was −45°C (RTNDT = 10°C). The maximum value of K_I for the final crack depth was 152 MPa•$\sqrt{m}$, and, of course, it occurred at the time of incipient warm prestressing (~5 min).

The value of 2.3 for $(K_I/K_{Ic})_{max}$ is large enough, relative to unity, to compensate for all uncertainties in the experiment and related posttest analysis, and the crack-tip temperature corresponding to this value was well below RTNDT. Thus, even though the value of $(K_I)_{max}$ for the final crack depth was substantially less than that predicted for the PWR LBLOCA, TSE-5A provided a convincing demonstration of the ability of warm prestressing to prevent crack initiation.

9.4.5 Arrest in a rising K_I field

The pretest analysis for TSE-5A (Sect. 4.2.2) indicated that the first two arrest events would take place in a rising K_I field, that is, with K_I increasing with crack depth. As shown in Fig. 9.17, which is a

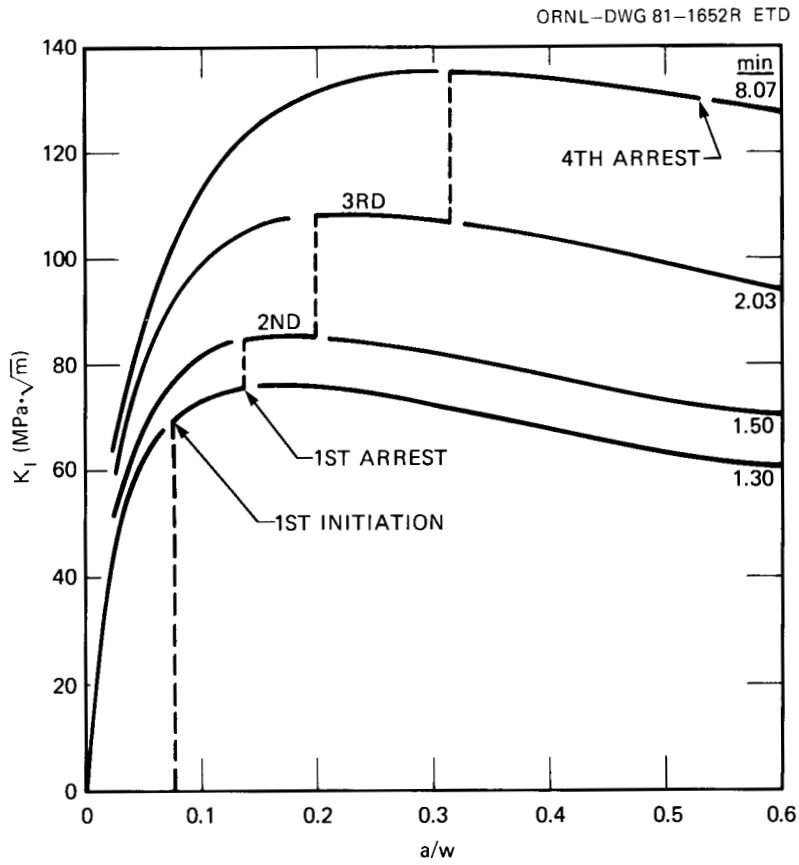

Fig. 9.17. K_I vs a/w and t for TSE-5A.

plot of K_I vs a/w for the times corresponding to the four initiation-arrest events and with the path of actual events superimposed, it appears that only the first arrest event took place in a rising K_I field. Furthermore, as illustrated in Fig. 9.18, the gradient (dK_I/da) was small compared to those calculated for two rather severe PWR overcooling accidents (LBLOCA and PTS transients*). Even so, the gradient is substantially greater than that for lab crack-arrest specimens, which have negative gradients. Thus, the TSE-5A data point provides an opportunity to compare K_{Ia} values measured in rising and falling K_I fields.

*The particular LBLOCA and PTS (pressurized thermal shock) transients considered are described in Refs. 4 and 5.

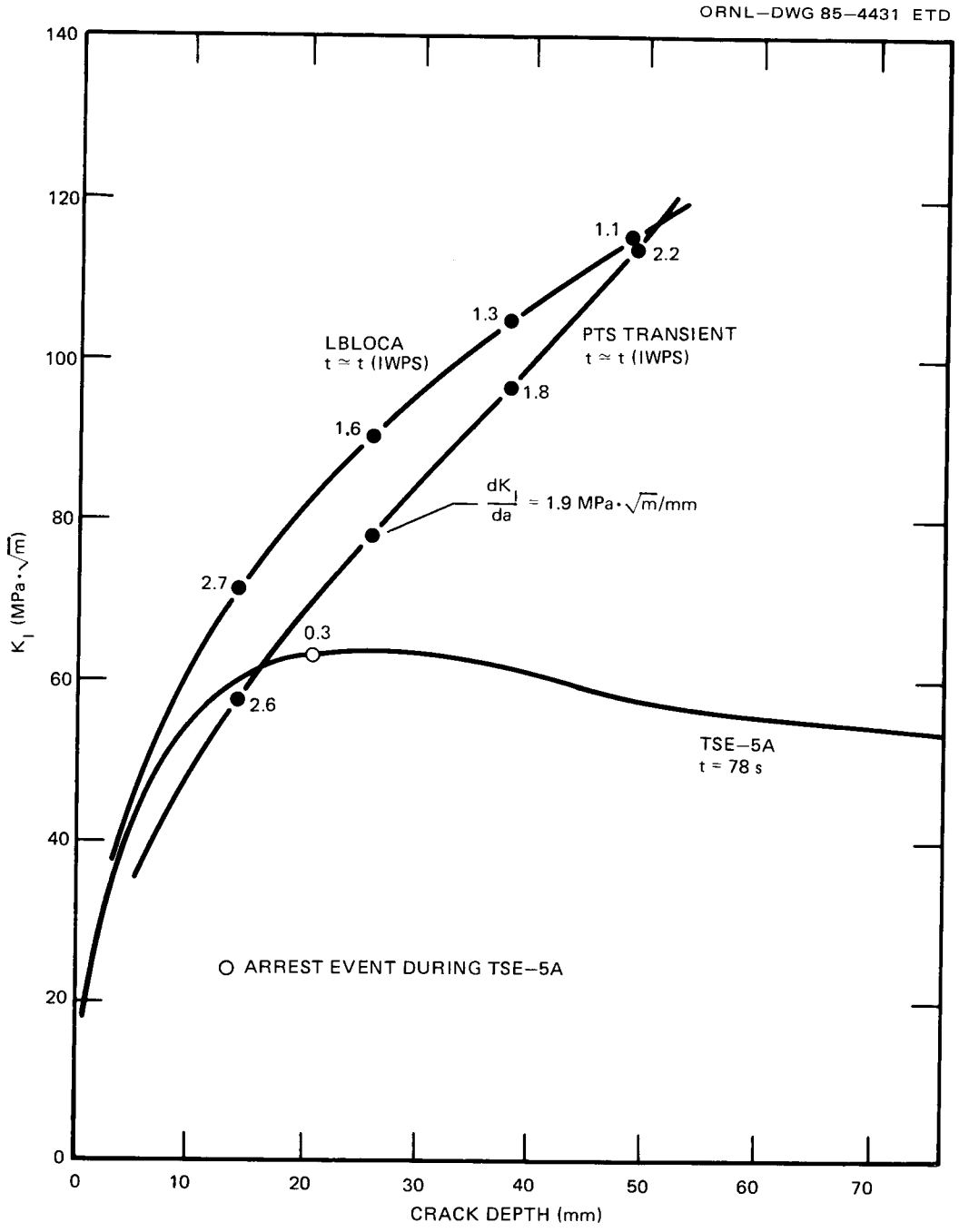

Fig. 9.18. Comparison of K_I vs a curves for TSE-5A and two PWR postulated severe overcooling accidents.

References

1. G. T. Hahn et al., *Critical Experiments, Measurements, and Analysis to Establish a Crack Arrest Methodology for Nuclear Pressure Vessel Steels*, Third Annual Progress Report, October 1976—September 1977, NUREG/CR-0057, BMI-1995, May 1978.

2. M. F. Kanninen, C. Popelar, and P. C. Gehlen, "Dynamic Analysis of Crack Propagation and Arrest in the Double-Cantilever-Beam Specimen," pp. 19—38 in *Fast Fracture and Crack Arrest*, ASTM-STP 627, July 1977.

3. W. L. Fourney et al., "Dynamic Run-Arrest Calculations," pp. 20—26 in *Heavy-Section Steel Technology Program Semiann. Prog. Rep. October 1983—March 1984*, NUREG/CR-3744, Vol. 1 (ORNL/TM-9154/V1), Martin Marietta Energy Systems, Inc., Oak Ridge Natl. Lab.

4. R. D. Cheverton, S. K. Iskander, and S. E. Bolt, *Applicability of LEFM to the Analysis of PWR Vessels Under LOCA-ECC Thermal-Shock Conditions*, NUREG/CR-0107 (ORNL/NUREG-40), Union Carbide Corp. Nuclear Div., Oak Ridge Natl. Lab., October 1978.

5. R. D. Cheverton and S. K. Iskander, "Thermal-Shock Investigations," pp. 76—83 in *Heavy-Section Steel Technology Program Quart. Prog. Rep. for January—March 1981*, NUREG/CR-2141/V1 (ORNL/TM-7822), Union Carbide Corp. Nuclear Div., Oak Ridge Natl. Lab.

10. TSE-6 RESULTS

10.1 Heat Transfer

The thermal shock for TSE-6 was intended to be at least as severe as that for TSE-5A, and, as indicated in Fig. 10.1, the two inner-surface (metal) temperature transients were essentially the same up to the time that the TSE-6 test cylinder was withdrawn from the liquid nitrogen. Radial distributions in temperature for TSE-6 at the two times that events took place are shown in Fig. 10.2, and distributions for additional times are shown in Fig. 10.3. As was the case with TSE-5 and TSE-5A, the indicated temperatures throughout the cylinder for times and crack depths of particular interest were very uniform (approximately ±5°C).

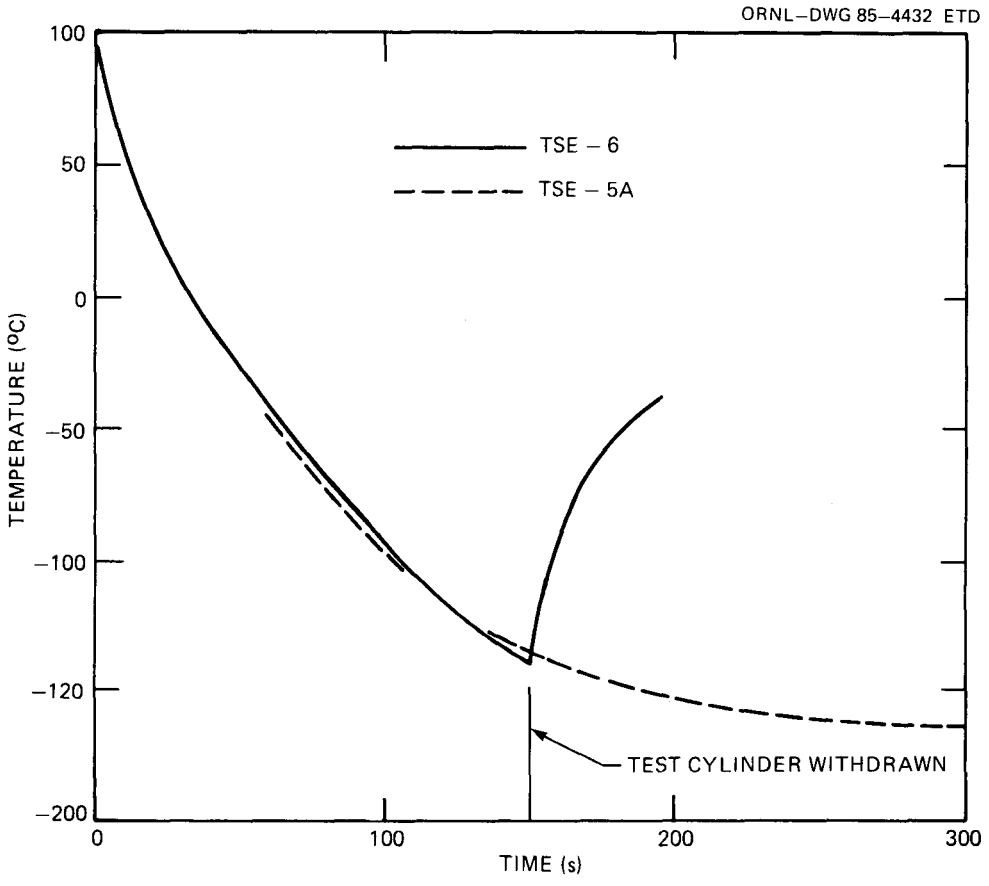

Fig. 10.1. Comparison of TSE-5A and TSE-6 inner-surface (metal) temperatures.

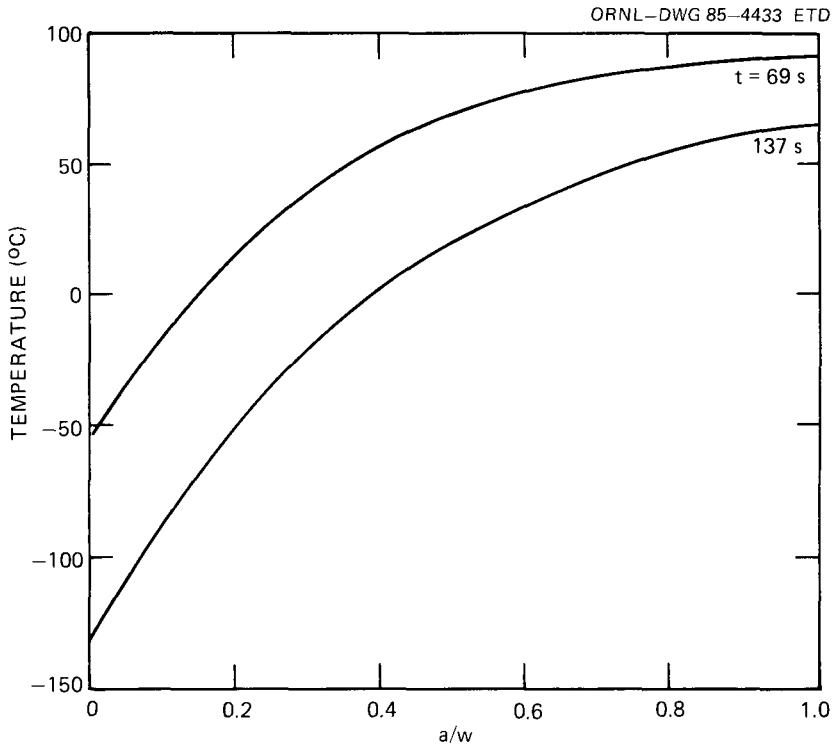

Fig. 10.2. TSE-6 measured radial temperature distributions for times at which events took place.

10.2 Events During TSE-6

As indicated in Fig. 10.4, which shows the final profile of the flaw near midlength of the test cylinder, the TSE-6 flaw penetrated very deep (>90%) into the wall of the test cylinder but did not extend all the way through, consistent with predictions. The COD data and a photograph of the full length of the fracture surface (Fig. 10.5) indicate that there were three initiation-arrest events involved. Two of these events, the first and last, were detected with COD gages that were connected to "slow" recorders, and the recorded output of the gages is shown in Fig. 10.6. The second event was detected with two COD gages that were connected to a fast-phenomena recorder, and the output for one of these gages is shown in Fig. 10.7. It is apparent that the second arrest event was the result of a momentary decrease in K_I because ~300 μs thereafter the third initiation-arrest event took place, presumably the result of a momentary increase in K_I (the time between arrest events was ~900 μs, the same as for TSE-5A). A dynamic analysis similar to that performed for TSE-5A was also attempted for TSE-6 (Sect. 9.2). This time the analysis indicated that the momentary arrest event would take place.[1]

The TSE-6 dynamic event appears to be the same type of dynamic event that took place during TSE-5A, and it is of interest to note that in TSE-5A the crack jump preceding the short duration of the arrest event was much shorter and the vessel wall was much stiffer. Thus, it is not clear

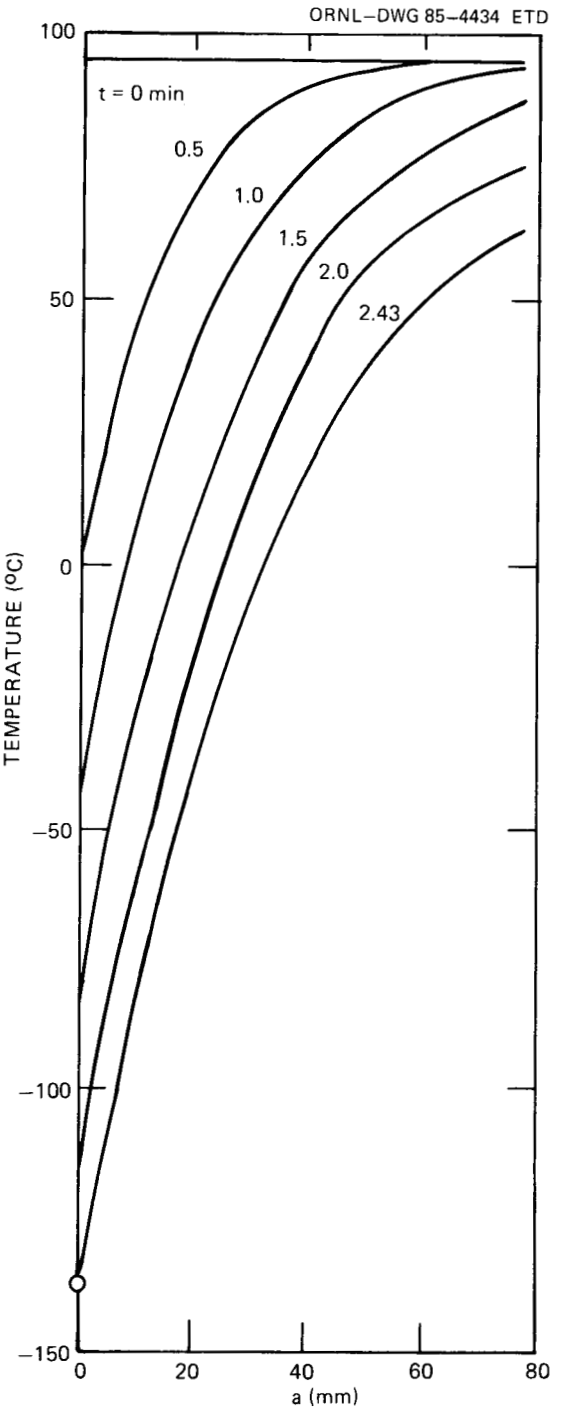

Fig. 10.3. TSE-6 measured radial temperature distributions for several times during transient.

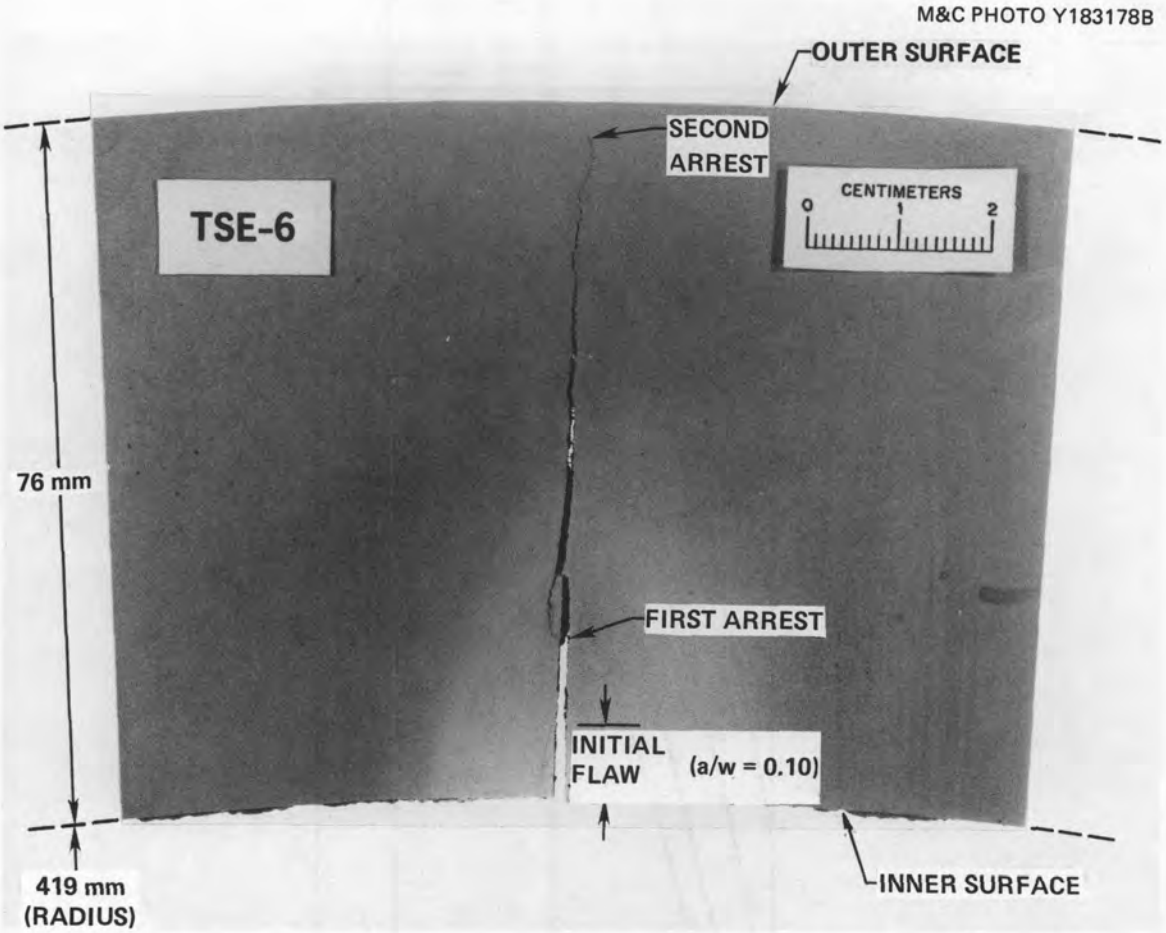

Fig. 10.4. Final radial profile of TSE-6 flaw near midlength of test cylinder.

that the longer crack jump and the less-stiff wall associated with TSE-6 contributed to this particular dynamic effect, which was a point of concern prior to TSE-6.

10.3 Crack Depths

As shown in Fig. 10.5, the initial flaw was uniform in depth (a/w = 0.10) and extended the full length of the test cylinder. Even so, the crack front associated with the first arrest event did not extend all the way to the ends, and the depth of the arrested front is somewhat less at midlength than elsewhere. Ignoring the tapering off at the ends of the flaw, the fractional depth (a/w) of the first arrested crack front varies from 0.21 to 0.32, and there is a 240-mm length in the lower half of the cylinder that has a uniform value of 0.28. With the exception of the tapering off at the ends, which is due to free-end effects, the variation of crack depth is probably due to small axial variations in fracture toughness.

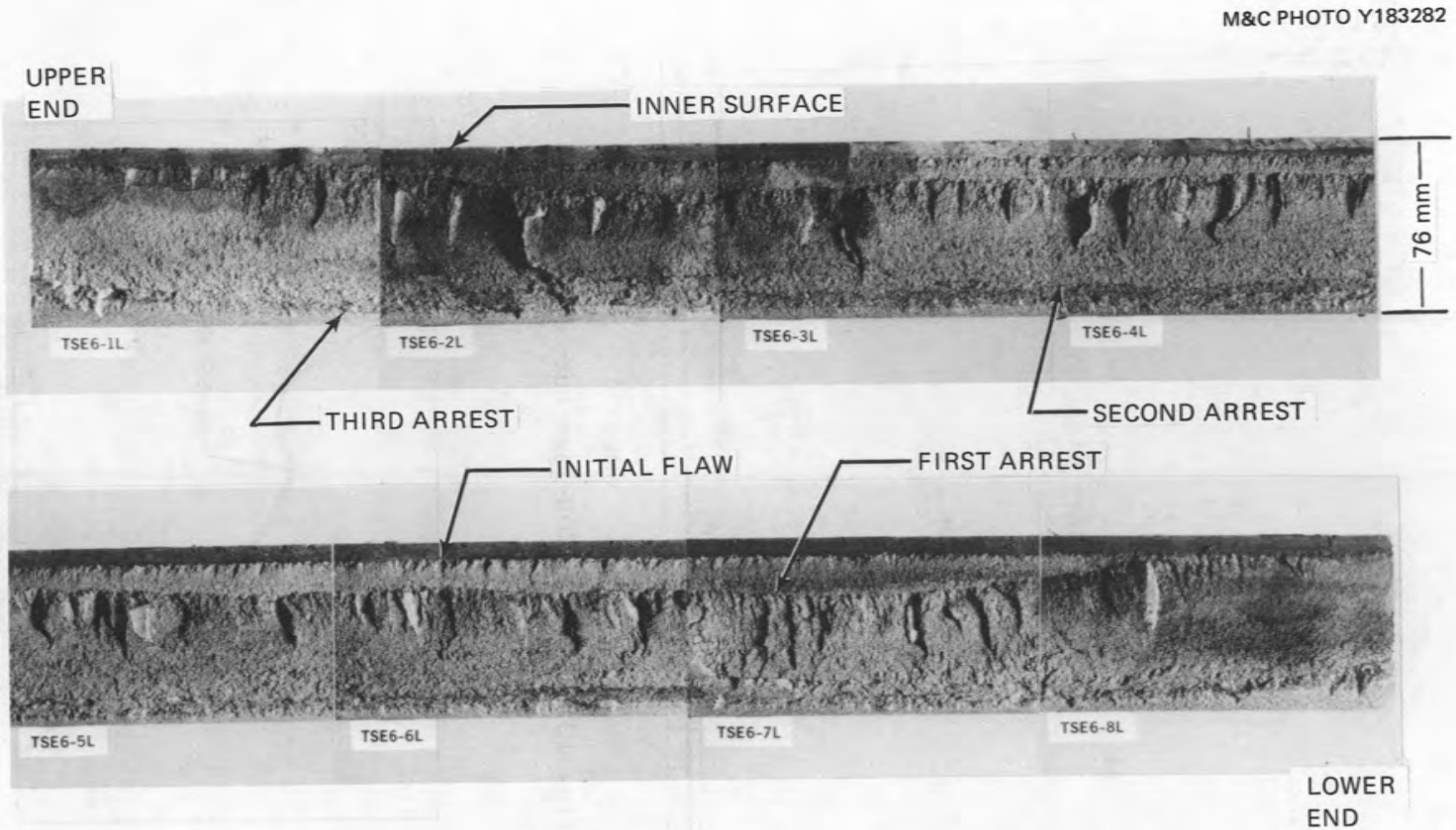

Fig. 10.5. Photograph of TSE-6 fracture surface.

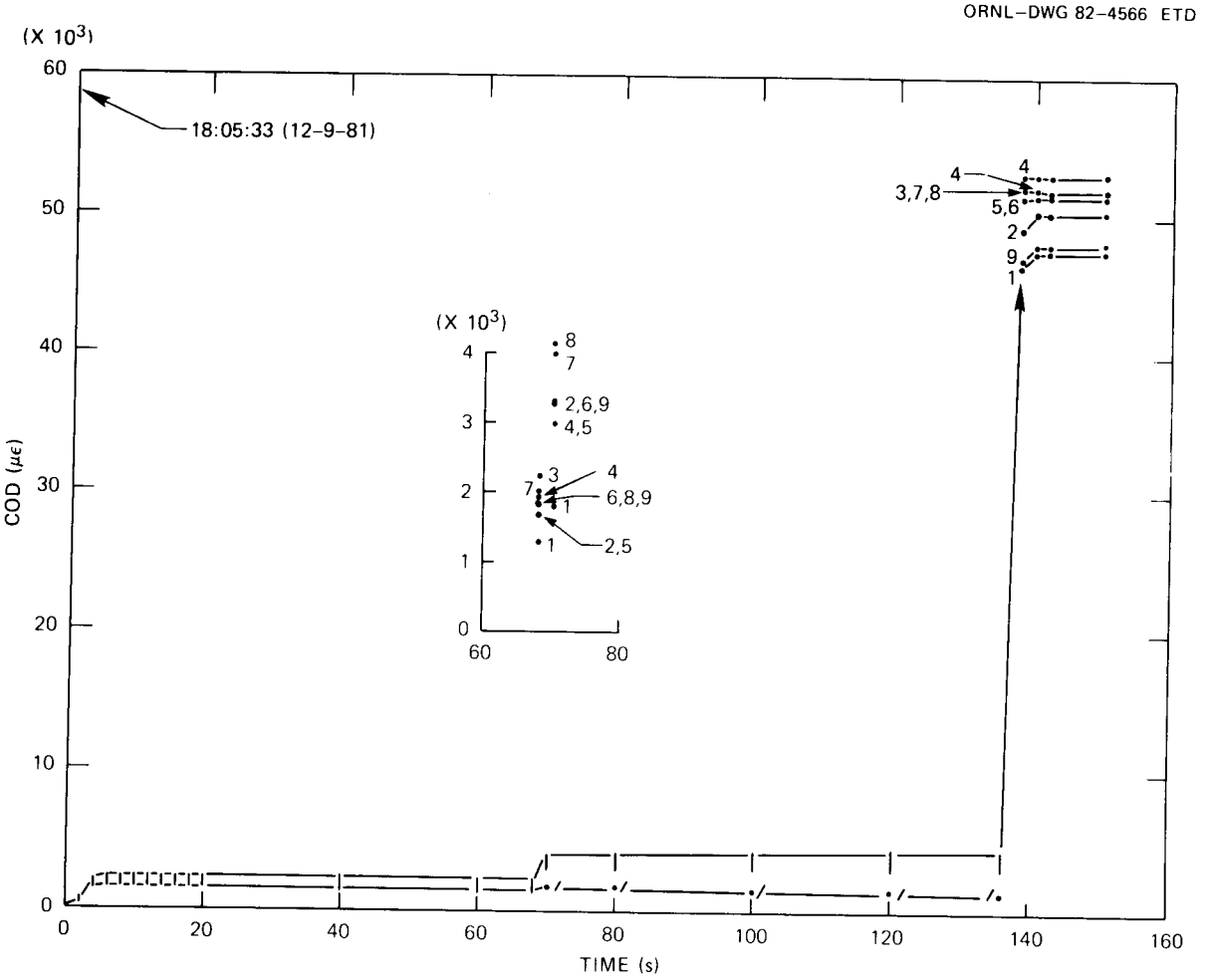

Fig. 10.6. TSE-6 COD-gage output vs time.

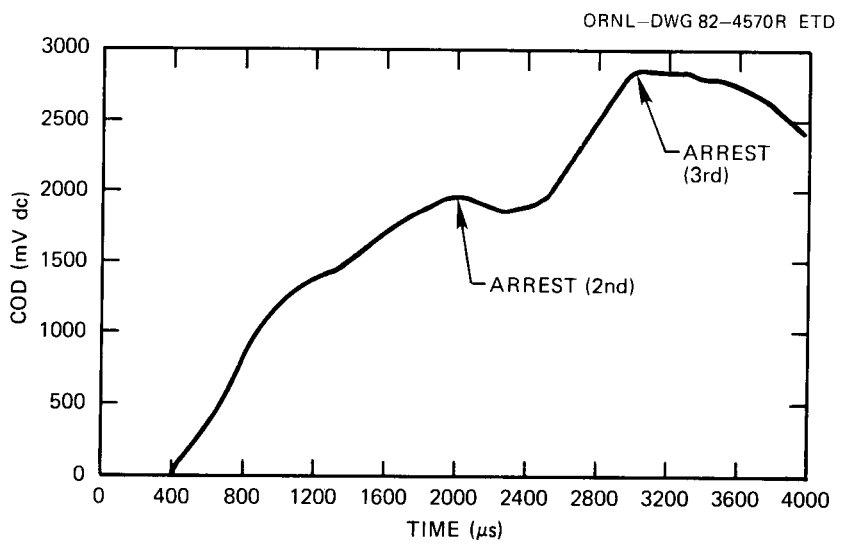

Fig. 10.7. TSE-6 COD output vs time for the second initiation-arrest event (gage 4).

The final crack depth was uniform over ~75% of the length of the test cylinder and was equal to 93% of the wall thickness (a/w = 0.93). At the ends of the cylinder, a/w = 0.82.

The crack depth associated with the very brief second arrest event was ~82% of the wall thickness (a/w = 0.82). Thus, this brief arrest event took place rather close to the site of the final arrest event, as was the case with TSE-5A.

10.4 Fracture-Mechanics Analysis

10.4.1 Posttest analysis based on design toughness curves

The pretest analysis for TSE-6 was based on toughness curves (TSE-6 design curves) deduced from the results of TSE-5 and indicated that only one initiation-arrest event would take place (see Fig. 4.9). Furthermore, a posttest analysis, based on actual temperatures and the design toughness curves, also indicates a single initiation-arrest event, as shown in Fig. 10.8. However, as discussed in Sect. 10.2, there were actually two "static" events and one "dynamic" event. As shown in Fig. 10.8, which includes the actual path of events, the first initiation-arrest event took place ~44 s earlier than "predicted," indicating that the actual fracture toughness was less than anticipated.

A quantitative comparison of K_{Ic} and K_{Ia} data can be obtained using Figs. 10.9 and 10.10, which correspond to Fig. 10.8 and are plots of T, K_I, K_{Ic}, and K_{Ia} vs a/w for the two times when events took place. These figures show that K_{Ic} and K_{Ia} for the first initiation-arrest event were ~40 and ~14% less, respectively, than the design values. For the second initiation and final arrest event, K_{Ic} and K_{Ia} were somewhat greater (24 and 18%, respectively) than the design values.

10.4.2. K_{Ic} and K_{Ia} values deduced from TSE-6

The calculated critical values of K_I corresponding to the first two initiation events and the first and last arrest events are listed in Table 10.1, which also includes for these events the times, crack depths, and crack-tip temperatures. These critical values of K_I are compared with the TSE-6 design curves and the lab small-specimen data in Fig. 10.11. As indicated in this figure, the values of K_{Ic} and K_{Ia} deduced from TSE-6 agree reasonably well with the curves corresponding to the final set of small-specimen data, although the K_{Ic} and K_{Ia} values corresponding to the second initiation event and the final arrest event seem somewhat high.

10.4.3 Posttest analysis based on final set of lab small-specimen K_J and K_{Ia} data

The few TSE-6 data points in Table 10.1 and Fig. 10.11 could not be used in a meaningful way to construct K_{Ic} and K_{Ia} curves for a final posttest analysis of TSE-6. Instead, a final analysis was performed

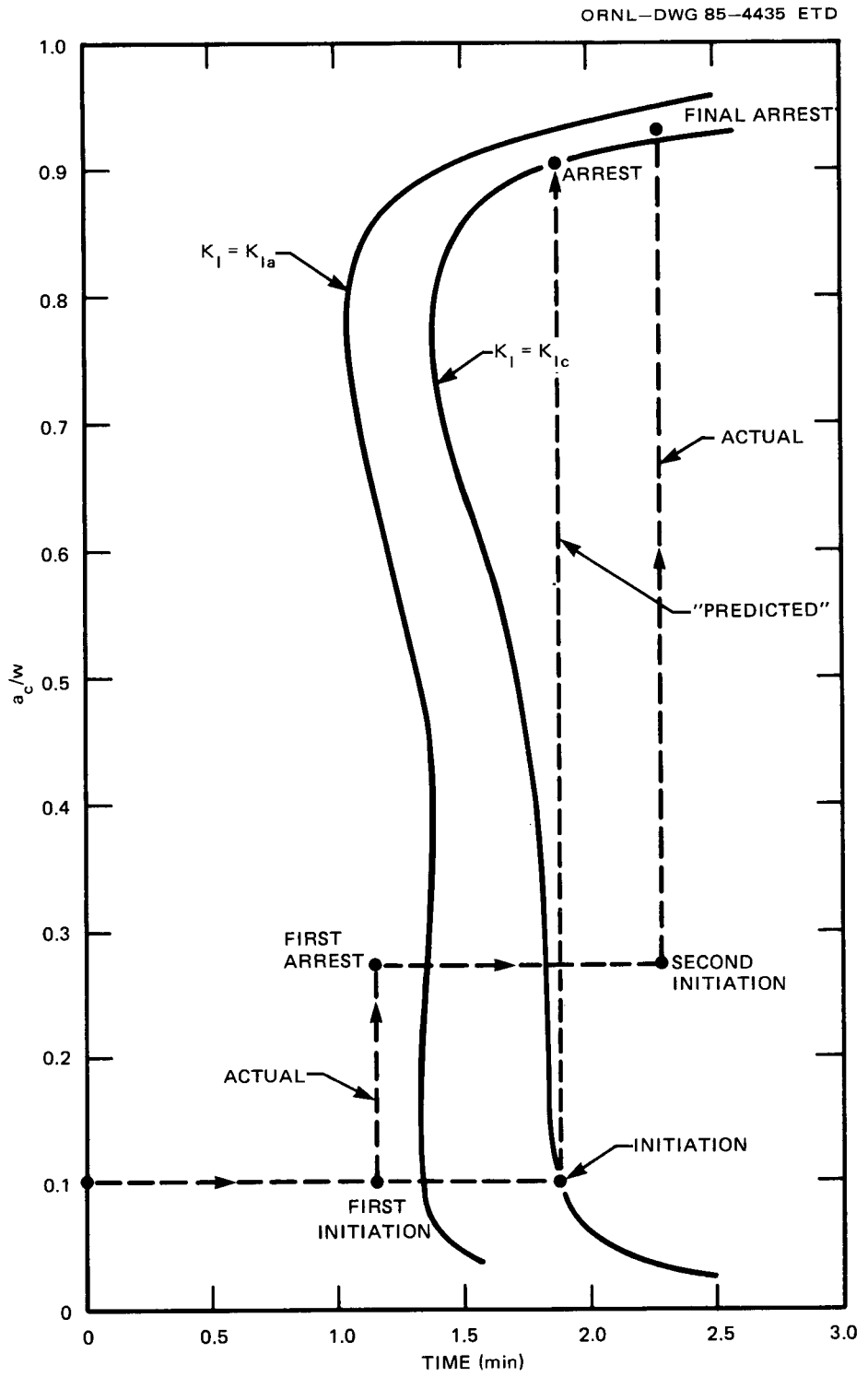

Fig. 10.8. TSE-6 posttest critical-crack-depth curves, based on measured temperatures and design toughness curves, with actual events superimposed.

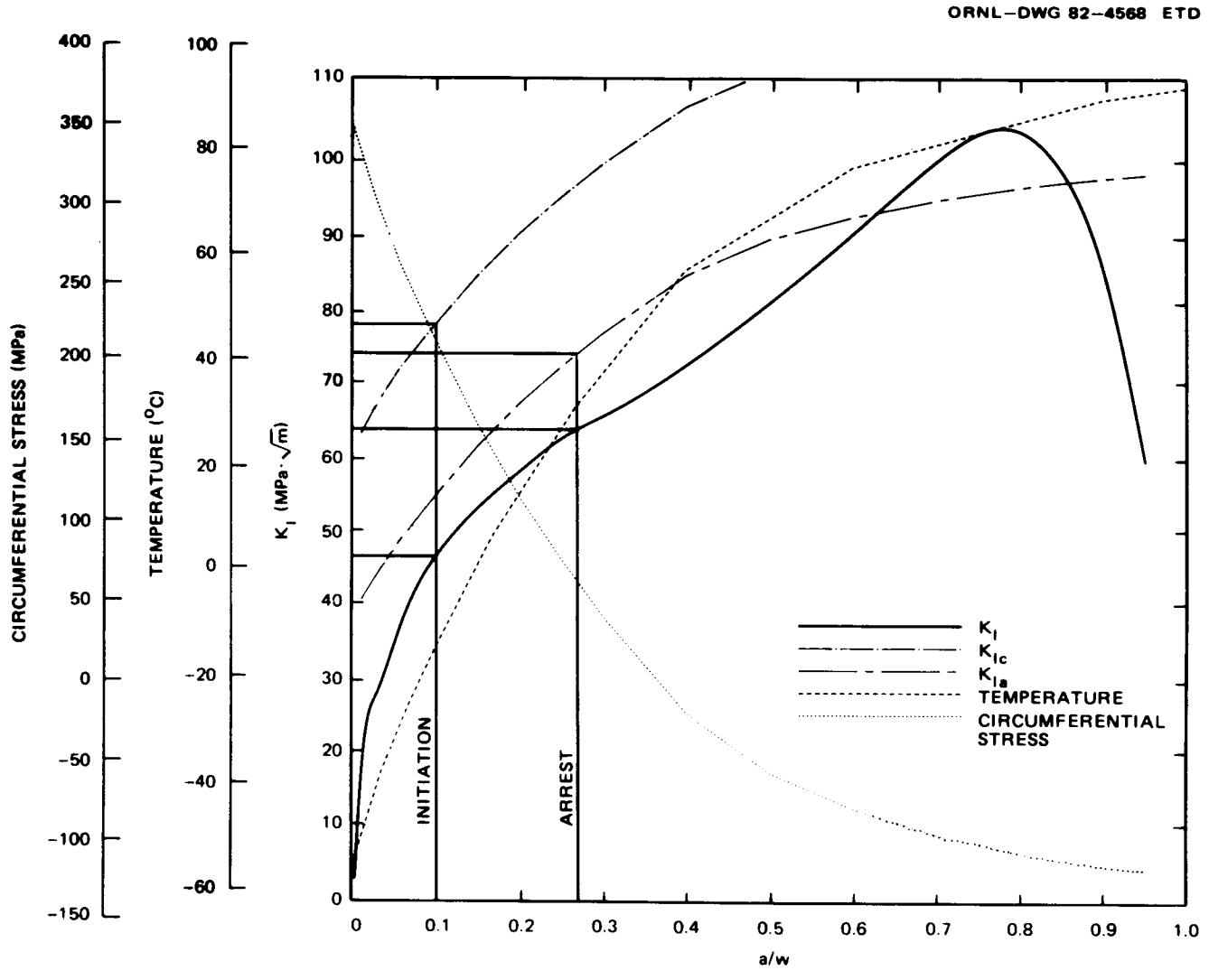

Fig. 10.9. Characteristic fracture-mechanics curves for TSE-6 at the time of the first initiation-arrest event (69 s), based on posttest analysis using measured temperatures and design toughness curves.

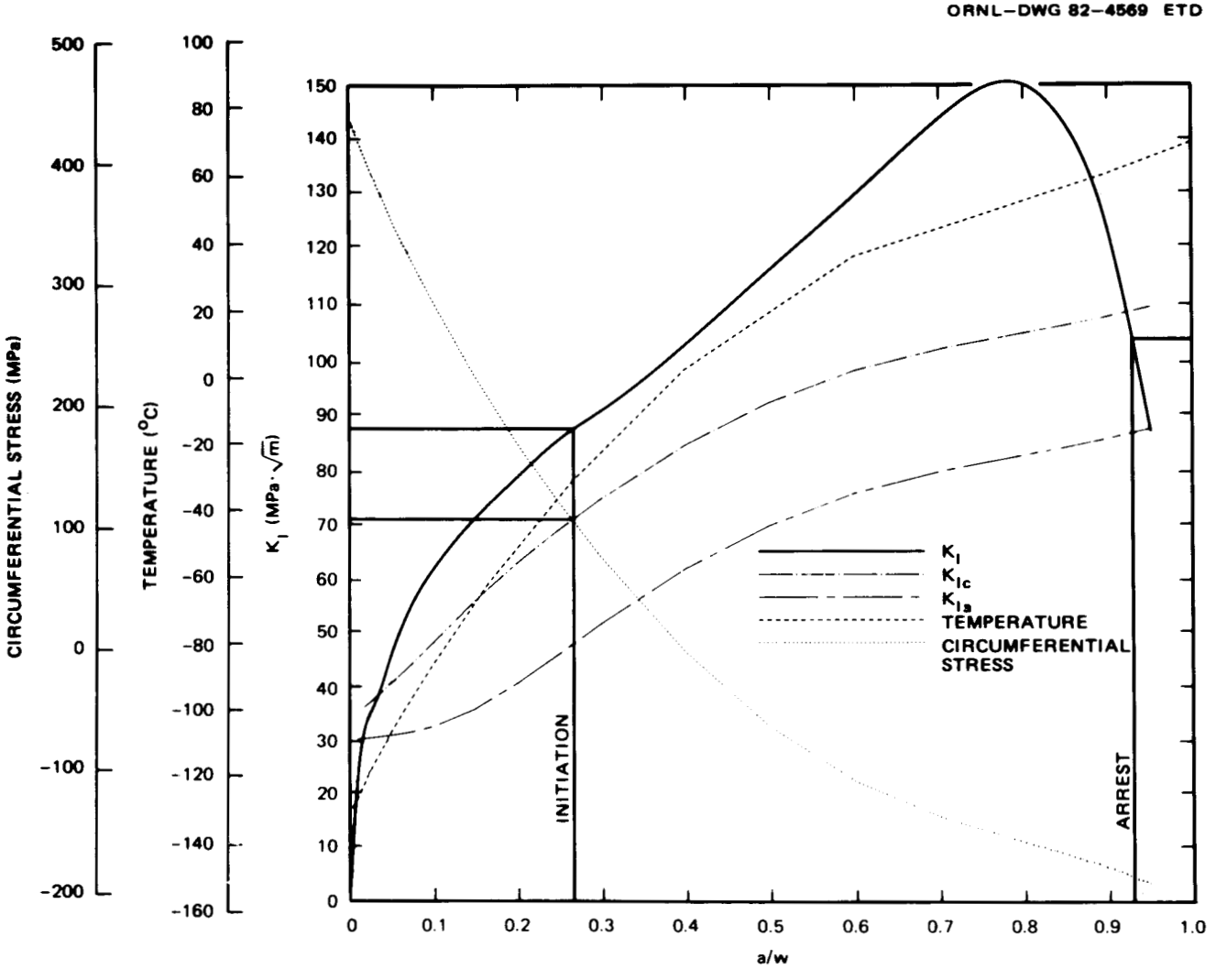

Fig. 10.10. Characteristic fracture-mechanics curves for TSE-6 at the time of the second initiation-arrest event (137 s), based on posttest analysis using measured temperatures and design toughness curves.

Table 10.1. Summary of events for TSE-6

Time (s)	Event	a/w	K_I (MPa·$\sqrt{m}$)	Temperature (°C)
69	Initiation	0.10	46	−13
	Arrest	0.28	63	32
137	Initiation	0.28[a]	87	−31
	Arrest	0.93[b]	105	63

[a]Second initiation event.

[b]Final arrest event.

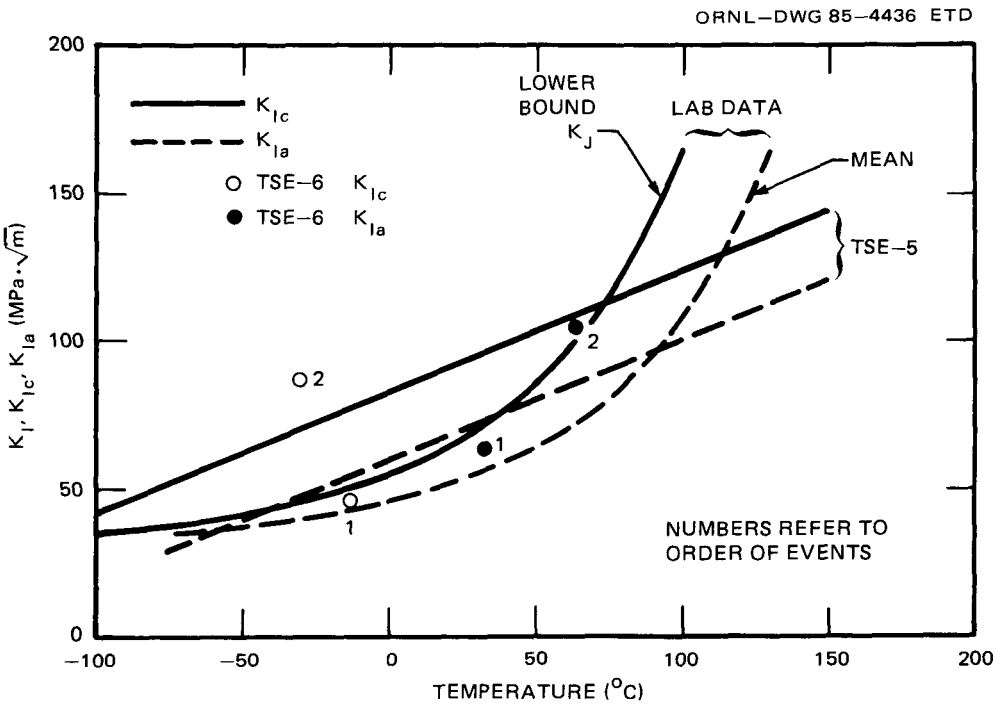

Fig. 10.11. Comparison of TSE-6 K_{Ic} and K_{Ia} values, TSE-6 K_{Ic} and K_{Ia} design curves (deduced from TSE-5 results), and small-specimen K_J, K_{Ic}, and K_{Ia} data.

using the small-specimen lower-bound K_J and the mean K_{Ia} curves shown in Figs. 7.7 and 10.11. The results are shown in Fig. 10.12, which is a set of critical-crack-depth curves with the actual events superimposed, and in Figs. 10.13 and 10.14, which are plots of temperature, K_I, K_{Ic} and K_{Ia} vs a/w for the two times at which events took place. (A complete set of digital output is included in Appendix F.) These results indicate reasonably good agreement between experiment and analysis for the first

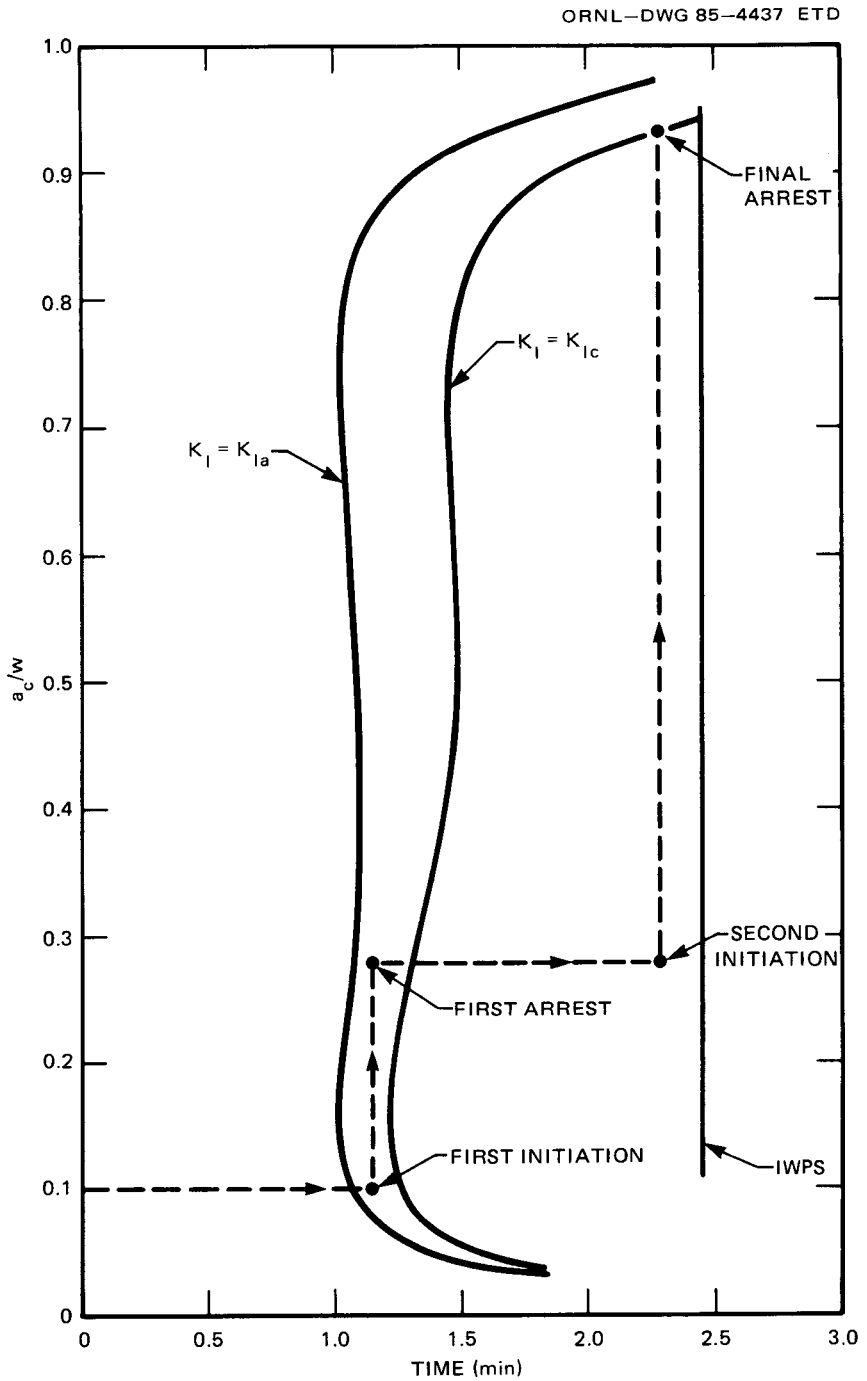

Fig. 10.12. TSE-6 posttest critical-crack-depth curves, based on measured temperatures and lab small-specimen lower-bound K_J and mean K_{Ia} data, with actual events superimposed.

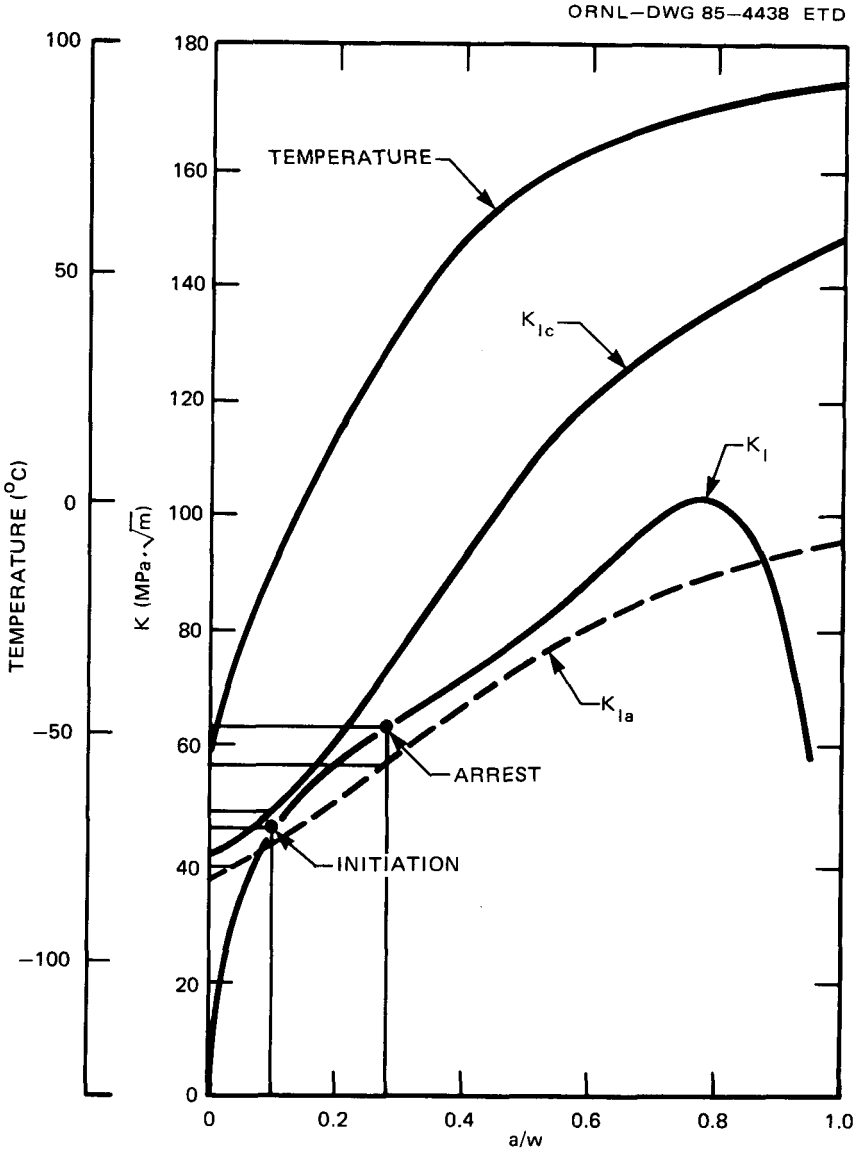

Fig. 10.13. Characteristic fracture-mechanics curves for TSE-6 at time of first initiation-arrest event (69 s), based on posttest analysis using small-specimen fracture-toughness data.

initiation, first arrest, and final arrest event and a rather large discrepancy for the second initiation event, consistent with the data in Fig. 10.11. The critical values of K_I corresponding to the first initiation and arrest events are ~6% less and ~12% greater, respectively, than the corresponding toughness curves. For the second initiation event, the critical value of K_I is ~88% greater than the initiation toughness curve.

A comparison of K_I and K_{Ia} for the final arrest event may not be very meaningful because of the proximity of the crack tip to the outer surface of the cylinder and because of the apparent very steep gradient in K_I, which makes the calculated critical value of K_I very sensitive to the effective crack depth. Probably the most important observation is

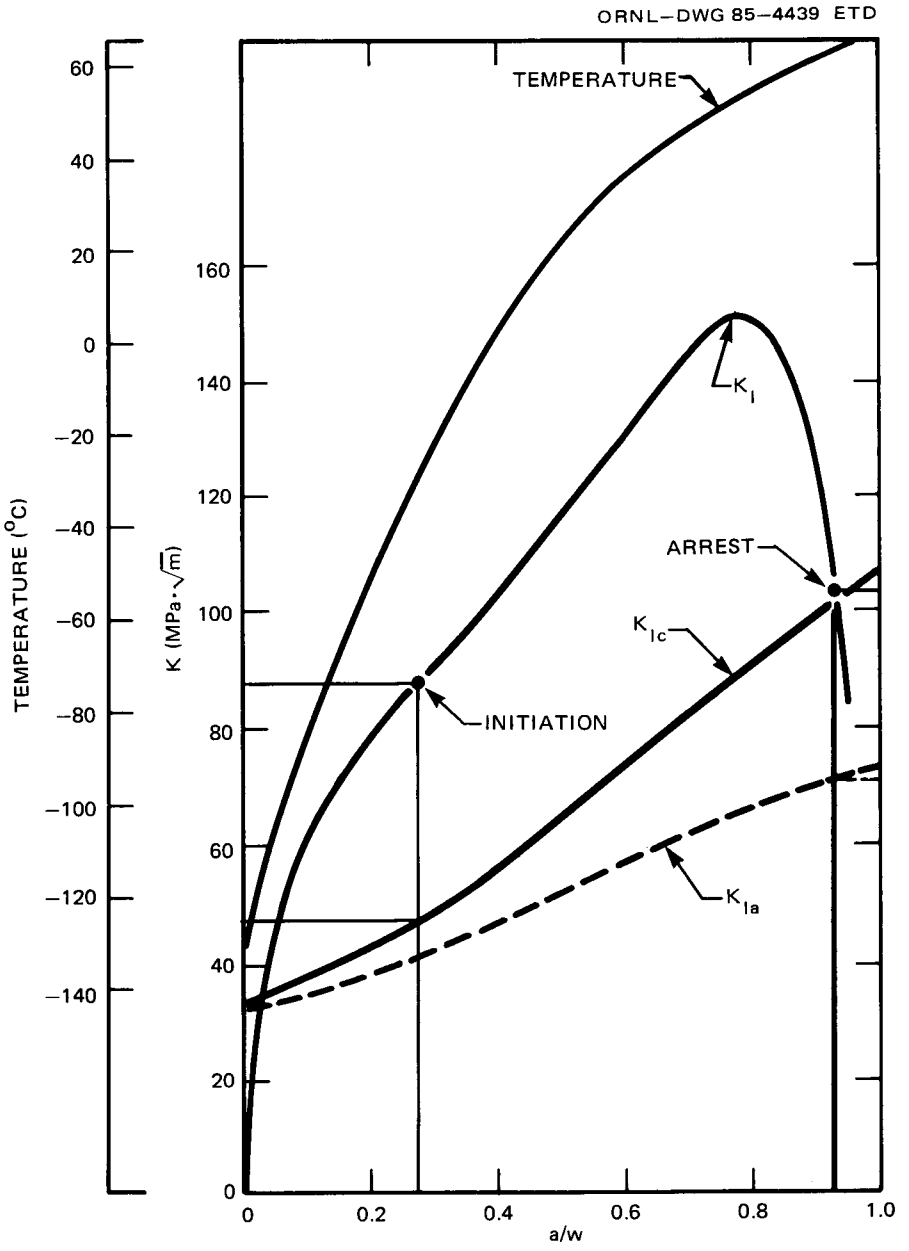

Fig. 10.14. Characteristic fracture-mechanics curves for TSE-6 at time of second initiation-arrest event (137 s), based on posttest analysis using small-specimen fracture-toughness data.

that almost irrespective of the value of K_{Ia}, the calculation would predict arrest deep in the wall ($a/w > 0.9$) and, indeed, that is what happened.

10.4.4 Arrest in a rising K_I field

The scope of TSE-6 did not include achieving arrest in a rising K_I field ($dK_I/da > 0$) nor was such an event expected since a single long

crack jump with arrest deep in the wall was desired and predicted. However, as shown in Fig. 10.15, the initial relatively short crack jump did result in arrest in a rising K_I field. As indicated in Fig. 10.15, the corresponding value of dK_I/da was ~0.8 MPa•$\sqrt{m}$/mm, which is about three times that achieved during TSE-5A but still significantly less than that estimated for two rather severe PWR postulated overcooling accidents (factor of two to three less). Even so, the value for TSE-6 is large enough for a meaningful comparison of K_{Ia} values corresponding to rising and falling K_I fields. Such a comparison is made in Chap. 11.

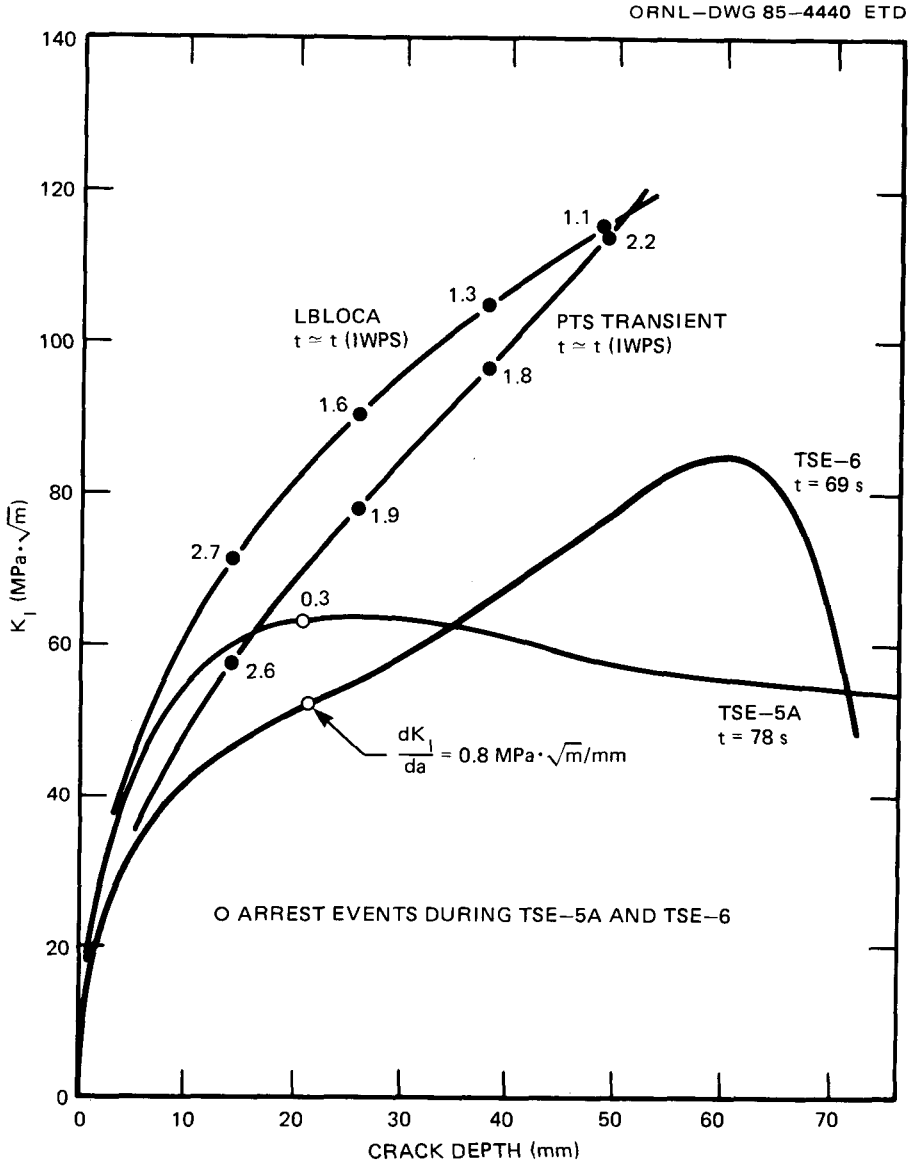

Fig. 10.15. Comparison of K_I vs a curves for TSE-5A, TSE-6, and two PWR postulated severe overcooling accidents.

Reference

1. W. L. Fourney et al., "Dynamic Run-Arrest Calculations," pp. 20–26 in *Heavy-Section Steel Technology Program Semiann. Prog. Rep. October 1983–March 1984*, NUREG/CR-3744, Vol. 1 (ORNL/TM-9154/V1), Martin Marietta Energy Systems, Inc., Oak Ridge Natl. Lab.

11. DISCUSSION OF RESULTS

11.1 Comparison of K_{Ic} and K_{Ia} Values Deduced from TSE-4, TSE-5, TSE-5A, TSE-6, and a French Thermal-Shock Experiment and Obtained from "Standard" Lab Specimens

An important objective of the thermal-shock program was to evaluate the validity of linear-elastic fracture mechanics for thermal-shock loading conditions. This was to be accomplished by comparing the K_{Ic} and K_{Ia} values deduced from the thermal-shock experiments with the data obtained using "standard" compact specimens. For a meaningful comparison it was necessary that K_I corresponding to the initiation and arrest events during the thermal-shock experiments be determined accurately and that the test-cylinder material be well characterized.

Valid crack-initiation-toughness data (K_{Ic}) were obtained over a reasonable temperature range for the TSE-5 and TSE-6 test cylinders, but because of the requirement for larger compact specimens, valid (K_{Ic}) data were not obtained for the TSE-5A test-cylinder material. In the absence of these specific data, the comparison for evaluating the validity of linear-elastic fracture mechanics in connection with TSE-5A was made with the ASME Sect. XI lower-bound K_{Ic} curve.[1]

Because the TSE-5 and TSE-6 test cylinders were from the same heat of material and were given the same heat treatment, it is of interest to compare the two sets of data, and this is done in Fig. 11.1. As indicated, the small-specimen and test-cylinder K_{Ic} data sets agree rather well, including the scatter, which is approximately ±35%. The K_{Ic} values for the second initiation events during the thermal-shock experiments are rather high, indicating an increase in toughness due to a prior arrest event. However, the third initiation event during TSE-5 did not exhibit the same enhancement of K_{Ic}. Furthermore, studies conducted by Rosenfield et al.[2,3] with compact specimens indicate that a crack-arrest event does not elevate the fracture toughness for a subsequent initiation event.

The TSE-5 and TSE-6 K_{Ia} values also agree reasonably well with each other, but the mean is ~20% above the mean of the small-specimen data. However, because of the apparent large scatter in K_{Ia} data and the small number of TSE-5 and TSE-6 data points, the 20% discrepancy is not considered to be a trend.

A comparison of all of the K_{Ic} values deduced from (1) TSE-5, TSE-5A, TSE-6; (2) a previous thermal-shock experiment, TSE-4 (Refs. 4 and 5); and (3) a French thermal-shock experiment[6] similar to the ORNL experiment with the ASME Sect. XI lower-bound K_{Ic} curve is presented in Fig. 11.2. It is apparent that all of the test-cylinder data points with the exception of one of the French points are above the ASME lower-bound curve and, with the exception of two points, are below an approximate upper bound of the K_{Ic} data that were used to generate the ASME lower-bound curve.[1] The two points above the upper-bound curve correspond to the second initiation events for TSE-5 and TSE-6.

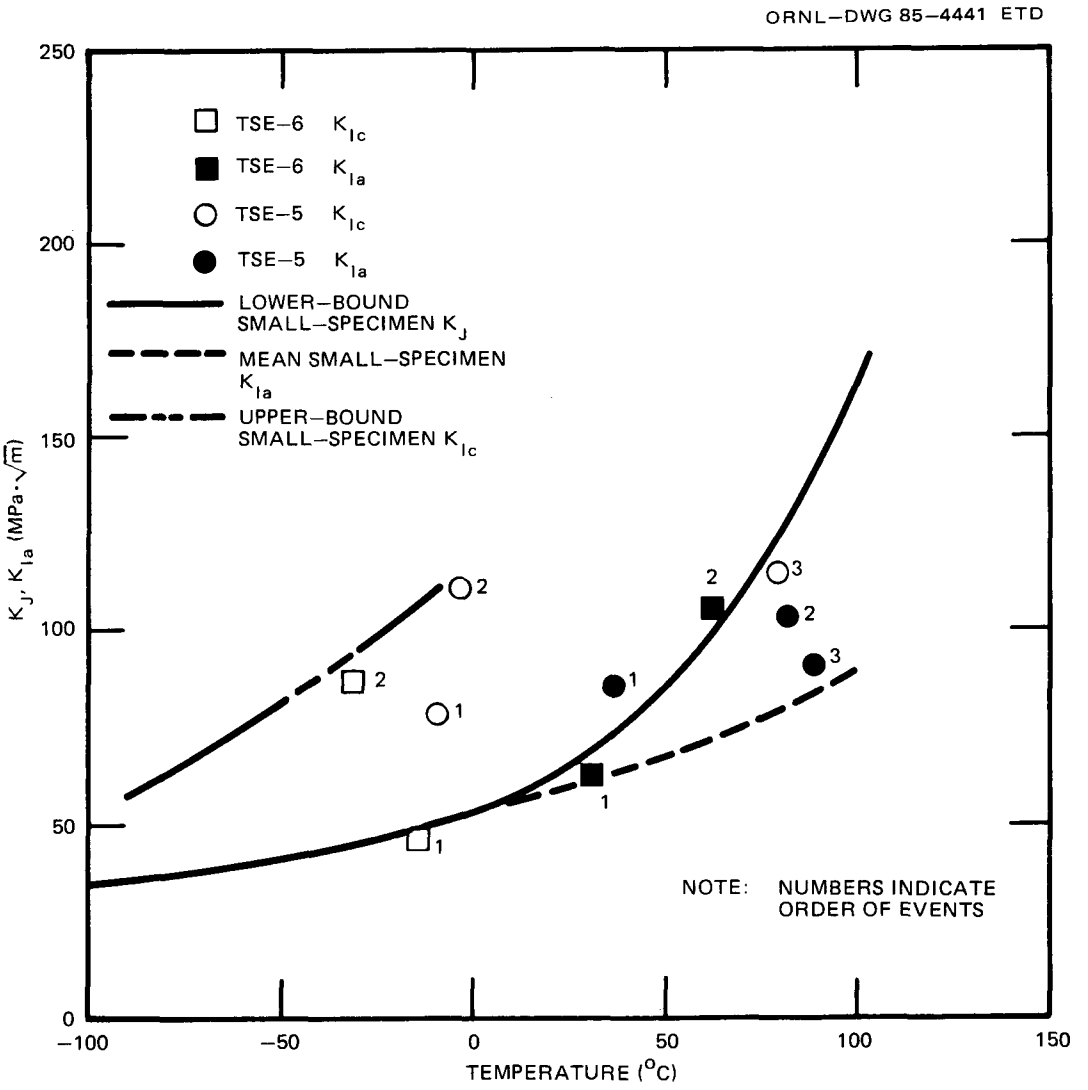

Fig. 11.1. Comparison of TSE-5 and TSE-6 K_{Ic} and K_{Ia} values with lower-bound K_J and mean K_{Ia} small-specimen data.

A similar comparison for the K_{Ia} data is presented in Fig. 11.3, which includes (1) 10 K_{Ia} values deduced from 4 ORNL thermal-shock experiments (TSE-4, TSE-5, TSE-5A, and TSE-6); (2) 3 K_{Ia} values deduced from the French thermal-shock experiment; (3) the 5th and 95th percentile curves corresponding to a Battelle-Columbus Laboratories small-specimen K_{Ia} data base[7,8] consisting of 233 data points for A 533 and A 508 material, including 25 data points obtained from the thermal-shock test-cylinder characterization studies; and (4) the ASME Sect. XI lower-bound K_{Ia} (K_{IR}) curve.[1] As indicated by Fig. 11.3, the scatter in the small-specimen data is approximately ±45%, and only a small fraction of the data points falls below the K_{IR} curve. All of the K_{Ia} values deduced from the ORNL thermal-shock experiments fall within the small-specimen

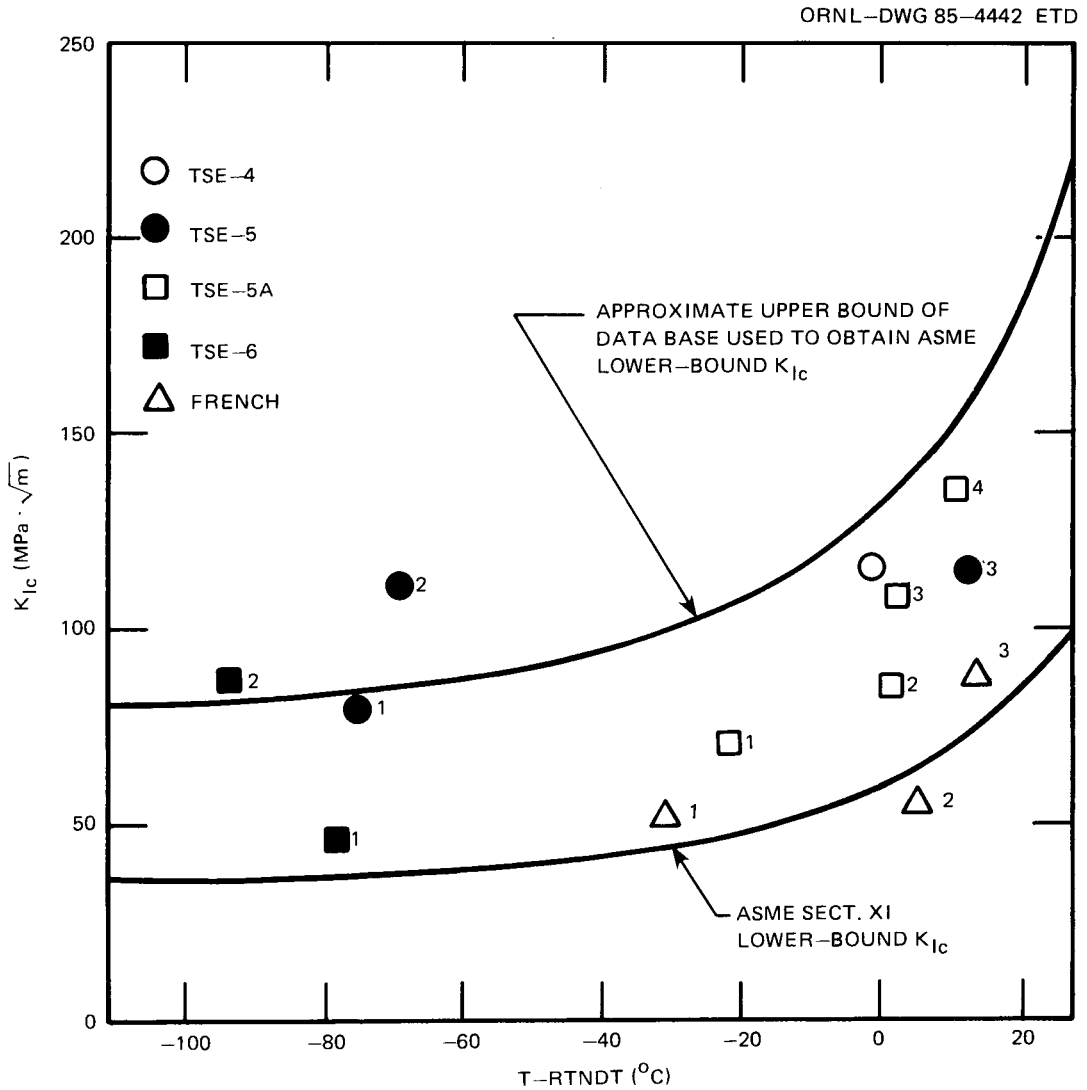

Fig. 11.2. Comparison of small-specimen and large-specimen K_{Ic} data.

scatter band and well above the K_{IR} curve, while the three French data points cluster about the K_{IR} curve.

A comparison of the ORNL and French thermal-shock-experiment data is of interest because the thermal-shock experiments were very similar. The test cylinders were similar in size and material and were thermally loaded by quenching in liquid nitrogen. However, the French fracture surfaces were very flat and void of unbroken ligaments,[6] while the ORNL surfaces were relatively rough and, in some cases, as shown in Figs. 9.10 and 11.4, had many unbroken ligaments. Since the restraining force of the ligaments was not accounted for in the calculation of critical values of K_I, the existence of ligaments on the ORNL surfaces could be a reason for the generally higher indicated values of fracture toughness relative to the French values.

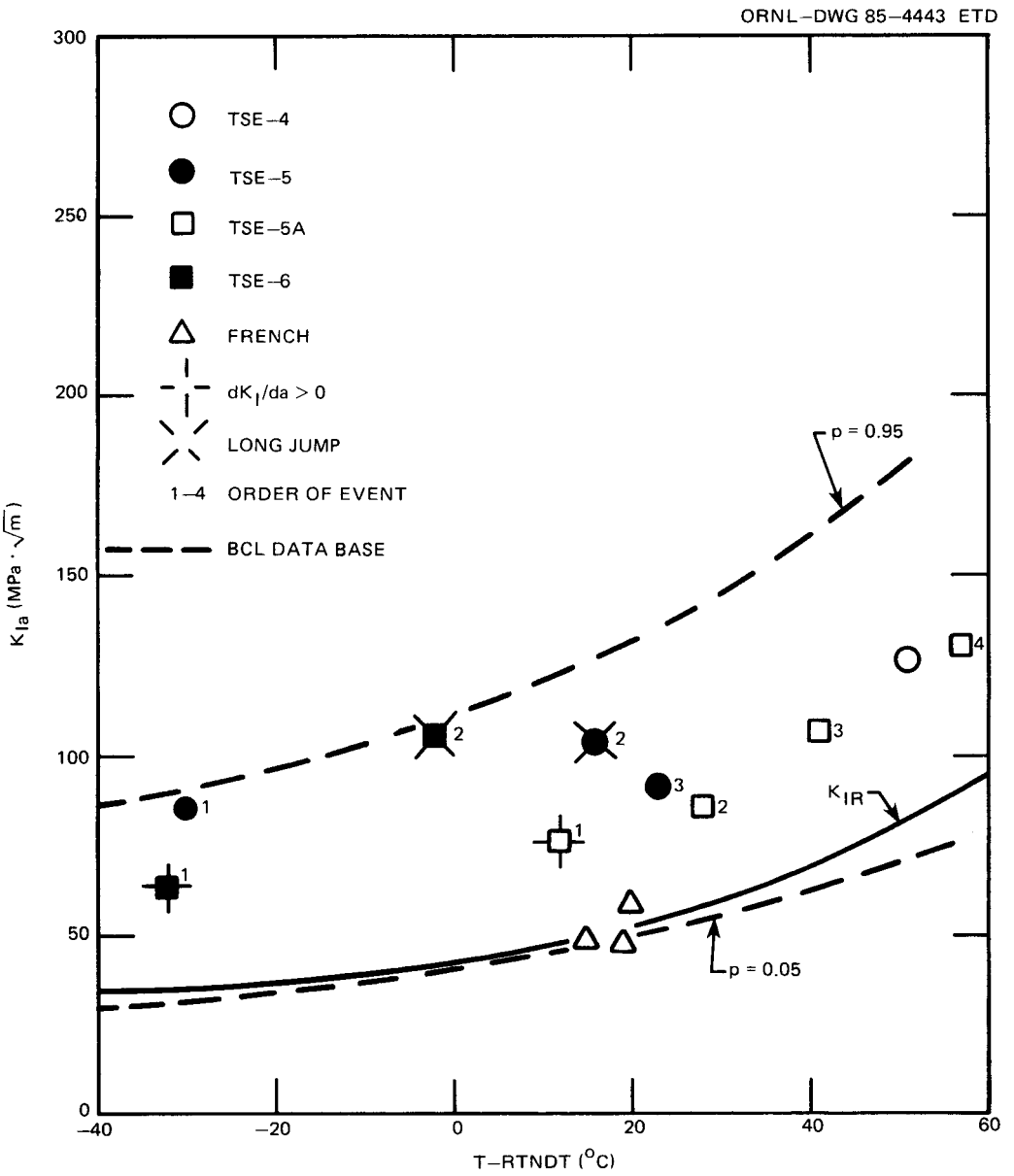

Fig. 11.3. Comparison of small-specimen and large-specimen K_{Ia} data.

It would seem that the large scatter in the small-specimen and in the test-cylinder K_{Ic} and K_{Ia} data would preclude drawing conclusions regarding the validity of linear-elastic fracture mechanics for thermal-shock loading conditions. However, if one accepts the apparent fact that both large and small specimens can exhibit large scatter in valid fracture-toughness data, then the coincidence of the scatter bands and a lack of significant anomalies during the thermal-shock experiments indicate that linear-elastic fracture mechanics is valid, at least for (T-RTNDT) < 20°C for crack-initiation events and (T-RTNDT) < 60°C for crack-arrest events.

M&C PHOTO Y175292A

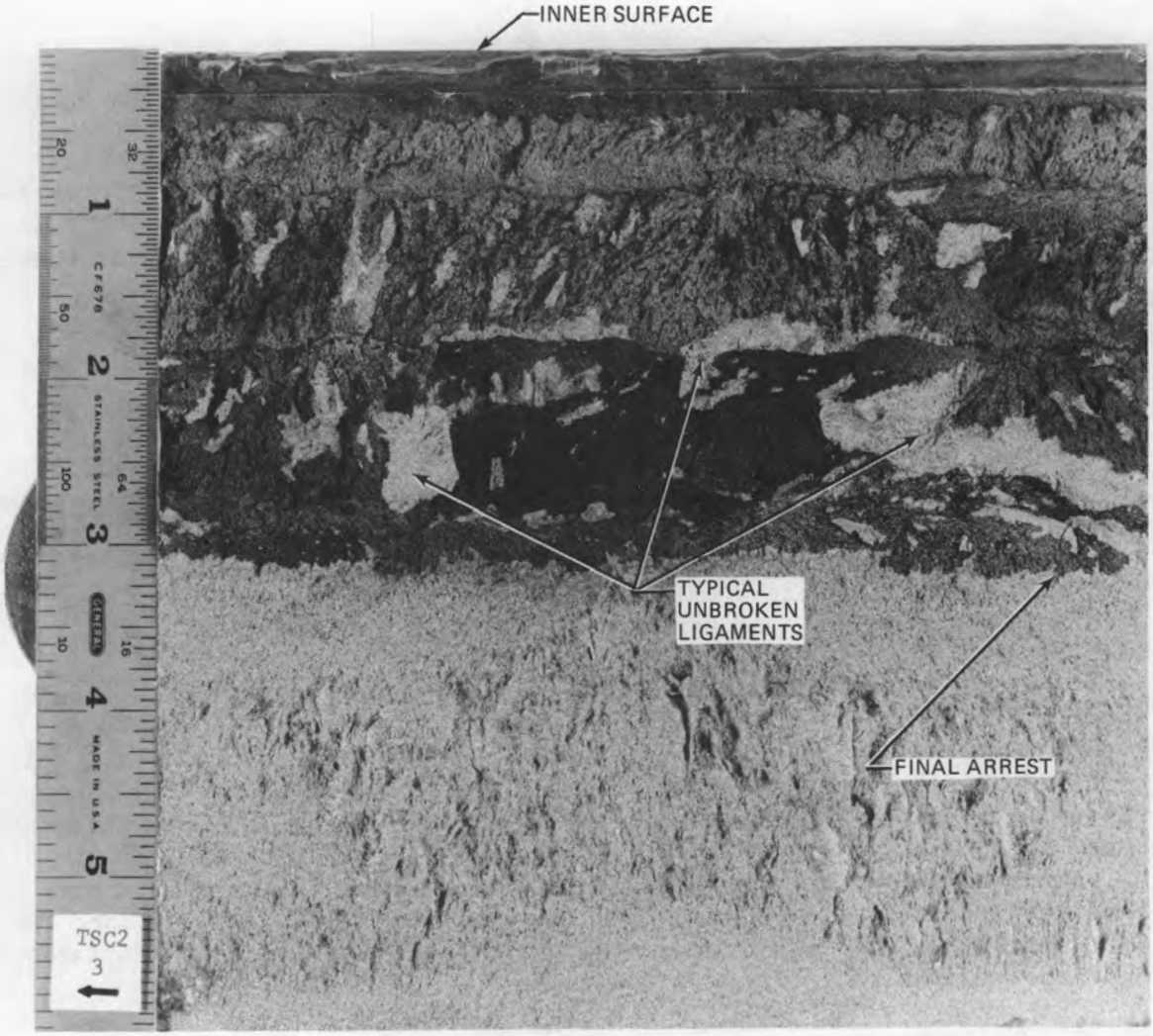

Fig. 11.4. Examples of unbroken ligaments (TSE-5A).

11.2 Arrest in a Rising K_I Field

The two data points in Fig. 11.3 that correspond to arrest in a rising K_I field (first arrest event for TSE-5A and TSE-6) fall well within the scatter band of the small-specimen data. This indicates that the critical value of K_I for arrest in a rising K_I field is about the same as that for a falling K_I field ($dK_I/da < 0$), which is the usual condition when obtaining small-specimen K_{Ia} data.

11.3 Dynamic Effects at Arrest

A dynamic effect at arrest would be manifest in a higher critical value of K_I than calculated with a static model.[9] As indicated by Fig. 11.3, the statically calculated values of K_{Ia} corresponding to arrest following the two long crack jumps (second arrest events for TSE-5 and TSE-6) are just below the upper bound of the small-specimen data. If dynamic effects were actually substantial, the static analysis would tend to yield low values of K_{Ia}. Thus, it is concluded on the basis of these data that dynamic effects were negligible.

11.4 Comparison of EB-Weld Flaws and Arrested Flaws

There is a lingering concern that flaws generated by the EB-weld process, which usually involves postweld hydrogen charging, and arrested flaws could exhibit a different effective fracture toughness (K_{Ic}) than fatigue flaws. Arrested flaws may have unbroken ligaments on the fracture surface that affect the critical load, and an EB-weld flaw, which is also an arrested flaw, may have a residual K_I value of unknown magnitude (see Sect. 8.4.4).

The lab small-specimen data obtained in connection with the thermal-shock program correspond to fatigue flaws, while the K_{Ic} data deduced from the thermal-shock experiments correspond to EB-weld flaws (all initial flaws) and arrested flaws. Thus, the thermal-shock program presented an opportunity to compare "K_{Ic}" values obtained from the three types of flaws (fatigue, EB weld, and arrested). As indicated by the K_{Ic} data in Fig. 11.2, there is no consistent trend to indicate a difference between the three types of flaws. Furthermore, as mentioned in Sect. 11.1, Rosenfield[7,8] found no significant difference between fatigue and arrested cracks in compact specimens.

11.5 Warm Prestressing

Warm prestressing with $\dot{K}_I < 0$ may have prevented reinitiation in each of the ORNL thermal-shock experiments. However, only in the case of TSE-5A was the calculated best estimate of $(K_I/K_{Ic})_{max}$ for the final crack depth large enough to account for the uncertainties in the experiment and analysis. As indicated in Sect. 9.4, the calculated best estimate of $(K_I/K_{Ic})_{max}$ (max with respect to time), using the deduced toughness curves in Fig. 9.15, was 2.3, and the corresponding crack-tip temperature was −45°C. With reference to Fig. 11.2, it can be seen that the factor of 2.3 more than accommodates the small-specimen upper-bound K_{Ic} curve and even an upper-bound curve through the maximum of the K_{Ic} values deduced from the thermal-shock experiments. Thus, it is concluded that warm prestressing with $\dot{K}_I < 0$ was adequately demonstrated.

References

1. T. U. Marston, ed., *Flaw Evaluation Procedures, ASME Section XI, Background and Application of ASME Section XI, Appendix A, Special Report*, EPRI NP-719-SR, American Society of Mechanical Engineers, Electric Power Research Institute, August 1978.

2. A. R. Rosenfield et al., "Fracture-Mechanics Analysis and Investigations," pp. 15–16 in *Heavy-Section Steel Technology Program Quart. Prog. Rep. April–June 1982*, NUREG/CR-2751, Vol. 2 (ORNL/TM-8369/V2), Union Carbide Corp. Nuclear Div., Oak Ridge Natl. Lab.

3. A. R. Rosenfield et al., "Fracture-Mechanics Analysis and Investigations," pp. 14–20 in *Heavy-Section Steel Technology Program Quart. Prog. Rep. July–September 1982*, NUREG/CR-2751, Vol. 3 (ORNL/TM-8369/V3), Union Carbide Corp. Nuclear Div., Oak Ridge Natl. Lab.

4. R. D. Cheverton and S. E. Bolt, *Pressure Vessel Fracture Studies Pertaining to a PWR LOCA-ECC Thermal Shock: Experiments TSE-3 and TSE-4 and Update of TSE-1 and TSE-2 Analysis*, ORNL/NUREG-22, Union Carbide Corp. Nuclear Div., Oak Ridge Natl. Lab., December 1977.

5. R. D. Cheverton and S. K. Iskander, *Application of Static and Dynamic Crack-Arrest Theory to Thermal-Shock Experiment TSE-4*, NUREG/CR-0767 (ORNL/NUREG-57), Union Carbide Corp. Nuclear Div., Oak Ridge Natl. Lab., June 1979.

6. A. Pellissier-Tanon, P. Sollogoub, and B. Houssin, "Crack Initiation and Arrest in an SA 508 Class-3 Cylinder Under Liquid Nitrogen Thermal-Shock Experiment," *Transactions of the 7th International Conference on Structural Mechanics in Reactor Technology*, Vols. G and H, Chicago, August 1983.

7. A. R. Rosenfield, "Validation of Compact-Specimen Crack-Arrest Data," Technical Briefs, *J. Eng. Mater. Technol.* 106, 207–208 (April 1984).

8. A. R. Rosenfield et al., "Crack-Arrest Studies at BCL," pp. 57–62 in *Heavy-Section Steel Technology Program Semiann. Prog. Rep. October–March 1984*, NUREG/CR-3744, Vol. 1 (ORNL/TM-9154/V1), Martin Marietta Energy Systems, Inc., Oak Ridge Natl. Lab.

9. J. K. Kalthoff, J. Beinert, and S. Winkler, "Measurements of Dynamic Stress Intensity Factors for Fast Running and Arresting Cracks in Double-Cantilever-Beam Specimens," pp. 161–76 in *Fast Fracture and Crack Arrest*, ASTM STP 627, July 1977.

Appendix A

INFORMATION PERTAINING TO THERMOCOUPLE THIMBLES

Radial temperature distributions in the wall of the TSE test cylinders were determined by measuring the temperatures along the length of a steel bar that constituted the core region of a thermocouple thimble that was inserted into a closely fitting, radially oriented hole in the wall of the cylinder. The rough stock for the core was taken from a prolongation of the test cylinders, and this was done in such a way that the longitudinal axis of the core, before removal of the rough stock from the prolongation, coincided with a radial line of the test cylinder. The final heat treatment for the core consisted of tempering at ~700°C for 4 h.

As shown in Figs. A.1 and A.2, the geometry of the core was a right circular cylinder. Twelve shallow, equally spaced grooves were machined

ORNL–PHOTO 6891–79R

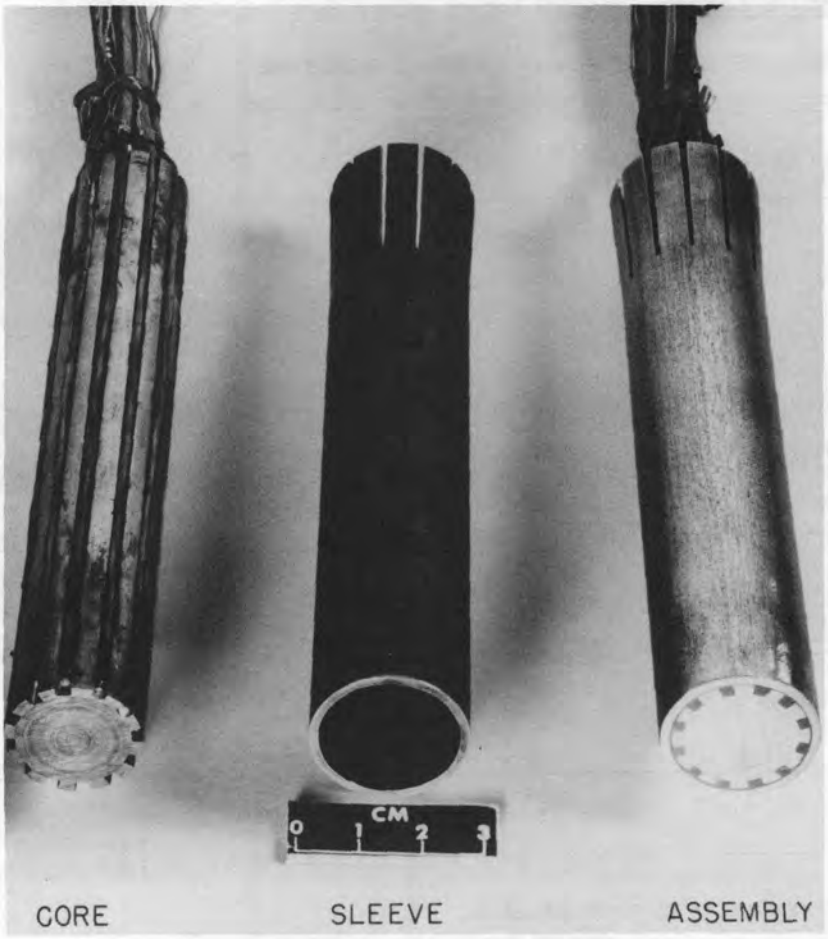

Fig. A.1. Thermocouple-thimble components and assembly for measuring radial temperature distribution in test cylinders during thermal-shock experiments.

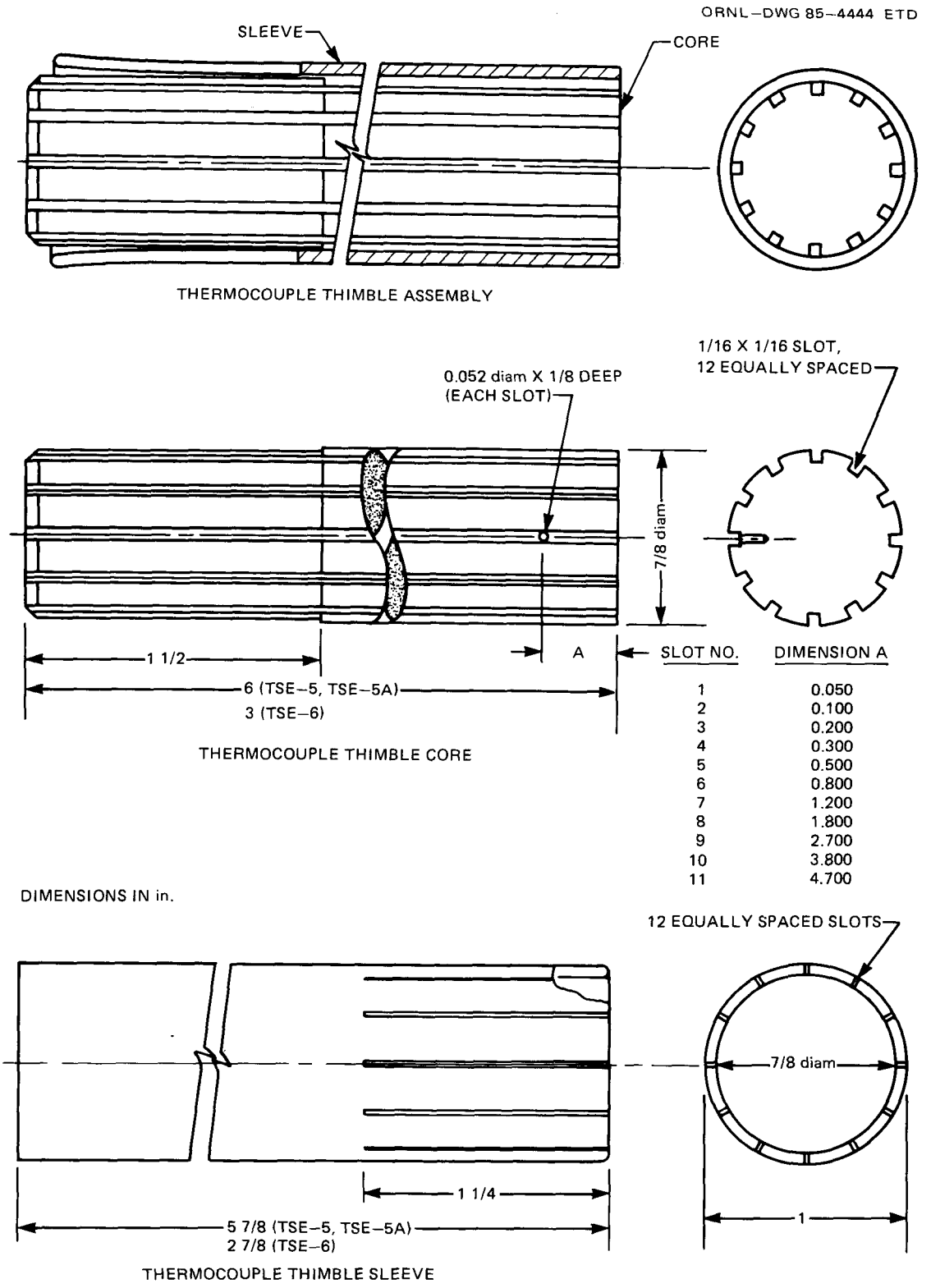

SLOT NO.	DIMENSION A
1	0.050
2	0.100
3	0.200
4	0.300
5	0.500
6	0.800
7	1.200
8	1.800
9	2.700
10	3.800
11	4.700

Fig A.2. Details of thermocouple thimbles used for TSE-5, TSE-5A, and TSE-6.

the full length of the bar to accommodate thermocouple leads. A shallow, small-diameter radial hole was drilled in each groove to accommodate the thermocouple junctions. These junctions were made by soldering pairs of leads in each hole. The holes were spaced apart along the length of the bar and were closer together near the "inner" end, where the temperature gradient would be the steepest.

A complete assembly of a thermocouple thimble includes the core, either 10 (TSE-6) or 12 (TSE-5, TSE-5A) thermocouples, and a steel sleeve that protects the thermocouples from abuse. Epoxy is used to bond these components together and to fill all voids.

After assembly, each thimble was subjected to an isothermal calibration at 100°C, room temperature, and liquid-nitrogen temperature. In addition, each thimble was subjected to a thermal shock by first coating the "inner" end of the thimble with rubber cement and then contacting that surface with liquid nitrogen. This was done to make sure that the junctions would not fail under thermal-shock conditions.

The diameter of the thermocouple-thimble was influenced by two considerations: (1) it had to be large enough to accommodate the 12 thermocouples without the thermal properties of the thermocouple leads and the epoxy having a significant effect on the temperatures in the core, and (2) it had to be large compared to local variations in the rubber-cement coating on the inner end of the thimble so that enhancement of the fluid-film heat transfer coefficient would be the same for the thimble as elsewhere.

The straight cylindrical shape of the core and the small clearance between the outside diameter of the thimble and the mating hole in the wall of the test cylinder introduce an error in the transient temperature indications. This is because during a thermal-shock experiment heat tends to travel along radial lines, and the cylindrical surface of the thimble cuts across these radial lines. The magnitude of the error depends, of course, upon the thermal resistance of the gap, and to complicate matters, the gap is not uniform around the thimble. If the gap resistance is assumed to be infinite, the maximum error can be estimated by comparing calculated temperatures for cylindrical and slab geometries. The results of such an analysis are shown in Fig. A.3 for typical TSE thermal-shock conditions. As indicated, at 2 min into the transient, the slab has a 6°C lower temperature at the inner surface, and at 5 min the difference is 14°C. The difference continues to increase for some time thereafter, and although the initiation and arrest events in each of the experiments were over before 5 min, the demonstration of warm prestressing required an extension of the experiment (TSE-5A) to ~15 min to obtain an estimate of $(K_I/K_{Ic})_{max}$. Thus, a further evaluation of the adequacy of the particular thimble design was in order.

Rather than attempt to estimate the actual thermal resistance of the gap, the TSE-5A test cylinder was equipped with three thimbles that had a rectangular cross section with all four sides of the thimble parallel to radial lines (see Fig. A.4). These 3 thimbles were located at the horizontal midplane of the test cylinder, and the other 12 thimble locations were equipped with the cylindrical thimbles. (The tapered holes in the cylinder wall were machined using electrical-discharge machining techniques, as illustrated to some extent in Fig. A.5.)

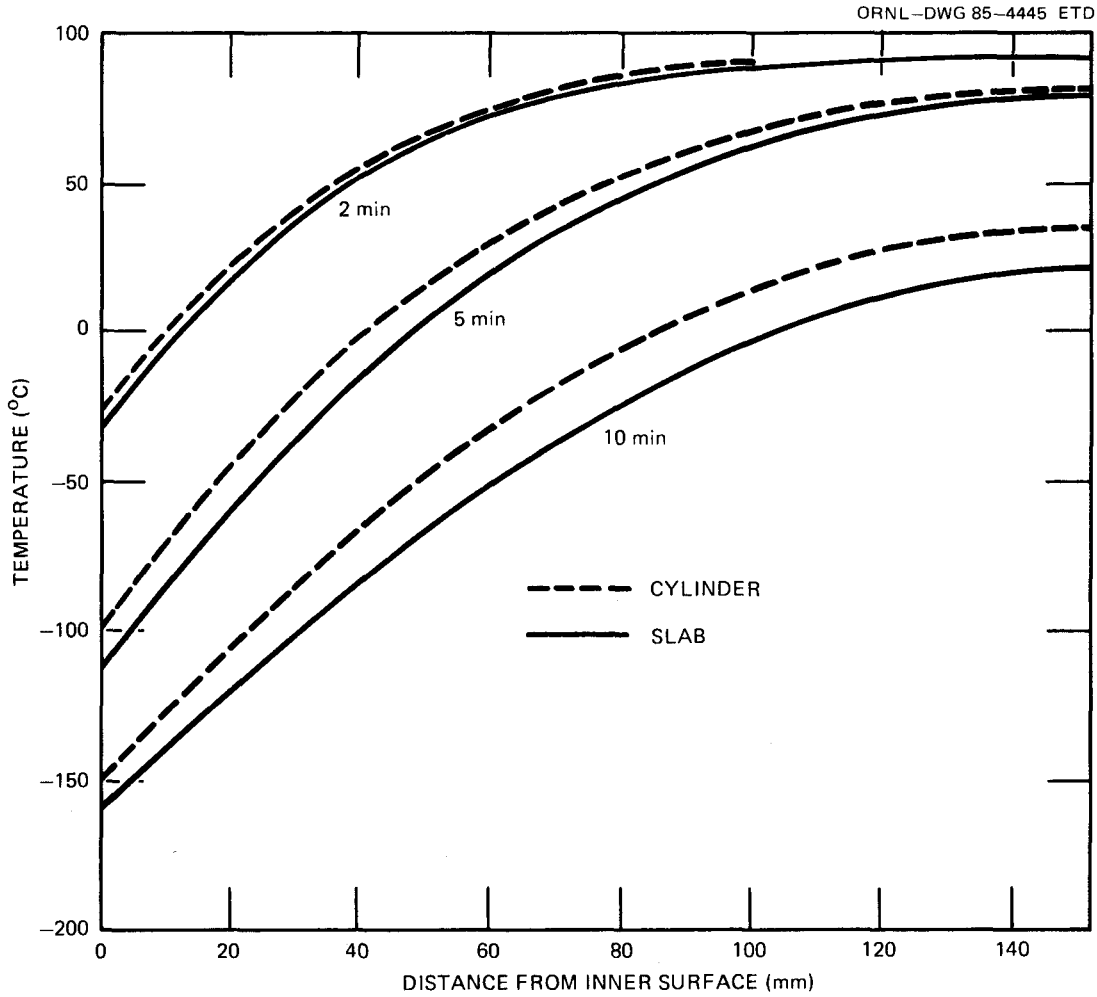

Fig. A.3. Comparison of temperatures for cylinder and slab geometries for typical TSE thermal-shock conditions.

Two thermal-shock experiments (a thermal-hydraulic experiment and TSE-5A) were conducted using the test cylinder equipped with both the cylindrical and tapered thimbles. In both tests there was no discernible difference in indicated temperatures measured with the two types of thimbles, implying that the interface resistance was negligible.

The wall thickness for the TSE-6 test cylinder was half that for the TSE-5 and TSE-5A test cylinders, for which w = 152 mm. Thus, the thimbles were reduced in length to 76 mm, and this eliminated thermocouples 10 and 11. Otherwise, the thimbles for TSE-6 were the same as those for TSE-5 and TSE-5A.

ORNL PHOTO 7330–80

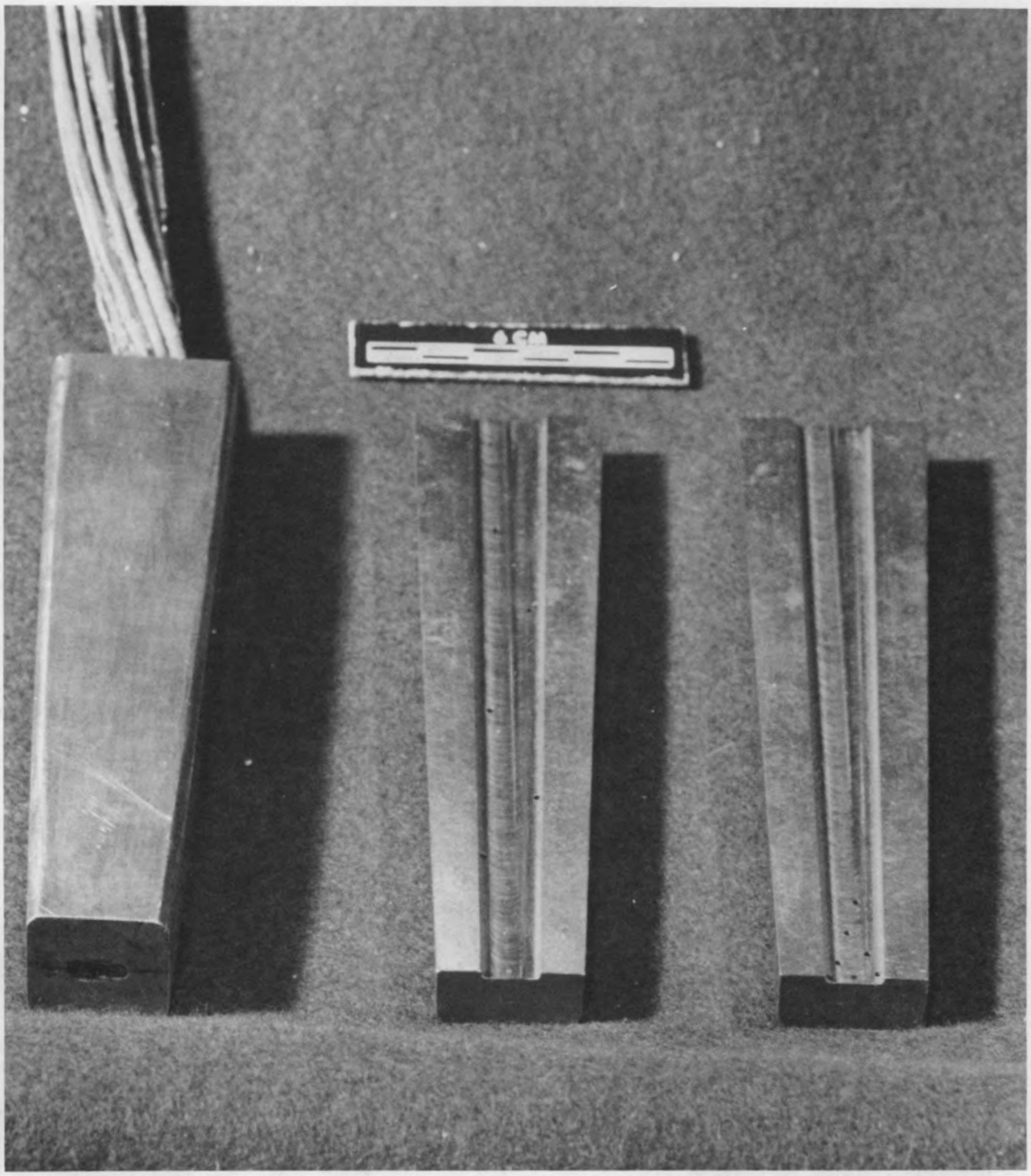

Fig. A.4. Tapered thermocouple-thimble components and assembly for measuring radial temperature distribution in TSE-5A test cylinder during thermal-shock experiment.

K/PH 80–2165A

Fig. A.5. Machining of tapered thermocouple-thimble holes in the TSE-5A test cylinder using the electrical discharge machining process.

Appendix B

CALIBRATION OF COD GAGES

During TSE-5, TSE-5A, and TSE-6, crack opening at the inner surface of the test cylinders was measured using Ailtech weldable strain gages (Fig. B.1). As illustrated in Fig. 6.8, the central portion of the gage was not bonded to the surface of the cylinder. This type of installation was used to prevent excessively high strain in the gage directly over the crack. The strain in the unbonded portion of the gage is essentially equal to the crack opening at the surface divided by the length of the unbonded section. If this strain is large compared with the strain associated with the surface stresses, then the output of the gage can be interpreted directly in terms of crack opening.

Even with a portion of the gage unbonded, the strain can be large enough for significant plastic deformation of the gage to take place. This and an unbonded section of the gage introduce the possibility of buckling of the unbonded portion when the thermal stresses subside and the crack closes, as illustrated in Fig. 6.8. This is of no concern because by the time buckling occurs, all of the data of interest have been recorded. Furthermore, the height of the buckle can be used to estimate the maximum crack opening.

Initially the COD gages were to be used only for detecting the time at which an initiation-arrest event took place, and such an event is clearly indicated by a step change in gage output as shown in Fig. 8.8. To accommodate a series of events, it was necessary that the gage not fail, and failure was prevented in most cases by not bonding the central portion of the gage, as discussed above.

Provided that temperature effects would not be excessive, there was also the possibility of using the COD-gage output indirectly to estimate crack depth. This was done by calculating the relation between crack

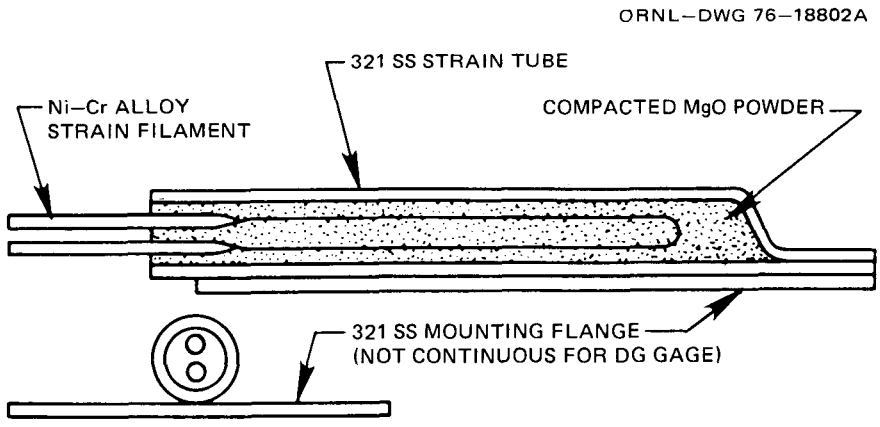

Fig. B.1. Details of Ailtech SG and DG-125 quarter-bridge strain gages.

opening at the inner surface and crack depth for the times in the transient at which initiation-arrest events took place. To improve the accuracy of this procedure, it was necessary to calibrate typical gages to obtain the relation between gage output and crack opening. This was done in an MTS testing machine, using the general arrangement and technique illustrated in Fig. B.2.

Calibrations were performed for two isothermal conditions: room temperature and liquid-nitrogen temperature (−196°C). Displacement-control loading (0.127 mm/min) was used, and loading was continued to failure of the gage. In all cases the gage output vs displacement was essentially linear up to the point of failure. Data pertaining to the COD gages used for TSE-5, TSE-5A, and TSE-6 are summarized in Table B.1.

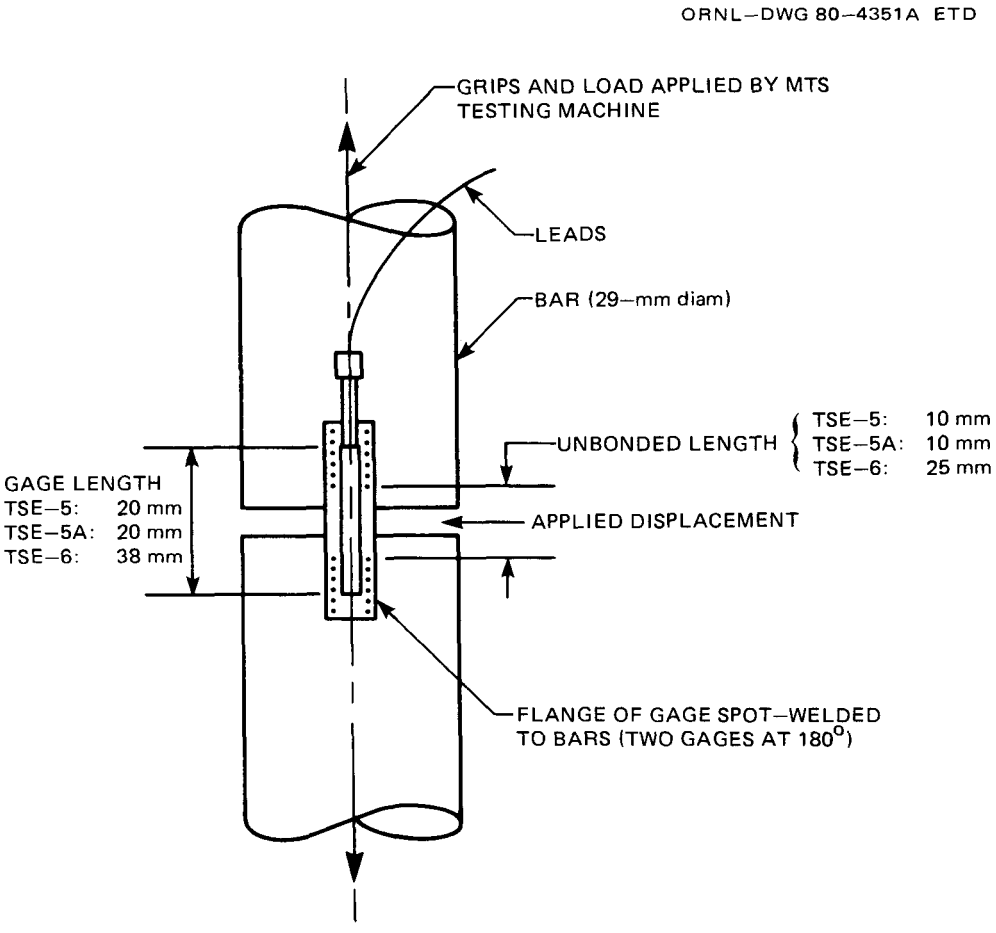

Fig. B.2. Installations of Ailtech COD gages for calibration.

Table B.1. Data pertaining to the COD gages used for TSE-5, TSE-5A, and TSE-6

Gage characteristics	TSE-5	TSE-5A	TSE-6
Gage No.	SG-125	SG-125	DG-125
Active length, mm	20	20	44
Unbonded length, mm	10	10	27
Average strain at failure, %	~7	~7	~8
Strain in unbonded length at failure, %	~14	~14	~13
$d(\varepsilon)/d(COD)$, mm^{-1}	0.040	0.040	0.021

Appendix C

MATERIAL PROPERTY DATA

A detailed discussion of the material property data for the three test cylinders (TSC-1, TSC-2, and TSC-3) and their prolongations (TSP-1, TSP-2, and TSP-3) is included in Chap. 7. This appendix is basically a compilation of digital data that correspond to the plotted data in Chap. 7 and is arranged in essentially the same order. Tables C.1—C.9 pertain to TSE-5 and TSE-6, while Tables C.10—C.13 pertain to TSE-5A. As mentioned in Chaps. 5 and 7, the test cylinders for the three experiments and their prolongations, which were used for characterizing the material, were from the same heat of SA 508 (class-2 chemistry) material. The TSE-5 and TSE-6 test cylinders (TSC-1 and TSC-3) were tempered at the same temperature (613°C), while TSC-2 was tempered at a higher temperature (679°C).

Table C.1. Tensile properties for TSP-1 tempered for 4 h and air cooled

Test temperature (°C)	Strength properties (MPa)		Total[a] elongation (%)	Reduction of area (%)
	Lower yield	Ultimate tensile		
		704°C temper		
−196	958	1037	18.4	24
−18	528	686	24.6	65
66	487	623	21.7	65
149	463	610	20.3	64
22	502	673	23.6	68
−101	613	782	27.5	62
107	476	612	21.4	67
− 59	553	715	25.1	66
−146	733	860	27.2	56
		677°C temper		
−18	627	766	21.0	62
66	592	722	19.5	61
149	557	695	18.1	64
23	603	741	18.5	60
−101	724	864	20.4	53
107	579	705	17.4	62
−59	653	801	22.4	61
−146	880	953	19.2	49
		649°C temper		
−123	803	934	23.7	55
−18	655	808	18.3	55
66	619	759	15.4	53
149	614[b]	743	18.1	60
22	632	783	16.6	54
−101	761	898	20.8	54
107	621[b]	741	18.1	62
−59	708	851	21.7	54
−146	855	972	20.5	46
		593°C temper		
−123	853[b]	1010	21.0	44
−18	719[b]	877	18.6	56
66	688[b]	831	17.4	53
149	653[b]	796	14.6	54
22	699[b]	850	17.7	52
−101	804[b]	961	17.3	47
107	666[b]	808	16.2	51
−59	743[b]	909	18.8	52
−146	925[b]	1050	18.8	35

[a]Gage length/gage diameter ratio (L/D) = 4 (calculated from L/D = 7 data).

[b]0.2% offset yield.

Table C.2. Tensile properties[a] for TSP-1 tempered at 613°C for 4 h and air cooled

Depth location[b]	Temperature (°C)	Strength (MPa)		Ductility (%)		
		Yield[c]	Ultimate	Total elongation[d]		Reduction of area
				L/D = 7	L/D = 4	
0.04	−18	734	881	13.9	19.2	55.1
0.04	38	711	842	12.7	17.6	55.9
0.04	93	678	816	12.5	17.2	55.0
0.21	−46	751	892	13.7	18.5	49.6
0.21	−18	727	869	13.7	18.8	55.4
0.21	10	710	850	13.0	17.4	54.8
0.21	38	696	828	13.0	18.1	54.9
0.21	93	666	799	11.7	16.2	55.2
0.21	177	647	789	12.5	17.3	54.4
0.21	288	660	803	12.5	17.6	54.2
0.50	−18	730	869	15.3	21.0	56.3
0.50	38	695	828	12.8	17.9	57.1
0.50	93	664	799	13.9	19.3	58.4
0.75	−18	719	864	14.6	20.2	59.2
0.75	38	687	820	13.4	18.7	57.7
0.75	93	662	793	13.2	18.6	59.9
0.96	−18	734	875	14.2	19.5	57.1
0.96	38	704	835	13.2	18.3	57.6
0.96	93	683	816	11.8	16.2	53.5

[a]Average of two specimens, both C oriented.

[b]Fraction of the 152-mm wall (inner surface = 0).

[c]0.2% offset; strain rate = 0.016/min.

[d]Gage length/gage diameter ratio (L/D) = 4 (calculated from L/D = 7 data).

Table C.3. Tensile properties[a] for TSC-1 tempered at 613°C for 4 h and air cooled

Depth location[b]	Temperature (°C)	Strength (MPa)		Ductility (%)		
		Yield[c]	Ultimate	Total elongation[d]		Reduction of area
				L/D = 7	L/D = 4	
0.04	−18	716	851	13.4	18.3	56.0
0.04	38	696	826	14.6	20.1	59.8
0.04	93	672	801	11.7	16.0	56.2
0.21	−46	731	869	13.6	19.4	55.8
0.21	−18	707	843	14.3	19.6	54.8
0.21	10	695	825	12.8	17.0	53.1
0.21	38	680	807	12.7	17.4	56.3
0.21	93	656	780	12.4	16.8	55.6
0.21	177	630	766	12.2	17.0	57.2
0.21	288	638	779	12.2	16.9	56.8
0.50	−18	702	839	13.4	19.8	53.4
0.50	38	677	802	12.8	17.6	57.0
0.50	93	655	776	11.5	15.9	55.4
0.75	−18	706	836	13.7	18.5	54.4
0.75	38	666	794	12.8	17.4	57.8
0.75	93	652	775	12.0	16.5	55.2
0.96	−18	714	849	14.1	19.2	56.0
0.96	38	685	808	12.2	16.8	55.8
0.96	93	662	783	11.6	15.8	54.8

[a]Average of two specimens, both C oriented.

[b]Fraction of the 152-mm wall (inner surface = 0).

[c]0.2% offset; strain rate = 0.016/min.

[d]Gage length/gage diameter ratio (L/D) = 4 (calculated from L/D = 7 data).

Table C.4. Static fracture toughness (K_J) from 1T compact specimens of TSP-1 tempered for 4 h and air cooled

Tempering temperature (°C)	Test temperature (°C)	K_J[a] (MPa•$\sqrt{m}$)
595	−46	37
	−18	81
	−18	81
	10	101
600	−46	38
	−46	38
	−46	80
	−18	97
	−18	64
	−18	99
	−18	62
	10	88
	10	66
	10	102
	10	67
	10	153
	38	200
	38	181
	38	96
	38	208
650	−46	110
	−18	115
	−18	110
	10	159

[a]K_J values calculated from J-integral at maximum load ($K_J^2 = EJ$).

Table C.5. Crack-arrest toughness data (K_{Ia}) for TSP-1 and TSP-3 tempered at 613°C for 4 h and air cooled

Test-cylinder prolongation	Test temperature (°C)	K_{Ia} (MPa•$\sqrt{m}$)
TSP-1[a]	28	59
	82	86
	84	73
	27	69
	81	105
TSP-3[b]	11	71
	9	62
	39	74
	66	68
	66	87
	78	69
	79	70
	79	72

[a]Ref. 1.

[b]Ref. 2.

Table C.6. Static fracture toughness (K_J) data from 1T and 2T compact specimens of TSP-1 tempered at 613°C for 4 h and air cooled

1T compact specimens		2T compact specimens	
Test temperature (°C)	K_J[a,b] (MPa•√m)	Test temperature (°C)	K_J[a,b] (MPa•√m)
−18	102	−18	105
	145		92
	111		51
	82		111
			80
32	114	32	221
	186		115
	153		105
	188		172
	164		
	202		
	70		
82	204	82	135
	128		255
	236		197
	200		161
	249		273
	240		277
	211		298
			284
		135	278
			274

[a]Depth location (d/w) = 0.33, w = 152 mm.

[b]K_J calculated from J-integral at maximum load (K_J^2 = EJ).

Table C.7. Static fracture toughness (K_J) data from 1T compact specimens of TSP-3 tempered at 613°C for 4 h and air cooled

Test temperature (°C)	Depth location[a] (d/w)	K_J[b] (MPa•$\sqrt{m}$)
10	0.63	135
		129
		110
		197
		87
		200
		169
		125
		177
		113
		201
		135
		128
		72
		175
−46	0.17	54
		57
		46
		64
		81
		72
		120
		93
		70
		100
−73	0.17	52
		42
		57
		61
		72
		40
		60
		38
		52
		59

[a] W = 152 mm.

[b] K_J calculated from J-integral at maximum load (K_J^2 = EJ).

Table C.8. Static fracture toughness (K_J) data from 1T compact specimens of TSC-3 tempered at 613°C for 4 h and air cooled

Test temperature (°C)	K_J[a,b] (MPa•$\sqrt{m}$)
−32	87
	104
	95
	138
	144
	49
	99
	80
	97
66	275
	164
	249
	270
	265
	263
	233
	264
	247

[a]Depth location (d/w) = 0.41, w = 76 mm.

[b]K_J calculated from J-integral at maximum load (K_J^2 = EJ).

Table C.9. Static fracture toughness (K_J) from 0.394T compact specimens of TSP-1 tempered at 613°C for 4 h and air cooled

Test temperature (°C)	Depth location[a] (d/w)	K_J[b] (MPa•$\sqrt{m}$)
−73	0.33	62
		100
		74
−46	0.33	53
		101
		41
−18	0.06	95
		57
		71
		106
	0.17	125
		65
		101
		123
		103
	0.33	184
		142
		124
		86
		134
	0.50	153
		159
		188
		150
		165
	0.67	86
		72
		135
		57
	0.83	167
		133
		176
		88
		161
10	0.33	125
		168
		205
		103
		214
		158
38	0.33	224
		149
		202
		197
		114
		183

[a] a_w = 152 mm.

[b] K_J calculated from J-integral at maximum load (K_J^2 = EJ).

Table C.10. Static fracture toughness (K_J) from 1T compact specimens of TSP-2 tempered at 677°C for 4 h and air cooled

Test temperature (°C)	Depth location[a] (d/w)	K_J[b] (MPa•$\sqrt{m}$)
−32	0.63	138
	0.17	91
		106
		121
		116
		99
		131
		135
		72
−4	0.17	112
	0.63	240
		224
		200
	0.17	249[c]
	0.17	180[c]
	0.63	275[c]
	0.63	210[c]
	0.36	240[c]
	0.17	143[c]
24	0.17	287
		233
		259
		268
		158
	0.63	222
		249
		279
		251
		296
		261[d]
		195[d]
		277[d]
		288[d]
		265[d]
		254[d]
38	0.63	276
	0.63	260
	0.17	277
	0.17	275
	0.17	220
	0.63	281
52	0.17	273
		279
		289
		289
		279
		334
	0.63	297
		310
		285
		322

[a] w = 152 mm.

[b] K_J calculated from J-integral at maximum load (K_J^2 = EJ).

[c] BCL 20% side grooved.[3]

[d] USNSRDC spring loaded.[4]

Table C.11. Static fracture toughness (K_J) from 1T compact specimens of TSP-2 tempered at 707°C for 4 h and air cooled

Test temperature (°C)	Depth location[a] (d/w)	K_J[b] (MPA•$\sqrt{m}$)
−73	0.63	126
−46	0.17	147
		137
		153
		88
		130
		134
	0.63	159
	0.63	162
	0.17	150
	0.63	149
	0.63	149
−4	0.63	295
	0.63	315
	0.17	211
	0.63	173
	0.63	211
	0.17	134
		230
		261
		234
	0.63	345
	0.17	150
38	0.63	293
		351
		234
	0.17	318
	0.63	328
		310
		364
	0.17	326
		332
		380
66	0.63	348
	0.63	308

[a] w = 152 mm.

[b] K_J calculated from J-integral at maximum load (K_J^2 = EJ).

Table C.12. Static crack-arrest toughness (K_{Ia}) from wedge-loaded compact specimens of TSP-2 tempered at 677°C for 4 h and air cooled[a,b]

Test temperature (°C)	K_{Ia} (MPa•$\sqrt{m}$)
0	82[c]
0	73[c]
22	80[c]
22	63[d]
27	65[d]
28	118[c]
28	97[c]
40	81[d]
42	81[d]
42	70[d]
51	134[c]
51	88[d]
53	94[d]
53	87[d]
53	95[d]
54	95[d]

[a]Ref. 3.

[b]Ref. 4.

[c]25 × 151 × 151-mm wedge-loaded compact specimens.

[d]25 × 102 × 151-mm wedge-loaded compact specimens.

Table C.13. Static fracture toughness (K_J) from 1T compact specimens of TSC-2 tempered at 679°C for 4 h and air cooled

Test temperature (°C)	K_J[a,b] (MPa•$\sqrt{m}$)
−32	79
	165
	161
	182
	74
	121
	94
	119
	160
	163
	100
−4	245
	106
	186
	229
	177
	112
	243
	149
	206
	261
	140
24	292
	235
	238
	262
	323
	338
	198
	334
	289
	247

[a]Depth location (d/w) = 0.23, w = 152 mm.

[b]K_J calculated from J-integral at maximum load (K_J^2 = EJ).

References

1. A. R. Rosenfield et al., *Critical Experiments, Measurements, and Analyses to Establish a Crack-Arrest Methodology for Nuclear-Pressure-Vessel Steels*, Progress Report for June—December 1979, NUREG/CR-1555 (BMI-2064), R5, June 1980.

2. A. R. Rosenfield et al., "BCL HSST Support Program," pp. 8—35 in *Heavy-Section Steel Technology Program Quart. Prog. Rep. January—March 1982*, NUREG/CR-2751, Vol. 1 (ORNL/TM-8369/V1), Union Carbide Corp. Nuclear Div., Oak Ridge Natl. Lab.

3. A. R. Rosenfield et al., *Critical Experiments, Measurements and Analyses to Establish a Crack-Arrest Methodology for Nuclear Pressure Vessel Steels*, NUREG/CR-1887 (BMI-2071), Appendix B, January 1981.

4. A. R. Rosenfield et al., "BCL HSST Support Program," pp. 7—39 in *Heavy-Section Steel Technology Program Quart. Prog. Rep. July—September 1982*, NUREG/CR-2751, Vol. 3 (ORNL/TM-8369/V3), Union Carbide Corp. Nuclear Div., Oak Ridge Natl. Lab.

Appendix D

DIGITAL OUTPUT FROM POSTTEST FRACTURE-MECHANICS ANALYSIS OF TSE-5

A standard set of OCA-P digital input-output for a posttest deterministic analysis of TSE-5, using fracture-toughness curves deduced from TSE-5, is included in this appendix. Values of K_I are for a two-dimensional axial flaw, and the English system of units is used throughout.

```
      TSE-5  13.5/19.5 IN. RAD. LN2(-320) TO = 205 DEG. F 8/1/79       OCA-P

 FRACTURE TOUGHNESS CODE (IF KICTYP = 6 , VALUES
 ARE READ IN & DESCRIBED LATER IN THIS RUN)    KICTYP =      6

 MAX. # OF TIME INTERVALS TO BE READ           NCYCLE =     60

 TIME INTERVAL # TO START PROCESSING DATA       ISKIP ◘      1

 CRACK SHAPE TO BE USED                        ICRKTP =      1
   =1 2-D;   =2 2-D,2-M;   =3 6-1,2-M;
   =4 6/1,2-D,&2-M;   =5 6/1,2-D

 REF TEMPERATURE FOR STRESS CALCULATIONS         TREF =   205.
   = 0 USE TEMP IN FIRST TIME INTERVAL

 WRITE TABLE-1 FOR TEMPS,KIC,ETC.THRU CYL. WALL
   = -1 THEN STOP;     =  0 NO PRINTING;
   = +1 CONTINUE PROCESSING KI VALUES            NOPT =      0

 UNITS SWITCH     =0 ENGLISH; =1 SI             ISISW =      0


TEMPERATURE PLOTTING
     ◘ 0 NO PLOTS,      = 1 PLOT       NPLOT ◘     0
KI RATIO PLOTTING
     = 0 NO PLOTS,      = 1 PLOT      KRPLOT =     0
KI PLOTTING
      = 0 NO PLOTS,     = 1 PLOT       KIPLT =     0
ENVELOPE PLOTTING
      = 0 NO PLOTS,     = 1 PLOT      KENPLT =     1
STRESS/TEMP/KI/KIC/KIA PLOTTING
      = 0 NO PLOTS,     = 1 PLOT      KALPLT =     0


TIME DEPENDENT PRESSURES                   NPR   =     0

   SEQ.NO.      TIME      PRESSURE
             (MINUTES)    (KSI)

.......................................
```

RADIATION DAMAGE/RUN CONTROL

RADIATION DAMAGE CALC SWITCH	IRTNSW	=	0
ATTENUATION CONSTANT	ATTCON	=	0.2400
STRESS INPUT SWITCH 0=CALC BY FE METHOD, 1=INPUT ON UNIT3 0=DEEPEST POINT, 1=MAX ON CRACK FRONT	ISTRSW	=	0

INCIPIENT INITIATION SEARCH CONTROL

INCIPIENT INITIATION SEARCH SWITCH 0=NO SEARCH, 1=SEARCH, 2=PARAMETRIC SEARCH	IBINSW	=	0
FLAW SHAPE CONTROL SWITCH 0=LONG(2-D), 1=(6 TO 1) ELLIPITICAL	ISEASW	=	0
MIN A/W USED ON THRESHOLD SEARCH	AWMIN	=	0.0249
MAX A/W USED ON THRESHOLD SEARCH	AWMAX	=	0.1510
UPPER LIMIT ON THRESHOLD SEARCH	TUPLIM	=	0.50D+20

TOUGHNESS PROPERTIES(-1 MEANS NOT INPUT)

FLUENCE, INSIDE SURFACE	F0	=	0.000E+00
REFERENCE TEMP., INITIAL	RTNDT0	=	0.000
PER CENT CU	CUPER	=	0.000
PER CENT P	PPER	=	0.000
PER CENT NI	PERNI	=	0.000
DELTA RTNDT(INNER SURFACE)	DRTNIN	=	-999.0

FINITE ELEMENT PARAMETERS (STRESS CALCULATIONS)

GEOMETRIC MODELING METHOD
= 0 USER SPECIFIED NO. OF ELEMENTS + G.P FACTOR.
= 1 USER SPEC. NO. OF ELEM.& A/W OF CLADDING-
BASE METAL INTERFACE MODEL = 0

NUMBER OF ELEMENTS---------- NUMEL = 15

INTEGRATION ORDER(# GAUSS POINTS) NGAUSS = 2

NUMBER OF NODAL POINTS---------- NUMNP = 31

GEOM.PROG.FACTOR = 1.13

FE MESH NODAL POINT COORDINATES

NODAL POINT NO.	R-COORD. (INCHES)	NODAL POINT NO.	R-COORD. (INCHES)
1	13.500	16	14.327
2	13.520	17	14.455
3	13.544	18	14.600
4	13.570	19	14.763
5	13.599	20	14.948
6	13.633	21	15.156
7	13.670	22	15.392
8	13.713	23	15.659
9	13.761	24	15.960
10	13.815	25	16.300
11	13.877	26	16.685
12	13.946	27	17.119
13	14.025	28	17.610
14	14.114	29	18.165
15	14.214	30	18.792
		31	19.500

ELEMENT CONNECTIVITY

ELEM. NO.	NODE NUMBERS I	J	K	MATERIAL NO.
1	1	2	3	1
2	3	4	5	1
3	5	6	7	1
4	7	8	9	1
5	9	10	11	1
6	11	12	13	1
7	13	14	15	1
8	15	16	17	1
9	17	18	19	1
10	19	20	21	1
11	21	22	23	1
12	23	24	25	1
13	25	26	27	1
14	27	28	29	1
15	29	30	31	1

MATERIAL PROPERTIES FOR STRESS CALCULATIONS

NUMBER OF MATERIALS ------ 1

TEMP(DEG.F)	MODULUS OF ELASTICITY(KSI) - E		
	(MAT 1)	(MAT 2)	(MAT 3)
70.0	2.800D+04	2.700D+04	0.000D+00

TEMP(DEG.F)	COEFF OF EXPANSION(PER DEG.F) - ALFA		
	(MAT 1)	(MAT 2)	(MAT 3)
70.0	6.500D-06	9.930D-06	0.000D+00

TEMP(DEG.F)	POISSONS RATIO - PNU		
	(MAT 1)	(MAT 2)	(MAT 3)
70.0	0.300	0.300	0.300

SELECTED TIME INTERVAL NUMBERS FOR KI CALCULATIONS

0	0	0	0	0	0	0	0	0	0
0	0	0	0	0	0	0	0	0	0
0	0	0	0	0	0	0	0	0	0
0	0	0	0	0	0	0	0	0	0
0	0	0	0	0	0	0	0	0	0
0	0	0	0	0	0	0	0	0	0
0									

CYLINDER DIMENSIONS (INCHES)

INNER RADIUS, RI = 13.500

OUTER RADIUS, RO = 19.500

WALL THICKNESS, W = 6.000

TEMPERATURE GRID GEOMETRY OVER CYLINDER WALL

GRID NO.	RADIUS
1	13.5000
2	13.7500
3	14.0000
4	14.2500
5	14.5000
6	14.7500
7	15.0000
8	15.2500
9	15.5000
10	16.0000
11	16.5000
12	17.5000
13	18.5000
14	19.5000

*** KIC (OR KIA) VALUES WERE READ IN FROM UNIT 56

MATERIAL IDENTIFICATION =TOUGHNESS PER 3/26/85 PHONE CALL WITH RDC

SEQ.NO.	TEMP.	KIC VALUE
1	-300.	27.
2	-250.	28.
3	-200.	31.
4	-150.	38.
5	-100.	48.
6	300.	130.

SEQ.NO.	TEMP.	KIA VALUE
1	-200.	27.
2	-150.	28.
3	-100.	31.
4	-50.	38.
5	0.	48.
6	400.	130.

CALCULATED 2-D CRACK DEPTH VALUES =
0.0000 0.1588 0.3353 0.4585 0.6088 0.9000 1.2088 1.5000 1.8071 2.4088
3.0000 3.6071 4.2441 4.8071 5.1000 5.4000

REF TEMPERATURE FOR STRESS CALCULATIONS TREF = 205.0 DEG.F

TSE-5 13.5/19.5 IN. RAD. LN2(-320) TO = 205 DEG. F 8/1/79 LONGIT. CRACK

KICTYP = 6, RTNDTO = 0.0 DEG., %CU = 0.000, FO =0.00E19

TEMPERATURE INTERVAL NUMBER = 1, TIME = 0.500 MIN., PRESSURE = 0.000 KSI

SEQ NO.	RADIUS IN.	DEPTH IN.	A/W	TEMPER. DEG.F	DLRTNDT DEG.F	CIRCUMF. STRESS KSI	KI	KIC	KI/KIC	KIA	KI/KIA	ELLIPTIC ANGLE
1	13.500	0.000	0.000	51.0	0.	36.65	0.00	79.37	0.000	58.68	0.000	
2	13.659	0.159	0.026	79.5	0.	28.86	23.28	85.21	0.273	64.61	0.360	
3	13.835	0.335	0.056	108.6	0.	20.99	29.56	91.16	0.324	70.63	0.418	
4	13.958	0.458	0.076	126.4	0.	16.18	31.65	94.81	0.334	74.32	0.426	
5	14.109	0.609	0.101	145.4	0.	11.12	31.91	98.67	0.323	78.22	0.408	
6	14.400	0.900	0.150	171.8	0.	4.12	30.04	104.04	0.289	83.65	0.359	
7	14.709	1.209	0.201	187.6	0.	0.00	27.43	107.25	0.256	86.88	0.316	
8	15.000	1.500	0.250	195.0	0.	-1.90	25.92	108.74	0.238	88.39	0.293	
9	15.307	1.807	0.301	200.5	0.	-3.25	23.65	109.87	0.215	89.52	0.264	
10	15.909	2.409	0.401	202.5	0.	-3.60	22.30	110.27	0.202	89.93	0.248	
11	16.500	3.000	0.500	205.0	0.	-4.07	21.68	110.77	0.196	90.43	0.240	
12	17.107	3.607	0.601	205.3	0.	-3.98	20.67	110.84	0.186	90.50	0.228	
13	17.744	4.244	0.707	204.9	0.	-3.72	19.29	110.75	0.174	90.41	0.213	
14	18.307	4.807	0.801	205.0	0.	-3.61	16.80	110.76	0.152	90.42	0.186	
15	18.600	5.100	0.850	205.0	0.	-3.56	14.56	110.77	0.131	90.44	0.161	
16	18.900	5.400	0.900	205.0	0.	-3.51	10.92	110.78	0.099	90.44	0.121	

TEMPERATURE INTERVAL NUMBER = 2, TIME = 1.000 MIN., PRESSURE = 0.000 KSI

SEQ NO.	RADIUS IN.	DEPTH IN.	A/W	TEMPER. DEG.F	DLRTNDT DEG.F	CIRCUMF. STRESS KSI	KI	KIC	KI/KIC	KIA	KI/KIA	ELLIPTIC ANGLE
1	13.500	0.000	0.000	-17.0	0.	50.68	0.00	65.34	0.000	44.44	0.000	
2	13.659	0.159	0.026	9.5	0.	43.24	33.65	70.82	0.475	50.00	0.673	
3	13.835	0.335	0.056	39.8	0.	34.87	45.01	77.07	0.584	56.35	0.799	
4	13.958	0.458	0.076	61.6	0.	28.93	49.95	81.55	0.612	60.89	0.820	
5	14.109	0.609	0.101	88.1	0.	21.79	52.12	86.98	0.599	66.40	0.785	
6	14.400	0.900	0.150	127.3	0.	11.31	51.96	94.98	0.547	74.49	0.697	
7	14.709	1.209	0.201	156.0	0.	3.73	49.83	100.82	0.494	80.40	0.620	
8	15.000	1.500	0.250	171.0	0.	-0.20	48.47	103.87	0.467	83.48	0.581	
9	15.307	1.807	0.301	183.1	0.	-3.24	45.46	106.33	0.428	85.95	0.529	
10	15.909	2.409	0.401	195.2	0.	-6.13	42.52	108.78	0.391	88.43	0.481	
11	16.500	3.000	0.500	200.0	0.	-7.07	41.62	109.76	0.379	89.41	0.466	
12	17.107	3.607	0.601	202.3	0.	-7.36	39.83	110.22	0.361	89.88	0.443	
13	17.744	4.244	0.707	203.5	0.	-7.38	36.96	110.47	0.335	90.13	0.410	
14	18.307	4.807	0.801	204.7	0.	-7.44	32.09	110.71	0.290	90.37	0.355	
15	18.600	5.100	0.850	205.1	0.	-7.41	27.79	110.79	0.251	90.45	0.307	
16	18.900	5.400	0.900	205.2	0.	-7.32	20.92	110.82	0.189	90.48	0.231	

TSE-5 13.5/19.5 IN. RAD. LN2(-320) TO = 205 DEG. F 8/1/79 LONGIT. CRACK

KICTYP = 6, RTNDTO = 0.0 DEG., %CU = 0.000, FO =0.00E19

TEMPERATURE INTERVAL NUMBER = 3, TIME = 1.500 MIN., PRESSURE = 0.000 KSI

SEQ NO.	RADIUS IN.	DEPTH IN.	A/W	TEMPER. DEG.F	DLRTNDT DEG.F	CIRCUMF. STRESS KSI	KI	KIC	KI/KIC	KIA	KI/KIA	ELLIPTIC ANGLE
1	13.500	0.000	0.000	-69.0	0.	61.32	0.00	54.51	0.000	34.87	0.000	
2	13.659	0.159	0.026	-38.4	0.	52.71	40.87	60.88	0.671	40.14	1.018	
3	13.835	0.335	0.056	-4.8	0.	43.37	55.11	67.86	0.812	46.98	1.173	
4	13.958	0.458	0.076	17.7	0.	37.16	61.81	72.52	0.852	51.73	1.195	
5	14.109	0.609	0.101	43.1	0.	30.23	65.85	77.74	0.847	57.03	1.155	
6	14.400	0.900	0.150	87.0	0.	18.37	68.67	86.74	0.792	66.16	1.038	
7	14.709	1.209	0.201	122.1	0.	9.01	68.12	93.91	0.725	73.41	0.928	
8	15.000	1.500	0.250	148.0	0.	2.25	67.61	99.20	0.682	78.76	0.858	
9	15.307	1.807	0.301	164.8	0.	-2.10	64.13	102.62	0.625	82.21	0.780	
10	15.909	2.409	0.401	187.7	0.	-7.76	60.67	107.26	0.566	86.89	0.698	
11	16.500	3.000	0.500	200.0	0.	-10.53	58.36	109.76	0.532	89.41	0.653	
12	17.107	3.607	0.601	203.2	0.	-10.91	55.04	110.41	0.498	90.07	0.611	
13	17.744	4.244	0.707	203.2	0.	-10.50	50.98	110.41	0.462	90.07	0.566	
14	18.307	4.807	0.801	204.6	0.	-10.48	44.36	110.69	0.401	90.35	0.491	
15	18.600	5.100	0.850	205.1	0.	-10.45	38.42	110.80	0.347	90.46	0.425	
16	18.900	5.400	0.900	205.3	0.	-10.32	28.96	110.84	0.261	90.50	0.320	

TEMPERATURE INTERVAL NUMBER = 4, TIME = 1.767 MIN., PRESSURE = 0.000 KSI

1	13.500	0.000	0.000	-90.0	0.	64.09	0.00	50.10	0.000	32.07	0.000	
2	13.659	0.159	0.026	-61.6	0.	56.00	43.11	56.06	0.769	36.04	1.196	
3	13.835	0.335	0.056	-29.4	0.	46.99	58.74	62.77	0.936	41.91	1.401	
4	13.958	0.458	0.076	-7.7	0.	40.98	66.42	67.26	0.988	46.37	1.432	
5	14.109	0.609	0.101	15.1	0.	34.66	71.65	71.98	0.995	51.17	1.400	
6	14.400	0.900	0.150	57.6	0.	23.06	76.86	80.74	0.952	60.07	1.279	
7	14.709	1.209	0.201	96.0	0.	12.78	77.81	88.58	0.878	68.02	1.144	
8	15.000	1.500	0.250	122.0	0.	5.90	79.03	93.90	0.842	73.40	1.077	
9	15.307	1.807	0.301	143.8	0.	0.21	76.27	98.35	0.776	77.90	0.979	
10	15.909	2.409	0.401	174.8	0.	-7.56	73.28	104.64	0.700	84.25	0.870	
11	16.500	3.000	0.500	192.0	0.	-11.58	71.06	108.13	0.657	87.78	0.810	
12	17.107	3.607	0.601	200.0	0.	-13.15	66.86	109.77	0.609	89.42	0.748	
13	17.744	4.244	0.707	202.7	0.	-13.31	61.22	110.31	0.555	89.97	0.681	
14	18.307	4.807	0.801	203.8	0.	-13.12	53.10	110.52	0.480	90.18	0.589	
15	18.600	5.100	0.850	204.1	0.	-13.00	46.05	110.59	0.416	90.25	0.510	
16	18.900	5.400	0.900	204.4	0.	-12.87	34.81	110.65	0.315	90.32	0.385	

TSE-5 13.5/19.5 IN. RAD. LN2(-320) TO = 205 DEG. F 8/1/79 LONGIT. CRACK

KICTYP = 6, RTNDTO = 0.0 DEG., %CU = 0.000, FO =0.00E19

TEMPERATURE INTERVAL NUMBER = 5, TIME = 2.000 MIN., PRESSURE = 0.000 KSI

SEQ NO.	RADIUS IN.	DEPTH IN.	A/W	TEMPER. DEG.F	DLRTNDT DEG.F	CIRCUMF. STRESS KSI	KI	KIC	KI/KIC	KIA	KI/KIA	ELLIPTIC ANGLE
1	13.500	0.000	0.000	-105.0	0.	66.07	0.00	46.95	0.000	30.54	0.000	
2	13.659	0.159	0.026	-76.7	0.	58.00	44.55	52.88	0.842	33.75	1.320	
3	13.835	0.335	0.056	-46.8	0.	49.53	61.11	59.15	1.033	38.58	1.584	
4	13.958	0.458	0.076	-26.7	0.	43.92	69.63	63.32	1.100	42.44	1.640	
5	14.109	0.609	0.101	-2.3	0.	37.15	75.50	68.39	1.104	47.52	1.589	
6	14.400	0.900	0.150	41.6	0.	25.16	81.27	77.44	1.049	56.72	1.433	
7	14.709	1.209	0.201	80.6	0.	14.68	83.19	85.44	0.974	64.83	1.283	
8	15.000	1.500	0.250	108.0	0.	7.37	85.01	91.04	0.934	70.51	1.206	
9	15.307	1.807	0.301	133.3	0.	0.80	82.25	96.20	0.855	75.73	1.086	
10	15.909	2.409	0.401	166.6	0.	-7.59	79.43	102.99	0.771	82.58	0.962	
11	16.500	3.000	0.500	182.0	0.	-11.14	78.12	106.11	0.736	85.73	0.911	
12	17.107	3.607	0.601	193.5	0.	-13.59	74.43	108.43	0.686	88.08	0.845	
13	17.744	4.244	0.707	201.0	0.	-14.95	67.77	109.96	0.616	89.62	0.756	
14	18.307	4.807	0.801	202.8	0.	-14.91	58.50	110.32	0.530	89.98	0.650	
15	18.600	5.100	0.850	203.1	0.	-14.76	50.73	110.39	0.460	90.05	0.563	
16	18.900	5.400	0.900	203.7	0.	-14.66	38.39	110.50	0.347	90.16	0.426	

TEMPERATURE INTERVAL NUMBER = 6, TIME = 2.500 MIN., PRESSURE = 0.000 KSI

SEQ NO.	RADIUS IN.	DEPTH IN.	A/W	TEMPER. DEG.F	DLRTNDT DEG.F	CIRCUMF. STRESS KSI	KI	KIC	KI/KIC	KIA	KI/KIA	ELLIPTIC ANGLE
1	13.500	0.000	0.000	-137.0	0.	71.77	0.00	40.42	0.000	28.49	0.000	
2	13.659	0.159	0.026	-110.5	0.	64.08	48.87	45.79	1.067	30.08	1.625	
3	13.835	0.335	0.056	-80.2	0.	55.47	67.64	52.15	1.297	33.28	2.032	
4	13.958	0.458	0.076	-59.0	0.	49.49	77.42	56.60	1.368	36.45	2.124	
5	14.109	0.609	0.101	-34.3	0.	42.59	84.45	61.75	1.368	40.95	2.062	
6	14.400	0.900	0.150	11.2	0.	30.08	92.25	71.18	1.296	50.36	1.832	
7	14.709	1.209	0.201	53.9	0.	18.55	95.57	79.97	1.195	59.29	1.612	
8	15.000	1.500	0.250	88.0	0.	9.48	98.20	86.96	1.129	66.37	1.479	
9	15.307	1.807	0.301	117.8	0.	1.69	95.13	93.05	1.022	72.54	1.311	
10	15.909	2.409	0.401	155.6	0.	-7.85	92.69	100.73	0.920	80.31	1.154	
11	16.500	3.000	0.500	180.0	0.	-13.67	90.49	105.70	0.856	85.32	1.061	
12	17.107	3.607	0.601	193.1	0.	-16.42	85.15	108.35	0.786	88.00	0.968	
13	17.744	4.244	0.707	198.5	0.	-17.15	77.71	109.46	0.710	89.11	0.872	
14	18.307	4.807	0.801	200.6	0.	-17.10	67.25	109.87	0.612	89.52	0.751	
15	18.600	5.100	0.850	201.2	0.	-16.99	58.32	110.00	0.530	89.66	0.650	
16	18.900	5.400	0.900	201.8	0.	-16.87	44.13	110.13	0.401	89.79	0.492	

TSE-5 13.5/19.5 IN. RAD. LN2(-320) TO = 205 DEG. F 8/1/79 LONGIT. CRACK

KICTYP = 6, RTNDTO = 0.0 DEG., %CU = 0.000, FO =0.00E19

TEMPERATURE INTERVAL NUMBER = 7, TIME = 2.967 MIN., PRESSURE = 0.000 KSI

SEQ NO.	RADIUS IN.	DEPTH IN.	A/W	TEMPER. DEG.F	DLRTNDT DEG.F	CIRCUMF. STRESS KSI	KI	KIC	KI/KIC	KIA	KI/KIA	ELLIPTIC ANGLE
1	13.500	0.000	0.000	-162.0	0.	74.40	0.00	35.96	0.000	27.66	0.000	
2	13.659	0.159	0.026	-135.2	0.	66.61	50.75	40.77	1.245	28.57	1.777	
3	13.835	0.335	0.056	-103.1	0.	57.48	70.23	47.35	1.483	30.71	2.287	
4	13.958	0.458	0.076	-80.2	0.	51.08	80.25	52.15	1.539	33.28	2.411	
5	14.109	0.609	0.101	-55.7	0.	44.20	87.52	57.29	1.528	37.01	2.365	
6	14.400	0.900	0.150	-13.1	0.	32.41	96.38	66.15	1.457	45.25	2.130	
7	14.709	1.209	0.201	27.2	0.	21.43	101.14	74.48	1.358	53.72	1.883	
8	15.000	1.500	0.250	59.0	0.	12.91	105.59	81.02	1.303	60.35	1.750	
9	15.307	1.807	0.301	87.9	0.	5.30	104.24	86.94	1.199	66.36	1.571	
10	15.909	2.409	0.401	129.7	0.	-5.41	104.49	95.48	1.094	75.00	1.393	
11	16.500	3.000	0.500	160.0	0.	-12.80	103.90	101.64	1.022	81.22	1.279	
12	17.107	3.607	0.601	180.4	0.	-17.44	98.57	105.79	0.932	85.41	1.154	
13	17.744	4.244	0.707	193.0	0.	-19.93	89.65	108.33	0.828	87.97	1.019	
14	18.307	4.807	0.801	198.9	0.	-20.77	77.00	109.53	0.703	89.18	0.863	
15	18.600	5.100	0.850	200.4	0.	-20.81	66.55	109.84	0.606	89.50	0.744	
16	18.900	5.400	0.900	201.1	0.	-20.63	50.30	109.98	0.457	89.64	0.561	

TEMPERATURE INTERVAL NUMBER = 8, TIME = 3.433 MIN., PRESSURE = 0.000 KSI

SEQ NO.	RADIUS IN.	DEPTH IN.	A/W	TEMPER. DEG.F	DLRTNDT DEG.F	CIRCUMF. STRESS KSI	KI	KIC	KI/KIC	KIA	KI/KIA	ELLIPTIC ANGLE
1	13.500	0.000	0.000	-183.0	0.	76.91	0.00	32.92	0.000	27.25	0.000	
2	13.659	0.159	0.026	-155.5	0.	68.91	52.47	37.04	1.416	27.83	1.885	
3	13.835	0.335	0.056	-125.8	0.	60.38	72.96	42.63	1.711	29.05	2.512	
4	13.958	0.458	0.076	-105.7	0.	54.66	84.01	46.80	1.795	30.47	2.757	
5	14.109	0.609	0.101	-81.5	0.	47.85	92.34	51.88	1.780	33.11	2.789	
6	14.400	0.900	0.150	-35.4	0.	35.07	102.24	61.52	1.662	40.73	2.510	
7	14.709	1.209	0.201	9.8	0.	22.80	107.31	70.89	1.514	50.06	2.143	
8	15.000	1.500	0.250	42.0	0.	14.11	112.12	77.52	1.446	56.81	1.974	
9	15.307	1.807	0.301	72.2	0.	6.17	111.04	83.72	1.326	63.09	1.760	
10	15.909	2.409	0.401	116.3	0.	-5.14	111.88	92.73	1.206	72.22	1.549	
11	16.500	3.000	0.500	150.0	0.	-13.40	111.45	99.60	1.119	79.17	1.408	
12	17.107	3.607	0.601	171.3	0.	-18.23	106.01	103.93	1.020	83.54	1.269	
13	17.744	4.244	0.707	184.6	0.	-20.88	97.03	106.63	0.910	86.25	1.125	
14	18.307	4.807	0.801	193.0	0.	-22.32	83.63	108.33	0.772	87.97	0.951	
15	18.600	5.100	0.850	195.9	0.	-22.68	72.33	108.92	0.664	88.57	0.817	
16	18.900	5.400	0.900	197.8	0.	-22.80	54.72	109.32	0.501	88.97	0.615	

TSE-5 13.5/19.5 IN. RAD. LN2(-320) TO = 205 DEG. F 8/1/79 LONGIT. CRACK

KICTYP = 6, RTNDTO = 0.0 DEG., %CU = 0.000, FO =0.00E19

TEMPERATURE INTERVAL NUMBER = 9, TIME = 4.000 MIN., PRESSURE = 0.000 KSI

SEQ NO.	RADIUS IN.	DEPTH IN.	A/W	TEMPER. DEG.F	DLRTNDT DEG.F	CIRCUMF. STRESS KSI	KI	KIC	KI/KIC	KIA	KI/KIA	ELLIPTIC ANGLE
1	13.500	0.000	0.000	-201.0	0.	78.34	0.00	30.90	0.000	27.00	0.000	
2	13.659	0.159	0.026	-175.0	0.	70.71	53.67	34.00	1.579	27.39	1.960	
3	13.835	0.335	0.056	-145.9	0.	62.31	74.92	38.74	1.934	28.14	2.663	
4	13.958	0.458	0.076	-125.7	0.	56.55	86.44	42.65	2.026	29.05	2.975	
5	14.109	0.609	0.101	-101.8	0.	49.78	95.23	47.63	1.999	30.83	3.089	
6	14.400	0.900	0.150	-57.4	0.	37.43	106.20	56.92	1.866	36.71	2.893	
7	14.709	1.209	0.201	-15.1	0.	25.85	112.83	65.72	1.717	44.82	2.517	
8	15.000	1.500	0.250	19.0	0.	16.65	118.96	72.78	1.634	51.99	2.288	
9	15.307	1.807	0.301	50.8	0.	8.21	118.60	79.34	1.495	58.65	2.022	
10	15.909	2.409	0.401	103.6	0.	-5.37	119.33	90.14	1.324	69.60	1.715	
11	16.500	3.000	0.500	140.0	0.	-14.31	118.54	97.57	1.215	77.11	1.537	
12	17.107	3.607	0.601	162.6	0.	-19.44	112.69	102.17	1.103	81.76	1.378	
13	17.744	4.244	0.707	176.9	0.	-22.28	103.09	105.06	0.981	84.68	1.217	
14	18.307	4.807	0.801	185.8	0.	-23.81	88.89	106.87	0.832	86.50	1.028	
15	18.600	5.100	0.850	189.0	0.	-24.22	76.92	107.52	0.715	87.15	0.883	
16	18.900	5.400	0.900	191.2	0.	-24.39	58.23	107.98	0.539	87.62	0.665	

TEMPERATURE INTERVAL NUMBER = 10, TIME = 5.000 MIN., PRESSURE = 0.000 KSI

1	13.500	0.000	0.000	-223.0	0.	77.99	0.00	29.21	0.000	27.00	0.000	
2	13.659	0.159	0.026	-198.9	0.	70.86	53.63	31.11	1.724	27.02	1.985	
3	13.835	0.335	0.056	-172.0	0.	63.01	75.22	34.43	2.184	27.44	2.741	
4	13.958	0.458	0.076	-153.2	0.	57.63	87.11	37.43	2.327	27.90	3.122	
5	14.109	0.609	0.101	-130.9	0.	51.25	96.43	41.62	2.317	28.78	3.351	
6	14.400	0.900	0.150	-87.6	0.	39.14	108.38	50.61	2.141	32.35	3.350	
7	14.709	1.209	0.201	-45.1	0.	27.47	115.77	59.50	1.946	38.89	2.977	
8	15.000	1.500	0.250	-12.0	0.	18.52	122.81	66.37	1.850	45.48	2.700	
9	15.307	1.807	0.301	17.3	0.	10.69	123.64	72.44	1.707	51.64	2.394	
10	15.909	2.409	0.401	68.2	0.	-2.51	127.43	82.90	1.537	62.26	2.047	
11	16.500	3.000	0.500	109.0	0.	-12.66	128.79	91.25	1.411	70.72	1.821	
12	17.107	3.607	0.601	139.0	0.	-19.71	123.28	97.36	1.266	76.90	1.603	
13	17.744	4.244	0.707	160.3	0.	-24.33	112.54	101.69	1.107	81.28	1.385	
14	18.307	4.807	0.801	173.0	0.	-26.77	96.61	104.28	0.926	83.89	1.152	
15	18.600	5.100	0.850	177.3	0.	-27.39	83.46	105.14	0.794	84.76	0.985	
16	18.900	5.400	0.900	180.1	0.	-27.64	63.17	105.71	0.598	85.33	0.740	

TSE-5 13.5/19.5 IN. RAD. LN2(-320) TO = 205 DEG. F 8/1/79 LONGIT. CRACK

KICTYP = 6, RTNDTO = 0.0 DEG., %CU = 0.000, FO =0.00E19

TEMPERATURE INTERVAL NUMBER = 11, TIME = 7.000 MIN., PRESSURE = 0.000 KSI

SEQ NO.	RADIUS IN.	DEPTH IN.	A/W	TEMPER. DEG.F	DLRTNDT DEG.F	CIRCUMF. STRESS KSI	KI	KIC	KI/KIC	KIA	KI/KIA	ELLIPTIC ANGLE
1	13.500	0.000	0.000	-252.0	0.	75.60	0.00	27.94	0.000	27.00	0.000	
2	13.659	0.159	0.026	-232.1	0.	69.60	52.39	28.71	1.825	27.00	1.940	
3	13.835	0.335	0.056	-207.9	0.	62.46	73.97	30.29	2.442	27.00	2.740	
4	13.958	0.458	0.076	-189.9	0.	57.28	85.91	32.07	2.679	27.14	3.165	
5	14.109	0.609	0.101	-169.1	0.	51.31	95.39	34.85	2.737	27.50	3.468	
6	14.400	0.900	0.150	-132.5	0.	40.92	108.49	41.29	2.627	28.69	3.781	
7	14.709	1.209	0.201	-93.0	0.	29.99	117.61	49.46	2.378	31.72	3.707	
8	15.000	1.500	0.250	-60.0	0.	20.95	125.93	56.39	2.233	36.29	3.470	
9	15.307	1.807	0.301	-26.1	0.	11.94	127.08	63.44	2.003	42.56	2.986	
10	15.909	2.409	0.401	27.7	0.	-2.03	131.28	74.57	1.761	53.81	2.440	
11	16.500	3.000	0.500	70.0	0.	-12.59	132.79	83.27	1.595	62.64	2.120	
12	17.107	3.607	0.601	102.4	0.	-20.27	127.14	89.91	1.414	69.36	1.833	
13	17.744	4.244	0.707	125.6	0.	-25.33	115.75	94.64	1.223	74.15	1.561	
14	18.307	4.807	0.801	138.1	0.	-27.67	99.37	97.17	1.023	76.71	1.295	
15	18.600	5.100	0.850	142.3	0.	-28.29	85.94	98.04	0.877	77.59	1.108	
16	18.900	5.400	0.900	145.5	0.	-28.64	65.14	98.69	0.660	78.25	0.833	

TEMPERATURE INTERVAL NUMBER = 12, TIME = 10.000 MIN., PRESSURE = 0.000 KSI

1	13.500	0.000	0.000	-278.0	0.	68.94	0.00	27.33	0.000	27.00	0.000	
2	13.659	0.159	0.026	-258.2	0.	63.02	47.57	27.76	1.714	27.00	1.762	
3	13.835	0.335	0.056	-236.7	0.	56.69	67.08	28.50	2.354	27.00	2.484	
4	13.958	0.458	0.076	-222.0	0.	52.39	78.09	29.27	2.668	27.00	2.892	
5	14.109	0.609	0.101	-203.8	0.	47.15	86.94	30.64	2.837	27.00	3.220	
6	14.400	0.900	0.150	-170.2	0.	37.60	99.06	34.70	2.855	27.48	3.605	
7	14.709	1.209	0.201	-134.8	0.	27.78	107.65	40.85	2.635	28.59	3.766	
8	15.000	1.500	0.250	-103.0	0.	19.16	115.18	47.37	2.432	30.72	3.750	
9	15.307	1.807	0.301	-76.2	0.	11.96	116.80	53.00	2.204	33.83	3.453	
10	15.909	2.409	0.401	-27.6	0.	-0.70	121.86	63.13	1.930	42.27	2.883	
11	16.500	3.000	0.500	11.0	0.	-10.38	124.36	71.13	1.748	50.31	2.472	
12	17.107	3.607	0.601	42.0	0.	-17.80	120.03	77.53	1.548	56.82	2.113	
13	17.744	4.244	0.707	66.3	0.	-23.24	109.88	82.52	1.332	61.87	1.776	
14	18.307	4.807	0.801	81.2	0.	-26.26	94.48	85.56	1.104	64.96	1.454	
15	18.600	5.100	0.850	86.8	0.	-27.24	81.73	86.70	0.943	66.12	1.236	
16	18.900	5.400	0.900	91.2	0.	-27.92	62.01	87.61	0.708	67.04	0.925	

TSE-5 13.5/19.5 IN. RAD. LN2(-320) TO = 205 DEG. F 8/1/79 LONGIT. CRACK

KICTYP = 6, RTNDTO = 0.0 DEG., %CU = 0.000, FO =0.00E19

TEMPERATURE INTERVAL NUMBER = 13, TIME = 15.000 MIN., PRESSURE = 0.000 KSI

SEQ NO.	RADIUS IN.	DEPTH IN.	A/W	TEMPER. DEG.F	DLRTNDT DEG.F	CIRCUMF. STRESS KSI	KI	KIC	KI/KIC	KIA	KI/KIA	ELLIPTIC ANGLE
1	13.500	0.000	0.000	-295.0	0.	55.10	0.00	27.07	0.000	27.00	0.000	
2	13.659	0.159	0.026	-279.5	0.	50.46	38.06	27.31	1.394	27.00	1.410	
3	13.835	0.335	0.056	-263.4	0.	45.66	53.79	27.63	1.947	27.00	1.992	
4	13.958	0.458	0.076	-252.7	0.	42.50	62.81	27.92	2.250	27.00	2.326	
5	14.109	0.609	0.101	-239.2	0.	38.57	70.21	28.40	2.472	27.00	2.600	
6	14.400	0.900	0.150	-212.0	0.	30.85	80.37	29.96	2.683	27.00	2.977	
7	14.709	1.209	0.201	-185.4	0.	23.42	87.75	32.62	2.690	27.21	3.225	
8	15.000	1.500	0.250	-162.0	0.	17.03	94.76	35.96	2.635	27.66	3.426	
9	15.307	1.807	0.301	-141.0	0.	11.34	96.95	39.65	2.445	28.32	3.423	
10	15.909	2.409	0.401	-98.8	0.	0.29	101.89	48.26	2.111	31.12	3.274	
11	16.500	3.000	0.500	-55.0	0.	-8.22	104.21	55.34	1.883	35.49	2.937	
12	17.107	3.607	0.601	-37.3	0.	-14.87	100.47	61.12	1.644	40.36	2.489	
13	17.744	4.244	0.707	-15.6	0.	-19.77	91.61	65.62	1.396	44.72	2.048	
14	18.307	4.807	0.801	-3.0	0.	-22.34	78.46	68.24	1.150	47.37	1.656	
15	18.600	5.100	0.850	1.3	0.	-23.05	67.75	69.13	0.980	48.27	1.403	
16	18.900	5.400	0.900	4.3	0.	-23.43	51.34	69.75	0.736	48.91	1.050	

TEMPERATURE INTERVAL NUMBER = 14, TIME = 20.000 MIN., PRESSURE = 0.000 KSI

SEQ NO.	RADIUS IN.	DEPTH IN.	A/W	TEMPER. DEG.F	DLRTNDT DEG.F	CIRCUMF. STRESS KSI	KI	KIC	KI/KIC	KIA	KI/KIA	ELLIPTIC ANGLE
1	13.500	0.000	0.000	-301.0	0.	42.62	0.00	27.00	0.000	27.00	0.000	
2	13.659	0.159	0.026	-289.6	0.	39.18	29.51	27.15	1.087	27.00	1.093	
3	13.835	0.335	0.056	-276.8	0.	35.38	41.72	27.35	1.525	27.00	1.545	
4	13.958	0.458	0.076	-267.9	0.	32.78	48.64	27.53	1.767	27.00	1.801	
5	14.109	0.609	0.101	-257.6	0.	29.79	54.32	27.77	1.956	27.00	2.012	
6	14.400	0.900	0.150	-237.0	0.	23.92	62.26	28.49	2.186	27.00	2.306	
7	14.709	1.209	0.201	-217.4	0.	18.41	68.09	29.57	2.303	27.00	2.522	
8	15.000	1.500	0.250	-200.0	0.	13.63	73.86	31.00	2.382	27.00	2.735	
9	15.307	1.807	0.301	-181.7	0.	8.71	75.44	33.09	2.280	27.27	2.766	
10	15.909	2.409	0.401	-149.6	0.	0.29	79.27	38.08	2.082	28.01	2.830	
11	16.500	3.000	0.500	-122.0	0.	-6.65	80.86	43.41	1.863	29.27	2.763	
12	17.107	3.607	0.601	-101.1	0.	-11.64	77.78	47.76	1.629	30.89	2.518	
13	17.744	4.244	0.707	-85.6	0.	-15.13	71.17	51.03	1.395	32.60	2.183	
14	18.307	4.807	0.801	-75.6	0.	-17.18	61.16	53.13	1.151	33.92	1.803	
15	18.600	5.100	0.850	-71.8	0.	-17.83	52.87	53.91	0.981	34.45	1.535	
16	18.900	5.400	0.900	-69.0	0.	-18.26	40.10	54.51	0.736	34.87	1.150	

TSE-5 13.5/19.5 IN. RAD. LN2(-3 2-D CRITICAL CRACK DEPTHS
KICTYP = 6, RTNDT0 = 0.0 DEGF, %CU = 0.000, F0 = 0.00E19

TIME	INITIATION	ARREST
1.24		0.076
1.27		0.056
1.29		0.101
1.44		0.150
1.47		0.026
1.50		0.026
1.50		0.168
1.59		0.201
1.67		0.250
1.77		0.022
1.77		0.290
1.78	0.101	
1.79	0.076	
1.81		0.301
1.88	0.150	
1.92	0.056	
2.00	0.051	0.020
2.00	0.184	0.371
2.06	0.201	
2.10		0.401
2.17	0.250	
2.30		0.500
2.35	0.026	
2.43	0.301	
2.50	0.025	0.016
2.50	0.323	0.566
2.58		0.601
2.71	0.401	
2.90	0.500	
2.91		0.707
2.97	0.021	0.015
2.97	0.525	0.719
3.33	0.601	
3.43	0.019	0.014
3.43	0.620	0.775
3.80		0.801
4.00	0.017	0.014
4.00	0.691	0.810
4.15	0.707	
5.00	0.015	0.013
5.00	0.763	0.846
5.25		0.850
6.53	0.801	
7.00	0.015	0.014
7.00	0.809	0.870
10.00	0.015	0.015
10.00	0.833	0.888
13.01		0.900
15.00	0.019	0.019
15.00	0.844	
20.00	0.024	0.024
20.00	0.844	

MAX ON INITIATION CURVE: A/W = 0.844, TIME = 20.00
MAX ON ARREST CURVE: A/W = 0.900, TIME = 13.01

Appendix E

DIGITAL OUTPUT FROM POSTTEST FRACTURE-MECHANICS ANALYSIS OF TSE-5A

A standard set of OCA-P digital input-output for a posttest deterministic analysis of TSE-5A, using fracture-toughness curves deduced from TSE-5A, is included in this appendix. Values of K_I are for a two-dimensional axial flaw, and the English system of units is used throughout.

```
      TSE5A EXPERIMENT (9-24-80) ZERO TIME 18:20:17                    OCA-P

FRACTURE TOUGHNESS CODE (IF KICTYP ■ 6 , VALUES
ARE READ IN & DESCRIBED LATER IN THIS RUN)    KICTYP =      6

MAX. # OF TIME INTERVALS TO BE READ           NCYCLE =     60

TIME INTERVAL # TO START PROCESSING DATA       ISKIP =      1

CRACK SHAPE TO BE USED                        ICRKTP =      1
  =1 2-D;   =2 2-D,2-M;   =3 6-1,2-M;
  =4 6/1,2-D,%2-M;   =5 6/1,2-D

REF TEMPERATURE FOR STRESS CALCULATIONS         TREF ■   200.
  = 0 USE TEMP IN FIRST TIME INTERVAL

WRITE TABLE-1 FOR TEMPS,KIC,ETC.THRU CYL. WALL
  = -1 THEN STOP;     =  0 NO PRINTING;
  = +1 CONTINUE PROCESSING KI VALUES            NOPT =      0

UNITS SWITCH     =0 ENGLISH; =1 SI             ISISW =      0


TEMPERATURE PLOTTING
     = 0 NO PLOTS,      = 1 PLOT       NPLOT =     0
KI RATIO PLOTTING
     = 0 NO PLOTS,      ■ 1 PLOT      KRPLOT =     0
KI PLOTTING
      = 0 NO PLOTS,     = 1 PLOT       KIPLT =     0
ENVELOPE PLOTTING
      = 0 NO PLOTS,     = 1 PLOT      KENPLT =     1
STRESS/TEMP/KI/KIC/KIA PLOTTING
      = 0 NO PLOTS,     = 1 PLOT      KALPLT =     0


TIME DEPENDENT PRESSURES                   NPR   =     0

   SEQ.NO.     TIME     PRESSURE
             (MINUTES)   (KSI)

.......................................
```

RADIATION DAMAGE/RUN CONTROL

RADIATION DAMAGE CALC SWITCH	IRTNSW	=	0
ATTENUATION CONSTANT	ATTCON	=	0.2400
STRESS INPUT SWITCH 0=CALC BY FE METHOD, 1=INPUT ON UNIT3 0=DEEPEST POINT, 1=MAX ON CRACK FRONT	ISTRSW	◘	0

INCIPIENT INITIATION SEARCH CONTROL

INCIPIENT INITIATION SEARCH SWITCH 0=NO SEARCH, 1=SEARCH, 2=PARAMETRIC SEARCH	IBINSW	◘	0
FLAW SHAPE CONTROL SWITCH 0=LONG(2-D), 1=(6 TO 1) ELLIPITICAL	ISEASW	=	0
MIN A/W USED ON THRESHOLD SEARCH	AWMIN	=	0.0249
MAX A/W USED ON THRESHOLD SEARCH	AWMAX	◘	0.1510
UPPER LIMIT ON THRESHOLD SEARCH	TUPLIM	=	0.50D+20

TOUGHNESS PROPERTIES(-1 MEANS NOT INPUT)

FLUENCE, INSIDE SURFACE	F0	◘	0.000E+00
REFERENCE TEMP., INITIAL	RTNDT0	◘	0.000
PER CENT CU	CUPER	=	0.000
PER CENT P	PPER	=	0.000
PER CENT NI	PERNI	=	0.000
DELTA RTNDT(INNER SURFACE)	DRTNIN	=	-999.0

FINITE ELEMENT PARAMETERS (STRESS CALCULATIONS)

GEOMETRIC MODELING METHOD
= 0 USER SPECIFIED NO. OF ELEMENTS + G.P FACTOR.
= 1 USER SPEC. NO. OF ELEM.& A/W OF CLADDING-
BASE METAL INTERFACE MODEL = 0

NUMBER OF ELEMENTS---------- NUMEL = 15

INTEGRATION ORDER(# GAUSS POINTS) NGAUSS = 2

NUMBER OF NODAL POINTS---------- NUMNP = 31

GEOM.PROG.FACTOR = 1.13

FE MESH NODAL POINT COORDINATES

NODAL POINT NO.	R-COORD. (INCHES)	NODAL POINT NO.	R-COORD. (INCHES)
1	13.500	16	14.327
2	13.520	17	14.455
3	13.544	18	14.600
4	13.570	19	14.763
5	13.599	20	14.948
6	13.633	21	15.156
7	13.670	22	15.392
8	13.713	23	15.659
9	13.761	24	15.960
10	13.815	25	16.300
11	13.877	26	16.685
12	13.946	27	17.119
13	14.025	28	17.610
14	14.114	29	18.165
15	14.214	30	18.792
		31	19.500

ELEMENT CONNECTIVITY

ELEM. NO.	NODE NUMBERS I	J	K	MATERIAL NO.
1	1	2	3	1
2	3	4	5	1
3	5	6	7	1
4	7	8	9	1
5	9	10	11	1
6	11	12	13	1
7	13	14	15	1
8	15	16	17	1
9	17	18	19	1
10	19	20	21	1
11	21	22	23	1
12	23	24	25	1
13	25	26	27	1
14	27	28	29	1
15	29	30	31	1

MATERIAL PROPERTIES FOR STRESS CALCULATIONS

NUMBER OF MATERIALS ------ 1

TEMP(DEG.F)	MODULUS OF ELASTICITY(KSI) - E		
	(MAT 1)	(MAT 2)	(MAT 3)
70.0	2.800D+04	2.700D+04	0.000D+00

TEMP(DEG.F)	COEFF OF EXPANSION(PER DEG.F) - ALFA		
	(MAT 1)	(MAT 2)	(MAT 3)
70.0	6.500D-06	9.930D-06	0.000D+00

TEMP(DEG.F)	POISSONS RATIO - PNU		
	(MAT 1)	(MAT 2)	(MAT 3)
70.0	0.300	0.300	0.300

SELECTED TIME INTERVAL NUMBERS FOR KI CALCULATIONS

0	0	0	0	0	0	0	0	0	0
0	0	0	0	0	0	0	0	0	0
0	0	0	0	0	0	0	0	0	0
0	0	0	0	0	0	0	0	0	0
0	0	0	0	0	0	0	0	0	0
0	0	0	0	0	0	0	0	0	0
0									

CYLINDER DIMENSIONS (INCHES)

INNER RADIUS, RI = 13.500

OUTER RADIUS, RO = 19.500

WALL THICKNESS, W = 6.000

TEMPERATURE GRID GEOMETRY OVER CYLINDER WALL

GRID NO.	RADIUS
1	13.5000
2	13.7500
3	14.0000
4	14.2500
5	14.5000
6	14.7500
7	15.0000
8	15.2500
9	15.5000
10	16.0000
11	16.5000
12	17.5000
13	18.5000
14	19.5000

*** KIC (OR KIA) VALUES WERE READ IN FROM UNIT 56

MATERIAL IDENTIFICATION =TOUGHNESS PER 3/26/85 PHONE CALL WITH RDC

SEQ.NO.	TEMP.	KIC VALUE
1	-300.	33.
2	-200.	35.
3	-100.	39.
4	-50.	45.
5	0.	57.
6	50.	88.
7	75.	125.
8	100.	185.
9	125.	260.
10	150.	400.
11	200.	680.

SEQ.NO.	TEMP.	KIA VALUE
1	-260.	33.
2	-160.	34.
3	-60.	35.
4	-10.	41.
5	40.	55.
6	90.	77.
7	140.	108.
8	165.	125.
9	190.	146.
10	240.	188.

CALCULATED 2-D CRACK DEPTH VALUES =
0.0000 0.1588 0.3353 0.4585 0.6088 0.9000 1.2088 1.5000 1.8071 2.4088
3.0000 3.6071 4.2441 4.8071 5.1000 5.4000

REF TEMPERATURE FOR STRESS CALCULATIONS TREF = 200.0 DEG.F

TSE5A EXPERIMENT (9-24-80) ZERO TIME 18:20:17 LONGIT. CRACK

KICTYP = 6, RTNDTO = 0.0 DEG., %CU = 0.000, FO =0.00E19

TEMPERATURE INTERVAL NUMBER = 1, TIME = 0.500 MIN., PRESSURE = 0.000 KSI

SEQ NO.	RADIUS IN.	DEPTH IN.	A/W	TEMPER. DEG.F	DLRTNDT DEG.F	CIRCUMF. STRESS KSI	KI	KIC	KI/KIC	KIA	KI/KIA	ELLIPTIC ANGLE
1	13.500	0.000	0.000	40.0	0.	38.18	0.00	78.56	0.000	55.00	0.000	
2	13.659	0.159	0.026	72.8	0.	29.25	23.88	120.71	0.198	68.33	0.349	
3	13.835	0.335	0.056	104.2	0.	20.78	29.89	195.31	0.153	85.20	0.351	
4	13.958	0.458	0.076	121.8	0.	16.06	31.87	246.89	0.129	96.19	0.331	
5	14.109	0.609	0.101	139.3	0.	11.36	32.21	335.27	0.096	107.57	0.299	
6	14.400	0.900	0.150	165.3	0.	4.46	30.63	490.09	0.062	125.26	0.245	
7	14.709	1.209	0.201	181.6	0.	0.22	28.04	580.47	0.048	138.66	0.202	
8	15.000	1.500	0.250	190.0	0.	-1.92	26.48	626.24	0.042	146.00	0.181	
9	15.307	1.807	0.301	194.8	0.	-3.09	24.32	651.87	0.037	150.12	0.162	
10	15.909	2.409	0.401	198.8	0.	-3.98	22.41	673.77	0.033	153.61	0.146	
11	16.500	3.000	0.500	200.0	0.	-4.10	21.85	680.00	0.032	154.61	0.141	
12	17.107	3.607	0.601	200.2	0.	-3.98	20.92	680.00	0.031	154.77	0.135	
13	17.744	4.244	0.707	199.9	0.	-3.76	19.52	679.68	0.029	154.55	0.126	
14	18.307	4.807	0.801	200.0	0.	-3.65	17.00	679.86	0.025	154.58	0.110	
15	18.600	5.100	0.850	200.0	0.	-3.59	14.73	680.00	0.022	154.61	0.095	
16	18.900	5.400	0.900	200.0	0.	-3.54	11.03	680.00	0.016	154.62	0.071	

TEMPERATURE INTERVAL NUMBER = 2, TIME = 1.000 MIN., PRESSURE = 0.000 KSI

SEQ NO.	RADIUS IN.	DEPTH IN.	A/W	TEMPER. DEG.F	DLRTNDT DEG.F	CIRCUMF. STRESS KSI	KI	KIC	KI/KIC	KIA	KI/KIA	ELLIPTIC ANGLE
1	13.500	0.000	0.000	-48.0	0.	57.04	0.00	45.33	0.000	35.86	0.000	
2	13.659	0.159	0.026	-10.4	0.	46.66	36.98	53.73	0.688	40.93	0.904	
3	13.835	0.335	0.056	27.7	0.	36.24	48.34	69.64	0.694	50.84	0.951	
4	13.958	0.458	0.076	50.8	0.	29.95	53.15	88.88	0.598	59.00	0.901	
5	14.109	0.609	0.101	75.4	0.	23.30	55.51	125.75	0.441	69.53	0.798	
6	14.400	0.900	0.150	112.7	0.	13.26	56.32	217.22	0.259	90.41	0.623	
7	14.709	1.209	0.201	141.7	0.	5.57	54.91	349.43	0.157	109.10	0.503	
8	15.000	1.500	0.250	162.0	0.	0.30	53.71	470.94	0.114	122.76	0.438	
9	15.307	1.807	0.301	175.2	0.	-3.07	50.40	545.46	0.092	133.21	0.378	
10	15.909	2.409	0.401	190.7	0.	-6.83	47.11	629.88	0.075	146.59	0.321	
11	16.500	3.000	0.500	198.0	0.	-8.39	45.44	669.27	0.068	152.90	0.297	
12	17.107	3.607	0.601	200.2	0.	-8.60	42.92	680.00	0.063	154.77	0.277	
13	17.744	4.244	0.707	199.9	0.	-8.19	39.68	679.48	0.058	154.52	0.257	
14	18.307	4.807	0.801	200.0	0.	-7.93	34.54	679.77	0.051	154.57	0.223	
15	18.600	5.100	0.850	200.0	0.	-7.81	29.95	680.00	0.044	154.62	0.194	
16	18.900	5.400	0.900	200.0	0.	-7.69	22.55	680.00	0.033	154.64	0.146	

TSE5A EXPERIMENT (9-24-80) ZERO TIME 18:20:17 LONGIT. CRACK

KICTYP = 6, RTNDT0 = 0.0 DEG., %CU = 0.000, F0 =0.00E19

SEQ NO.	RADIUS IN.	DEPTH IN.	A/W	TEMPER. DEG.F	DLRTNDT DEG.F	CIRCUMF. STRESS KSI	KI	KIC	KI/KIC	KIA	KI/KIA	ELLIPTIC ANGLE
TEMPERATURE INTERVAL NUMBER = 3, TIME = 1.233 MIN., PRESSURE = 0.000 KSI												
1	13.500	0.000	0.000	-82.0	0.	63.96	0.00	40.69	0.000	34.05	0.000	
2	13.659	0.159	0.026	-41.7	0.	52.80	41.67	46.44	0.897	36.43	1.144	
3	13.835	0.335	0.056	-1.3	0.	41.72	54.88	56.55	0.970	42.84	1.281	
4	13.958	0.458	0.076	22.7	0.	35.15	60.79	66.71	0.911	49.27	1.234	
5	14.109	0.609	0.101	47.5	0.	28.37	64.20	85.46	0.751	57.75	1.112	
6	14.400	0.900	0.150	88.5	0.	17.29	66.56	156.21	0.426	76.20	0.873	
7	14.709	1.209	0.201	122.4	0.	8.27	65.78	249.34	0.264	96.60	0.681	
8	15.000	1.500	0.250	145.0	0.	2.33	65.46	369.48	0.177	111.22	0.589	
9	15.307	1.807	0.301	164.1	0.	-2.57	61.88	483.00	0.128	124.32	0.498	
10	15.909	2.409	0.401	186.0	0.	-7.95	58.02	604.58	0.096	142.51	0.407	
11	16.500	3.000	0.500	195.0	0.	-9.89	56.02	653.15	0.086	150.32	0.373	
12	17.107	3.607	0.601	199.0	0.	-10.49	53.02	674.41	0.079	153.72	0.345	
13	17.744	4.244	0.707	200.2	0.	-10.39	48.70	680.00	0.072	154.80	0.315	
14	18.307	4.807	0.801	200.1	0.	-10.01	42.26	680.00	0.062	154.69	0.273	
15	18.600	5.100	0.850	200.0	0.	-9.82	36.65	679.80	0.054	154.57	0.237	
16	18.900	5.400	0.900	199.9	0.	-9.65	27.63	679.56	0.041	154.54	0.179	
TEMPERATURE INTERVAL NUMBER = 4, TIME = 1.300 MIN., PRESSURE = 0.000 KSI												
1	13.500	0.000	0.000	-94.0	0.	66.36	0.00	39.51	0.000	33.81	0.000	
2	13.659	0.159	0.026	-53.8	0.	55.20	43.42	44.39	0.978	35.41	1.226	
3	13.835	0.335	0.056	-13.0	0.	43.97	57.44	52.98	1.084	40.43	1.421	
4	13.958	0.458	0.076	12.1	0.	37.10	63.76	61.58	1.035	46.21	1.380	
5	14.109	0.609	0.101	39.4	0.	29.65	67.31	78.10	0.862	54.80	1.228	
6	14.400	0.900	0.150	82.7	0.	17.96	69.53	142.12	0.489	73.18	0.950	
7	14.709	1.209	0.201	117.2	0.	8.78	68.91	230.73	0.299	93.25	0.739	
8	15.000	1.500	0.250	141.0	0.	2.53	68.60	345.22	0.199	108.64	0.631	
9	15.307	1.807	0.301	160.1	0.	-2.37	65.02	459.75	0.141	121.36	0.536	
10	15.909	2.409	0.401	182.8	0.	-7.96	61.42	587.05	0.105	139.71	0.440	
11	16.500	3.000	0.500	193.0	0.	-10.21	59.47	642.40	0.093	148.60	0.400	
12	17.107	3.607	0.601	197.6	0.	-10.96	56.37	667.22	0.084	152.57	0.369	
13	17.744	4.244	0.707	199.5	0.	-11.00	51.82	677.25	0.077	154.17	0.336	
14	18.307	4.807	0.801	200.0	0.	-10.75	44.92	679.77	0.066	154.57	0.291	
15	18.600	5.100	0.850	200.0	0.	-10.59	38.94	680.00	0.057	154.62	0.252	
16	18.900	5.400	0.900	200.0	0.	-10.42	29.35	680.00	0.043	154.63	0.190	

TSE5A EXPERIMENT (9-24-80) ZERO TIME 18:20:17 LONGIT. CRACK

KICTYP = 6, RTNDTO = 0.0 DEG., %CU = 0.000, FO =0.00E19

TEMPERATURE INTERVAL NUMBER = 5, TIME = 1.500 MIN., PRESSURE = 0.000 KSI

SEQ NO.	RADIUS IN.	DEPTH IN.	A/W	TEMPER. DEG.F	DLRTNDT DEG.F	CIRCUMF. STRESS KSI	KI	KIC	KI/KIC	KIA	KI/KIA	ELLIPTIC ANGLE
1	13.500	0.000	0.000	-122.0	0.	71.97	0.00	37.48	0.000	33.72	0.000	
2	13.659	0.159	0.026	-79.6	0.	60.17	47.21	40.96	1.153	34.12	1.383	
3	13.835	0.335	0.056	-37.8	0.	48.63	62.81	47.18	1.331	36.83	1.705	
4	13.958	0.458	0.076	-12.3	0.	41.62	70.16	53.17	1.320	40.55	1.730	
5	14.109	0.609	0.101	17.6	0.	33.46	74.44	64.08	1.162	47.75	1.559	
6	14.400	0.900	0.150	64.5	0.	20.77	77.33	106.43	0.727	64.59	1.197	
7	14.709	1.209	0.201	101.7	0.	10.84	77.40	189.09	0.409	83.67	0.925	
8	15.000	1.500	0.250	128.0	0.	3.88	77.57	273.67	0.283	100.22	0.774	
9	15.307	1.807	0.301	150.4	0.	-1.90	73.85	402.72	0.183	114.77	0.643	
10	15.909	2.409	0.401	177.0	0.	-8.46	70.35	555.53	0.127	134.76	0.522	
11	16.500	3.000	0.500	190.0	0.	-11.39	68.12	626.24	0.109	146.00	0.467	
12	17.107	3.607	0.601	195.9	0.	-12.42	64.61	658.08	0.098	151.11	0.428	
13	17.744	4.244	0.707	198.8	0.	-12.67	59.33	673.77	0.088	153.61	0.386	
14	18.307	4.807	0.801	199.9	0.	-12.51	51.37	679.23	0.076	154.48	0.332	
15	18.600	5.100	0.850	200.0	0.	-12.35	44.50	680.00	0.065	154.65	0.288	
16	18.900	5.400	0.900	200.1	0.	-12.16	33.55	680.00	0.049	154.70	0.217	

TEMPERATURE INTERVAL NUMBER = 6, TIME = 2.033 MIN., PRESSURE = 0.000 KSI

1	13.500	0.000	0.000	-180.0	0.	82.16	0.00	35.40	0.000	34.01	0.000	
2	13.659	0.159	0.026	-139.2	0.	70.67	54.77	36.63	1.495	33.85	1.618	
3	13.835	0.335	0.056	-97.5	0.	59.00	74.17	39.21	1.891	33.76	2.197	
4	13.958	0.458	0.076	-70.8	0.	51.59	83.82	42.00	1.996	34.45	2.433	
5	14.109	0.609	0.101	-39.4	0.	42.94	90.15	46.88	1.923	36.67	2.458	
6	14.400	0.900	0.150	13.0	0.	28.66	96.03	61.98	1.550	46.45	2.067	
7	14.709	1.209	0.201	56.8	0.	16.87	98.11	95.81	1.024	61.37	1.599	
8	15.000	1.500	0.250	90.0	0.	8.06	100.00	159.89	0.625	77.00	1.299	
9	15.307	1.807	0.301	118.7	0.	0.59	96.59	235.96	0.409	94.25	1.025	
10	15.909	2.409	0.401	157.7	0.	-9.20	93.29	445.84	0.209	119.67	0.780	
11	16.500	3.000	0.500	178.0	0.	-13.93	90.95	560.94	0.162	135.59	0.671	
12	17.107	3.607	0.601	188.7	0.	-16.07	86.36	619.13	0.139	144.86	0.596	
13	17.744	4.244	0.707	195.1	0.	-17.06	79.16	653.65	0.121	150.40	0.526	
14	18.307	4.807	0.801	198.4	0.	-17.33	68.34	671.34	0.102	153.23	0.446	
15	18.600	5.100	0.850	199.2	0.	-17.24	59.13	675.77	0.088	153.93	0.384	
16	18.900	5.400	0.900	199.5	0.	-17.02	44.61	677.18	0.066	154.16	0.289	

TSE5A EXPERIMENT (9-24-80) ZERO TIME 18:20:17 LONGIT. CRACK

KICTYP = 6, RTNDTO = 0.0 DEG., %CU = 0.000, FO =0.00E19

TEMPERATURE INTERVAL NUMBER = 7, TIME = 2.500 MIN., PRESSURE = 0.000 KSI

SEQ NO.	RADIUS IN.	DEPTH IN.	A/W	TEMPER. DEG.F	DLRTNDT DEG.F	CIRCUMF. STRESS KSI	KI	KIC	KI/KIC	KIA	KI/KIA	ELLIPTIC ANGLE
1	13.500	0.000	0.000	-212.0	0.	86.43	0.00	34.77	0.000	33.75	0.000	
2	13.659	0.159	0.026	-174.9	0.	75.84	58.27	35.52	1.641	34.02	1.713	
3	13.835	0.335	0.056	-135.0	0.	64.58	79.84	36.82	2.169	33.81	2.361	
4	13.958	0.458	0.076	-108.6	0.	57.20	90.89	38.34	2.370	33.69	2.698	
5	14.109	0.609	0.101	-78.3	0.	48.79	98.65	41.10	2.400	34.16	2.888	
6	14.400	0.900	0.150	-26.2	0.	34.46	107.20	49.63	2.160	38.28	2.800	
7	14.709	1.209	0.201	21.3	0.	21.60	111.18	65.97	1.685	48.86	2.276	
8	15.000	1.500	0.250	58.0	0.	11.81	114.72	97.32	1.179	61.86	1.855	
9	15.307	1.807	0.301	90.6	0.	3.28	112.05	161.45	0.694	77.34	1.449	
10	15.909	2.409	0.401	136.8	0.	-8.44	109.90	320.31	0.343	105.91	1.038	
11	16.500	3.000	0.500	165.0	0.	-15.19	108.03	488.16	0.221	125.00	0.864	
12	17.107	3.607	0.601	181.6	0.	-18.76	102.36	580.58	0.176	138.68	0.738	
13	17.744	4.244	0.707	191.1	0.	-20.43	93.54	632.05	0.148	146.94	0.637	
14	18.307	4.807	0.801	196.0	0.	-21.00	80.65	658.58	0.122	151.19	0.533	
15	18.600	5.100	0.850	197.4	0.	-20.99	69.76	665.91	0.105	152.36	0.458	
16	18.900	5.400	0.900	198.0	0.	-20.80	52.69	669.35	0.079	152.91	0.345	

TEMPERATURE INTERVAL NUMBER = 8, TIME = 3.067 MIN., PRESSURE = 0.000 KSI

1	13.500	0.000	0.000	-233.0	0.	87.44	0.00	34.35	0.000	33.45	0.000	
2	13.659	0.159	0.026	-197.0	0.	77.13	59.12	35.06	1.686	33.90	1.744	
3	13.835	0.335	0.056	-159.1	0.	66.36	81.38	35.93	2.265	34.00	2.394	
4	13.958	0.458	0.076	-134.7	0.	59.49	93.10	36.83	2.528	33.81	2.754	
5	14.109	0.609	0.101	-107.8	0.	51.93	101.86	38.40	2.653	33.70	3.023	
6	14.400	0.900	0.150	-58.5	0.	38.26	112.54	43.67	2.577	35.09	3.207	
7	14.709	1.209	0.201	-10.7	0.	25.25	118.23	53.64	2.204	40.86	2.893	
8	15.000	1.500	0.250	27.0	0.	15.13	123.39	69.21	1.783	50.62	2.438	
9	15.307	1.807	0.301	60.6	0.	6.28	121.82	100.79	1.209	62.94	1.936	
10	15.909	2.409	0.401	111.6	0.	-6.74	121.88	214.07	0.569	89.70	1.359	
11	16.500	3.000	0.500	145.0	0.	-14.89	120.98	369.48	0.327	111.22	1.088	
12	17.107	3.607	0.601	167.6	0.	-19.99	115.26	502.96	0.229	127.02	0.907	
13	17.744	4.244	0.707	182.9	0.	-23.08	105.06	587.89	0.179	139.84	0.751	
14	18.307	4.807	0.801	190.5	0.	-24.24	90.33	628.67	0.144	146.39	0.617	
15	18.600	5.100	0.850	192.6	0.	-24.38	78.10	640.41	0.122	148.28	0.527	
16	18.900	5.400	0.900	193.9	0.	-24.31	59.05	647.46	0.091	149.41	0.395	

TSE5A EXPERIMENT (9-24-80) ZERO TIME 18:20:17 LONGIT. CRACK

KICTYP = 6, RTNDTO = 0.0 DEG., %CU = 0.000, FO =0.00E19

TEMPERATURE INTERVAL NUMBER = 9, TIME = 3.500 MIN., PRESSURE = 0.000 KSI

SEQ NO.	RADIUS IN.	DEPTH IN.	A/W	TEMPER. DEG.F	DLRTNDT DEG.F	CIRCUMF. STRESS KSI	KI	KIC	KI/KIC	KIA	KI/KIA	ELLIPTIC ANGLE
1	13.500	0.000	0.000	-243.0	0.	87.00	0.00	34.15	0.000	33.29	0.000	
2	13.659	0.159	0.026	-213.0	0.	78.23	59.49	34.75	1.712	33.73	1.763	
3	13.835	0.335	0.056	-177.5	0.	68.10	82.64	35.46	2.331	34.01	2.429	
4	13.958	0.458	0.076	-152.8	0.	61.11	94.82	36.13	2.625	33.96	2.792	
5	14.109	0.609	0.101	-126.4	0.	53.68	104.02	37.24	2.794	33.75	3.083	
6	14.400	0.900	0.150	-79.2	0.	40.51	115.87	41.00	2.826	34.13	3.395	
7	14.709	1.209	0.201	-32.6	0.	27.75	122.80	48.23	2.546	37.44	3.280	
8	15.000	1.500	0.250	5.0	0.	17.63	129.25	58.77	2.199	44.35	2.914	
9	15.307	1.807	0.301	40.0	0.	8.36	128.51	78.57	1.636	55.01	2.336	
10	15.909	2.409	0.401	95.1	0.	-5.78	129.58	172.70	0.750	79.83	1.623	
11	16.500	3.000	0.500	132.0	0.	-14.84	129.33	293.89	0.440	102.82	1.258	
12	17.107	3.607	0.601	159.3	0.	-21.13	123.22	455.16	0.271	120.80	1.020	
13	17.744	4.244	0.707	177.6	0.	-24.93	111.91	558.84	0.200	135.27	0.827	
14	18.307	4.807	0.801	185.4	0.	-26.09	96.17	601.40	0.160	142.00	0.677	
15	18.600	5.100	0.850	187.7	0.	-26.25	83.23	613.84	0.136	144.00	0.578	
16	18.900	5.400	0.900	189.5	0.	-26.26	63.03	623.33	0.101	145.53	0.433	

TEMPERATURE INTERVAL NUMBER = 10, TIME = 4.000 MIN., PRESSURE = 0.000 KSI

1	13.500	0.000	0.000	-252.0	0.	86.28	0.00	33.97	0.000	33.14	0.000	
2	13.659	0.159	0.026	-221.4	0.	77.38	58.89	34.58	1.703	33.62	1.752	
3	13.835	0.335	0.056	-187.9	0.	67.74	81.89	35.24	2.324	33.97	2.411	
4	13.958	0.458	0.076	-165.3	0.	61.32	94.27	35.75	2.637	34.02	2.771	
5	14.109	0.609	0.101	-139.7	0.	54.07	103.76	36.61	2.834	33.85	3.065	
6	14.400	0.900	0.150	-93.3	0.	41.12	115.93	39.58	2.929	33.82	3.428	
7	14.709	1.209	0.201	-48.4	0.	28.79	123.53	45.27	2.729	35.83	3.448	
8	15.000	1.500	0.250	-13.0	0.	19.20	130.82	52.98	2.469	40.43	3.236	
9	15.307	1.807	0.301	21.0	0.	10.18	131.04	65.80	1.992	48.76	2.688	
10	15.909	2.409	0.401	75.7	0.	-3.97	133.84	126.50	1.058	69.71	1.920	
11	16.500	3.000	0.500	118.0	0.	-14.43	134.29	233.46	0.575	93.78	1.432	
12	17.107	3.607	0.601	146.9	0.	-21.15	128.19	381.22	0.336	112.47	1.140	
13	17.744	4.244	0.707	166.9	0.	-25.38	117.09	499.01	0.235	126.47	0.926	
14	18.307	4.807	0.801	179.2	0.	-27.67	100.53	567.49	0.177	136.61	0.736	
15	18.600	5.100	0.850	183.1	0.	-28.19	86.81	589.05	0.147	140.02	0.620	
16	18.900	5.400	0.900	185.4	0.	-28.29	65.63	601.52	0.109	142.02	0.462	

TSE5A EXPERIMENT (9-24-80) ZERO TIME 18:20:17 LONGIT. CRACK

KICTYP = 6, RTNDTO = 0.0 DEG., %CU = 0.000, FO =0.00E19

TEMPERATURE INTERVAL NUMBER = 11, TIME = 4.500 MIN., PRESSURE = 0.000 KSI

SEQ NO.	RADIUS IN.	DEPTH IN.	A/W	TEMPER. DEG.F	DLRTNDT DEG.F	CIRCUMF. STRESS KSI	KI	KIC	KI/KIC	KIA	KI/KIA	ELLIPTIC ANGLE
1	13.500	0.000	0.000	-257.0	0.	84.40	0.00	33.87	0.000	33.05	0.000	
2	13.659	0.159	0.026	-228.1	0.	75.94	57.71	34.45	1.675	33.53	1.721	
3	13.835	0.335	0.056	-197.6	0.	67.11	80.56	35.05	2.298	33.90	2.376	
4	13.958	0.458	0.076	-177.0	0.	61.22	93.11	35.47	2.625	34.02	2.737	
5	14.109	0.609	0.101	-151.2	0.	53.93	102.73	36.18	2.840	33.95	3.026	
6	14.400	0.900	0.150	-106.7	0.	41.45	115.02	38.48	2.989	33.70	3.413	
7	14.709	1.209	0.201	-63.4	0.	29.54	123.34	42.97	2.870	34.80	3.544	
8	15.000	1.500	0.250	-30.0	0.	20.43	131.22	48.78	2.690	37.76	3.475	
9	15.307	1.807	0.301	3.1	0.	11.61	132.28	58.09	2.277	43.89	3.014	
10	15.909	2.409	0.401	58.8	0.	-2.83	136.00	98.37	1.383	62.19	2.187	
11	16.500	3.000	0.500	102.0	0.	-13.56	137.38	189.90	0.723	83.86	1.638	
12	17.107	3.607	0.601	134.0	0.	-21.10	131.46	304.93	0.431	104.14	1.262	
13	17.744	4.244	0.707	156.6	0.	-25.99	119.97	439.71	0.273	118.95	1.009	
14	18.307	4.807	0.801	169.9	0.	-28.50	103.02	515.75	0.200	128.82	0.800	
15	18.600	5.100	0.850	174.3	0.	-29.15	89.02	540.74	0.165	132.50	0.672	
16	18.900	5.400	0.900	177.4	0.	-29.45	67.39	557.77	0.121	135.10	0.499	

TEMPERATURE INTERVAL NUMBER = 12, TIME = 5.000 MIN., PRESSURE = 0.000 KSI

1	13.500	0.000	0.000	-262.0	0.	82.85	0.00	33.77	0.000	33.00	0.000	
2	13.659	0.159	0.026	-235.6	0.	75.06	56.89	34.30	1.659	33.41	1.703	
3	13.835	0.335	0.056	-205.1	0.	66.24	79.53	34.90	2.279	33.82	2.351	
4	13.958	0.458	0.076	-183.8	0.	60.18	91.80	35.32	2.599	33.99	2.701	
5	14.109	0.609	0.101	-160.3	0.	53.47	101.36	35.89	2.824	34.00	2.981	
6	14.400	0.900	0.150	-118.9	0.	41.80	114.26	37.67	3.033	33.71	3.390	
7	14.709	1.209	0.201	-77.2	0.	30.31	123.01	41.22	2.984	34.20	3.597	
8	15.000	1.500	0.250	-42.0	0.	20.74	131.13	46.39	2.827	36.40	3.602	
9	15.307	1.807	0.301	-9.1	0.	11.95	132.21	54.11	2.443	41.18	3.210	
10	15.909	2.409	0.401	44.1	0.	-1.87	136.75	82.15	1.665	56.47	2.422	
11	16.500	3.000	0.500	87.0	0.	-12.57	139.17	152.41	0.913	75.39	1.846	
12	17.107	3.607	0.601	122.1	0.	-20.91	133.50	248.01	0.538	96.38	1.385	
13	17.744	4.244	0.707	147.3	0.	-26.46	121.57	383.37	0.317	112.69	1.079	
14	18.307	4.807	0.801	160.8	0.	-29.04	104.35	463.99	0.225	121.88	0.856	
15	18.600	5.100	0.850	165.4	0.	-29.73	90.23	490.62	0.184	125.33	0.720	
16	18.900	5.400	0.900	169.0	0.	-30.13	68.39	510.68	0.134	128.10	0.534	

TSE5A EXPERIMENT (9-24-80) ZERO TIME 18:20:17 LONGIT. CRACK

KICTYP = 6, RTNDTO = 0.0 DEG., %CU = 0.000, FO =0.00E19

TEMPERATURE INTERVAL NUMBER = 13, TIME = 6.000 MIN., PRESSURE = 0.000 KSI

SEQ NO.	RADIUS IN.	DEPTH IN.	A/W	TEMPER. DEG.F	DLRTNDT DEG.F	CIRCUMF. STRESS KSI	KI	KIC	KI/KIC	KIA	KI/KIA	ELLIPTIC ANGLE
1	13.500	0.000	0.000	-270.0	0.	79.73	0.00	33.61	0.000	33.00	0.000	
2	13.659	0.159	0.026	-244.4	0.	72.19	54.71	34.12	1.603	33.27	1.645	
3	13.835	0.335	0.056	-216.9	0.	64.18	76.65	34.67	2.211	33.68	2.276	
4	13.958	0.458	0.076	-198.3	0.	58.82	88.82	35.03	2.535	33.89	2.621	
5	14.109	0.609	0.101	-175.5	0.	52.33	98.35	35.50	2.770	34.02	2.891	
6	14.400	0.900	0.150	-135.3	0.	41.01	111.02	36.80	3.017	33.81	3.283	
7	14.709	1.209	0.201	-97.8	0.	30.57	120.24	39.18	3.069	33.76	3.562	
8	15.000	1.500	0.250	-65.0	0.	21.61	128.99	42.75	3.017	34.72	3.715	
9	15.307	1.807	0.301	-32.4	0.	12.90	130.58	48.26	2.706	37.46	3.486	
10	15.909	2.409	0.401	20.5	0.	-0.88	136.19	65.53	2.078	48.60	2.802	
11	16.500	3.000	0.500	65.0	0.	-12.03	138.66	107.20	1.293	64.81	2.139	
12	17.107	3.607	0.601	99.8	0.	-20.34	133.33	184.54	0.723	82.57	1.615	
13	17.744	4.244	0.707	125.8	0.	-26.11	121.78	263.53	0.462	98.80	1.233	
14	18.307	4.807	0.801	141.2	0.	-29.17	104.59	346.29	0.302	108.76	0.962	
15	18.600	5.100	0.850	146.7	0.	-30.08	90.43	379.97	0.238	112.33	0.805	
16	18.900	5.400	0.900	151.0	0.	-30.66	68.55	405.80	0.169	115.11	0.596	

TEMPERATURE INTERVAL NUMBER = 14, TIME = 7.000 MIN., PRESSURE = 0.000 KSI

SEQ NO.	RADIUS IN.	DEPTH IN.	A/W	TEMPER. DEG.F	DLRTNDT DEG.F	CIRCUMF. STRESS KSI	KI	KIC	KI/KIC	KIA	KI/KIA	ELLIPTIC ANGLE
1	13.500	0.000	0.000	-275.0	0.	75.92	0.00	33.51	0.000	33.00	0.000	
2	13.659	0.159	0.026	-253.1	0.	69.38	52.39	33.95	1.543	33.12	1.582	
3	13.835	0.335	0.056	-227.2	0.	61.83	73.65	34.46	2.137	33.54	2.196	
4	13.958	0.458	0.076	-208.9	0.	56.55	85.34	34.83	2.450	33.78	2.526	
5	14.109	0.609	0.101	-188.6	0.	50.72	94.64	35.22	2.687	33.97	2.786	
6	14.400	0.900	0.150	-152.3	0.	40.42	107.59	36.14	2.977	33.96	3.168	
7	14.709	1.209	0.201	-115.6	0.	30.23	116.84	37.87	3.086	33.70	3.468	
8	15.000	1.500	0.250	-84.0	0.	21.59	125.62	40.48	3.103	34.00	3.695	
9	15.307	1.807	0.301	-54.7	0.	13.71	127.83	44.25	2.889	35.34	3.617	
10	15.909	2.409	0.401	-1.3	0.	-0.23	133.85	56.56	2.366	42.84	3.124	
11	16.500	3.000	0.500	41.0	0.	-10.85	137.01	79.40	1.725	55.36	2.475	
12	17.107	3.607	0.601	76.3	0.	-19.32	132.46	127.67	1.038	69.98	1.893	
13	17.744	4.244	0.707	104.8	0.	-25.76	121.07	196.63	0.616	85.52	1.416	
14	18.307	4.807	0.801	121.8	0.	-29.27	103.83	247.12	0.420	96.23	1.079	
15	18.600	5.100	0.850	127.8	0.	-30.29	89.70	272.89	0.329	100.11	0.896	
16	18.900	5.400	0.900	132.2	0.	-30.90	67.98	295.10	0.230	102.96	0.660	

TSE5A EXPERIMENT (9-24-80) ZERO TIME 18:20:17 LONGIT. CRACK

KICTYP = 6, RTNDTO = 0.0 DEG., %CU = 0.000, FO =0.00E19

TEMPERATURE INTERVAL NUMBER = 15, TIME = 8.000 MIN., PRESSURE = 0.000 KSI

SEQ NO.	RADIUS IN.	DEPTH IN.	A/W	TEMPER. DEG.F	DLRTNDT DEG.F	CIRCUMF. STRESS KSI	KI	KIC	KI/KIC	KIA	KI/KIA	ELLIPTIC ANGLE
1	13.500	0.000	0.000	-280.0	0.	72.70	0.00	33.41	0.000	33.00	0.000	
2	13.659	0.159	0.026	-259.4	0.	66.54	50.22	33.82	1.485	33.01	1.521	
3	13.835	0.335	0.056	-234.8	0.	59.35	70.64	34.31	2.059	33.42	2.114	
4	13.958	0.458	0.076	-217.4	0.	54.35	81.89	34.66	2.363	33.68	2.432	
5	14.109	0.609	0.101	-199.0	0.	49.04	90.96	35.02	2.598	33.88	2.684	
6	14.400	0.900	0.150	-164.4	0.	39.18	103.73	35.78	2.899	34.02	3.049	
7	14.709	1.209	0.201	-129.2	0.	29.39	112.69	37.10	3.038	33.77	3.337	
8	15.000	1.500	0.250	-100.0	0.	21.38	121.54	39.00	3.116	33.74	3.603	
9	15.307	1.807	0.301	-69.5	0.	13.21	123.62	42.16	2.932	34.50	3.583	
10	15.909	2.409	0.401	-18.9	0.	-0.02	129.39	51.41	2.517	39.40	3.284	
11	16.500	3.000	0.500	23.0	0.	-10.54	132.52	66.88	1.981	49.37	2.684	
12	17.107	3.607	0.601	56.7	0.	-18.62	128.06	95.70	1.338	61.33	2.088	
13	17.744	4.244	0.707	83.3	0.	-24.62	117.40	143.45	0.818	73.46	1.598	
14	18.307	4.807	0.801	100.5	0.	-28.20	100.90	186.34	0.542	83.00	1.216	
15	18.600	5.100	0.850	107.0	0.	-29.36	87.23	202.20	0.431	86.89	1.004	
16	18.900	5.400	0.900	112.0	0.	-30.13	66.15	215.19	0.307	89.96	0.735	

TEMPERATURE INTERVAL NUMBER = 16, TIME = 10.000 MIN., PRESSURE = 0.000 KSI

1	13.500	0.000	0.000	-287.0	0.	66.23	0.00	33.26	0.000	33.00	0.000	
2	13.659	0.159	0.026	-267.9	0.	60.53	45.70	33.65	1.358	33.00	1.385	
3	13.835	0.335	0.056	-246.8	0.	54.33	64.38	34.07	1.890	33.22	1.938	
4	13.958	0.458	0.076	-232.1	0.	50.04	74.86	34.37	2.178	33.46	2.237	
5	14.109	0.609	0.101	-213.6	0.	44.75	83.16	34.73	2.394	33.73	2.466	
6	14.400	0.900	0.150	-181.7	0.	35.70	94.48	35.37	2.671	34.00	2.779	
7	14.709	1.209	0.201	-151.0	0.	27.14	103.07	36.18	2.848	33.95	3.036	
8	15.000	1.500	0.250	-124.0	0.	19.72	111.18	37.37	2.975	33.73	3.296	
9	15.307	1.807	0.301	-97.1	0.	12.48	113.32	39.24	2.888	33.77	3.356	
10	15.909	2.409	0.401	-50.3	0.	0.24	118.88	44.96	2.644	35.68	3.332	
11	16.500	3.000	0.500	-13.0	0.	-9.12	122.17	52.98	2.306	40.43	3.022	
12	17.107	3.607	0.601	18.2	0.	-16.61	118.61	64.36	1.843	47.92	2.475	
13	17.744	4.244	0.707	44.2	0.	-22.55	108.94	82.28	1.324	56.52	1.927	
14	18.307	4.807	0.801	61.5	0.	-26.22	93.61	102.04	0.917	63.32	1.478	
15	18.600	5.100	0.850	68.0	0.	-27.42	80.90	112.08	0.722	66.14	1.223	
16	18.900	5.400	0.900	73.0	0.	-28.23	61.35	121.02	0.507	68.41	0.897	

TSE5A EXPERIMENT (9-24-80) ZERO TIME 18:20:17 LONGIT. CRACK

KICTYP = 6, RTNDTO = 0.0 DEG., %CU = 0.000, F0 =0.00E19

TEMPERATURE INTERVAL NUMBER = 17, TIME = 12.000 MIN., PRESSURE = 0.000 KSI

SEQ NO.	RADIUS IN.	DEPTH IN.	A/W	TEMPER. DEG.F	DLRTNDT DEG.F	CIRCUMF. STRESS KSI	KI	KIC	KI/KIC	KIA	KI/KIA	ELLIPTIC ANGLE
1	13.500	0.000	0.000	-293.0	0.	60.23	0.00	33.14	0.000	33.00	0.000	
2	13.659	0.159	0.026	-275.7	0.	55.06	41.56	33.49	1.241	33.00	1.259	
3	13.835	0.335	0.056	-257.2	0.	49.58	58.62	33.87	1.731	33.05	1.774	
4	13.958	0.458	0.076	-244.4	0.	45.86	68.27	34.12	2.001	33.27	2.052	
5	14.109	0.609	0.101	-228.1	0.	41.16	76.00	34.45	2.206	33.53	2.267	
6	14.400	0.900	0.150	-198.9	0.	32.88	86.52	35.02	2.471	33.89	2.553	
7	14.709	1.209	0.201	-170.8	0.	25.02	94.48	35.62	2.653	34.02	2.777	
8	15.000	1.500	0.250	-145.0	0.	17.95	101.84	36.40	2.798	33.90	3.004	
9	15.307	1.807	0.301	-119.7	0.	11.16	103.55	37.62	2.753	33.71	3.072	
10	15.909	2.409	0.401	-77.9	0.	0.26	108.80	41.14	2.644	34.17	3.184	
11	16.500	3.000	0.500	-43.0	0.	-8.53	111.61	46.21	2.415	36.31	3.074	
12	17.107	3.607	0.601	-14.9	0.	-15.27	108.24	52.46	2.063	40.08	2.700	
13	17.744	4.244	0.707	8.2	0.	-20.52	99.51	59.99	1.659	45.17	2.203	
14	18.307	4.807	0.801	23.8	0.	-23.83	85.63	67.35	1.271	49.62	1.726	
15	18.600	5.100	0.850	29.9	0.	-24.97	74.06	71.05	1.042	51.56	1.436	
16	18.900	5.400	0.900	34.7	0.	-25.78	56.20	74.42	0.755	53.17	1.057	

TEMPERATURE INTERVAL NUMBER = 18, TIME = 14.000 MIN., PRESSURE = 0.000 KSI

1	13.500	0.000	0.000	-298.0	0.	54.58	0.00	33.04	0.000	33.00	0.000	
2	13.659	0.159	0.026	-283.6	0.	50.23	37.82	33.33	1.135	33.00	1.146	
3	13.835	0.335	0.056	-266.5	0.	45.18	53.42	33.68	1.586	33.00	1.619	
4	13.958	0.458	0.076	-254.1	0.	41.58	62.13	33.93	1.831	33.10	1.877	
5	14.109	0.609	0.101	-239.7	0.	37.43	69.12	34.22	2.020	33.34	2.073	
6	14.400	0.900	0.150	-213.9	0.	30.08	78.90	34.73	2.272	33.72	2.340	
7	14.709	1.209	0.201	-186.4	0.	22.43	85.87	35.27	2.435	33.98	2.527	
8	15.000	1.500	0.250	-165.0	0.	16.53	92.66	35.76	2.591	34.02	2.724	
9	15.307	1.807	0.301	-141.7	0.	10.30	94.42	36.53	2.585	33.87	2.788	
10	15.909	2.409	0.401	-103.1	0.	0.20	98.93	38.75	2.553	33.72	2.934	
11	16.500	3.000	0.500	-72.0	0.	-7.61	101.74	41.85	2.431	34.39	2.958	
12	17.107	3.607	0.601	-45.8	0.	-13.91	98.67	45.71	2.159	36.05	2.737	
13	17.744	4.244	0.707	-24.6	0.	-18.72	90.64	50.00	1.813	38.51	2.354	
14	18.307	4.807	0.801	-10.8	0.	-21.63	78.08	53.62	1.456	40.85	1.911	
15	18.600	5.100	0.850	-5.2	0.	-22.68	67.59	55.29	1.223	41.98	1.610	
16	18.900	5.400	0.900	-0.6	0.	-23.49	51.34	56.80	0.904	43.01	1.194	

TSE5A EXPERIMENT (9-24-80) ZERO TIME 18:20:17 LONGIT. CRACK

KICTYP = 6, RTNDTO = 0.0 DEG., %CU = 0.000, FO =0.00E19

TEMPERATURE INTERVAL NUMBER = 19, TIME = 16.000 MIN., PRESSURE = 0.000 KSI

SEQ NO.	RADIUS IN.	DEPTH IN.	A/W	TEMPER. DEG.F	DLRTNDT DEG.F	CIRCUMF. STRESS KSI	KI	KIC	KI/KIC	KIA	KI/KIA	ELLIPTIC ANGLE
1	13.500	0.000	0.000	-302.0	0.	49.50	0.00	33.00	0.000	33.00	0.000	
2	13.659	0.159	0.026	-288.2	0.	45.36	34.21	33.24	1.029	33.00	1.037	
3	13.835	0.335	0.056	-272.0	0.	40.62	48.20	33.57	1.436	33.00	1.461	
4	13.958	0.458	0.076	-260.7	0.	37.32	55.98	33.80	1.656	33.00	1.696	
5	14.109	0.609	0.101	-248.0	0.	33.68	62.25	34.05	1.828	33.20	1.875	
6	14.400	0.900	0.150	-225.0	0.	27.11	71.11	34.51	2.061	33.57	2.118	
7	14.709	1.209	0.201	-201.0	0.	20.44	77.51	34.98	2.216	33.87	2.289	
8	15.000	1.500	0.250	-180.0	0.	14.68	83.53	35.40	2.359	34.01	2.456	
9	15.307	1.807	0.301	-159.4	0.	9.15	84.94	35.92	2.365	34.00	2.498	
10	15.909	2.409	0.401	-125.7	0.	0.33	89.29	37.28	2.395	33.74	2.646	
11	16.500	3.000	0.500	-97.0	0.	-6.89	91.77	39.25	2.338	33.77	2.718	
12	17.107	3.607	0.601	-74.1	0.	-12.39	89.11	41.59	2.142	34.31	2.597	
13	17.744	4.244	0.707	-55.2	0.	-16.69	82.13	44.17	1.859	35.31	2.326	
14	18.307	4.807	0.801	-41.7	0.	-19.57	70.80	46.44	1.525	36.43	1.943	
15	18.600	5.100	0.850	-36.3	0.	-20.62	61.26	47.48	1.290	37.00	1.655	
16	18.900	5.400	0.900	-31.9	0.	-21.40	46.51	48.38	0.961	37.53	1.239	

TEMPERATURE INTERVAL NUMBER = 20, TIME = 18.000 MIN., PRESSURE = 0.000 KSI

SEQ NO.	RADIUS IN.	DEPTH IN.	A/W	TEMPER. DEG.F	DLRTNDT DEG.F	CIRCUMF. STRESS KSI	KI	KIC	KI/KIC	KIA	KI/KIA	ELLIPTIC ANGLE
1	13.500	0.000	0.000	-303.0	0.	44.09	0.00	33.00	0.000	33.00	0.000	
2	13.659	0.159	0.026	-290.4	0.	40.31	30.43	33.20	0.917	33.00	0.922	
3	13.835	0.335	0.056	-276.0	0.	36.11	42.85	33.49	1.280	33.00	1.299	
4	13.958	0.458	0.076	-266.2	0.	33.25	49.79	33.68	1.478	33.00	1.509	
5	14.109	0.609	0.101	-255.1	0.	30.04	55.41	33.91	1.634	33.08	1.675	
6	14.400	0.900	0.150	-233.9	0.	24.02	63.24	34.33	1.842	33.44	1.892	
7	14.709	1.209	0.201	-214.6	0.	18.59	69.13	34.71	1.991	33.71	2.051	
8	15.000	1.500	0.250	-195.0	0.	13.29	74.66	35.10	2.127	33.92	2.201	
9	15.307	1.807	0.301	-178.8	0.	8.87	76.33	35.43	2.154	34.01	2.244	
10	15.909	2.409	0.401	-146.1	0.	0.30	80.10	36.36	2.203	33.91	2.362	
11	16.500	3.000	0.500	-121.0	0.	-6.00	82.46	37.54	2.197	33.71	2.446	
12	17.107	3.607	0.601	-100.2	0.	-11.01	80.19	38.99	2.057	33.74	2.377	
13	17.744	4.244	0.707	-82.7	0.	-15.00	73.91	40.62	1.820	34.03	2.172	
14	18.307	4.807	0.801	-70.4	0.	-17.64	63.71	42.05	1.515	34.46	1.849	
15	18.600	5.100	0.850	-65.4	0.	-18.61	55.13	42.69	1.291	34.70	1.589	
16	18.900	5.400	0.900	-61.4	0.	-19.33	41.86	43.26	0.968	34.92	1.199	

TSE5A EXPERIMENT (9-24-80) ZERO TIME 18:20:17 LONGIT. CRACK

KICTYP = 6, RTNDTO = 0.0 DEG., %CU = 0.000, FO =0.00E19

SEQ NO.	RADIUS IN.	DEPTH IN.	A/W	TEMPER. DEG.F	DLRTNDT DEG.F	CIRCUMF. STRESS KSI	KI	KIC	KI/KIC	KIA	KI/KIA	ELLIPTIC ANGLE
TEMPERATURE INTERVAL NUMBER = 21, TIME = 20.000 MIN., PRESSURE = 0.000 KSI												
1	13.500	0.000	0.000	-305.0	0.	39.41	0.00	33.00	0.000	33.00	0.000	
2	13.659	0.159	0.026	-293.5	0.	35.98	27.18	33.13	0.820	33.00	0.823	
3	13.835	0.335	0.056	-281.1	0.	32.33	38.29	33.38	1.147	33.00	1.160	
4	13.958	0.458	0.076	-272.8	0.	29.90	44.56	33.55	1.328	33.00	1.350	
5	14.109	0.609	0.101	-262.9	0.	27.04	49.67	33.75	1.472	33.00	1.505	
6	14.400	0.900	0.150	-245.0	0.	21.92	56.87	34.11	1.667	33.26	1.710	
7	14.709	1.209	0.201	-226.4	0.	16.73	62.26	34.48	1.805	33.55	1.856	
8	15.000	1.500	0.250	-210.0	0.	12.21	67.32	34.80	1.934	33.77	1.993	
9	15.307	1.807	0.301	-193.1	0.	7.67	68.60	35.13	1.953	33.93	2.022	
10	15.909	2.409	0.401	-165.9	0.	0.55	72.36	35.74	2.025	34.02	2.127	
11	16.500	3.000	0.500	-142.0	0.	-5.47	74.43	36.52	2.038	33.87	2.197	
12	17.107	3.607	0.601	-122.9	0.	-10.08	72.18	37.43	1.928	33.72	2.140	
13	17.744	4.244	0.707	-107.6	0.	-13.55	66.48	38.41	1.731	33.70	1.973	
14	18.307	4.807	0.801	-97.0	0.	-15.79	57.39	39.25	1.462	33.77	1.700	
15	18.600	5.100	0.850	-92.6	0.	-16.67	49.72	39.65	1.254	33.83	1.470	
16	18.900	5.400	0.900	-88.7	0.	-17.38	37.80	40.01	0.945	33.90	1.115	
TEMPERATURE INTERVAL NUMBER = 22, TIME = 25.000 MIN., PRESSURE = 0.000 KSI												
1	13.500	0.000	0.000	-308.0	0.	29.31	0.00	33.00	0.000	33.00	0.000	
2	13.659	0.159	0.026	-300.5	0.	27.05	20.34	33.00	0.616	33.00	0.616	
3	13.835	0.335	0.056	-291.5	0.	24.37	28.77	33.17	0.867	33.00	0.872	
4	13.958	0.458	0.076	-285.0	0.	22.49	33.50	33.30	1.006	33.00	1.015	
5	14.109	0.609	0.101	-278.1	0.	20.47	37.38	33.44	1.118	33.00	1.133	
6	14.400	0.900	0.150	-264.8	0.	16.66	42.98	33.71	1.275	33.00	1.302	
7	14.709	1.209	0.201	-250.8	0.	12.73	47.05	33.99	1.384	33.16	1.419	
8	15.000	1.500	0.250	-238.0	0.	9.24	50.89	34.25	1.486	33.37	1.525	
9	15.307	1.807	0.301	-225.9	0.	5.97	51.94	34.49	1.506	33.56	1.548	
10	15.909	2.409	0.401	-205.0	0.	0.49	54.88	34.90	1.572	33.83	1.622	
11	16.500	3.000	0.500	-187.0	0.	-4.05	56.50	35.26	1.603	33.98	1.663	
12	17.107	3.607	0.601	-172.6	0.	-7.52	54.92	35.57	1.544	34.02	1.614	
13	17.744	4.244	0.707	-160.8	0.	-10.21	50.67	35.88	1.412	34.00	1.490	
14	18.307	4.807	0.801	-152.4	0.	-12.00	43.80	36.14	1.212	33.96	1.290	
15	18.600	5.100	0.850	-148.8	0.	-12.72	37.97	36.26	1.047	33.93	1.119	
16	18.900	5.400	0.900	-145.6	0.	-13.33	28.88	36.38	0.794	33.90	0.852	

TSE5A EXPERIMENT (9-24-80) ZERO TIME 18:20:17 LONGIT. CRACK

KICTYP = 6, RTNDTO = 0.0 DEG., %CU = 0.000, F0 =0.00E19

TEMPERATURE INTERVAL NUMBER = 23, TIME = 30.000 MIN., PRESSURE = 0.000 KSI

SEQ NO.	RADIUS IN.	DEPTH IN.	A/W	TEMPER. DEG.F	DLRTNDT DEG.F	CIRCUMF. STRESS KSI	KI	KIC	KI/KIC	KIA	KI/KIA	ELLIPTIC ANGLE
1	13.500	0.000	0.000	-313.0	0.	22.02	0.00	33.00	0.000	33.00	0.000	
2	13.659	0.159	0.026	-306.4	0.	20.06	15.16	33.00	0.459	33.00	0.459	
3	13.835	0.335	0.056	-300.2	0.	18.20	21.41	33.00	0.649	33.00	0.649	
4	13.958	0.458	0.076	-296.3	0.	17.05	25.05	33.07	0.758	33.00	0.759	
5	14.109	0.609	0.101	-291.2	0.	15.56	28.09	33.18	0.847	33.00	0.851	
6	14.400	0.900	0.150	-280.5	0.	12.50	32.25	33.40	0.966	33.00	0.977	
7	14.709	1.209	0.201	-270.3	0.	9.64	35.35	33.60	1.052	33.00	1.071	
8	15.000	1.500	0.250	-261.0	0.	7.08	38.32	33.79	1.134	33.00	1.161	
9	15.307	1.807	0.301	-251.3	0.	4.48	39.10	33.98	1.150	33.15	1.179	
10	15.909	2.409	0.401	-235.3	0.	0.27	41.19	34.30	1.201	33.41	1.233	
11	16.500	3.000	0.500	-222.0	0.	-3.07	42.35	34.57	1.225	33.61	1.260	
12	17.107	3.607	0.601	-211.6	0.	-5.56	41.26	34.77	1.187	33.75	1.223	
13	17.744	4.244	0.707	-202.7	0.	-7.60	38.18	34.95	1.092	33.85	1.128	
14	18.307	4.807	0.801	-195.9	0.	-9.07	32.96	35.08	0.940	33.91	0.972	
15	18.600	5.100	0.850	-193.1	0.	-9.64	28.53	35.13	0.812	33.93	0.841	
16	18.900	5.400	0.900	-190.7	0.	-10.08	21.68	35.18	0.616	33.95	0.638	

TSE5A EXPERIMENT (9-24-80) ZERO 2-D CRITICAL CRACK DEPTHS
KICTYP = 6, RTNDT0 = 0.0 DEGF, %CU = 0.000, F0 = 0.00E19

TIME	INITIATION	ARREST
1.03		0.056
1.07		0.076
1.09		0.026
1.15		0.101
1.23		0.023
1.23		0.124
1.25	0.056	
1.28	0.076	
1.30	0.033	0.022
1.30	0.082	0.141
1.33	0.026	
1.34		0.150
1.39	0.101	
1.50	0.023	0.019
1.50	0.120	0.187
1.56		0.201
1.68	0.150	
1.73		0.250
2.00		0.301
2.01	0.201	
2.03	0.018	0.016
2.03	0.204	0.311
2.35	0.250	
2.43		0.401
2.50	0.016	0.015
2.50	0.269	0.423
2.84	0.301	
2.84		0.500
3.07	0.016	0.015
3.07	0.334	0.549
3.42		0.601
3.50	0.015	0.015
3.50	0.373	0.612
3.91	0.401	
4.00	0.016	0.015
4.00	0.413	0.671
4.45		0.707
4.50	0.016	0.015
4.50	0.459	0.711
5.00	0.016	0.016
5.00	0.489	0.741
5.23	0.500	
6.00	0.017	0.016
6.00	0.552	0.788
6.33		0.801
6.88	0.601	
7.00	0.017	0.017
7.00	0.611	0.822
7.96		0.850
8.00	0.018	0.017
8.00	0.670	0.851
8.72	0.707	
10.00	0.019	0.019
10.00	0.782	0.884
10.47	0.801	

TSE5A EXPERIMENT (9-24-80) ZERO 2-D CRITICAL CRACK DEPTHS
KICTYP = 6, RTNDT0 = 0.0 DEGF, %CU = 0.000, F0 = 0.00E19

TIME	INITIATION	ARREST
11.29		0.900
11.74	0.850	
12.00	0.021	0.021
12.00	0.857	
14.00	0.023	0.023
14.00	0.885	
16.00	0.026	0.026
16.00	0.894	
16.52	0.026	
16.64		0.026
18.00	0.033	0.033
18.00	0.895	
20.00	0.043	0.042
20.00	0.891	
22.19		0.900
22.63	0.056	
22.78		0.056
25.00	0.076	0.074
25.00	0.859	0.872
25.12	0.076	
25.29		0.076
26.00	0.850	
27.14		0.850
27.17	0.101	
27.36		0.101
28.89	0.801	
29.44	0.150	
29.56		0.801
29.65		0.150
30.00	0.171	0.163
30.00	0.764	0.784

MAX ON INITIATION CURVE: A/W = 0.895, TIME = 18.00

MAX ON ARREST CURVE: A/W = 0.900, TIME = 22.19

Appendix F

DIGITAL OUTPUT FROM POSTTEST FRACTURE-MECHANICS ANALYSIS OF TSE-6

A standard set of OCA-P digital input-output for a posttest deterministic analysis of TSE-6, using small-specimen lower-bound K_J and mean K_{Ia} fracture-toughness curves, is included in this appendix. Values of K_I are for a two-dimensional axial flaw, and the English system of units is used throughout.

```
      TSE6    12/9/81     TO 3M 14S                                    OCA-P

FRACTURE TOUGHNESS CODE (IF KICTYP = 6 , VALUES
ARE READ IN & DESCRIBED LATER IN THIS RUN)    KICTYP =      6

MAX. # OF TIME INTERVALS TO BE READ           NCYCLE =     60

TIME INTERVAL # TO START PROCESSING DATA       ISKIP =      1

CRACK SHAPE TO BE USED                        ICRKTP =      1
  =1 2-D;   =2 2-D,2-M;   =3 6-1,2-M;
  =4 6/1,2-D,&2-M;   =5 6/1,2-D

REF TEMPERATURE FOR STRESS CALCULATIONS         TREF =     0.
  = 0 USE TEMP IN FIRST TIME INTERVAL

WRITE TABLE-1 FOR TEMPS,KIC,ETC.THRU CYL. WALL
  = -1 THEN STOP;     =  0 NO PRINTING;
  = +1 CONTINUE PROCESSING KI VALUES            NOPT =      0

UNITS SWITCH     =0 ENGLISH; =1 SI            ISISW =      0


TEMPERATURE PLOTTING
     = 0 NO PLOTS,      = 1 PLOT       NPLOT =     1
KI RATIO PLOTTING
     = 0 NO PLOTS,      = 1 PLOT      KRPLOT =     0
KI PLOTTING
      = 0 NO PLOTS,     = 1 PLOT       KIPLT =     0
ENVELOPE PLOTTING
      = 0 NO PLOTS,     = 1 PLOT      KENPLT =     1
STRESS/TEMP/KI/KIC/KIA PLOTTING
      = 0 NO PLOTS,     = 1 PLOT      KALPLT =     0


TIME DEPENDENT PRESSURES                  NPR   =     0

   SEQ.NO.     TIME     PRESSURE
             (MINUTES)    (KSI)

.......................................
```

RADIATION DAMAGE/RUN CONTROL

RADIATION DAMAGE CALC SWITCH	IRTNSW	=	0
ATTENUATION CONSTANT	ATTCON	=	0.2400
STRESS INPUT SWITCH 0=CALC BY FE METHOD, 1=INPUT ON UNIT3 0=DEEPEST POINT, 1=MAX ON CRACK FRONT	ISTRSW	=	0

INCIPIENT INITIATION SEARCH CONTROL

INCIPIENT INITIATION SEARCH SWITCH 0=NO SEARCH, 1=SEARCH, 2=PARAMETRIC SEARCH	IBINSW	=	0
FLAW SHAPE CONTROL SWITCH 0=LONG(2-D), 1=(6 TO 1) ELLIPITICAL	ISEASW	=	0
MIN A/W USED ON THRESHOLD SEARCH	AWMIN	=	0.0249
MAX A/W USED ON THRESHOLD SEARCH	AWMAX	=	0.1510
UPPER LIMIT ON THRESHOLD SEARCH	TUPLIM	=	0.50D+20

TOUGHNESS PROPERTIES(-1 MEANS NOT INPUT)

FLUENCE, INSIDE SURFACE	F0	=	0.000E+00
REFERENCE TEMP., INITIAL	RTNDT0	=	0.000
PER CENT CU	CUPER	=	0.000
PER CENT P	PPER	=	0.000
PER CENT NI	PERNI	=	0.000
DELTA RTNDT(INNER SURFACE)	DRTNIN	=	-999.0

FINITE ELEMENT PARAMETERS (STRESS CALCULATIONS)

GEOMETRIC MODELING METHOD
= 0 USER SPECIFIED NO. OF ELEMENTS + G.P FACTOR.
= 1 USER SPEC. NO. OF ELEM.& A/W OF CLADDING-
BASE METAL INTERFACE MODEL = 0

NUMBER OF ELEMENTS---------- NUMEL = 15

INTEGRATION ORDER(# GAUSS POINTS) NGAUSS = 2

NUMBER OF NODAL POINTS---------- NUMNP = 31

GEOM.PROG.FACTOR = 1.13

FE MESH NODAL POINT COORDINATES

NODAL POINT NO.	R-COORD. (INCHES)	NODAL POINT NO.	R-COORD. (INCHES)
1	16.500	16	16.914
2	16.510	17	16.978
3	16.522	18	17.050
4	16.535	19	17.132
5	16.550	20	17.224
6	16.566	21	17.328
7	16.585	22	17.446
8	16.606	23	17.579
9	16.631	24	17.730
10	16.658	25	17.900
11	16.688	26	18.092
12	16.723	27	18.310
13	16.762	28	18.555
14	16.807	29	18.832
15	16.857	30	19.146
		31	19.500

ELEMENT CONNECTIVITY

ELEM. NO.	NODE NUMBERS I	J	K	MATERIAL NO.
1	1	2	3	1
2	3	4	5	1
3	5	6	7	1
4	7	8	9	1
5	9	10	11	1
6	11	12	13	1
7	13	14	15	1
8	15	16	17	1
9	17	18	19	1
10	19	20	21	1
11	21	22	23	1
12	23	24	25	1
13	25	26	27	1
14	27	28	29	1
15	29	30	31	1

MATERIAL PROPERTIES FOR STRESS CALCULATIONS

NUMBER OF MATERIALS ------ 1

TEMP(DEG.F)	MODULUS OF ELASTICITY(KSI) - E (MAT 1)	(MAT 2)	(MAT 3)
70.0	2.800D+04	2.700D+04	0.000D+00

TEMP(DEG.F)	COEFF OF EXPANSION(PER DEG.F) - ALFA (MAT 1)	(MAT 2)	(MAT 3)
70.0	6.500D-06	9.930D-06	0.000D+00

TEMP(DEG.F)	POISSONS RATIO - PNU (MAT 1)	(MAT 2)	(MAT 3)
70.0	0.300	0.300	0.300

SELECTED TIME INTERVAL NUMBERS FOR KI CALCULATIONS

0	0	0	0	0	0	0	0	0	0
0	0	0	0	0	0	0	0	0	0
0	0	0	0	0	0	0	0	0	0
0	0	0	0	0	0	0	0	0	0
0	0	0	0	0	0	0	0	0	0
0	0	0	0	0	0	0	0	0	0
0									

CYLINDER DIMENSIONS (INCHES)

INNER RADIUS, RI = 16.500

OUTER RADIUS, RO = 19.500

WALL THICKNESS, W = 3.000

TEMPERATURE GRID GEOMETRY OVER CYLINDER WALL

GRID NO.	RADIUS
1	16.5000
2	16.5500
3	16.6000
4	16.7000
5	16.8000
6	17.0000
7	17.3000
8	17.7000
9	18.3000
10	19.2000
11	19.5000

*** KIC (OR KIA) VALUES WERE READ IN FROM UNIT 56

MATERIAL IDENTIFICATION =TOUGHNESS PER 2/19/85 PHONE CALL WITH RDC

SEQ.NO.	TEMP.	KIC VALUE
1	-148.	32.
2	-58.	38.
3	-13.	43.
4	32.	50.
5	77.	61.
6	122.	77.
7	167.	107.
8	212.	150.
9	235.	182.

SEQ.NO.	TEMP.	KIA VALUE
1	-94.	32.
2	-4.	38.
3	41.	43.
4	86.	50.
5	131.	61.
6	176.	77.
7	221.	106.
8	266.	150.
9	289.	182.

CALCULATED 2-D CRACK DEPTH VALUES =
0.0000 0.0299 0.0794 0.1676 0.2292 0.3044 0.4500 0.6044 0.7500 0.9035
1.2044 1.5000 1.8035 2.1221 2.4035 2.5500 2.7000 2.8551

REF TEMPERATURE FOR STRESS CALCULATIONS TREF = 203.0 DEG.F

TSE6 12/9/81 TO 3M 14S LONGIT. CRACK

KICTYP = 6, RTNDTO = 0.0 DEG., %CU = 0.000, FO =0.00E19

TEMPERATURE INTERVAL NUMBER = 1, TIME = 0.000 MIN., PRESSURE = 0.000 KSI

SEQ NO.	RADIUS IN.	DEPTH IN.	A/W	TEMPER. DEG.F	DLRTNDT DEG.F	CIRCUMF. STRESS KSI	KI	KIC	KI/KIC	KIA	KI/KIA	ELLIPTIC ANGLE
1	16.500	0.000	0.000	202.0	0.	0.31	0.00	138.54	0.000	92.58	0.000	
2	16.530	0.030	0.010	202.0	0.	0.31	0.10	138.53	0.001	92.58	0.001	
3	16.579	0.079	0.026	202.0	0.	0.31	0.16	138.55	0.001	92.59	0.002	
4	16.668	0.168	0.056	201.9	0.	0.33	0.25	138.44	0.002	92.52	0.003	
5	16.729	0.229	0.076	202.2	0.	0.25	0.29	138.80	0.002	92.74	0.003	
6	16.804	0.304	0.101	203.0	0.	0.04	0.26	139.68	0.002	93.28	0.003	
7	16.950	0.450	0.150	203.2	0.	0.01	0.20	139.82	0.001	93.36	0.002	
8	17.104	0.604	0.201	202.9	0.	0.08	0.24	139.48	0.002	93.16	0.003	
9	17.250	0.750	0.250	202.9	0.	0.06	0.27	139.59	0.002	93.22	0.003	
10	17.404	0.904	0.301	203.1	0.	0.03	0.29	139.71	0.002	93.30	0.003	
11	17.704	1.204	0.401	203.0	0.	0.05	0.35	139.64	0.003	93.25	0.004	
12	18.000	1.500	0.500	202.9	0.	0.08	0.48	139.50	0.003	93.17	0.005	
13	18.304	1.804	0.601	203.0	0.	0.04	0.62	139.65	0.004	93.26	0.007	
14	18.622	2.122	0.707	203.6	0.	-0.11	0.69	140.31	0.005	93.66	0.007	
15	18.904	2.404	0.801	204.1	0.	-0.24	0.64	140.86	0.005	94.00	0.007	
16	19.050	2.550	0.850	204.2	0.	-0.24	0.56	140.94	0.004	94.04	0.006	
17	19.200	2.700	0.900	204.0	0.	-0.18	0.47	140.76	0.003	93.94	0.005	
18	19.355	2.855	0.952	203.6	0.	-0.10	0.32	140.26	0.002	93.64	0.003	

TEMPERATURE INTERVAL NUMBER = 2, TIME = 0.167 MIN., PRESSURE = 0.000 KSI

1	16.500	0.000	0.000	127.0	0.	17.89	0.00	79.96	0.000	59.89	0.000	
2	16.530	0.030	0.010	132.4	0.	16.47	5.65	82.91	0.068	61.38	0.092	
3	16.579	0.079	0.026	141.4	0.	14.07	8.28	88.34	0.094	64.05	0.129	
4	16.668	0.168	0.056	154.9	0.	10.50	10.24	97.43	0.105	68.52	0.149	
5	16.729	0.229	0.076	162.6	0.	8.45	11.14	103.15	0.108	71.47	0.156	
6	16.804	0.304	0.101	171.5	0.	6.12	11.47	110.05	0.104	75.26	0.152	
7	16.950	0.450	0.150	184.7	0.	2.66	11.29	121.27	0.093	81.93	0.138	
8	17.104	0.604	0.201	193.3	0.	0.39	10.80	129.49	0.083	87.01	0.124	
9	17.250	0.750	0.250	197.9	0.	-0.80	10.45	134.18	0.078	89.90	0.116	
10	17.404	0.904	0.301	200.7	0.	-1.51	10.18	137.14	0.074	91.72	0.111	
11	17.704	1.204	0.401	203.0	0.	-2.07	10.41	139.66	0.075	93.27	0.112	
12	18.000	1.500	0.500	203.3	0.	-2.11	11.38	140.00	0.081	93.48	0.122	
13	18.304	1.804	0.601	203.0	0.	-1.99	12.76	139.64	0.091	93.25	0.137	
14	18.622	2.122	0.707	202.9	0.	-1.92	14.37	139.48	0.103	93.16	0.154	
15	18.904	2.404	0.801	202.9	0.	-1.90	14.97	139.54	0.107	93.20	0.161	
16	19.050	2.550	0.850	203.0	0.	-1.90	14.27	139.60	0.102	93.23	0.153	
17	19.200	2.700	0.900	203.0	0.	-1.89	12.39	139.64	0.089	93.26	0.133	
18	19.355	2.855	0.952	203.0	0.	-1.88	8.57	139.65	0.061	93.26	0.092	

TSE6 12/9/81 TO 3M 14S LONGIT. CRACK

KICTYP = 6, RTNDTO = 0.0 DEG., %CU = 0.000, FO =0.00E19

TEMPERATURE INTERVAL NUMBER = 3, TIME = 0.333 MIN., PRESSURE = 0.000 KSI

SEQ NO.	RADIUS IN.	DEPTH IN.	A/W	TEMPER. DEG.F	DLRTNDT DEG.F	CIRCUMF. STRESS KSI	KI	KIC	KI/KIC	KIA	KI/KIA	ELLIPTIC ANGLE
1	16.500	0.000	0.000	74.0	0.	29.09	0.00	60.16	0.000	47.82	0.000	
2	16.530	0.030	0.010	83.6	0.	26.54	9.14	62.91	0.145	49.63	0.184	
3	16.579	0.079	0.026	99.1	0.	22.44	13.30	67.86	0.196	52.89	0.251	
4	16.668	0.168	0.056	120.6	0.	16.74	16.37	76.72	0.213	58.16	0.281	
5	16.729	0.229	0.076	129.8	0.	14.29	17.97	81.48	0.221	60.67	0.296	
6	16.804	0.304	0.101	137.4	0.	12.25	19.24	85.89	0.224	62.86	0.306	
7	16.950	0.450	0.150	153.5	0.	7.98	20.67	96.48	0.214	68.04	0.304	
8	17.104	0.604	0.201	168.8	0.	3.97	21.18	107.90	0.196	74.05	0.286	
9	17.250	0.750	0.250	179.2	0.	1.26	21.45	116.42	0.184	78.98	0.272	
10	17.404	0.904	0.301	187.0	0.	-0.78	21.50	123.41	0.174	83.24	0.258	
11	17.704	1.204	0.401	196.1	0.	-3.10	22.53	132.27	0.170	88.73	0.254	
12	18.000	1.500	0.500	200.3	0.	-4.12	24.61	136.68	0.180	91.44	0.269	
13	18.304	1.804	0.601	202.0	0.	-4.49	27.29	138.55	0.197	92.59	0.295	
14	18.622	2.122	0.707	202.8	0.	-4.60	30.42	139.37	0.218	93.09	0.327	
15	18.904	2.404	0.801	203.0	0.	-4.59	31.57	139.62	0.226	93.24	0.339	
16	19.050	2.550	0.850	203.0	0.	-4.56	30.07	139.64	0.215	93.26	0.322	
17	19.200	2.700	0.900	203.0	0.	-4.52	26.11	139.64	0.187	93.26	0.280	
18	19.355	2.855	0.952	203.0	0.	-4.48	18.06	139.64	0.129	93.26	0.194	

TEMPERATURE INTERVAL NUMBER = 4, TIME = 0.500 MIN., PRESSURE = 0.000 KSI

SEQ NO.	RADIUS IN.	DEPTH IN.	A/W	TEMPER. DEG.F	DLRTNDT DEG.F	CIRCUMF. STRESS KSI	KI	KIC	KI/KIC	KIA	KI/KIA	ELLIPTIC ANGLE
1	16.500	0.000	0.000	41.0	0.	34.99	0.00	51.99	0.000	42.80	0.000	
2	16.530	0.030	0.010	49.4	0.	32.74	11.16	53.89	0.207	43.92	0.254	
3	16.579	0.079	0.026	63.0	0.	29.13	16.67	57.21	0.291	45.94	0.363	
4	16.668	0.168	0.056	81.0	0.	24.30	21.72	62.14	0.350	49.12	0.442	
5	16.729	0.229	0.076	93.2	0.	21.03	24.50	65.89	0.372	51.60	0.475	
6	16.804	0.304	0.101	109.9	0.	16.63	26.16	71.95	0.363	55.43	0.472	
7	16.950	0.450	0.150	130.1	0.	11.24	27.95	81.66	0.342	60.76	0.460	
8	17.104	0.604	0.201	145.1	0.	7.26	29.60	90.76	0.326	65.22	0.454	
9	17.250	0.750	0.250	158.8	0.	3.68	30.78	100.25	0.307	69.95	0.440	
10	17.404	0.904	0.301	170.7	0.	0.57	31.39	109.42	0.287	74.90	0.419	
11	17.704	1.204	0.401	186.2	0.	-3.42	33.52	122.65	0.273	82.78	0.405	
12	18.000	1.500	0.500	194.6	0.	-5.51	36.83	130.73	0.282	87.77	0.420	
13	18.304	1.804	0.601	199.0	0.	-6.57	40.83	135.34	0.302	90.62	0.451	
14	18.622	2.122	0.707	201.5	0.	-7.09	45.36	138.04	0.329	92.28	0.492	
15	18.904	2.404	0.801	202.6	0.	-7.26	46.98	139.22	0.337	93.00	0.505	
16	19.050	2.550	0.850	202.9	0.	-7.27	44.72	139.51	0.321	93.18	0.480	
17	19.200	2.700	0.900	203.0	0.	-7.24	38.86	139.64	0.278	93.26	0.417	
18	19.355	2.855	0.952	203.0	0.	-7.19	26.89	139.67	0.193	93.27	0.288	

TSE6 12/9/81 TO 3M 14S LONGIT. CRACK

KICTYP = 6, RTNDTO = 0.0 DEG., %CU = 0.000, FO =0.00E19

TEMPERATURE INTERVAL NUMBER = 5, TIME = 0.667 MIN., PRESSURE = 0.000 KSI

SEQ NO.	RADIUS IN.	DEPTH IN.	A/W	TEMPER. DEG.F	DLRTNDT DEG.F	CIRCUMF. STRESS KSI	KI	KIC	KI/KIC	KIA	KI/KIA	ELLIPTIC ANGLE
1	16.500	0.000	0.000	11.0	0.	39.98	0.00	46.28	0.000	39.53	0.000	
2	16.530	0.030	0.010	19.3	0.	37.75	12.82	47.70	0.269	40.34	0.318	
3	16.579	0.079	0.026	33.4	0.	33.97	19.28	50.39	0.383	41.88	0.460	
4	16.668	0.168	0.056	53.3	0.	28.63	25.32	54.82	0.462	44.48	0.569	
5	16.729	0.229	0.076	64.1	0.	25.75	28.85	57.50	0.502	46.12	0.625	
6	16.804	0.304	0.101	77.9	0.	22.04	31.58	61.25	0.516	48.53	0.651	
7	16.950	0.450	0.150	108.1	0.	14.05	34.26	71.22	0.481	54.99	0.623	
8	17.104	0.604	0.201	129.9	0.	8.27	35.67	81.54	0.437	60.70	0.588	
9	17.250	0.750	0.250	140.0	0.	5.60	37.57	87.48	0.429	63.63	0.590	
10	17.404	0.904	0.301	150.2	0.	2.92	39.38	94.16	0.418	66.88	0.589	
11	17.704	1.204	0.401	173.3	0.	-3.06	43.07	111.52	0.386	76.10	0.566	
12	18.000	1.500	0.500	187.3	0.	-6.61	47.31	123.69	0.383	83.42	0.567	
13	18.304	1.804	0.601	194.1	0.	-8.24	52.43	130.21	0.403	87.45	0.600	
14	18.622	2.122	0.707	198.2	0.	-9.14	58.24	134.44	0.433	90.07	0.647	
15	18.904	2.404	0.801	200.5	0.	-9.60	60.34	136.90	0.441	91.58	0.659	
16	19.050	2.550	0.850	201.3	0.	-9.74	57.44	137.81	0.417	92.14	0.623	
17	19.200	2.700	0.900	202.0	0.	-9.83	49.92	138.54	0.360	92.58	0.539	
18	19.355	2.855	0.952	202.6	0.	-9.90	34.53	139.14	0.248	92.95	0.371	

TEMPERATURE INTERVAL NUMBER = 6, TIME = 0.833 MIN., PRESSURE = 0.000 KSI

1	16.500	0.000	0.000	-16.0	0.	44.02	0.00	42.43	0.000	37.22	0.000	
2	16.530	0.030	0.010	-7.7	0.	41.78	14.16	43.50	0.325	37.89	0.374	
3	16.579	0.079	0.026	6.4	0.	37.99	21.42	45.54	0.470	39.11	0.548	
4	16.668	0.168	0.056	26.9	0.	32.50	28.39	49.09	0.578	41.14	0.690	
5	16.729	0.229	0.076	38.6	0.	29.34	32.48	51.46	0.631	42.50	0.764	
6	16.804	0.304	0.101	52.8	0.	25.51	35.72	54.69	0.653	44.40	0.805	
7	16.950	0.450	0.150	77.9	0.	18.80	39.98	61.26	0.653	48.53	0.824	
8	17.104	0.604	0.201	102.4	0.	12.30	43.04	69.06	0.623	53.65	0.802	
9	17.250	0.750	0.250	122.9	0.	6.89	45.20	77.87	0.581	58.78	0.769	
10	17.404	0.904	0.301	139.6	0.	2.53	46.59	87.20	0.534	63.49	0.734	
11	17.704	1.204	0.401	160.2	0.	-2.83	51.16	101.35	0.505	70.52	0.725	
12	18.000	1.500	0.500	175.4	0.	-6.66	57.29	113.24	0.506	77.10	0.743	
13	18.304	1.804	0.601	187.1	0.	-9.55	63.72	123.52	0.516	83.31	0.765	
14	18.622	2.122	0.707	194.4	0.	-11.27	70.58	130.60	0.540	87.69	0.805	
15	18.904	2.404	0.801	197.9	0.	-11.97	73.00	134.11	0.544	89.86	0.812	
16	19.050	2.550	0.850	199.0	0.	-12.18	69.48	135.31	0.513	90.60	0.767	
17	19.200	2.700	0.900	200.0	0.	-12.35	60.39	136.37	0.443	91.25	0.662	
18	19.355	2.855	0.952	201.0	0.	-12.50	41.78	137.47	0.304	91.93	0.454	

TSE6 12/9/81 TO 3M 14S LONGIT. CRACK

KICTYP = 6, RTNDTO = 0.0 DEG., %CU = 0.000, FO =0.00E19

TEMPERATURE INTERVAL NUMBER = 7, TIME = 1.000 MIN., PRESSURE = 0.000 KSI

SEQ NO.	RADIUS IN.	DEPTH IN.	A/W	TEMPER. DEG.F	DLRTNDT DEG.F	CIRCUMF. STRESS KSI	KI	KIC	KI/KIC	KIA	KI/KIA	ELLIPTIC ANGLE
1	16.500	0.000	0.000	-42.0	0.	47.79	0.00	39.63	0.000	35.29	0.000	
2	16.530	0.030	0.010	-33.0	0.	45.36	15.37	40.52	0.379	35.93	0.428	
3	16.579	0.079	0.026	-18.5	0.	41.48	23.29	42.12	0.553	37.02	0.629	
4	16.668	0.168	0.056	2.4	0.	35.83	31.07	44.93	0.691	38.75	0.802	
5	16.729	0.229	0.076	14.9	0.	32.45	35.64	46.93	0.759	39.91	0.893	
6	16.804	0.304	0.101	29.9	0.	28.44	39.32	49.67	0.792	41.47	0.948	
7	16.950	0.450	0.150	56.3	0.	21.34	44.29	55.55	0.797	44.92	0.986	
8	17.104	0.604	0.201	82.8	0.	14.31	47.98	62.66	0.766	49.46	0.970	
9	17.250	0.750	0.250	105.3	0.	8.36	50.64	70.16	0.722	54.34	0.932	
10	17.404	0.904	0.301	123.6	0.	3.58	52.44	78.18	0.671	58.95	0.890	
11	17.704	1.204	0.401	146.3	0.	-2.32	58.14	91.50	0.635	65.59	0.887	
12	18.000	1.500	0.500	164.2	0.	-6.89	65.51	104.37	0.628	72.11	0.908	
13	18.304	1.804	0.601	179.1	0.	-10.59	73.01	116.41	0.627	78.98	0.924	
14	18.622	2.122	0.707	188.9	0.	-12.92	80.85	125.20	0.646	84.35	0.959	
15	18.904	2.404	0.801	193.8	0.	-13.96	83.57	129.91	0.643	87.26	0.958	
16	19.050	2.550	0.850	195.5	0.	-14.31	79.52	131.64	0.604	88.34	0.900	
17	19.200	2.700	0.900	197.0	0.	-14.60	69.11	133.21	0.519	89.31	0.774	
18	19.355	2.855	0.952	198.5	0.	-14.86	47.82	134.83	0.355	90.30	0.530	

TEMPERATURE INTERVAL NUMBER = 8, TIME = 1.133 MIN., PRESSURE = 0.000 KSI

1	16.500	0.000	0.000	-62.0	0.	50.38	0.00	37.87	0.000	33.94	0.000	
2	16.530	0.030	0.010	-53.1	0.	47.97	16.23	38.62	0.420	34.53	0.470	
3	16.579	0.079	0.026	-38.0	0.	43.91	24.65	40.01	0.616	35.57	0.693	
4	16.668	0.168	0.056	-15.7	0.	37.90	32.86	42.46	0.774	37.24	0.882	
5	16.729	0.229	0.076	-3.1	0.	34.49	37.73	44.13	0.855	38.28	0.986	
6	16.804	0.304	0.101	11.9	0.	30.46	41.74	46.42	0.899	39.61	1.054	
7	16.950	0.450	0.150	39.3	0.	23.11	47.24	51.62	0.915	42.58	1.109	
8	17.104	0.604	0.201	64.8	0.	16.32	51.59	57.68	0.894	46.24	1.116	
9	17.250	0.750	0.250	85.4	0.	10.84	55.25	63.45	0.871	49.99	1.105	
10	17.404	0.904	0.301	104.9	0.	5.72	57.96	69.99	0.828	54.23	1.069	
11	17.704	1.204	0.401	136.4	0.	-2.47	64.28	85.26	0.754	62.55	1.028	
12	18.000	1.500	0.500	157.7	0.	-7.90	71.89	99.46	0.723	69.55	1.034	
13	18.304	1.804	0.601	172.1	0.	-11.48	80.20	110.58	0.725	75.56	1.061	
14	18.622	2.122	0.707	182.6	0.	-13.95	89.10	119.41	0.746	80.79	1.103	
15	18.904	2.404	0.801	189.1	0.	-15.41	92.21	125.34	0.736	84.44	1.092	
16	19.050	2.550	0.850	191.7	0.	-15.96	87.75	127.87	0.686	86.00	1.020	
17	19.200	2.700	0.900	194.0	0.	-16.43	76.26	130.16	0.586	87.42	0.872	
18	19.355	2.855	0.952	196.1	0.	-16.86	52.77	132.32	0.399	88.75	0.595	

TSE6 12/9/81 TO 3M 14S LONGIT. CRACK

KICTYP = 6, RTNDTO = 0.0 DEG., %CU = 0.000, FO =0.00E19

TEMPERATURE INTERVAL NUMBER = 9, TIME = 1.167 MIN., PRESSURE = 0.000 KSI

SEQ NO.	RADIUS IN.	DEPTH IN.	A/W	TEMPER. DEG.F	DLRTNDT DEG.F	CIRCUMF. STRESS KSI	KI	KIC	KI/KIC	KIA	KI/KIA	ELLIPTIC ANGLE
1	16.500	0.000	0.000	-66.0	0.	50.84	0.00	37.54	0.000	33.68	0.000	
2	16.530	0.030	0.010	-57.1	0.	48.44	16.39	38.28	0.428	34.26	0.478	
3	16.579	0.079	0.026	-42.0	0.	44.38	24.89	39.63	0.628	35.29	0.705	
4	16.668	0.168	0.056	-19.7	0.	38.36	33.22	41.98	0.791	36.93	0.899	
5	16.729	0.229	0.076	-7.1	0.	34.95	38.17	43.58	0.876	37.94	1.006	
6	16.804	0.304	0.101	7.9	0.	30.92	42.25	45.77	0.923	39.24	1.077	
7	16.950	0.450	0.150	35.3	0.	23.55	47.89	50.78	0.943	42.10	1.137	
8	17.104	0.604	0.201	60.6	0.	16.80	52.41	56.62	0.926	45.58	1.150	
9	17.250	0.750	0.250	81.3	0.	11.32	56.25	62.23	0.904	49.18	1.144	
10	17.404	0.904	0.301	101.5	0.	5.99	59.07	68.73	0.859	53.45	1.105	
11	17.704	1.204	0.401	135.4	0.	-2.81	65.29	84.68	0.771	62.26	1.049	
12	18.000	1.500	0.500	156.8	0.	-8.25	72.79	98.79	0.737	69.20	1.052	
13	18.304	1.804	0.601	170.1	0.	-11.55	81.29	108.97	0.746	74.64	1.089	
14	18.622	2.122	0.707	180.5	0.	-13.99	90.48	117.56	0.770	79.67	1.136	
15	18.904	2.404	0.801	187.5	0.	-15.60	93.68	123.89	0.756	83.54	1.121	
16	19.050	2.550	0.850	190.5	0.	-16.22	89.15	126.69	0.704	85.27	1.045	
17	19.200	2.700	0.900	193.0	0.	-16.73	77.47	129.16	0.600	86.80	0.892	
18	19.355	2.855	0.952	195.2	0.	-17.20	53.60	131.35	0.408	88.16	0.608	

TEMPERATURE INTERVAL NUMBER = 10, TIME = 1.333 MIN., PRESSURE = 0.000 KSI

SEQ NO.	RADIUS IN.	DEPTH IN.	A/W	TEMPER. DEG.F	DLRTNDT DEG.F	CIRCUMF. STRESS KSI	KI	KIC	KI/KIC	KIA	KI/KIA	ELLIPTIC ANGLE
1	16.500	0.000	0.000	-90.0	0.	54.12	0.00	35.71	0.000	32.15	0.000	
2	16.530	0.030	0.010	-81.2	0.	51.74	17.48	36.36	0.481	32.71	0.534	
3	16.579	0.079	0.026	-65.4	0.	47.49	26.60	37.59	0.708	33.72	0.789	
4	16.668	0.168	0.056	-42.7	0.	41.35	35.59	39.56	0.900	35.24	1.010	
5	16.729	0.229	0.076	-29.7	0.	37.83	41.02	40.86	1.004	36.17	1.134	
6	16.804	0.304	0.101	-13.0	0.	33.34	45.44	42.80	1.062	37.46	1.213	
7	16.950	0.450	0.150	16.1	0.	25.52	51.54	47.13	1.094	40.02	1.288	
8	17.104	0.604	0.201	42.0	0.	18.58	56.64	52.21	1.085	42.93	1.319	
9	17.250	0.750	0.250	63.7	0.	12.83	61.06	57.41	1.064	46.07	1.325	
10	17.404	0.904	0.301	86.2	0.	6.91	64.26	63.67	1.009	50.14	1.282	
11	17.704	1.204	0.401	125.5	0.	-3.30	70.81	79.16	0.895	59.47	1.191	
12	18.000	1.500	0.500	148.3	0.	-9.11	78.74	92.84	0.848	66.24	1.189	
13	18.304	1.804	0.601	161.1	0.	-12.26	88.14	102.01	0.864	70.86	1.244	
14	18.622	2.122	0.707	172.2	0.	-14.88	98.38	110.65	0.889	75.60	1.301	
15	18.904	2.404	0.801	180.9	0.	-16.89	101.97	117.90	0.865	79.88	1.277	
16	19.050	2.550	0.850	184.7	0.	-17.71	97.04	121.30	0.800	81.95	1.184	
17	19.200	2.700	0.900	188.0	0.	-18.40	84.33	124.35	0.678	83.82	1.006	
18	19.355	2.855	0.952	190.8	0.	-19.03	58.34	126.98	0.459	85.45	0.683	

TSE6 12/9/81 TO 3M 14S LONGIT. CRACK

KICTYP = 6, RTNDTO = 0.0 DEG., %CU = 0.000, FO =0.00E19

SEQ NO.	RADIUS IN.	DEPTH IN.	A/W	TEMPER. DEG.F	DLRTNDT DEG.F	CIRCUMF. STRESS KSI	KI	KIC	KI/KIC	KIA	KI/KIA	ELLIPTIC ANGLE
TEMPERATURE INTERVAL NUMBER = 11, TIME = 1.500 MIN., PRESSURE = 0.000 KSI												
1	16.500	0.000	0.000	-113.0	0.	56.67	0.00	34.14	0.000	31.90	0.000	
2	16.530	0.030	0.010	-103.4	0.	54.06	18.28	34.78	0.526	31.90	0.573	
3	16.579	0.079	0.026	-88.0	0.	49.91	27.85	35.86	0.777	32.28	0.863	
4	16.668	0.168	0.056	-64.5	0.	43.57	37.44	37.66	0.994	33.77	1.109	
5	16.729	0.229	0.076	-50.4	0.	39.74	43.11	38.86	1.109	34.71	1.242	
6	16.804	0.304	0.101	-34.1	0.	35.33	47.83	40.41	1.184	35.85	1.334	
7	16.950	0.450	0.150	-4.4	0.	27.36	54.51	43.94	1.241	38.16	1.428	
8	17.104	0.604	0.201	23.3	0.	19.96	60.03	48.41	1.240	40.75	1.473	
9	17.250	0.750	0.250	46.4	0.	13.81	64.76	53.19	1.217	43.51	1.488	
10	17.404	0.904	0.301	69.4	0.	7.75	68.30	58.91	1.159	47.01	1.453	
11	17.704	1.204	0.401	108.5	0.	-2.42	76.00	71.39	1.065	55.09	1.380	
12	18.000	1.500	0.500	133.7	0.	-8.85	85.16	83.67	1.018	61.76	1.379	
13	18.304	1.804	0.601	150.2	0.	-12.94	95.43	94.13	1.014	66.87	1.427	
14	18.622	2.122	0.707	163.7	0.	-16.17	106.41	103.93	1.024	71.88	1.480	
15	18.904	2.404	0.801	173.5	0.	-18.47	110.25	111.72	0.987	76.21	1.447	
16	19.050	2.550	0.850	178.0	0.	-19.45	104.93	115.40	0.909	78.37	1.339	
17	19.200	2.700	0.900	182.0	0.	-20.33	91.18	118.90	0.767	80.48	1.133	
18	19.355	2.855	0.952	185.7	0.	-21.17	63.11	122.25	0.516	82.53	0.765	
TEMPERATURE INTERVAL NUMBER = 12, TIME = 1.667 MIN., PRESSURE = 0.000 KSI												
1	16.500	0.000	0.000	-135.0	0.	58.90	0.00	32.72	0.000	31.90	0.000	
2	16.530	0.030	0.010	-125.5	0.	56.32	19.02	33.32	0.571	31.90	0.596	
3	16.579	0.079	0.026	-109.4	0.	51.98	29.01	34.37	0.844	31.90	0.909	
4	16.668	0.168	0.056	-85.4	0.	45.49	39.00	36.05	1.082	32.44	1.202	
5	16.729	0.229	0.076	-71.3	0.	41.65	44.99	37.12	1.212	33.34	1.349	
6	16.804	0.304	0.101	-54.0	0.	36.99	49.96	38.54	1.296	34.47	1.449	
7	16.950	0.450	0.150	-23.6	0.	28.81	57.02	41.53	1.373	36.63	1.557	
8	17.104	0.604	0.201	5.0	0.	21.17	62.93	45.32	1.389	38.98	1.614	
9	17.250	0.750	0.250	29.2	0.	14.72	67.98	49.55	1.372	41.40	1.642	
10	17.404	0.904	0.301	52.3	0.	8.63	71.86	54.57	1.317	44.33	1.621	
11	17.704	1.204	0.401	90.5	0.	-1.33	80.84	65.00	1.244	51.02	1.584	
12	18.000	1.500	0.500	119.0	0.	-8.64	91.15	75.98	1.200	57.75	1.578	
13	18.304	1.804	0.601	140.2	0.	-13.93	101.93	87.59	1.164	63.68	1.601	
14	18.622	2.122	0.707	155.3	0.	-17.56	113.34	97.72	1.160	68.66	1.651	
15	18.904	2.404	0.801	164.9	0.	-19.77	117.46	104.90	1.120	72.40	1.622	
16	19.050	2.550	0.850	169.4	0.	-20.79	111.88	108.38	1.032	74.31	1.505	
17	19.200	2.700	0.900	174.0	0.	-21.84	97.28	112.10	0.868	76.43	1.273	
18	19.355	2.855	0.952	179.1	0.	-22.93	67.34	116.36	0.579	78.95	0.853	

TSE6 12/9/81 TO 3M 14S LONGIT. CRACK

KICTYP = 6, RTNDTO = 0.0 DEG., %CU = 0.000, FO =0.00E19

TEMPERATURE INTERVAL NUMBER = 13, TIME = 1.833 MIN., PRESSURE = 0.000 KSI

SEQ NO.	RADIUS IN.	DEPTH IN.	A/W	TEMPER. DEG.F	DLRTNDT DEG.F	CIRCUMF. STRESS KSI	KI	KIC	KI/KIC	KIA	KI/KIA	ELLIPTIC ANGLE
1	16.500	0.000	0.000	-155.0	0.	61.09	0.00	31.90	0.000	31.90	0.000	
2	16.530	0.030	0.010	-145.4	0.	58.47	19.74	32.07	0.616	31.90	0.619	
3	16.579	0.079	0.026	-130.0	0.	54.32	30.18	33.03	0.914	31.90	0.946	
4	16.668	0.168	0.056	-105.9	0.	47.79	40.79	34.61	1.179	31.90	1.279	
5	16.729	0.229	0.076	-91.1	0.	43.76	47.09	35.64	1.321	32.08	1.468	
6	16.804	0.304	0.101	-74.0	0.	39.14	52.41	36.91	1.420	33.16	1.580	
7	16.950	0.450	0.150	-42.2	0.	30.58	60.01	39.61	1.515	35.27	1.701	
8	17.104	0.604	0.201	-12.3	0.	22.58	66.33	42.89	1.547	37.51	1.768	
9	17.250	0.750	0.250	12.1	0.	16.07	71.87	46.46	1.547	39.64	1.813	
10	17.404	0.904	0.301	35.7	0.	9.85	76.26	50.85	1.500	42.14	1.810	
11	17.704	1.204	0.401	76.5	0.	-0.82	86.22	60.87	1.416	48.28	1.786	
12	18.000	1.500	0.500	108.9	0.	-9.13	97.22	71.57	1.358	55.20	1.761	
13	18.304	1.804	0.601	133.2	0.	-15.21	108.37	83.41	1.299	61.63	1.758	
14	18.622	2.122	0.707	149.1	0.	-19.02	120.20	93.38	1.287	66.51	1.807	
15	18.904	2.404	0.801	158.2	0.	-21.06	124.53	99.84	1.247	69.74	1.786	
16	19.050	2.550	0.850	162.4	0.	-22.04	118.64	102.96	1.152	71.37	1.662	
17	19.200	2.700	0.900	167.0	0.	-23.10	103.18	106.50	0.969	73.27	1.408	
18	19.355	2.855	0.952	172.5	0.	-24.23	71.44	110.86	0.644	75.72	0.943	

TEMPERATURE INTERVAL NUMBER = 14, TIME = 2.000 MIN., PRESSURE = 0.000 KSI

1	16.500	0.000	0.000	-175.0	0.	63.09	0.00	31.90	0.000	31.90	0.000	
2	16.530	0.030	0.010	-165.5	0.	60.50	20.41	31.90	0.640	31.90	0.640	
3	16.579	0.079	0.026	-149.4	0.	56.16	31.22	31.90	0.979	31.90	0.979	
4	16.668	0.168	0.056	-124.7	0.	49.46	42.17	33.37	1.264	31.90	1.322	
5	16.729	0.229	0.076	-110.2	0.	45.50	48.76	34.32	1.421	31.90	1.529	
6	16.804	0.304	0.101	-93.0	0.	40.84	54.37	35.50	1.531	31.96	1.701	
7	16.950	0.450	0.150	-60.5	0.	32.10	62.43	37.99	1.643	34.03	1.834	
8	17.104	0.604	0.201	-29.6	0.	23.80	69.14	40.88	1.691	36.18	1.911	
9	17.250	0.750	0.250	-4.1	0.	17.02	75.01	43.99	1.705	38.19	1.964	
10	17.404	0.904	0.301	19.9	0.	10.66	79.72	47.81	1.668	40.41	1.973	
11	17.704	1.204	0.401	61.6	0.	-0.22	90.59	56.86	1.593	45.73	1.981	
12	18.000	1.500	0.500	97.4	0.	-9.43	102.28	67.29	1.520	52.52	1.947	
13	18.304	1.804	0.601	125.3	0.	-16.40	113.62	79.04	1.437	59.41	1.913	
14	18.622	2.122	0.707	141.3	0.	-20.25	125.71	88.27	1.424	64.01	1.964	
15	18.904	2.404	0.801	149.2	0.	-21.94	130.35	93.45	1.395	66.54	1.959	
16	19.050	2.550	0.850	153.1	0.	-22.88	124.29	96.14	1.293	67.87	1.831	
17	19.200	2.700	0.900	158.0	0.	-24.07	108.17	99.69	1.085	69.66	1.553	
18	19.355	2.855	0.952	164.8	0.	-25.43	74.90	104.77	0.715	72.33	1.036	

TSE6 12/9/81 TO 3M 14S LONGIT. CRACK

KICTYP = 6, RTNDTO = 0.0 DEG., %CU = 0.000, FO =0.00E19

TEMPERATURE INTERVAL NUMBER = 15, TIME = 2.167 MIN., PRESSURE = 0.000 KSI

SEQ NO.	RADIUS IN.	DEPTH IN.	A/W	TEMPER. DEG.F	DLRTNDT DEG.F	CIRCUMF. STRESS KSI	KI	KIC	KI/KIC	KIA	KI/KIA	ELLIPTIC ANGLE
1	16.500	0.000	0.000	-192.0	0.	64.08	0.00	31.90	0.000	31.90	0.000	
2	16.530	0.030	0.010	-182.5	0.	61.49	20.74	31.90	0.650	31.90	0.650	
3	16.579	0.079	0.026	-166.4	0.	57.13	31.74	31.90	0.995	31.90	0.995	
4	16.668	0.168	0.056	-142.5	0.	50.64	42.98	32.25	1.333	31.90	1.347	
5	16.729	0.229	0.076	-128.1	0.	46.71	49.81	33.16	1.502	31.90	1.561	
6	16.804	0.304	0.101	-109.9	0.	41.80	55.56	34.34	1.618	31.90	1.742	
7	16.950	0.450	0.150	-76.6	0.	32.81	63.77	36.71	1.737	33.00	1.932	
8	17.104	0.604	0.201	-45.6	0.	24.52	70.71	39.29	1.800	35.04	2.018	
9	17.250	0.750	0.250	-20.2	0.	17.74	76.86	41.92	1.833	36.89	2.083	
10	17.404	0.904	0.301	4.3	0.	11.26	81.82	45.22	1.810	38.92	2.102	
11	17.704	1.204	0.401	47.6	0.	-0.06	93.07	53.47	1.741	43.67	2.131	
12	18.000	1.500	0.500	84.1	0.	-9.44	105.19	63.05	1.668	49.72	2.116	
13	18.304	1.804	0.601	112.3	0.	-16.50	117.12	72.94	1.606	56.02	2.091	
14	18.622	2.122	0.707	129.4	0.	-20.64	129.79	81.27	1.597	60.56	2.143	
15	18.904	2.404	0.801	138.8	0.	-22.69	134.61	86.70	1.553	63.25	2.128	
16	19.050	2.550	0.850	143.4	0.	-23.81	128.34	89.61	1.432	64.66	1.985	
17	19.200	2.700	0.900	149.0	0.	-25.16	111.69	93.33	1.197	66.48	1.680	
18	19.355	2.855	0.952	156.3	0.	-26.67	77.34	98.47	0.785	69.04	1.120	

TEMPERATURE INTERVAL NUMBER = 16, TIME = 2.267 MIN., PRESSURE = 0.000 KSI

1	16.500	0.000	0.000	-201.0	0.	64.07	0.00	31.90	0.000	31.90	0.000	
2	16.530	0.030	0.010	-191.4	0.	61.45	20.73	31.90	0.650	31.90	0.650	
3	16.579	0.079	0.026	-176.0	0.	57.28	31.76	31.90	0.995	31.90	0.995	
4	16.668	0.168	0.056	-152.0	0.	50.76	43.09	31.90	1.351	31.90	1.351	
5	16.729	0.229	0.076	-136.9	0.	46.65	49.86	32.60	1.530	31.90	1.563	
6	16.804	0.304	0.101	-119.0	0.	41.80	55.60	33.74	1.648	31.90	1.743	
7	16.950	0.450	0.150	-86.4	0.	33.02	63.90	35.97	1.776	32.38	1.974	
8	17.104	0.604	0.201	-55.5	0.	24.74	70.95	38.41	1.847	34.37	2.065	
9	17.250	0.750	0.250	-29.5	0.	17.80	77.10	40.89	1.886	36.19	2.130	
10	17.404	0.904	0.301	-4.1	0.	11.10	81.98	43.98	1.864	38.19	2.147	
11	17.704	1.204	0.401	39.6	0.	-0.32	93.01	51.68	1.800	42.62	2.182	
12	18.000	1.500	0.500	74.1	0.	-9.19	105.27	60.19	1.749	47.84	2.201	
13	18.304	1.804	0.601	100.2	0.	-15.74	117.80	68.28	1.725	53.16	2.216	
14	18.622	2.122	0.707	118.2	0.	-20.09	131.13	75.59	1.735	57.54	2.279	
15	18.904	2.404	0.801	130.0	0.	-22.79	136.16	81.57	1.669	60.71	2.243	
16	19.050	2.550	0.850	136.0	0.	-24.25	129.82	85.05	1.526	62.44	2.079	
17	19.200	2.700	0.900	143.0	0.	-25.93	112.96	89.36	1.264	64.54	1.750	
18	19.355	2.855	0.952	151.4	0.	-27.76	78.23	95.01	0.823	67.31	1.162	

TSE6 12/9/81 TO 3M 14S LONGIT. CRACK

KICTYP = 6, RTNDTO = 0.0 DEG., %CU = 0.000, FO =0.00E19

TEMPERATURE INTERVAL NUMBER = 17, TIME = 2.300 MIN., PRESSURE = 0.000 KSI

SEQ NO.	RADIUS IN.	DEPTH IN.	A/W	TEMPER. DEG.F	DLRTNDT DEG.F	CIRCUMF. STRESS KSI	KI	KIC	KI/KIC	KIA	KI/KIA	ELLIPTIC ANGLE
1	16.500	0.000	0.000	-204.0	0.	64.14	0.00	31.90	0.000	31.90	0.000	
2	16.530	0.030	0.010	-194.4	0.	61.52	20.75	31.90	0.651	31.90	0.651	
3	16.579	0.079	0.026	-179.0	0.	57.35	31.79	31.90	0.997	31.90	0.997	
4	16.668	0.168	0.056	-155.0	0.	50.83	43.14	31.90	1.352	31.90	1.352	
5	16.729	0.229	0.076	-139.9	0.	46.71	49.93	32.41	1.540	31.90	1.565	
6	16.804	0.304	0.101	-122.0	0.	41.86	55.67	33.55	1.659	31.90	1.745	
7	16.950	0.450	0.150	-89.4	0.	33.09	64.00	35.76	1.790	32.19	1.988	
8	17.104	0.604	0.201	-58.5	0.	24.81	71.07	38.15	1.863	34.17	2.080	
9	17.250	0.750	0.250	-32.5	0.	17.86	77.25	40.57	1.904	35.97	2.147	
10	17.404	0.904	0.301	-7.1	0.	11.17	82.15	43.57	1.886	37.94	2.166	
11	17.704	1.204	0.401	36.6	0.	-0.26	93.24	51.04	1.827	42.25	2.207	
12	18.000	1.500	0.500	71.0	0.	-9.11	105.60	59.35	1.779	47.30	2.233	
13	18.304	1.804	0.601	97.3	0.	-15.68	118.25	67.23	1.759	52.48	2.253	
14	18.622	2.122	0.707	115.6	0.	-20.12	131.66	74.38	1.770	56.85	2.316	
15	18.904	2.404	0.801	127.7	0.	-22.92	136.70	80.34	1.702	60.08	2.275	
16	19.050	2.550	0.850	133.9	0.	-24.42	130.33	83.81	1.555	61.83	2.108	
17	19.200	2.700	0.900	141.0	0.	-26.12	113.39	88.09	1.287	63.93	1.774	
18	19.355	2.855	0.952	149.5	0.	-27.96	78.52	93.65	0.839	66.63	1.178	

TEMPERATURE INTERVAL NUMBER = 18, TIME = 2.400 MIN., PRESSURE = 0.000 KSI

SEQ NO.	RADIUS IN.	DEPTH IN.	A/W	TEMPER. DEG.F	DLRTNDT DEG.F	CIRCUMF. STRESS KSI	KI	KIC	KI/KIC	KIA	KI/KIA	ELLIPTIC ANGLE
1	16.500	0.000	0.000	-211.0	0.	64.09	0.00	31.90	0.000	31.90	0.000	
2	16.530	0.030	0.010	-202.1	0.	61.65	20.77	31.90	0.651	31.90	0.651	
3	16.579	0.079	0.026	-187.0	0.	57.57	31.88	31.90	0.999	31.90	0.999	
4	16.668	0.168	0.056	-163.7	0.	51.20	43.32	31.90	1.358	31.90	1.358	
5	16.729	0.229	0.076	-149.0	0.	47.22	50.23	31.90	1.575	31.90	1.575	
6	16.804	0.304	0.101	-131.0	0.	42.33	56.07	32.97	1.700	31.90	1.758	
7	16.950	0.450	0.150	-98.4	0.	33.53	64.54	35.12	1.837	31.90	2.023	
8	17.104	0.604	0.201	-67.6	0.	25.29	71.79	37.41	1.919	33.57	2.138	
9	17.250	0.750	0.250	-41.5	0.	18.33	78.15	39.67	1.970	35.32	2.212	
10	17.404	0.904	0.301	-15.9	0.	11.55	83.20	42.44	1.961	37.23	2.235	
11	17.704	1.204	0.401	28.6	0.	-0.08	94.53	49.42	1.913	41.33	2.288	
12	18.000	1.500	0.500	63.0	0.	-8.90	107.25	57.21	1.875	45.94	2.334	
13	18.304	1.804	0.601	89.3	0.	-15.51	120.40	64.62	1.863	50.77	2.372	
14	18.622	2.122	0.707	109.1	0.	-20.33	134.19	71.63	1.873	55.24	2.429	
15	18.904	2.404	0.801	122.9	0.	-23.57	139.24	77.86	1.788	58.78	2.369	
16	19.050	2.550	0.850	129.7	0.	-25.20	132.67	81.45	1.629	60.65	2.188	
17	19.200	2.700	0.900	137.0	0.	-26.91	115.39	85.63	1.348	62.73	1.840	
18	19.355	2.855	0.952	145.1	0.	-28.71	79.89	90.73	0.881	65.21	1.225	

TSE6 12/9/81 TO 3M 14S LONGIT. CRACK

KICTYP = 6, RTNDTO = 0.0 DEG., %CU = 0.000, FO =0.00E19

TEMPERATURE INTERVAL NUMBER = 19, TIME = 2.500 MIN., PRESSURE = 0.000 KSI

SEQ NO.	RADIUS IN.	DEPTH IN.	A/W	TEMPER. DEG.F	DLRTNDT DEG.F	CIRCUMF. STRESS KSI	KI	KIC	KI/KIC	KIA	KI/KIA	ELLIPTIC ANGLE
1	16.500	0.000	0.000	-215.0	0.	63.97	0.00	31.90	0.000	31.90	0.000	
2	16.530	0.030	0.010	-206.8	0.	61.71	20.77	31.90	0.651	31.90	0.651	
3	16.579	0.079	0.026	-192.1	0.	57.72	31.93	31.90	1.001	31.90	1.001	
4	16.668	0.168	0.056	-168.6	0.	51.33	43.41	31.90	1.361	31.90	1.361	
5	16.729	0.229	0.076	-154.0	0.	47.36	50.34	31.90	1.578	31.90	1.578	
6	16.804	0.304	0.101	-136.0	0.	42.46	56.21	32.66	1.721	31.90	1.762	
7	16.950	0.450	0.150	-103.4	0.	33.67	64.72	34.78	1.861	31.90	2.029	
8	17.104	0.604	0.201	-72.6	0.	25.43	72.03	37.01	1.946	33.25	2.166	
9	17.250	0.750	0.250	-46.5	0.	18.47	78.44	39.21	2.001	34.98	2.243	
10	17.404	0.904	0.301	-20.9	0.	11.68	83.54	41.84	1.997	36.84	2.268	
11	17.704	1.204	0.401	23.6	0.	0.06	95.00	48.47	1.960	40.78	2.329	
12	18.000	1.500	0.500	57.8	0.	-8.75	107.91	55.92	1.930	45.15	2.390	
13	18.304	1.804	0.601	84.3	0.	-15.38	121.29	63.10	1.922	49.75	2.438	
14	18.622	2.122	0.707	104.8	0.	-20.39	135.26	69.95	1.934	54.21	2.495	
15	18.904	2.404	0.801	119.4	0.	-23.83	140.34	76.14	1.843	57.84	2.426	
16	19.050	2.550	0.850	126.5	0.	-25.52	133.70	79.71	1.677	59.76	2.237	
17	19.200	2.700	0.900	134.0	0.	-27.28	116.28	83.85	1.387	61.85	1.880	
18	19.355	2.855	0.952	142.1	0.	-29.11	80.50	88.82	0.906	64.28	1.252	

TEMPERATURE INTERVAL NUMBER = 20, TIME = 2.667 MIN., PRESSURE = 0.000 KSI

1	16.500	0.000	0.000	-125.0	0.	39.83	0.00	33.35	0.000	31.90	0.000	
2	16.530	0.030	0.010	-123.1	0.	39.27	13.09	33.48	0.391	31.90	0.410	
3	16.579	0.079	0.026	-120.7	0.	38.53	20.64	33.63	0.614	31.90	0.647	
4	16.668	0.168	0.056	-117.6	0.	37.52	29.61	33.83	0.875	31.90	0.928	
5	16.729	0.229	0.076	-114.1	0.	36.46	35.49	34.07	1.042	31.90	1.112	
6	16.804	0.304	0.101	-107.6	0.	34.63	41.00	34.50	1.188	31.90	1.285	
7	16.950	0.450	0.150	-92.7	0.	30.49	49.88	35.52	1.404	31.98	1.560	
8	17.104	0.604	0.201	-74.0	0.	25.36	58.01	36.91	1.572	33.17	1.749	
9	17.250	0.750	0.250	-54.1	0.	20.01	65.08	38.54	1.689	34.46	1.888	
10	17.404	0.904	0.301	-32.3	0.	14.21	70.72	40.59	1.743	35.98	1.965	
11	17.704	1.204	0.401	8.6	0.	3.47	82.40	45.88	1.796	39.31	2.096	
12	18.000	1.500	0.500	42.3	0.	-5.26	94.67	52.27	1.811	42.97	2.203	
13	18.304	1.804	0.601	70.3	0.	-12.37	106.87	59.15	1.807	47.17	2.266	
14	18.622	2.122	0.707	93.8	0.	-18.19	119.07	66.07	1.802	51.72	2.302	
15	18.904	2.404	0.801	110.7	0.	-22.28	123.22	72.31	1.704	55.64	2.214	
16	19.050	2.550	0.850	118.5	0.	-24.11	117.24	75.74	1.548	57.62	2.035	
17	19.200	2.700	0.900	126.0	0.	-25.84	101.90	79.43	1.283	59.61	1.709	
18	19.355	2.855	0.952	133.3	0.	-27.55	70.55	83.47	0.845	61.66	1.144	

TSE6 12/9/81 TO 3M 14S LONGIT. CRACK

KICTYP = 6, RTNDTO = 0.0 DEG., %CU = 0.000, FO =0.00E19

TEMPERATURE INTERVAL NUMBER = 21, TIME = 3.000 MIN., PRESSURE = 0.000 KSI

SEQ NO.	RADIUS IN.	DEPTH IN.	A/W	TEMPER. DEG.F	DLRTNDT DEG.F	CIRCUMF. STRESS KSI	KI	KIC	KI/KIC	KIA	KI/KIA	ELLIPTIC ANGLE
1	16.500	0.000	0.000	-57.0	0.	22.16	0.00	38.28	0.000	34.27	0.000	
2	16.530	0.030	0.010	-56.3	0.	21.93	7.30	38.35	0.190	34.32	0.213	
3	16.579	0.079	0.026	-56.0	0.	21.79	11.58	38.37	0.302	34.34	0.337	
4	16.668	0.168	0.056	-54.9	0.	21.39	16.76	38.46	0.436	34.41	0.487	
5	16.729	0.229	0.076	-53.2	0.	20.86	20.14	38.62	0.522	34.52	0.583	
6	16.804	0.304	0.101	-50.9	0.	20.18	23.41	38.82	0.603	34.68	0.675	
7	16.950	0.450	0.150	-45.3	0.	18.57	29.00	39.32	0.738	35.06	0.827	
8	17.104	0.604	0.201	-37.5	0.	16.38	34.44	40.06	0.860	35.61	0.967	
9	17.250	0.750	0.250	-28.4	0.	13.90	39.46	41.00	0.962	36.27	1.088	
10	17.404	0.904	0.301	-17.5	0.	10.97	43.78	42.24	1.037	37.10	1.180	
11	17.704	1.204	0.401	6.4	0.	4.64	52.73	45.53	1.158	39.11	1.348	
12	18.000	1.500	0.500	31.0	0.	-1.76	61.50	49.89	1.233	41.59	1.479	
13	18.304	1.804	0.601	52.2	0.	-7.18	69.70	54.55	1.278	44.31	1.573	
14	18.622	2.122	0.707	66.6	0.	-10.78	78.37	58.16	1.347	46.54	1.684	
15	18.904	2.404	0.801	78.2	0.	-13.55	82.33	61.34	1.342	48.59	1.695	
16	19.050	2.550	0.850	86.2	0.	-15.69	78.95	63.67	1.240	50.13	1.575	
17	19.200	2.700	0.900	97.0	0.	-18.53	68.93	67.14	1.027	52.43	1.315	
18	19.355	2.855	0.952	111.6	0.	-21.81	47.84	72.66	0.658	55.85	0.856	

TEMPERATURE INTERVAL NUMBER = 22, TIME = 3.233 MIN., PRESSURE = 0.000 KSI

1	16.500	0.000	0.000	-33.0	0.	16.34	0.00	40.52	0.000	35.93	0.000	
2	16.530	0.030	0.010	-32.3	0.	16.13	5.38	40.59	0.132	35.98	0.149	
3	16.579	0.079	0.026	-32.0	0.	15.99	8.51	40.62	0.209	36.01	0.236	
4	16.668	0.168	0.056	-31.5	0.	15.79	12.33	40.67	0.303	36.04	0.342	
5	16.729	0.229	0.076	-30.5	0.	15.47	14.85	40.78	0.364	36.12	0.411	
6	16.804	0.304	0.101	-28.9	0.	14.99	17.30	40.95	0.423	36.23	0.478	
7	16.950	0.450	0.150	-24.7	0.	13.77	21.46	41.41	0.518	36.55	0.587	
8	17.104	0.604	0.201	-19.3	0.	12.25	25.53	42.03	0.607	36.96	0.691	
9	17.250	0.750	0.250	-13.3	0.	10.61	29.37	42.76	0.687	37.43	0.785	
10	17.404	0.904	0.301	-5.7	0.	8.55	32.76	43.76	0.748	38.06	0.861	
11	17.704	1.204	0.401	12.3	0.	3.78	39.67	46.49	0.853	39.65	1.000	
12	18.000	1.500	0.500	30.6	0.	-1.00	46.45	49.83	0.932	41.56	1.118	
13	18.304	1.804	0.601	46.1	0.	-4.95	52.93	53.13	0.996	43.47	1.218	
14	18.622	2.122	0.707	56.7	0.	-7.60	59.96	55.63	1.078	44.97	1.333	
15	18.904	2.404	0.801	66.4	0.	-9.93	63.40	58.11	1.091	46.51	1.363	
16	19.050	2.550	0.850	73.7	0.	-11.93	60.97	60.08	1.015	47.77	1.276	
17	19.200	2.700	0.900	84.0	0.	-14.66	53.30	63.02	0.846	49.70	1.072	
18	19.355	2.855	0.952	98.1	0.	-17.84	37.02	67.51	0.548	52.66	0.703	

TSE6 12/9/81 TO 3M 14S 2-D CRITICAL CRACK DEPTHS
KICTYP = 6, RTNDTO = 0.0 DEGF, %CU = 0.000, FO = 0.00E19

TIME	INITIATION	ARREST
1.02		0.150
1.03		0.201
1.04		0.707
1.04		0.801
1.05		0.250
1.07		0.101
1.07		0.601
1.08		0.301
1.10		0.500
1.11		0.401
1.11		0.850
1.13		0.082
1.13		0.857
1.16		0.076
1.17		0.075
1.17		0.865
1.23	0.150	
1.24	0.201	
1.26	0.101	
1.27	0.250	
1.32		0.056
1.32	0.301	
1.32		0.900
1.33	0.076	
1.33	0.076	0.055
1.33	0.309	0.901
1.44	0.401	
1.47	0.707	
1.48	0.500	
1.48	0.601	
1.50	0.057	0.043
1.50	0.768	0.919
1.51	0.056	
1.52	0.801	
1.62	0.850	
1.67	0.046	0.036
1.67	0.860	0.934
1.83	0.036	0.031
1.83	0.892	0.945
1.88	0.900	
1.94		0.952
2.00	0.029	0.028
2.00	0.912	
2.17	0.027	0.027
2.17	0.925	
2.27	0.027	0.027
2.27	0.931	
2.30	0.027	0.027
2.30	0.933	
2.40	0.027	0.027
2.40	0.938	
2.44	0.026	0.026
2.50	0.026	0.026
2.50	0.942	
2.50	0.026	

TSE6 12/9/81 TO 3M 14S 2-D CRITICAL CRACK DEPTHS
KICTYP = 6, RTNDTO = 0.0 DEGF, %CU = 0.000, F0 = 0.00E19

TIME	INITIATION	ARREST
2.50		0.026
2.62	0.056	
2.64		0.056
2.67	0.071	0.064
2.67	0.933	
2.69	0.076	
2.74		0.076
2.77	0.101	
2.82		0.101
2.83		0.952
2.87	0.150	
2.92		0.150
2.93	0.201	
2.98	0.250	
2.99		0.201
3.00	0.276	0.215
3.00	0.904	0.936
3.03	0.301	
3.03	0.900	
3.07		0.250
3.12	0.401	
3.13		0.301
3.18	0.500	
3.23	0.601	
3.23	0.606	0.401
3.23	0.854	0.910

MAX ON INITIATION CURVE: A/W = 0.942, TIME = 2.50

MAX ON ARREST CURVE: A/W = 0.952, TIME = 2.83

NUREG/CR-4249
ORNL-6163
Dist. Category RF

Internal Distribution

1-5. D. G. Ball
6. B. R. Bass
7. S. E. Bolt
8. R. H. Bryan
9. J. W. Bryson
10-14. R. D. Cheverton
15. J. M. Corum
16. W. R. Corwin
17. J. S. Crowell
18. D. M. Eissenberg
19. J. A. Getsi
20. S. K. Iskander
21. J. J. McGowan
22. J. G. Merkle
23. A. P. Malinauskas
24. R. K. Nanstad
25. D. J. Naus
26. J. C. Petrykowski
27-31. C. E. Pugh
32. G. C. Robinson
33. H. E. Trammell
34-38. G. D. Whitman
39. ORNL Patent Office
40. Central Research Library
41. Document Reference Section
42-43. Laboratory Records Department
44. Laboratory Records (RC)

External Distribution

45. C. Z. Serpan, Division of Engineering Technology, Nuclear Regulatory Commission, Washington, DC 20555
46. M. Vagins, Division of Engineering Technology, Nuclear Regulatory Commission, Washington, DC 20555
47. Director, Division of Reactor Safety Research, Nuclear Regulatory Commission, Washington, DC 20555
48. Office of Assistant Manager for Energy Research and Development, Department of Energy, Oak Ridge Operations Office, Oak Ridge, TN 37831
49-50. Technical Information Center, DOE, Oak Ridge, TN 37831
51-325. Given distribution as shown in Category RF (NTIS-10)

NRC FORM 335 (2-84) NRCM 1102, 3201, 3202

U.S. NUCLEAR REGULATORY COMMISSION

BIBLIOGRAPHIC DATA SHEET

SEE INSTRUCTIONS ON THE REVERSE

1. REPORT NUMBER (Assigned by TIDC, add Vol. No., if any)

NUREG/CR-4249
ORNL-6163

2. TITLE AND SUBTITLE

Pressure Vessel Fracture Studies Pertaining to the PWR Thermal-Shock Issue: Experiments TSE-5, TSE-5A, and TSE-6

3. LEAVE BLANK

4. DATE REPORT COMPLETED

MONTH	YEAR
May	1985

5. AUTHOR(S)

R. D. Cheverton, D. G. Ball,* S. E. Bolt, S. K. Iskander,* and R. K. Nanstad

6. DATE REPORT ISSUED

MONTH	YEAR
June	1985

7. PERFORMING ORGANIZATION NAME AND MAILING ADDRESS (Include Zip Code)

Oak Ridge National Laboratory
P.O. Box X
Oak Ridge, Tennessee 37831

8. PROJECT/TASK/WORK UNIT NUMBER

9. FIN OR GRANT NUMBER

B0119

10. SPONSORING ORGANIZATION NAME AND MAILING ADDRESS (Include Zip Code)

Division of Engineering Technology
Office of Nuclear Regulatory Research
U.S. Nuclear Regulatory Commission
Washington, DC 20555

11a. TYPE OF REPORT

b. PERIOD COVERED (Inclusive dates)

12. SUPPLEMENTARY NOTES

13. ABSTRACT (200 words or less)

Thermal-shock experiments TSE-5, TSE-5A, and TSE-6 were conducted for the purpose of investigating the behavior of surface flaws under pressurized-water-reactor (PWR) overcooling-accident conditions. These experiments were the fifth, sixth, and seventh in a series of thermal-shock experiments conducted with large steel cylinders (A508, class-2 chemistry; 991-mm OD × 76- and 152-mm wall × 1.2-m length) as a part of the Heavy-Section Steel Technology (HSST) Program for this purpose.

For each of these experiments the initial flaw was on the inner surface and extended the full length of the cylinder. The thermal shock was applied to the inner surface only, and this was accomplished by effectively dunking the test cylinder, initially at ∿93°C, into a large volume of liquid nitrogen.

Results of the experiments have confirmed that (1) linear-elastic fracture mechanics (LEFM) is valid for thermal-shock loading, (2) crack arrest will take place in accordance with recently developed crack-arrest concepts, (3) the crack-arrest toughness values for rising and falling K_I fields are the same, (4) warm prestressing is effective in preventing crack initiation, (5) thermal shock alone cannot drive a flaw all the way through the wall, (6) dynamic effects for PWR-vessel thermal-shock loading conditions are negligible, (7) in the absence of cladding and under severe thermal-shock loading conditions finite-length flaws will extend on the surface to become very long, and (8) there can be very large scatter in small-specimen fracture-toughness data.

14. DOCUMENT ANALYSIS a. KEYWORDS DESCRIPTORS

Nuclear reactor pressure vessels
Thermal shock
Fracture mechanics
Thermal-shock experiments

b. IDENTIFIERS/OPEN ENDED TERMS

15. AVAILABILITY STATEMENT

Unlimited

16. SECURITY CLASSIFICATION

(This page)
Unclassified

(This report)
Unclassified

17. NUMBER OF PAGES

18. PRICE

*Computing and Telecommunications Division